AD_____

Award Number: DAMD17-99-1-9564

TITLE: Role of Angiogenesis in the Etiology and Prevention of Ovarian Cancer

Project 1: Effect of Angiogenesis Inhibitors in Preventing Ovarian Cancer Growth

PRINCIPAL INVESTIGATOR: Sundaram Ramakrishnan, Ph.D.

CONTRACTING ORGANIZATION: University of Minnesota
Minneapolis, Minnesota 55455-2070

REPORT DATE: October 2002

TYPE OF REPORT: Annual

PREPARED FOR: U.S. Army Medical Research and Materiel Command
Fort Detrick, Maryland 21702-5012

REPORT DOCUMENTATION PAGE

Form Approved
OMB No. 074-0188

1. AGENCY USE ONLY (Leave blank)	2. REPORT DATE	3. REPORT TYPE AND DATES COVERED
	October 2002	Annual (1 Oct 01 - 30 Sep 02)

4. TITLE AND SUBTITLE
Role of Angiogenesis in the Etiology and Prevention of Ovarian Cancer, Project 1: Effect of Angiogenesis Inhibitors in Preventing Ovarian Cancer Growth

5. FUNDING NUMBERS
DAMD17-99-1-9564

6. AUTHOR(S):
Sundaram Ramakrishnan, Ph.D.

7. PERFORMING ORGANIZATION NAME(S) AND ADDRESS(ES)
University of Minnesota
Minneapolis, Minnesota 55455-2070

E-Mail: sunda001@tc.umn.edu

8. PERFORMING ORGANIZATION REPORT NUMBER

9. SPONSORING / MONITORING AGENCY NAME(S) AND ADDRESS(ES)
U.S. Army Medical Research and Materiel Command
Fort Detrick, Maryland 21702-5012

10. SPONSORING / MONITORING AGENCY REPORT NUMBER

11. SUPPLEMENTARY NOTES
Original contains color plates: All DTIC reproductions will be in black and white.

12a. DISTRIBUTION / AVAILABILITY STATEMENT
Approved for Public Release; Distribution Unlimited

12b. DISTRIBUTION CODE

13. Abstract ***(Maximum 200 Words)*** *(abstract should contain no proprietary or confidential information)*

Primary growth of ovarian cancer and its spreading in the peritoneal cavity as micrometastases are dependent on angiogenesis. Therefore, angiogenesis inhibitors can be used in the prevention and treatment of ovarian cancers. One of the objectives of Project 1 is the development of a genetically reengineered angiostatic protein, endostatin. During expression cloning of human endostatin, a single point mutation was identified. Mutation lead to the substitution of Proline 125 to an Alanine residue. Mutant endostatin (P125A) was expressed in soluble form in large quantities to evaluate its effect against ovarian cancer growth. Native human endostatin was used in parallel studies to determine relative efficacy. P125A endostatin was more potent than native endostatin in inhibiting endothelial cell proliferation and migration in vitro. Mutant endostatin also bound endothelial cells better than the native protein. Furthermore, mutant endostatin inhibited ovarian cancer growth in athymic mice more effectively when compared to native endostatin.

14. SUBJECT TERMS
ovarian cancer, angiogenesis inhibitors

15. NUMBER OF PAGES
259

16. PRICE CODE

17. SECURITY CLASSIFICATION OF REPORT	18. SECURITY CLASSIFICATION OF THIS PAGE	19. SECURITY CLASSIFICATION OF ABSTRACT	20. LIMITATION OF ABSTRACT
Unclassified	Unclassified	Unclassified	Unlimited

Table of Contents

Cover	1.
SF 298	2.
Table of Contents	3.
Introduction	4.
Body	4.-9.
Key Research Accomplishments	9.
Reportable Outcomes	9.-10.
Conclusions	10.-11.
References	11.
Appendices	12.

(4) INTRODUCTION:

Establishment of new blood supply (angiogenesis) is necessary for ovarian cancers to grow and spread inside the peritoneum (1 –3). Angiognesis is a complex process involving growth factors and matrix degrading proteases (4) . Angiogenesis can also be inhibited by a number of proteolytic fragments of the coagulation cascade. One of the well-studied antiangiogenic molecule is endostatin, which, is produced by the proteolysis of collagen type XVIII that is selectively expressed on vascular basement membrane (5,6). We have earlier shown that a mouse endostatin is effective in inhibiting ovarian cancer growth in athymic mice (7). Furthermore, endostatin treatment delayed the appearance of malignant lesions in a transgenic mouse line, which has been genetically modified to develop mammary adenocarcinomas (8). These studies demonstrated the potential of using antiangiogenic molecules to prevent and treat ovarian cancer. While native endostatin was effective in inhibiting cancer growth, its biological activity can be further improved by genetically redesigning the molecule to enhance bioavailability, tumor homing and potency. Structure-function studies are necessary to accomplish this goal. Endostatin binds to integrins and glypicans expressed on endothelial cell surface (9,10). Regions of endostatin involved in binding these molecules are not completely understood. During expression cloning of human endostatin, we identified a mutant protein containing a substitution of proline to an alanine (P125A) . Pro_{125}, is located immediately upstream to Asn-Gly-Arg (NGR) sequence. NGR containing peptides target tumor vasculature and inhibit endothelial membrane associated aminopeptidase N activity. Therefore investigations were carried out with the mutant endostatin and the native protein.

(5) BODY :

Hypothesis and Purpose : Ovarian cancer growth and peritoneal spread is dependent on neovascularization. Furthermore, angiogenic growth factors such as VEGF play an important role in the development of malignant ascites. Therefore, inhibition angiogenesis will have a significant impact on the development of ovarian cancer. The purpose of the present study is to determine the effect of angiogenesis inhibitors on ovarian cancer growth.

Task 1 : Large-scale production of angiostatin and endostatin. Evaluate their efficacy in ovarian cancer model systems. This task was largely completed. Fermentation conditions were optimized and production of recombinant protein was streamlined. Year 1 and 2 were spent on Task 1 and experiments related to Task were initiated during the same period. During expression cloning of human endostatin, a novel mutant endostatin was generated (P125A). Mutant endostatin was found to be better in inhibiting endothelial cell proliferation , migration and angiogenesis (Summarized earlier in 2001 Annual report). Additional studies were carried out using this mutant protein. In a collaborative study we determined the efficacy of the mutant endostatin to inhibit tumor growth in a transgenic animal model (Int. J. Cancer, 2002, a copy attached). Major findings from

this study are that mutant endostatin is better in inhibiting ovarian and breast cancer growth. Endostatin treatment inhibits angiogenesis related gene expression at the tumor site.

Results related to Task 1 completed in Year 3 : An immunocopetent mouse model for ovarian cancer was used to determine the biological efficacy of human endostatin. LM3, a mouse epithelial ovarian cancer cell line was obtained from Japan. This cell line produces aggressive growth of ovarian cancer (ascites and solid tumors) in C3H/Balb c F1 mice (syngenic). Human endostatin treated significantly inhibited the subcutaneous growth of LM3 tumors (Fig. 1) . These preliminary studies are now extended to i.p. model . Intraperitoneal growth of ovarian cancer is difficult of follow . Transgenic expression of surrogate markers can be used to follow the growth during antiangiogenic therapy. For this purpose, we obtained an ovarian cancer cell line established in Dr. Hamilton's laboratory (Fox Chase Cancer Center), which secretes heat stable alkaline phosphatase enzyme. Serum levels of alkaline phosphatase had been used as a marker to follow the therapeutic efficacy. This model is currently used to determine the effect of endostatin treatment.

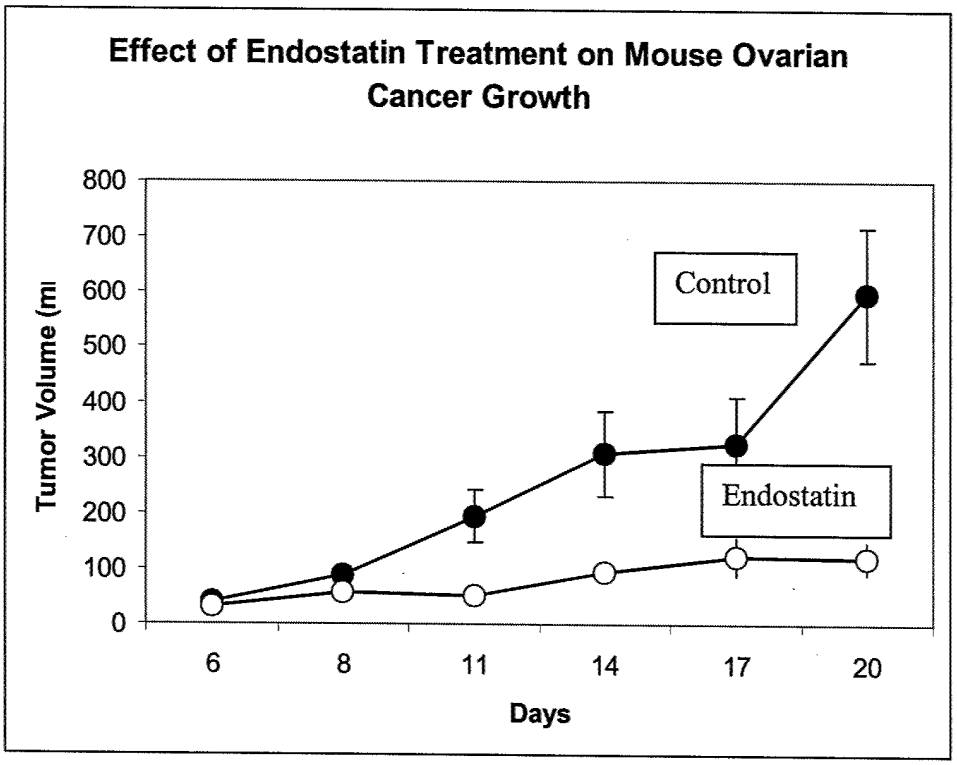

Fig.1 : Effect of Human Endostatin on LM-3, ovarian cancer growth. Groups of 10 mice were implanted with 2 x 105 cells on day 0. Treatment with endostatin started on day 3. Once a week injection of 400 ug/mouse in alginate encapsulated beads. A total of two injections were given on day 3 and day 10. Values are mean +/- SE.

Task # 2 : Alternate methods to improve antitumor activity of angiostatin and endostatin. Angiogenic inhibitors in combination with chemotherapy for example are likely to be synergistic in inhibiting ovarian cancer growth. Two strategies were proposed ; a) combination treatment with chemotherapy and an angiogenesis inhibitor and b) genetic modification of endostatin to improve its bioavailability and potency. For the later approach, endostatin was modified with specific vascular targeting motifs. Construction and preliminary characterization of these constructs began in year two instead of year three as originally proposed . A summary of these constructs was provided in the last annual report (Year 2001).

Results Related to the Task # 2 completed in Year 3 :

Carboplatin Differentially Up-regulates VEGF Expression in Endothelial Cells

Preliminary studies showed that ovarian cancer cells were at least two orders in magnitude more sensitive to carboplatin when compared to endothelial cells. The apparent differences in sensitivity are due to a number of factors. Tumor cells are more sensitive due to impaired DNA repair pathways and genetic instability. On the other hand, endothelial cells are protected from chemotherapeutic drugs by selective upregulation of survival factors such as VEGF. VEGF is known to protect endothelial cells from apoptosis induced by radiation. Therefore, we determined the effect of carboplatin on VEGF expression. Both ovarian and endothelial cell cultures were treated with their respective TCID50 concentration of Carboplatin and VEGF levels in the conditioned media were measured by ELISA. Carboplatin treatment did not alter the level of VEGF secreted by the tumor cell line at both 24 and 48-hour time points. VEGF concentrations ranged between 47.8 and 58.4 pg/1x10^6 cells. However, treatment of HUVEC with Carboplatin resulted in a five-fold increase of VEGF levels at 24 hours (22.8 pg/1x10^6 cells for control versus 129.4 pg/1x10^6 cells for Carboplatin treated cultures). An even more pronounced effect was seen at the 48 hour time point with a twelve-fold increase in VEGF levels in Carboplatin treated HUVEC (17.9 pg/1x10^6 cells for control cells versus 224.2 pg/1x10^6 cells for Carboplatin treated cells). These values were statistically significant as determined by the Student's t-test ($p < 0.038$). Our results indicate that Carboplatin induced expression of VEGF in endothelial cells could act as an anti-apoptotic factor, which partially rescues these cells from the cytotoxic effects of this drug.

Carboplatin Specifically Up-regulates VEGF Expression in Tumor Vessels *In vivo*

To determine whether Carboplatin could induce VEGF expression *in vivo*, a nude mouse model was employed. MA148 tumor cells, the same carcinoma cell line used for the *in vitro* experiments, were transplanted s.c. into the hind leg of athymic nude mice. After ten days, small palpable tumors were established and treatment was initiated. A low dose of Carboplatin (32.5 mg/kg/dose) was then administered every three days for five doses, at which point the animals were sacrificed and tumor tissues were harvested. Sections were prepared and immunochemically stained for VEGF and CD-31. As shown in Fig. 2A, PBS treated control animals showed a consistent but low expression of VEGF

in the tumor tissue. In contrast, Carboplatin treated animals displayed increased expression of VEGF in the vasculature (Fig. 2B). Staining of the tissues with specific antibodies to the endothelial cell marker CD-31 was used to identify vascular structures in the tumor tissue (Fig. 2 C and D). A subsequent overlay of the images showed a clear co-localization of VEGF in the tumor vasculature of Carboplatin treated animals (Fig. 2 F). In contrast, no significant co-localization was seen in the PBS treated control tissue (Fig. 2 E). These results provide evidence that Carboplatin treatment significantly increases the expression of the survival factor VEGF in tumor vessels *in vivo*.

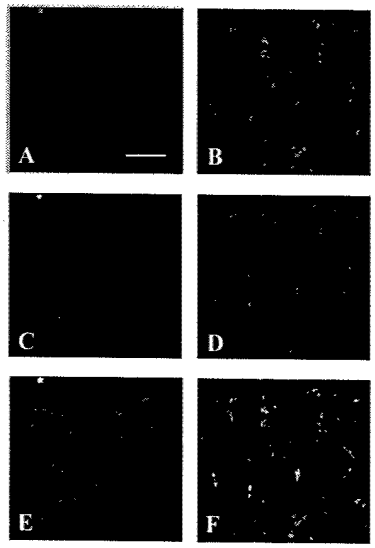

Antibody to VEGF Significantly Improves The Anti-Tumor Effects of Carboplatin

Subsequently, experiments were carried out to determine the therapeutic benefit of anti-VEGF antibodies during Carboplatin chemotherapy. MA148 cells were inoculated s.c. into the hind leg of athymic, nude mice and tumors were allowed to establish for ten days. Animals were then randomized and divided into four treatment groups. Tumor growth was then monitored by caliper measurements and the experiments were terminated once tumor volumes reached about 3,000 mm^3. Data in Fig. 3 show the effect of antibodies to VEGF and carboplatin from three independent experiments. Histogram in panel D shows the respective control where in nonspecific IgG was used as control. These studies clearly demonstrate that chemotherapy induces selective stress response in vascular endothelial cells by producing VEGF and that intervening the stress response with an antibody to VEGF produces synergistic inhibition of ovarian cancer growth. Details from these experiments are given in a manuscript communicated for publication (attached).

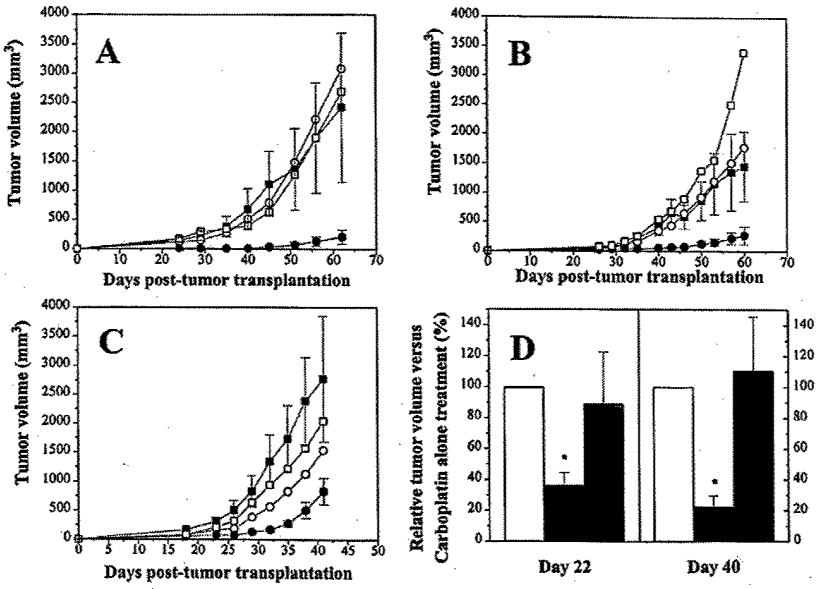

Fig.3

Antibody to VEGF Significantly Improves The Anti-Tumor Effect of Carboplatin. Human epithelial ovarian carcinoma (MA148) tumors were established by injecting athymic nude mice s.c. in the right flank with 2 x 10^6 tumor cells. Tumors were allowed to establish for ten days and animals were subsequently randomized and divided into treatment groups. Solid tumor growth was then monitored by caliper measurements as described in "Materials and Methods". Open square symbol - PBS control, Closed squares – Carboplatin, Closed Circle symbols - Carboplatin + anti-VEGF IgG, Open circle symbols - anti-VEGF IgG. A-C shows the results of three independent experiments (n = 4-6 animals per group per experiment). Data points show the mean tumor volume with respective standard error bars. D, summary of inhibition of tumor growth with the addition of anti-VEGF IgG or pre-immune control IgG to Carboplatin therapy. Results are expressed as mean tumor volumes relative to mean Carboplatin treated volumes ($V/V^{carboplatin}$). Two time points were chosen for analysis. Day 22 (end of Carboplatin treatment) and day 40 (end of antibody treatment). □ Carboplatin, Solid bars - Carboplatin + anti-VEGF IgG, Grey bars represent Carboplatin + pre-immune IgG. * statistical significance as determined by Student's t-test ($p < 0.033$ for both values compared to Carboplatin alone treatment).

These studies will be extended to endostatin treatment in combination with carboplatin and or Taxol in year 4.

Task # 3. Investigate genetically engineered endostatin to inhibit ovarian cancer growth. Experiments were initiated in year 2 to make and characterize vascular targeting endostatin to improve bioavailability and efficacy. These constructs are currently being investigated for efficacy in inhibiting ovarian cancer growth in different model systems. These studies will be completed in Year 4.

Major work related to Task # 3 completed :

- NH2 and COOH terminal modification of endostatin with RGD sequence.
- Characterization of biological activity (Abstract presented at Keystone meeting 2001- a copy attached)
- NGR-endostatin was constructed, expressed in yeast.
- Biological activity and aminopeptidase inhibition was characterized (Abstract presented at the AACR meeting, 2002 – a copy attached).

We will continue to evaluate the efficacy of the mutated endostatin against ovarian cancer in the year 4.

(6) KEY RESEARCH ACCOMPLISHMENTS IN YEAR 3:

- Endostatin is effective in inhibiting ovarian cancer growth in immunocompetent mouse model
- Mutant endostatin (P125A) is a potent inhibitor of angiogenesis
- P125A-endostatin inhibit human ovarian cancer growth in athymic mice more efficiently than the native protein
- P125A-endostatin treatment inhibits expression of angiogenic growth factors and their respective receptors in the tumors.
- Carboplatin treatment differentially induces the expression of survival factors (VEGF) in the endothelial cells *in vitro* and *in vivo*.
- Interfering with this pathway potentiates the efficacy of chemotherapy of ovarian cancer.
- Addition of vascular targeting sequence to P125A endostatin improves tumor homing and enhances anti-tumor activity.
-

(7) REPORTABLE OUTCOMES :

Manuscripts :

1. Calvo, A., Yokoyama, Y., Smith, L.E., Shih, S-C., Ramakrishnan, S., Feldman, A., Libuti, S., Green, J.E. Inhibition of the mammary gland

adenocarcinoma angiogenic switch in C3(1)/SV40 transgenic mice by a mutated form of human endostatin. (Int. J. Cancer, 101: 224-234,2002)

2. Ruud P.M. Dings, Yumi Yokoyama, S. Ramakrishnan, Arjan W. Griffioen, Kevin H. Mayo. The designed angiostatic peptide anginex synergistically improves chemotherapy and anti-angiogenesis therapy with angiostatin. Cancer Research, 2002 (in press). (Collaborative study with Project 3).

3. Robert Wild, Ruud P.M. Dings and S. Ramakrishnan. Carboplatin selectively induces the VEGF stress response in endothelial cells : Synergistic inhibition of tumor growth by combination treatment with antibody to VEGF. (communicated).

4. Yumi Yokoyama and S. Ramakrishnan. Substitution of a single amino acid residue in human endostatin potentiates inhibition of cancer growth. (communicated).

Abstracts :

1. Improved Inhibition of Tumor Growth by Genetic Modification of Endostatin with an NGR-motif . Yumi Yokoyama[1] and S. Ramakrishnan[1,2,3]
Abstract # 897, p117. Proc. Am. Assoc. Cancer Res., April 7, 2002.

2. **Substitution of A Single Amino Acid Residue in Human Endostatin Potentiates Inhibition of Ovarian Cancer Growth**
Yumi Yokoyama[1] and S. Ramakrishnan[1,2,3]
Keystone Meeting on Angiogenesis, Barniff, Alberta, CA 2002

3. Transfection of ovarian cancer cells with mutated human endostatins suppresses tumor growth. Indira V. Subramanian, Yumi Yokoyama, Rahel Ghebre, Blair Harkness and S. Ramakrisnnan.

Abstract # 4574, p 308. Proc. Am. Assoc. Cancer Res., April 7, 2002.

4. Isolation and in vitro characterization of human anti-VEGF scFV fragments. S. Wang, J. Hong, Y. Yokoyama, S. Ramakrishnan and Soldano Ferrone.

Abstract # 4801, p316. Proc. Am. Assoc. Cancer Res., April 7, 2002.

(9) **CONCLUSIONS** :

We conclude from the studies carried out in Year 3 that human endostatin is able to inhibit ovarian cancer growth in immunocompetent mouse model system. Antiangiogenic therapies can synergies with chemotherapy in inhibiting ovarian cancer growth. Chemotherapeutic drugs such as carboplatin induces stress response signals in endothelial cells leading to the expression of survival factor, VEGF. Interfering with this pathway potentiates the efficacy of chemotherapy. Genetic modification of endostatin improves its activity and tumor homing. Finally, treatment of tumor bearing mice with endostatin down regulates expression of angiogenic growth factors and their receptors. These studies will help in developing antiangiogenic methods to prevent and /or treat ovarian cancer.

(10) **REFERENCES** :

1. O'Reilly, M.S., T. Boehm, Y. Shing, N. Fukai, G. Vasios, W.S. Lane, E. Flynn, J.R. Birkhead, B.R. Olsen, and J. Folkman. 1997. Endostatin: an endogenous inhibitor of angiogenesis and tumor growth. *Cell*. 88:277-285.
2. Dhanabal, M., R. Ramchandran, R. Volk, I.E. Stillman, M. Lombardo, M.L. Iruela-Arispe, M. Simons, and V.P. Sukhatme. 1999. Endostatin: yeast production, mutants, and antitumor effect in renal cell carcinoma. *Cancer Res*. 59:189-197.
3. Boehm, T., J. Folkman, T. Browder, and M.S. O'Reilly. 1997. Antiangiogenic therapy of experimental cancer does not induce acquired drug resistance. *Nature*. 390:404-407.
4. Boehm, T., S. O'Reilly M, K. Keough, J. Shiloach, R. Shapiro, and J. Folkman. 1998. Zinc-binding of endostatin is essential for its antiangiogenic activity. *Biochem Biophys Res Commun*. 252:190-194.
5. Yamaguchi, N., B. Anand-Apte, M. Lee, T. Sasaki, N. Fukai, R. Shapiro, I. Que, C. Lowik, R. Timpl, and B.R. Olsen. 1999. Endostatin inhibits VEGF-induced endothelial cell migration and tumor growth independently of zinc binding. *Embo J.* 18:4414-4423.
6. Sasaki, T., H. Larsson, J. Kreuger, M. Salmivirta, L. Claesson-Welsh, U. Lindahl, E. Hohenester, and R. Timpl. 1999. Structural basis and potential role of heparin/heparan sulfate binding to the angiogenesis inhibitor endostatin. *Embo J.* 18:6240-6248.
7. Rehn, M., T. Veikkola, E. Kukk-Valdre, H. Nakamura, M. Ilmonen, C. Lombardo, T. Pihlajaniemi, K. Alitalo, and K. Vuori. 2001. Interaction of endostatin with integrins implicated in angiogenesis. *Proc Natl Acad Sci U S A*. 98:1024-1029.
8. Karumanchi, S.A., V. Jha, R. Ramchandran, A. Karihaloo, L. Tsiokas, B. Chan, M. Dhanabal, J.I. Hanai, G. Venkataraman, Z. Shriver, N. Keiser, R. Kalluri, H. Zeng, D. Mukhopadhyay, R.L. Chen, A.D. Lander, K. Hagihara, Y. Yamaguchi, R. Sasisekharan, L. Cantley, and V.P. Sukhatme. 2001. Cell surface glypicans are low-affinity endostatin receptors. *Mol Cell*. 7:811-822.
9. Dhanabal, M., R. Ramchandran, M.J. Waterman, H. Lu, B. Knebelmann, M. Segal, and V.P. Sukhatme. 1999. Endostatin induces endothelial cell apoptosis. *J Biol Chem*. 274:11721-11726.
10. Shichiri, M., and Y. Hirata. 2001. Antiangiogenesis signals by endostatin. *Faseb J*. 15:1044-1053.

(11) **APPENDICES** :

1. Calvo, A., Yokoyama, Y., Smith, L.E., Shih, S-C., Ramakrishnan, S., Feldman, A., Libuti, S., Green, J.E. Inhibition of the mammary gland adenocarcinoma angiogenic switch in C3(1)/SV40 transgenic mice by a mutated form of human endostatin. (Int. J. Cancer, 101: 224-234,2002)

3. Robert Wild, Ruud P.M. Dings and S. Ramakrishnan. Carboplatin selectively induces the VEGF stress response in endothelial cells : Synergistic inhibition of tumor growth by combination treatment with antibody to VEGF. (communicated).

Abstracts :

1. Improved Inhibition of Tumor Growth by Genetic Modification of Endostatin with an NGR-motif . Yumi Yokoyama[1] and S. Ramakrishnan[1,2,3]
Abstract # 897, p179. Proc. Am. Assoc. Cancer Res., April 7, 2002.

2. **Substitution of A Single Amino Acid Residue in Human Endostatin Potentiates Inhibition of Ovarian Cancer Growth**
Yumi Yokoyama[1] and S. Ramakrishnan[1,2,3]
Keystone Meeting on Angiogenesis, Barniff, Alberta, CA 2002

3. Transfection of ovarian cancer cells with mutated human endostatins suppresses tumor growth. Indira V. Subramanian, Yumi Yokoyama, Rahel Ghebre, Blair Harkness and S. Ramakrisnnan.

Abstract # 4574, p 923. Proc. Am. Assoc. Cancer Res., April 7, 2002.

4. Isolation and in vitro characterization of human anti-VEGF scFV fragments. S. Wang, J. Hong, Y. Yokoyama, S. Ramakrishnan and Soldano Ferrone.

Abstract # 4801, p969-970. Proc. Am. Assoc. Cancer Res., April 7, 2002.

APPENDIX

Project 1

Int. J. Cancer: **101**, 224–234 (2002)

Publication of the International Union Against Cancer

INHIBITION OF THE MAMMARY CARCINOMA ANGIOGENIC SWITCH IN C3(1)/SV40 TRANSGENIC MICE BY A MUTATED FORM OF HUMAN ENDOSTATIN

Alfonso CALVO[1], Yumi YOKOYAMA[3], Lois E. SMITH[2], Iqbal ALI[4], Shu-Ching SHIH[2], Andrew L. FELDMAN[5], Steven K. LIBUTTI[5], Ramakrishnan SUNDARAM[3] and Jeffrey E. GREEN[1]*

[1]*Laboratory of Cell Regulation and Carcinogenesis, National Cancer Institute, NIH, Bethesda, MD, USA*
[2]*Children's Hospital, Harvard Medical School, Boston, MA, USA*
[3]*Department of Pharmacology, University of Minnesota, Minneapolis, MN, USA*
[4]*Division of Cancer Prevention and Center for Cancer Research, National Cancer Institute, NIH, Bethesda, MD, USA*
[5]*Surgery Branch, National Cancer Institute, NIH, Bethesda, MD, USA*

Cancer therapies based on the inhibition of angiogenesis by endostatin have recently been developed. We demonstrate that a mutated form of human endostatin (P125A) can inhibit the angiogenic switch in the C3(1)/Tag mammary cancer model. P125A has a stronger growth-inhibitory effect on endothelial cell proliferation than wild-type endostatin. We characterize the angiogenic switch, which occurs during the transition from preinvasive lesions to invasive carcinoma in this model, and which is accompanied by a significant increase in total protein levels of vascular endothelial growth factor (VEGF) and an invasion of blood vessels. Expression of the $VEGF_{188}$ mRNA isoform, however, is suppressed in invasive carcinomas. The VEGF receptors fetal liver kinase-1 (Flk-1) and Fms-like tyrosine kinase-1 (Flt-1) become highly expressed in epithelial tumor and endothelial cells in the mammary carcinomas, suggesting a potential autocrine effect for VEGF on tumor cell growth. Angiopoietin-2 mRNA levels are also increased during tumor progression. CD-31 (platelet-endothelial cell adhesion molecule [PECAM]) staining revealed that blood vessels developed in tumors larger than 1 mm The administration of P125A human endostatin in C3(1)/Tag females resulted in a significant delay in tumor onset, decreased tumor multiplicity and tumor burden and prolonged survival of the animals. Endostatin treatment did not reduce the number of preinvasive lesions, proliferation rates or apoptotic index, compared with controls. However, mRNA levels of a variety of proangiogenic factors (VEGF, VEGF receptors Flk-1 and Flt-1, angiopoietin-2, Tie-1, cadherin-5 and PECAM) were significantly decreased in the endostatin-treated group compared with controls. These results demonstrate that P125A endostatin inhibits the angiogenic switch during mammary gland adenocarcinoma tumor progression in the C3(1)/Tag transgenic model.

Key words: *angiogenesis; endostatin; vascular endothelial growth factor; mammary cancer*

The growth and metastatic spread of solid tumors is critically dependent on the formation of new blood vessels through angiogenesis.[1,2] During this process, the effects of proangiogenic factors dominate over the antiangiogenic factors, resulting in the *angiogenic switch*.[2] A large variety of growth factors modulate tumor angiogenesis, including those that alter the extracellular matrix as well as those that promote endothelial cell proliferation and migration.[3] Among the proangiogenic factors described, vascular endothelial growth factor (VEGF) has been shown to be frequently upregulated in a variety of tumors[4] and has been well characterized.[4,5] The 2 high-affinity VEGF receptors fetal liver kinase-1 (Flk-1) and Fms-like tyrosine kinase-1 (Flt-1), members of the tyrosine kinase receptor family, transduce the activity of this growth factor.[5] The activation of intracellular signaling pathways by these receptors involves their autophosphorylation and, as a consequence, the stimulation of endothelial cell proliferation (especially in the case of the Flk-1 receptor), migration, tubule formation, and angiogenesis *in vivo*.[5–7] Although the expression of VEGF receptors was initially localized to endothelial cells, recent studies have shown that epithelial and tumor cells from various tissues also express VEGF receptors and respond to stimulation by VEGF.[8–10]

Another family of vascular growth factors, angiopoietins, has recently been characterized.[11] Angiopoietin-1 mediates cell-cell interactions between endothelial cells and other neighboring cells, such as smooth muscle cells.[12,13] In contrast to VEGF, angiopoietin-1 does not directly stimulate endothelial cell growth. Angiopoietin-2 is typically expressed at sites of vascular remodeling in the adult[14] and in tumors, where it stimulates endothelial cell growth and angiogenesis.[11,14] Moreover, angiopoietin-2 acts in a complementary and coordinated way with VEGF in order to promote tumor angiogenesis.[11]

Inhibition of angiogenesis has emerged as a promising strategy to treat both primary and metastatic tumors by shifting the balance from a proangiogenic to an antiangiogenic state. Endostatin, a 20 kDa fragment derived from the COOH-terminal domain of collagen XVIII, has been shown to have a therapeutic effect on tumor growth and metastasis in several animal models.[15–19] The dose, schedule and species specificity in the administration of endostatin seem to be critical factors that determine its *in vivo* effect.[18,19] We have previously demonstrated that recombinant mouse endostatin significantly inhibits mammary tumor progression in C3(1)/Tag transgenic mice.[20] This animal model recapitulates many of the histopathologic and molecular alterations leading to malignant transformation observed in human breast cancer.[21,22] Preinvasive lesions predictably develop in C3(1)/Tag mice at about 12 weeks of age and progress to invasive carcinoma over several weeks in 100% of female mice.[21,22]

We characterize here the angiogenic switch in C3(1)/Tag mammary gland adenocarcinomas and evaluate the antiangiogenic properties of P125A, a mutated form of human endostatin in which an alanine residue is substituted for proline at position 125. We demonstrate that P125A has a stronger *in vitro* inhibitory effect on

Grant sponsor: USMRMC; Grant number: DAMD 17-99-19564; Grant sponsor: the Gynecologic Group; Grant sponsor: NIH.

The first two authors contributed equally to this paper.

*Correspondence to: Laboratory of Cell Regulation and Carcinogenesis, National Cancer Institute, NIH, Building 41, Room C629, 41 Library Drive, Bethesda, MD 20892, USA. Fax: +301-496-8395.
E-mail: jegreen@nih.gov

Received 2 April 2002; Revised 5 June 2002; Accepted 6 June 2002

DOI 10.1002/ijc.10589

endothelial cell growth and *in vivo* tumor growth inhibition in a xenograft model than wild-type human endostatin.

Our results provide evidence that P125A endostatin inhibits the angiogenic switch and mammary tumor progression in a transgenic mammary cancer model and that human endostatin can be structurally modified to improve its efficacy.

MATERIAL AND METHODS

Mice

Heterozygous C3(1)/Tag transgenic females in the FVB/N background were bred as previously described.[21] The chronologic development of histopathologic lesions in C3(1)/Tag mice has been previously described.[21,22] Virgin 12-week-old FVB/N female mice were used as controls.

All studies were carried out in accordance with the guidelines of the Animal Care and Use Committee and the procedures outlined in the *Guide for the Care and Use of Laboratory Animals* (NIH publication No. 86-23, 1985).

Cloning, expression and purification of wild-type and mutant human endostatin (p125a)

The following primers were used to amplify human endostatin: GGGGAATTCCACAGCCACCGCGACTTCCAG (sense, 5′-3′) and GGGGCGG CCGCCTACTTGGAGGCAGTCATGAAGCT (antisense, 5′-3′). The PCR products were cloned into pPICZ-α vector and sequenced. After sequencing, clones containing wild-type endostatin and additional clones containing a spontaneous single-point mutation at a position 125 (P125A) were identified. The wild-type (P125) and the mutated endostatin (P125A) were subsequently cloned under the control of alcohol oxidase (AOX) promoter and expressed in *Pichia pastoris*.

Large-scale production of the modified endostatin was carried out in a 10 L bioreactor. Briefly, an overnight seed culture was inoculated into basal salt medium with glycerol as the carbon source until the wet weight of the cultures reached about 200 g/L. Glycerol feed was then restricted, and methanol was introduced as the sole carbon source. Expression was maintained for 100 hr under the following conditions. Feed rate of methanol medium was adjusted to about 75 ml/hr allowing slow growth (mut+ strain) during the induction phase. Temperature was maintained at 29°C, and the dissolved O_2 levels varied between 40 and 60%. The bioreactor (New Brunswick BioFlow 3000, Chicago, IL) was automatically controlled to regulate O_2 feed, agitation and temperature. Every 24 hr, a small aliquot of the culture was aspirated to determine cell density, viability and protein induction (SDS-PAGE 15% gel). After completion of the incubation, cultures were harvested and centrifuged at 15,000*g* to remove cells. Cell-free supernatant was then concentrated and desalted by buffer exchange using a Millipore (Bedford, MA) tangential flow membrane cassette (5,000 m.wt cutoff). Concentrated medium from the bioreactor was then aliquoted and stored at −70°C until purification.

Initial purification of the wild-type and mutated endostatin was accomplished by affinity chromatography on heparin linked to ceramic beads (Sigma, St. Louis, MO). Samples were loaded at a rate of 1.0 ml/min, and the matrix was washed with Tris-HCl buffer (0.01 M, pH 7.6) to remove unbound proteins. Absorbance at 280 nm was continuously monitored. Bound proteins were eluted by a salt gradient (0–1.0 M NaCl). Typically, endostatin is eluted from the column at 300 mM NaCl. Eluted proteins were then further purified by a Mono-S column using FPLC. Loading and washing were carried out in 0.01 M Tris-HCl, pH 7.6. Bound proteins were eluted by a NaCl gradient (0–1.0 M). Purified proteins were filter sterilized and stored at −70°C. Protein purity was confirmed by gel analysis.

Endothelial cell proliferation assay

Bovine adrenal gland capillary endothelial cells (BCE) were obtained from Clonetics (San Diego, CA). The endothelial cell proliferation assay was performed as previously described[1] to compare the functional activity between wild-type and P125A (mutated) endostatin. Experiments were performed in triplicate.

Tumor growth inhibition in xenograft model

A xenograft model for ovarian carcinoma was used to compare the *in vivo* efficacy of both endostatin proteins. For this purpose, wild-type and P125A-endostatin diluted in alginic acid were dropped into 0.1 M $CaCl_2$ solution to encapsulate endostatin in alginate beads. This method was used to allow a slow release of endostatin and to prolong its effect *in vivo*. Ovarian carcinoma cells (10^6 MA148) were injected subcutaneously in the flank of athymic mice ($n = 5$). Seven days after cell injection, mice were randomly distributed and treated with the wild-type and P125A-endostatin (dose 20 mg/kg) encapsulated in alginate beads by subcutaneous injections, once a week. Tumor growth was measured by calipers.

Treatment of C3(1)/Tag transgenic animals

Female C3(1)/Tag transgenic mice ($n = 8$) were treated at 12 weeks of age by daily intraperitoneal injection of P125A human endostatin (20 mg/kg weight). Control animals ($n = 10$) received PBS over the same period of time.

Body weight (measured weekly) and tumor volume (evaluated twice a week) were measured in transgenic animals after the onset of tumor formation. Mammary tumor size was measured with a caliper, and tumor volume was calculated using the formula: largest diameter × (the smallest diameter)^2 × 0.4.[23] Three animals of each group were euthanized at 15 weeks of age upon termination of the treatment. The remaining animals were followed after cessation of therapy up to 25 weeks of age. Animals were euthanized when tumors reached 1.5 cm^3 or animals appeared sickly.

Whole-mount preparations and histology

Transgenic and control animals were euthanized by CO_2 asphyxiation. Mammary gland whole-mount preparations were spread onto a slide and fixed in 70% ethanol for 30 min. After rehydratation in distilled water, tissues were stained by immersion in a solution consisting of 0.2% carmine and 0.5% aluminium potassium sulfate (in H_2O) overnight. The sections were dehydrated through a progressive increase in ethanol concentration to 100%, cleared in xylene and mounted in Permount (Fisher Scientific, Fair Lawn, NJ).

For histology, mammary glands were immediately fixed in fresh 4% paraformaldehyde overnight, embedded in paraffin, cut (4 μm in thickness) and stained with hematoxylin and eosin. Histopathologic lesions were evaluated following the criteria previously described.[22] For CD-31 immunostaining, the dissected tissues were immediately immersed in O.C.T. (Tissue-Tek, Sakura, Japan) and frozen on a mixture of dry ice and isopentane (Fluka, Milwaukee, WI).

Immunohistochemistry and TUNEL analysis

Paraffin sections were rehydrated through decreasing concentrations of ethanol. The antigen retrieval technique was used for all immunohistochemistry. Slides were immersed in citric acid (pH 6) and heated in a microwave oven twice for 5 min. Mouse monoclonal (Neomarkers, Freemont, CA) and rabbit polyclonal (Santa Cruz Biotechnology, Santa Cruz, CA) anti-VEGF antibodies were used at a 1:200 dilution. Rabbit polyclonal antibodies, anti-Flt-1 and anti-Flk-1 (Santa Cruz Biotechnology), were used at a 1:100 dilution, and mouse monoclonal anti-Ki-67 antibody (Dako, Glostrup, Denmark) was diluted 1:10,000. Cryostat sections were stained with anti-CD-31 antibody (PharMingen, San Diego, CA) at a 1:100 dilution. The avidin-biotin complex method (Vectastatin ABC Elite kit, Vector, Burlingame, CA) was used to visualize the bound antibodies. Omission of the primary antibody and replacement of the primary antibody by nonimmune IgG were used as a negative control for immunohistochemistry.

Apoptotic cells were identified using the TUNEL *in situ* end-labeling technique (Apoptag; Oncor, Gaithersburgh, MD). Labeled

cells for Ki-67 and for TUNEL staining were quantified using a Zeiss Axioplan microscope and Optimas software (version 6.51.199, Media Cybernetics). At least 1,000 cells/section of mammary gland were counted in randomly selected fields. Final data were expressed as a percentage of positively stained epithelial cells with respect to the total number of epithelial cells examined.

Protein extraction and ELISA analysis

Tissues were homogenized in RIPA buffer containing proteinase inhibitors (1 × PBS, 1% NP40, 0.5% sodium deoxycholate, 0.1% SDS, 10 μg/mL phenylmethylsulfonyl fluoride [PMSF]), maintained at 4°C for 45 min and cleared by centrifugation. Protein concentration was measured with the Bio-Rad (Hercules, CA) Protein Assay according to the manufacturer's instructions.

Murine VEGF concentrations in mammary gland and tumor lysates were measured using a quantitative sandwich enzyme immunoassay (Quantikine; R&D Systems, Minneapolis, MN) according to the manufacturer's instructions. Briefly, each sample was incubated in duplicate wells of a microplate coated with anti-VEGF polyclonal antibody. Unbound substances were washed from the plate, and peroxidase-linked anti-VEGF polyclonal antibody was added. After incubation and further washing, H_2O_2 and tetramethylbenzidine were added. The reaction was stopped with HCl, and optical densities were read at 450 nm (correction wavelength, 540 nm) on a Multiskan plate reader (Titertek, Huntsville, AL). VEGF concentrations were calculated by comparison with a standard curve generated using a 4-parameter logistic curve-fit and on-board software. VEGF concentrations were normalized to total protein concentrations.

RNA extraction and RT-PCR for VEGF isoforms

Total RNA was extracted from frozen tissues using the RNeasy mini kit (Qiagen, Valencia, CA) according to the manufacturer's protocol. The quality of the RNA was assessed by running aliquots on formaldehyde-agarose gels. Two micrograms of total RNA were incubated with DNAseI (Life Technologies, Gaithersburg, MD) for 20 min. Reverse transcription was performed with the SuperScript II kit (Life Technologies), according to the manufacturer's protocol. The cDNA was amplified with Taq polymerase (Life Technologies) using a PTC-100 M.J. Research thermocycler (Watertown, MA). The sequence of the primers for the detection of $VEGF_{120}$, $VEGF_{164}$ and $VEGF_{188}$ and the conditions used for the PCR were adjusted from those previously described.[24] The following primer sequences were used: 5′-ctg ctc tct tgg gtg cac tg-3′ (forward primer, located in exon 1) and 5′-cac cgc ctt ggc ttg tca ca-3′ (reverse primer, located in exon 8). The conditions used for PCR were as follows: 40 cycles at 94°C for 1 min, 56°C for 2 min and 72°C for 3 min. Negative controls included the omission of the reverse-transcriptase.

Quantitative real time RT-PCR analysis

For cDNA preparation, 1 μg total RNA was treated with DNase I (Ambion, Austin, TX) to remove any contaminating genomic DNA. The DNased RNA (100 ng) was then converted into cDNA by using murine leukemia virus reverse transcriptase (Life Technologies).

PCR primers targeting murine VEGF, Flt-1, Flk-1, angiopoietin-2, Tie-1, platelet-endothelial cell adhesion molecule (PECAM; CD-31), VE-cadherin (cadherin-5) and cyclophilin were designed by using Primer Express software (Applied BioSystems, Foster City, CA) and are listed in Table I (5′ to 3′).The specificity of each primer to the sequence of choice was confirmed using the NCBI Blast module (http://www.ncbi.nlm.nih.gov/). All the primers were synthesized by Genemed Synthesis (South San Francisco, CA). To verify each primer set, amplicons generated from the PCR reaction were analyzed for their respective specific melting point temperatures using the first derivative primer melting curve software supplied by Applied BioSystems. Quantitative analysis of gene expression was performed using the SYBR Green master mix kit (Applied BioSystems) and the ABI Prism 7700 Sequence Detection System (TaqMan). SYBR Green dye intercalation into the minor groove of double-stranded DNA reaches an emission maximum at 530 nm. The level of gene expression was calculated after normalizing to the cyclophilin level in each sample and is presented as relative units. Samples were analyzed in triplicate to assess the accuracy of the measurements.

Statistical analysis

The 2-sided Student's *t*-test was used to evaluate whether significant differences existed between the mean values of the groups analyzed. The Mann-Whitney test was used to analyze tumor volumes. The log rank test was used to determine differences in survival curves.

RESULTS

Wild-type endostatin and mutant P125A endostatin were expressed in soluble form in *Pichia pastoris*. Both proteins were purified to near homogeneity. The wild-type and P125A-endostatin contain 183 amino acid residues. The expected molecular weight of wild-type endostatin is 20,095 and that of the P125A mutant is 20,068. MacVector protein analysis software was used to determine the expected molecular weight from the primary sequence. P125A substitution does alter the pI of the protein (pI 9.91). In SDS-PAGE, both wild-type and P125A-endostatin migrated to a relative position corresponding to 21 kDa under nonreducing conditions (Fig. 1*a*).

Biologic activities of wild-type (P125) and mutant (P125A) endostatin

Inhibition of endothelial cell proliferation. To evaluate whether the P125A mutation affected the biologic activity of endostatin, an inhibition assay of endothelial cell proliferation was performed. Serum-starved endothelial cells were stimulated with human basic fibroblast growth factor (FGF). Growth factor-induced endothelial cell proliferation was inhibited by both wild-type and mutant endostatin. Dose-response curves demonstrated a better inhibitory effect of P125A-endostatin compared with the wild-type protein (Fig. 1*b*). A concentration of 1 μg/ml wild-type endostatin was required to inhibit proliferation by 8.6%, whereas P125A-endostatin produced a similar level of inhibition at a concentration of 0.33 μg/ml. At a concentration of 3 μg/ml, wild-type endostatin inhibited proliferation by 22.2%, and an equivalent inhibition was

TABLE I – TaqMan PRIMER SEQUENCES[1]

Gene	Forward	Reverse
Ang-2	1478--TTAGCACAAAGGATTCGGACAAT--1500	1598--TTTTGTGGGTAGTACTGTCCATTCA--1574
Flt-1	2421--GAGGAGGATGAGGGTGTCTATAGGT--2445	2536--GTGATCAGCTCCAGGTTTGACTT--2514
FLK-1	4570--GCCCTGCTGTGGTCTCACTAC--4590	4632--CAAAGCATTGCCCATTCGAT--4666
Tie-1	742--CAAGGTCACACACACGGTGAA--762	863--GCCAGTCTAGGGTATTGAAGTAGGA--839
PECAM	1652--GAGCCCAATCACGTTTCAGTTT--1673	1769--TCCTTCCTGCTTCTTGCTAGCT--1748
VE-cadherin	1853--TCCTCTGCATCCTCACTATCACA--1875	1974--GTAAGTGACCAACTGCTCGTGAAT--1951
VEGF	805--GGAGATCCTTCGAGGAGCACTT--826	933--GGCGATTTAGCAGCAGATATAAGAA--909

[1]Ang-2, Angiopoietin-2; Flt-1, Fms-like tyrosine kinase; KDR, PECAM, platelet-endothelial cell adhesion molecule; VE, vascular endothelial; VEGF, vascular endothelial growth factor.

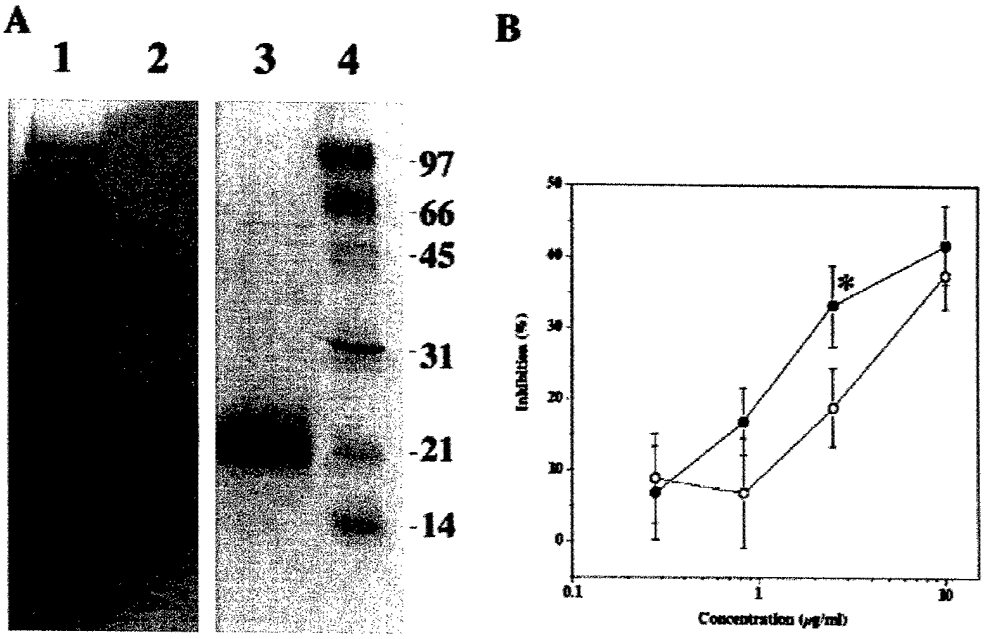

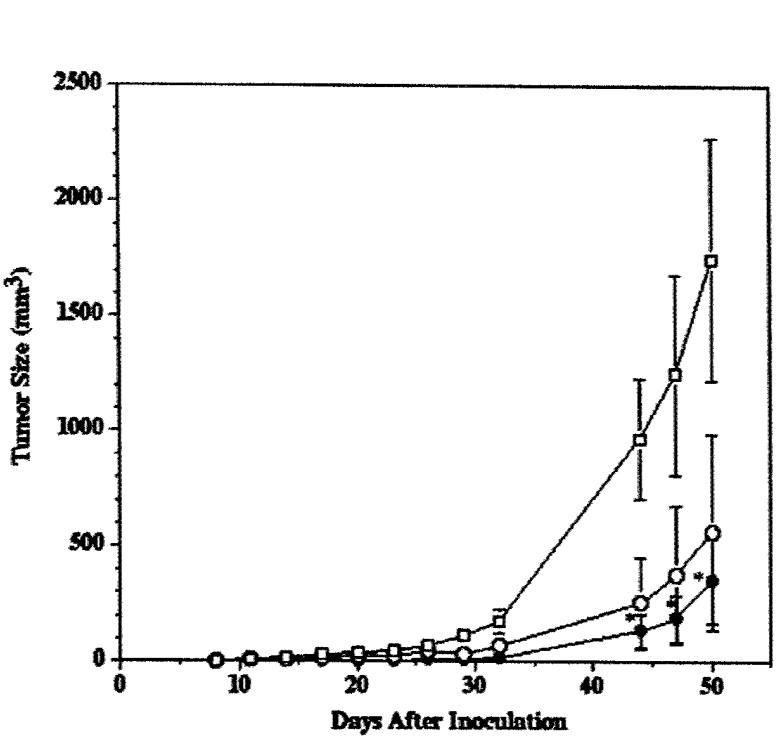

FIGURE 1 – Comparison between wild-type endostatin (P125) and P125A mutated human endostatin. (*a*) SDS-PAGE (15%) for wild-type (lane 2) and P125A-endostatin (lane 3) shows a single band of 21 kDa under nonreducing conditions for both types of endostatin. Protein markers (lanes 1 and 4). (*b*) Inhibition of endothelial cell proliferation. Growth factor-induced (FGF) endothelial cell proliferation is inhibited by both wild-type and mutant endostatin. However, P125A-endostatin has a significantly increased inhibitory effect on BCE cell growth compared with wild-type endostatin ($p < 0.05$). Open circles, wild-type endostatin; closed circles, P125A-endostatin. The experiments were done in triplicate. (*c*) Mean tumor growth of MA148 cells in nude mice treated with wild-type endostatin, P125A-endostatin or PBS. Tumor growth is significantly inhibited by both wild-type and P125A-endostatin, compared with PBS-treated (control) mice. No statistical differences were found between wild-type and P125A-endostatin groups. Open circles, wild-type endostatin; closed circles, P125A-endostatin; squares, PBS. Bars indicate SEM. Five animals per group were used.

observed by P125A-endostatin at a concentration of 1.23 μg/ml. Based on these data, P125A endostatin appears to be about 2- to 3-fold more potent in inhibiting endothelial cell proliferation compared with the wild-type protein. Experiments were performed in triplicate.

Inhibition of tumor growth in a xenograft model of ovarian cancer. The ability of wild-type and P125A-endostatin to inhibit tumor growth *in vivo* was assessed using the MA148 ovarian carcinoma model xenografted into nude mice. Tumors in the control mice grew exponentially, reaching a mean volume of 1,747 mm^3 on day 50. Animals treated with wild-type or P125A-endostatin exhibited a significant reduction in tumor growth ($p < 0.05$) compared with untreated animals. On day 50, mice treated with wild-type endostatin had a mean tumor volume of 564 $mm,^3$, an inhibition of 67.8% compared with controls. Throughout the observation period, mice treated with P125A-endostatin exhibited the slowest tumor growth. At the termination of the experiment on day 50, P125A-endostatin-treated mice exhibited a mean tumor volume of 351 $mm,^3$, a reduction of 80% in tumor volume (statistically significant, $p < 0.05$) compared with controls, although this

was not statistically different from mice treated with the wild-type endostatin (Fig. 1*c*). Five animals per group were used.

The angiogenic switch in C3(1)/Tag mammary gland tumors

To determine alterations in the expression of several major regulators of angiogenesis during mammary tumor progression in C3(1)/Tag transgenic mice, we studied the expression patterns of the angiogenic factors VEGF and angiopoietin-2.

Immunohistochemical analyses of VEGF receptors Flk-1 and Flt-1, and the endothelial marker CD-31 (PECAM) were also examined during tumor progression. As previously described,[21,22] C3(1)/Tag transgenic females develop preinvasive lesions in the mammary glands (mammary intraepithelial neoplasia [MIN]) at about 12 weeks of age, followed by the development of invasive carcinomas at about 16 weeks of age. Total VEGF protein levels were dramatically increased ($p < 0.001$) during the transition from preinvasive mammary intraepithelial neoplasia to invasive carcinoma, as evaluated by ELISA (Fig. 2*a*).Twelve-week-old FVB/N nontransgenic females and 12- or 15-week-old transgenic C3(1)/Tag females exhibited similar levels of VEGF protein (less than 100 pg/mg total protein). During the transition from preneoplastic lesions to invasive tumors in transgenic animals, an 8-fold increase in VEGF levels was found (Fig. 2*a*). Three mice per group were used for these experiments.

Immunohistochemical analysis revealed relatively weak VEGF staining in the epithelial cells and in most endothelial cells of the blood vessels in the mammary glands of 12-week-old nontransgenic FVB/N. MIN lesions in 12-week-old C3(1)/Tag mice also stained positively for VEGF (Fig. 2*b*). However, tumors from 18–20-week-old animals stained strongly positive for VEGF (Fig. 2*c*). Both the tumor cells and the endothelial cells stained strongly positive. The substitution of nonimmune serum for the primary antibody produced no staining (result not shown). The 2 different antibodies used for VEGF staining gave identical staining patterns.

Evaluation of the VEGF isoforms by RT-PCR revealed that normal mammary glands and mammary glands with preinvasive lesions expressed the 3 VEGF isoforms, $VEGF_{120}$, $VEGF_{164}$ and $VEGF_{188}$. Tumors, however, expressed $VEGF_{120}$ and $VEGF_{164}$ but not $VEGF_{188}$ (Fig. 3).

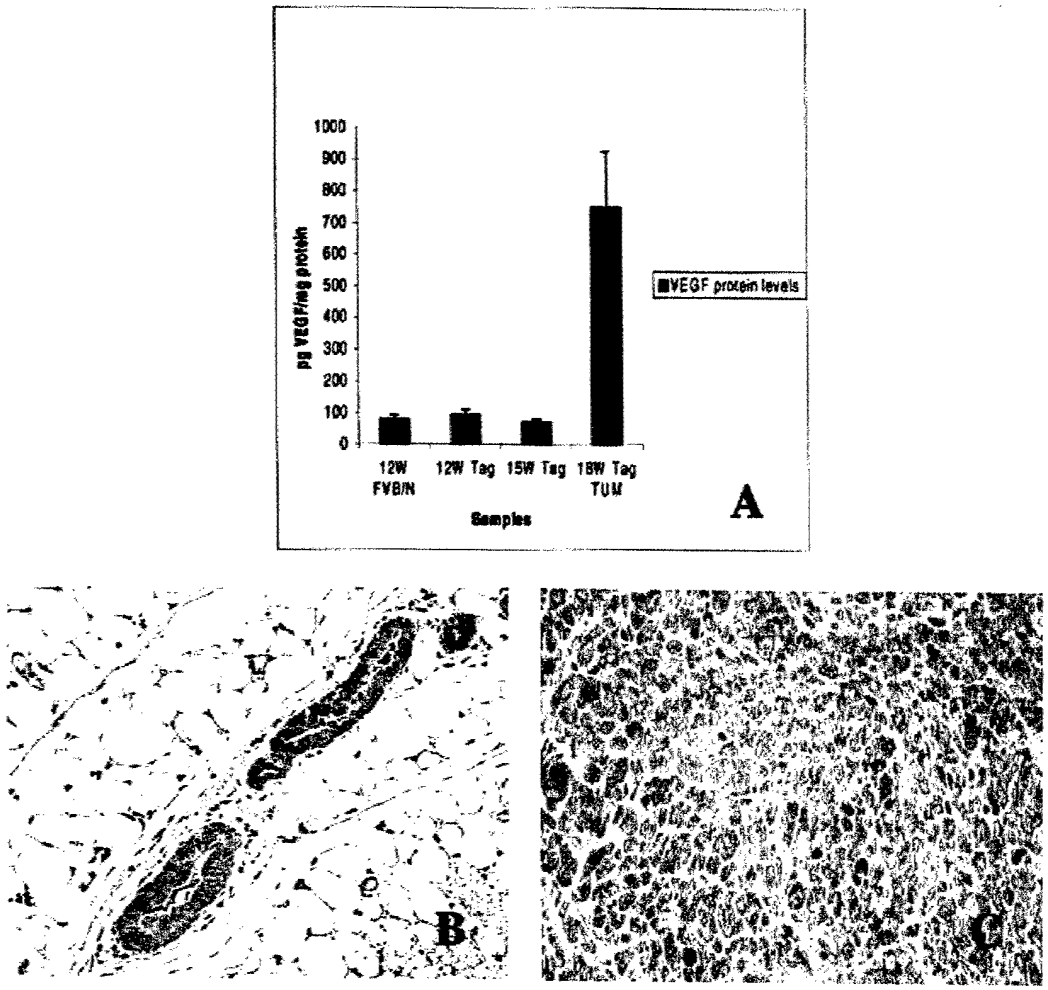

FIGURE 2 – Vascular endothelial growth factor (VEGF) protein expression in mammary glands and tumors from C3(1)/Tag females or control animals. (*a*) ELISA analysis. Mammary glands from control FVB/N females have a mean value of 82 ± 12.1 pg/mg total protein at 12 weeks of age. Mammary glands from 12- and 15-week-old C3(1)/Tag females with preinvasive lesions have similar values (93 ± 15 and 70 ± 8.9 pg/mg total protein, respectively). However, tumors from 18-week-old C3(1)Tag females exhibit an 8-fold increase ($p < 0.001$) in VEGF protein values. Three mice per group were used in these experiments. (*b*) Immunohistochemical analysis of mammary glands of 12-week-old C3(1)/Tag females with preinvasive lesions shows VEGF staining in the epithelium of the ducts and end buds. Normal mammary glands of control animals at the same age exhibit the same pattern of staining. (*c*) Mammary tumor of a 20-week-old C3(1)/Tag mouse with stronger staining for VEGF than epithelial cells in preinvasive lesions. (Magnification ×400.)

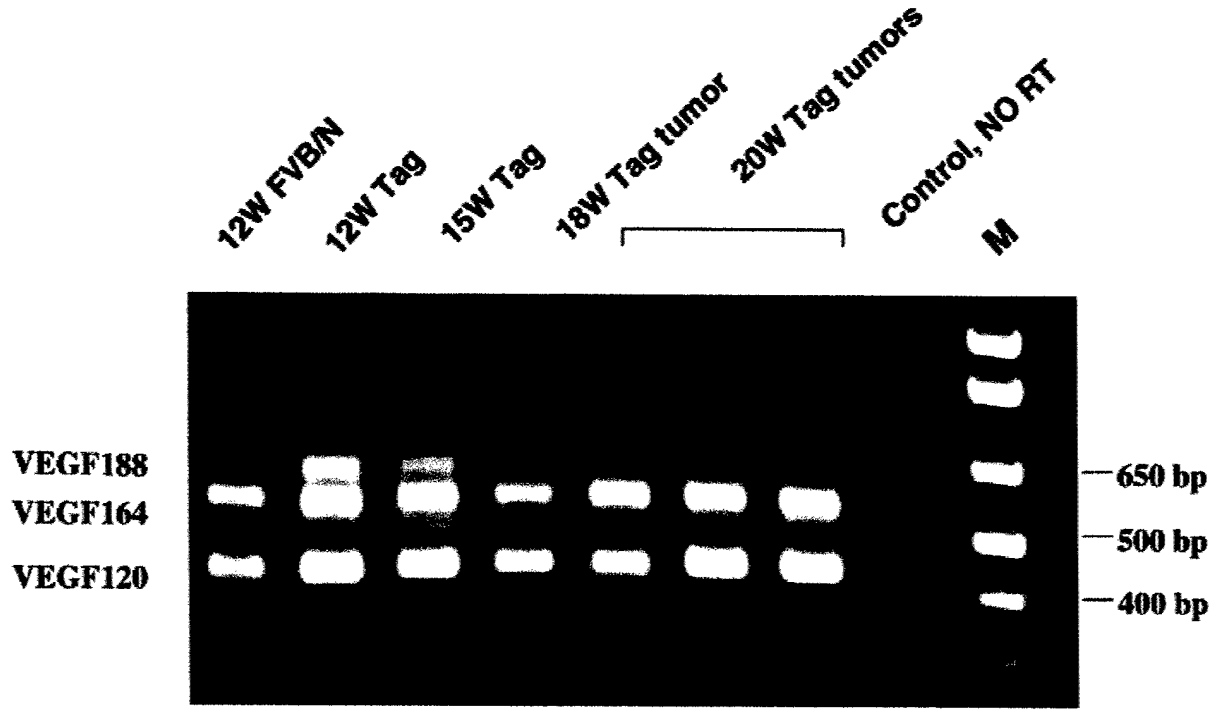

FIGURE 3 – RT-PCR for vascular endothelial growth factor (VEGF) isoforms in mammary glands and tumors from C3(1)/Tag females or control animals. Mammary glands from transgenic animals with preneoplastic lesions (12- and 15-week-old) and from FVB/N control mice express the 3 VEGF isoforms. The expected size for $VEGF_{120}$ (431 bp), $VEGF_{164}$ (563 bp) and $VEGF_{188}$ (635 bp) bands are found in these animals. Tumors from 18- or 20-week-old females only express $VEGF_{120}$ and $VEGF_{164}$, but not $VEGF_{188}$.

Immunohistochemistry for the VEGF-receptor Flk-1 revealed that mammary epithelium from 12-week-old control FVB/N mice exhibited barely detectable staining in the epithelium (Fig. 4*a*), whereas the endothelial cells of some blood vessels stained positively for Flk-1. In mammary glands from 12-week-old transgenic animals, Flk-1 staining was detected in the cellular apex and basal compartment of the premalignant epithelial cells (Fig. 4*b,c*). Invasive carcinomas were characterized by strong Flk-1 staining in both tumor (Fig. 4*d*) and endothelial cells. The VEGF receptor Flt-1, however, was undetectable by immunohistochemistry in epithelial and endothelial cells, in both 12-week-old FVB/N control mammary glands and MIN lesions in C3(1)/Tag mammary glands (Fig. 4*e*). However, both tumor cells and blood vessels stained positively for Flt-1 in invasive carcinomas (Fig. 4*f*).

The angiogenic switch in C3(1)/Tag mammary tumors was also characterized by an increase in angiopoietin-2 mRNA levels during the transition from MIN to adenocarcinoma. Tumors from 18-week-old transgenic animals exhibited a 2.5-fold increase ($p < 0.01$) in angiopoietin-2 mRNA levels compared with that observed in transgenic mice with preinvasive lesions or nontransgenic mice (data not shown).

Tumor vascularization was studied using CD-31 immunostaining. In mammary glands of C3(1)/Tag mice with preinvasive lesions, endothelial cells of the capillary network surrounding the adipocytes (Fig. 5*a,b*) and larger vessels within the mammary glands stained positively for CD-31. No staining was observed in the epithelial cells, as expected. Normal mammary glands from nontransgenic control mice exhibited a similar staining pattern for CD-31 (data not shown). No CD-31 staining was observed in more advanced lesions, such as high-grade MIN and early invasive carcinomas (microscopic), which were found in most animals after 15 weeks of age, indicating that blood vessel recruitment had not yet occurred (Fig. 5*c*). Intratumoral vessels were observed by CD-31 staining when tumors reached an approximate volume of 1 mm^3 in size (Fig. 5*d*). Larger palpable tumors were highly vascularized (Fig. 5*e,f*).

P125A-endostatin inhibits mammary adenocarcinoma development and growth, decreases tumor number and prolongs the survival of C3(1)/Tag mice

To evaluate whether P125A-endostatin is able to inhibit tumor angiogenesis in C3(1)/Tag mice, we treated 12-week-old animals ($n = 8$) with the highly active form of endostatin, P125A, daily for 3 weeks. The administration of P125A-endostatin for this 3-week period significantly delayed tumor onset ($p = 0.011$, Fig. 6*a*).In the control group, the earliest tumor onset occurred at 16 weeks of age, whereas in the endostatin-treated group, tumor onset occurred at 18 weeks of age. By this age all the animals in the control group had developed tumors, whereas only 1 endostatin-treated animal had palpable tumors. However, despite the delay in tumor appearance, 100% of the treated mice developed palpable tumors by 21 weeks of age. Three mice per group were used in these experiments.

Tumor burden in the group of animals treated with endostatin was very significantly decreased, compared with controls, from week 16 to week 21 ($p < 0.01$, Fig. 6*b*). In the control group, the mean cumulative tumor burden was $1,481 \pm 510$ mm^3 at 19 weeks of age (1 month after the cessation of treatment). However, in the group of animals treated with endostatin, the mean value was 70 ± 32 mm^3 at the same age (an approximate 20-fold decrease). At 22 weeks of age (the end point of survival for the control animals), the mean cumulative tumor burden for control animals was $2,420 \pm 820$ $mm,^3$, whereas the group of animals treated with endostatin exhibited an approximately 2-fold decrease, with a mean value of $1,230 \pm 331$ mm^3 ($p < 0.05$).

A significant decrease in the mean number of tumors per animal (MNT) was observed in mice treated with endostatin compared with controls, from 16 weeks to 19 weeks of age. At 18 weeks of age, the MNT for controls was 1.2 ± 0.3, whereas for treated

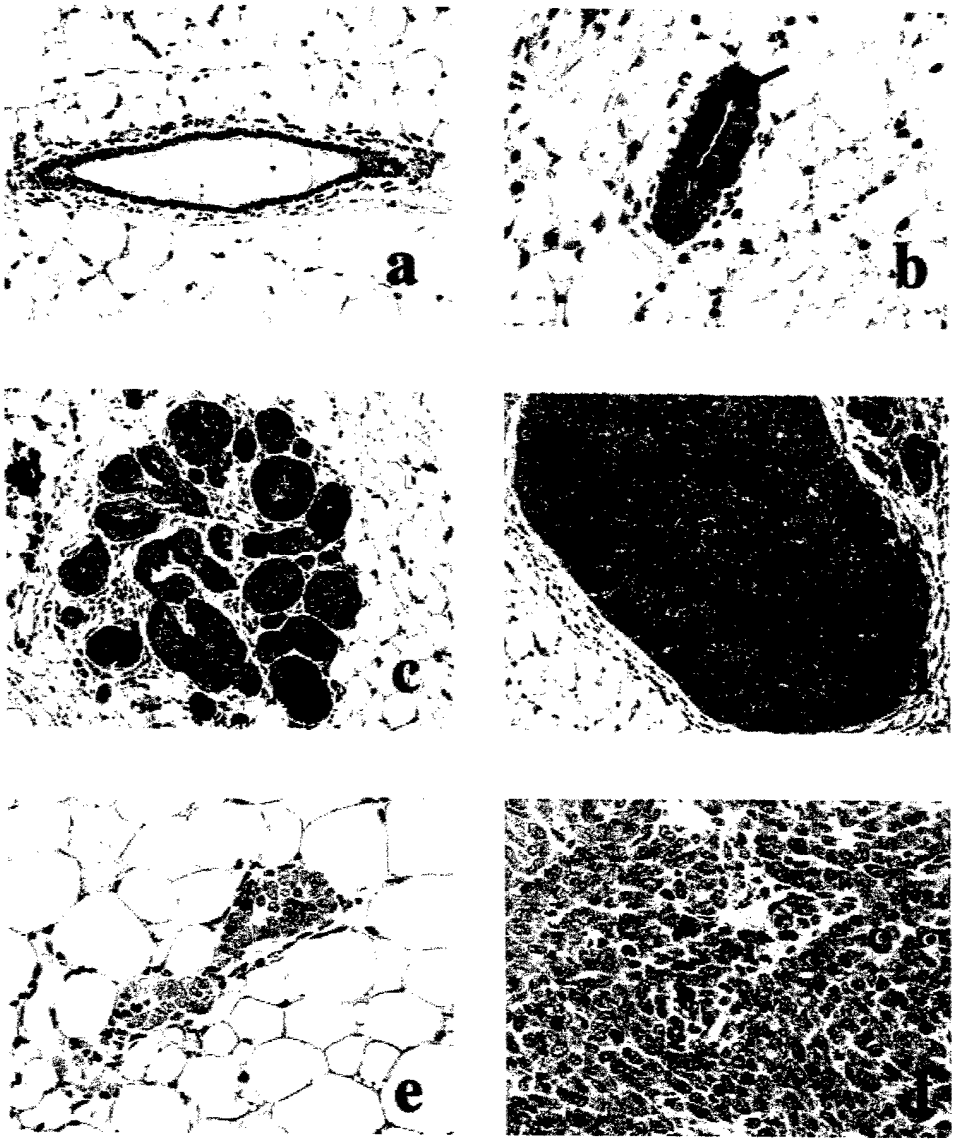

FIGURE 4 – Immunohistochemical analysis of VEGF receptors (Flk-1 and Flt-1) in mammary glands and tumors from C3(1)/Tag females or control animals. (*a*) In control animals, no staining for Flk-1 is observed in the epithelium, and faint staining is seen in blood vessels. (*b*) Flk-1 stains positively in MIN lesions in 12-week-old transgenic animals, mainly in the apex (arrow) and basal zone of the epithelium. (*c*) An increase in Flk-1 immunostaining is observed in more advanced lesions. (*d*) Strong Flk-1 staining is observed in tumors. (*e*) Lack of Flt-1 immunostaining in a preinvasive mammary lesion from a 12-week-old C3(1)/Tag mouse. The same result is observed in normal mammary glands from control females (not shown). (*f*) Tumor cells from C3(1)/Tag animals exhibit strong staining for Flt-1. (Magnification, a, c, d, ×200; b, e, f, ×400.)

animals it was significantly lower, 0.2 ± 0.2 ($p < 0.05$). At 19 weeks of age, the MNT remained significantly different ($p < 0.05$): 1.8 ± 0.2 for controls, and 0.8 ± 0.3 for treated animals. However, due to the prolonged survival of endostatin-treated animals after this age and the lack of continued treatment with endostatin, the MNT became similar for both groups by 20 weeks of age (2.2 ± 0.2 for controls and 2.6 ± 0.6 for treated mice).

Survival curves demonstrated that endostatin-treated animals lived significantly longer than PBS-treated mice (3–4-week increase in survival, $p = 0.0086$, Fig. 6*c*). No signs of toxicity or weight loss were observed as a result of the endostatin treatment.

P125A-endostatin downregulates the expression of angiogenic factors in preinvasive mammary glands but does not inhibit MIN formation

To determine the preventive effect of endostatin on the angiogenic switch and tumor development in C3(1)/Tag mice, analyses were performed on mammary glands at 15 weeks of age (after cessation of treatment) to identify changes in the histopathology, rates of proliferation and apoptosis, as well as mRNA levels of a battery of angiogenic factors.

Histopathologic evaluation showed no remarkable differences in lesion formation at 15 weeks of age between the control and endostatin-treated animals. Mammary gland whole mounts and histologic analysis revealed that both groups of animals had the typical pathologic lesions found in C3(1)/Tag mice at this age, with multiple MIN lesions and some high-grade MIN. Control mice had 22.1 ± 7 MIN lesions per mammary gland, whereas P125A-endostatin-treated mice had 27.2 ± 8.2 MIN lesions, which was not statistically different. Cellular proliferation, as evaluated by Ki-67 staining, was observed only in epithelial cells in both treated and untreated mice. No endothelial proliferation was ever observed at this stage of tumor progression. Quantification of Ki-67-positive cells was similar between both groups of mice (82 ± 12.7 in controls and 79 ± 10.9 in treated mice). Similarly, TUNEL staining was positive for apoptosis only in epithelial cells, but not in endothelial cells, in both treated and untreated animals. The apoptotic index of epithelial cells was similar in controls and endostatin-treated mice (12.3 ± 7.2 in controls and 12.1 ± 9.7 in treated mice).

Despite similarities in histopathology, differences in mRNA levels of angiogenic factors were found between control animals and animals treated with endostatin as measured by real-time RT-PCR. VEGF mRNA levels were decreased about 50% ($p < 0.01$) in mammary glands from treated animals, compared with controls. Total VEGF protein levels were also measured by

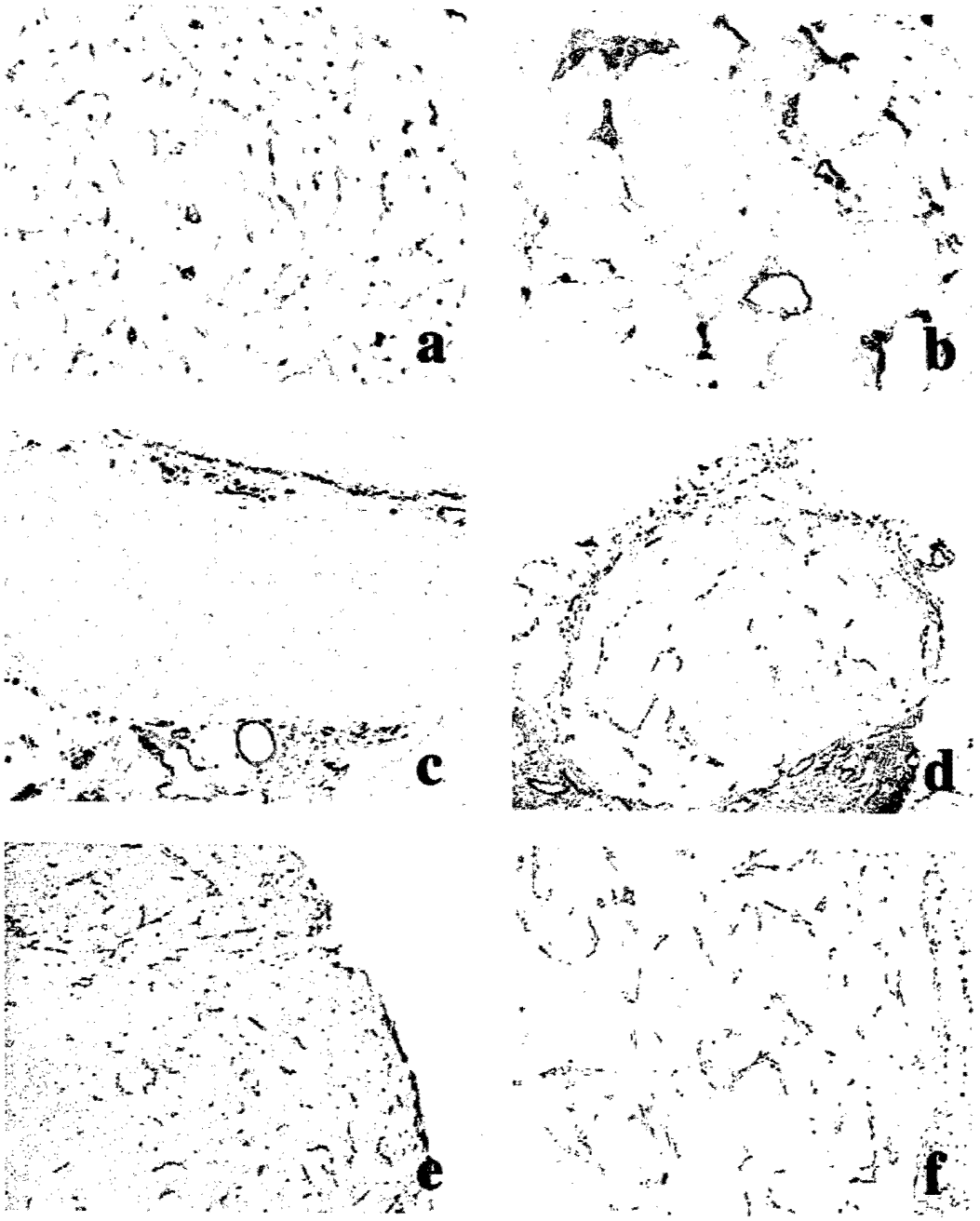

FIGURE 5 – CD-31 (PECAM) immunostaining in mammary glands and tumors from C3(1)/Tag females. (*a*) At 12 weeks of age, numerous blood vessels positive for CD-31 can be observed surrounding the adipocytes or the premalignant epithelium, but not inside the epithelium. (*b*) MIN lesion in a 15-week-old female, showing similar CD-31 staining to that seen at 12 weeks of age. (*c*) High-grade MIN in a 15-week-old mouse. No blood vessels invading the MIN lesion are apparent. (*d*) In small tumors (approximately 1 mm^3 in size,), intratumoral blood vessel invasion is observed. (*e*) Larger tumors are highly vascularized. (*f*) Another tumor with a more glandular histologic pattern, also exhibiting abundant vascularization. (Magnification, a, c, ×200; b, ×400; d–f, ×40.)

ELISA, in 15-week-old PBS- or P125A-treated mice. Control animals had an average value (± SEM) of 71.3 ± 7.2 pg VEGF/mg total protein. Mice treated with P125A-endostatin exhibited significantly lower values compared with controls (48.1 ± 9, $p < 0.05$; approximate 32% decrease). Angiopoietin-2 mRNA levels were also significantly decreased, by 44% ($p < 0.01$). Endostatin treatment resulted in a significant decrease in mRNA levels of VEGF receptors Flk-1 (33%; $p < 0.05$) and Flt-1 (27%; $p < 0.05$). Tie-1 and cadherin-5 mRNA levels were decreased by 31% ($p < 0.05$) and 19% ($p = 0.1$), respectively, in the mice treated with endostatin, compared with the animals treated with PBS. PECAM (CD-31) mRNA levels were decreased by 33% ($p < 0.05$).

DISCUSSION

Previous studies have shown that the administration of murine endostatin inhibits tumor growth and metastasis in mouse models.[15–19] However, in our experience, the efficacy of human endostatin in mouse models has been problematic. We observed no

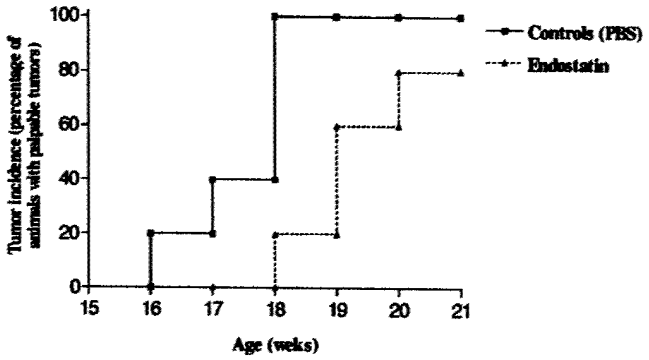

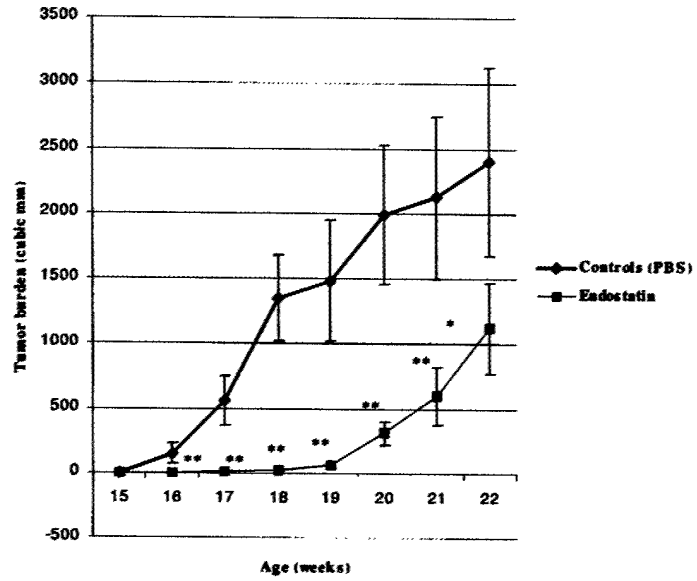

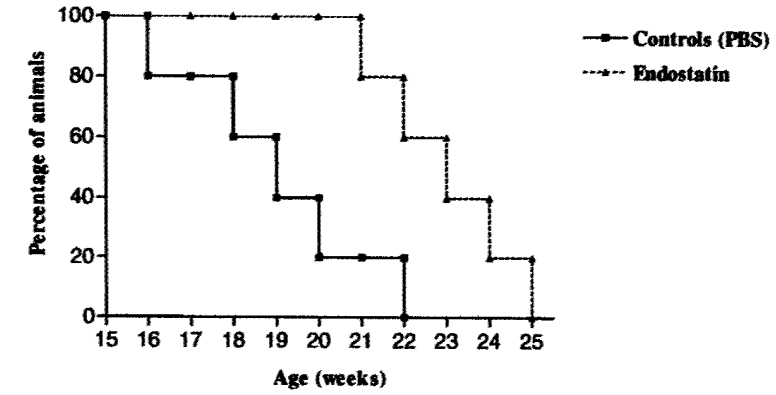

FIGURE 6 – Effect of P125A-endostatin on mammary tumor growth and survival. (*a*) Comparison of tumor incidence between endostatin-treated and untreated females. There is a significant delay in tumor incidence between the groups ($p = 0.011$). (*b*) Tumor burden in endostatin-treated animals was very significantly decreased from week 16 to week 21 ($p < 0.01$), compared with control mice (**, $p < 0.01$; *, $p < 0.05$. (*c*) Survival curves. The increase in survival in the P125A-endostatin-treated mice is statistically significant ($p = 0.0086$). Eight C3(1)/Tag transgenic mice were treated with P125A-endostatin, and 10 mice were injected with PBS (controls).

effect on mammary tumor development and progression when C3(1)/Tag mice were treated with human endostatin (Calvo and Green, unpublished observations). In the present study we have characterized a mutated form of human endostatin that exhibits enhanced activity compared with the wild type.

The spontaneous P125A mutation that occurred during the cloning process is located immediately before the NGR, a endothelial cell homing motif for endostatin.[32] Through the use of phage display libraries, this motif was shown to contain homing sequences for tumor vasculature.[32] Our characterization of this mutated form of human endostatin (P125A) demonstrated increased inhibition of endothelial cell proliferation and *in vivo* xenograft tumor growth compared with wild-type endostatain.

Due to this enhanced activity, we decided to investigate further the inhibitory effects of P125A-endostatin on C3(1)/Tag mammary gland lesion progression. We have demonstrated that a limited course of P125A-endostatin retards tumor onset and decreases tumor growth and multiplicity. P125A-endostatin appears to inhibit the angiogenic switch and tumor growth by downregulating the expression of a variety of proangiogenic factors at the prein-

vasive to invasive transition stage. The therapeutic efficacy of P125A-endostatin on mammary tumor development in transgenic mice is similar to that for recombinant murine endostatin, on which we have previously reported.[20]

Some studies have suggested that the main effect of endostatin might be related to the prevention of primary tumor development as well as metastatic progression, rather than regression of large established tumors.[16,17] Bergers *et al.*[18] demonstrated in the RIP1-Tag transgenic model of pancreatic islet cell carcinoma that recombinant endostatin is highly effective in inhibiting tumor progression from hyperplastic lesions to invasive carcinomas but that endostatin has much less effect in treating large, established tumors. Moreover, in other mouse models in which transplantable tumor cell lines have been used, the strongest therapeutic effect has been described when endostatin was given shortly after the implantation of tumor cells.[25] Similar preventive effects have been observed with angiostatin.[26]

C3(1)/Tag females develop preinvasive alterations in the mammary glands at about 12 weeks of age and invasive carcinomas after about 16 weeks of age.[21,22] We have shown in the present study that the transition from preinvasive lesions to invasive carcinomas is accompanied by an increase in expression of the proangiogenic factors VEGF and angiopoietin-2, as well as VEGF receptors Flk-1 and Flt-1, thus establishing a mechanism for the angiogenic switch in this tumor model. Even though we have observed VEGF expression in epithelial and endothelial cells in the virgin normal mammary gland, the expression of Flk-1 and Flt-1 is very low and is restricted to endothelial cells. Flk-1 is first expressed in epithelial cells in preinvasive lesions, whereas Flt-1 is undetectable at this stage. In contrast, both epithelial and endothelial cells of tumors express high levels of Flk-1 and Flt-1.

These results suggest that angiogenesis in this model of mammary tumor progression is activated not only by an increase in VEGF but also by an increase in the expression of VEGF receptors. Since we have demonstrated that VEGF receptors are localized on the tumor epithelial cells, our results suggest that VEGF may be acting as an autocrine factor on tumor cells in addition to its paracrine effects on endothelial cell growth. Other studies have also suggested that VEGF may have autocrine effects. For instance, in the rat hormone-induced mammary tumor model, Xie *et al.*[9] showed coexpression of VEGF and its receptors in tumor cells. Enhanced expression and activation of Flk-1 has recently been reported in human breast carcinoma as well, in which an increase in VEGF levels has been also described.[27]

Although the overall amount of VEGF in C3(1)/Tag mammary adenocarcinomas is higher than that in control mammary glands or in mammary tissues with early MIN lesions, there is also a change in the isoforms of VEGF that are being produced. It has been shown that VEGF isoforms act in different, yet coordinated ways to promote tumor angiogenesis.[30] The RT-PCR analysis presented in our study demonstrates that normal and mammary glands with MIN lesions express the 3 VEGF isoforms 120, 164 and 188. However, there is no expression of the $VEGF_{188}$ mRNA isoform in the invasive carcinomas. A recent study has similarly demonstrated that, unlike $VEGF_{120}$ and $VEGF_{165}$, $VEGF_{188}$ mRNA is not increased in several types of tumors.[28] However, another report has described elevated levels of $VEGF_{188}$ associated with increased tumor aggressiveness in lung cancer.[29] $VEGF_{188}$ remains attached to the extracellular matrix (ECM) and causes high intratumoral microvascularization, but little or no recruitment of peripheral vasculature. The functional significance of the consistent loss of $VEGF_{188}$ mRNA in C3(1)/Tag tumors remains unclear and is being investigated further.

Histopathologic examination of the mammary glands from 15-week-old mice (immediately after the treatment period) revealed no differences between the control and treated animals. Both groups had similar histopatholgic alterations, both qualitatively and quantitatively, consisting of low-grade MIN and, less frequently, high-grade MIN lesions. The proliferation and apoptosis indexes were also similar between both groups. Interestingly, we did not observe positive TUNEL staining in the endothelial cells of animals treated with endostatin. This result suggests that endostatin does not cause apoptosis of endothelial cells in preinvasive mammary lesions. It has been reported that endostatin induces apoptosis in endothelial cells *in vitro*.[31] Bergers *et al.*[18] noted that RIP1-Tag transgenic mice treated with endostatin in a prevention-type study had no changes in histology, blood vessel density or apoptotic index at the preinvasive stage. However, apoptotic figures were observed (in both endothelial and tumor cells) in animals treated with established invasive tumors.

Our results suggest that the preventive effect of endostatin is mediated by effects other than apoptosis in this mammary tumor model. This is consistent with our observations comparing the expression of a battery of angiogenic factors in preneoplastic mammary glands between endostatin-treated or untreated mice. Endostatin treatment resulted in the downregulation of VEGF, Flk-1, Fl-1, angiopoietin-2, PECAM (CD-31), Tie-1 and cadherin-5 mRNA levels. Total VEGF protein levels were also decreased in P125A-treated mice compared with controls. This downregulation of angiogenic factors prior to or during the angiogenic switch would presumably lead to a disruption of the normal process of tumor angiogenesis and, therefore, to the inhibition of tumor growth that we have observed in C3(1)/Tag mice. In addition, any tumor-promoting effects through potential VEGF autocrine mechanisms would also be inhibited.

Shichiri and Hirata[31] have recently demonstrated *in vitro* that the main effect of endostatin on endothelial cells is a strong inhibition of cell migration, rather than the induction of endothelial cell apoptosis or cell cycle arrest. These authors have demonstrated that endostatin downregulates genes associated with cell migration and angiogenesis, such as endothelin-1, ET_B receptor, integrin αv, integrin-$\beta 3$, FAK, cadherin-5 and PECAM. We similarly demonstrate *in vivo* that endostatin is associated with reduced expression of cadherin-5 and PECAM. Our results are consistent with the notion that a major effect of endostatin is the prevention of endothelial cell recruitment, migration and vessel formation. This explanation would be consistent with the strong inhibition of endostatin on rapid tumor growth in animal models but only modest effects on large established tumors.

In summary, we have demonstrated that the downregulation of angiogenic factors in C3(1)/Tag transgenic mice by the P125A mutated form of human endostatin is associated with the inhibition of tumor growth. These results suggest that endostatin might be effective in inhibiting the transition of ductal carcinoma in *situ* to invasive carcinomas and warrant further investigation.

ACKNOWLEDGEMENTS

We are grateful to Dr. M. Anver for critical histological analysis, and to L. Birely for excellent technical assistance. A.C. is supported by a Fulbright-MEC fellowship at the NIH.

REFERENCES

1. O'Reilly MS, Boehm T, Shing Y, Fukai N, Vasios G, Lane WS, Flynn E, Birkhead JR, Olsen BR, Folkman J. Endostatin: an endogenous inhibitor of angiogenesis and tumor growth. Cell 1997;88:277–85.
2. Hanahan D, Christofori G, Naik P, Arbeit J. Transgenic mouse models of tumour angiogenesis: the angiogenic switch, its molecular controls, and prospects for preclinical therapeutic models. Eur J Cancer 1996; 32:2386–93.
3. Cavallaro U, Christofori G. Molecular mechanisms of tumor angiogenesis and tumor progression. J Neurooncol 2000;50:63–70.
4. Ferrara N, Alitalo K. Clinical applications of angiogenic growth factors and their inhibitors. Nat Med 1999;5:1359–64.

5. Ferrara N. Role of vascular endothelial growth factor in the regulation of angiogenesis. Kidney Int 1999;56:794–814.
6. Veikkola T, Alitalo K. VEGFs, receptors and angiogenesis. Semin Cancer Biol 1999;9:211–20.
7. Hiratsuka S, Maru Y, Okada A, Seiki M, Noda T, Shibuya M. Involvement of Flt-1 tyrosine kinase (vascular endothelial growth factor receptor-1) in pathological angiogenesis. Cancer Res 2001;61: 1207–13.
8. Von Marschall Z, Cramer T, Hocker M, Burde R, Plath T, Schirner M, Heidenreich R, Breier G, Riecken EO, Wiedenmann B, Rosewicz S. De novo expression of vascular endothelial growth factor in human pancreatic cancer: evidence for an autocrine mitogenic loop. Gastroenterology 2000;119:1358–72.
9. Xie B, Tam NN, Tsao SW, Wong YC. Co-expression of vascular endothelial growth factor (VEGF) and its receptors (flk-1 and flt-1) in hormone-induced mammary cancer in the Noble rat. Br J Cancer 1999;81:1335–43.
10. Ferrer FA, Miller LJ, Lindquist R, Kowalczyk P, Laudone VP, Albertsen PC, Kreutzer DL. Expression of vascular endothelial growth factor receptors in human prostate cancer. Urology 1999;54:567–72.
11. Holash J, Wiegand SJ, Yancopoulos GD. New model of tumor angiogenesis: dynamic balance between vessel regression and growth mediated by angiopoietins and VEGF. Oncogene 1999;18:5356–62.
12. Folkman J, D'Amore PA. Blood vessel formation: what is its molecular basis? Cell 1996;87:1153–5.
13. Suri C, Jones PF, Patan S, Bartunkova S, Maisonpierre PC, Davis S, Sato TN, Yancopoulos GD. Requisite role of angiopoietin-1, a ligand for the TIE2 receptor, during embryonic angiogenesis. Cell 1996;87: 1171–80.
14. Maisonpierre PC, Suri C, Jones PF, Bartunkova S, Wiegand SJ, Radziejewski C, Compton D, McClain J, Aldrich TH, Papadopoulos N, Daly TJ, Davis S, et al. Angiopoietin-2, a natural antagonist for Tie2 that disrupts in vivo angiogenesis. Science 1997;277:55–60.
15. Chen QR, Kumar D, Stass SA, Mixson AJ. Liposomes complexed to plasmids encoding angiostatin and endostatin inhibit breast cancer in nude mice. Cancer Res 1999;59:3308–12.
16. Yoon SS, Eto H, Lin CM, Nakamura H, Pawlik TM, Song SU, Tanabe KK. Mouse endostatin inhibits the formation of lung and liver metastases. Cancer Res 1999;59:6251–6.
17. Ding I, Sun JZ, Fenton B, Liu WM, Kimsely P, Okunieff P, Min W. Intratumoral administration of endostatin plasmid inhibits vascular growth and perfusion in MCa-4 murine mammary carcinomas. Cancer Res 2001;61:526–31.
18. Bergers G, Javaherian K, Lo KM, Folkman J, Hanahan D. Effects of angiogenesis inhibitors on multistage carcinogenesis in mice. Science 1999;284:808–12.
19. Kuo CJ, Farnebo F, Yu EY, Christofferson R, Swearingen RA, Carter R, Von Recum HA, Yuan J, Kamihara J, Flynn E, D'Amato R, Folkman J, et al. Comparative evaluation of the antitumor activity of antiangiogenic proteins delivered by gene transfer. Proc Natl Acad Sci 2001;98:4605–10.
20. Yokoyama Y, Green JE, Sukhatme VP, Ramakrishnan S. Effect of endostatin on spontaneous tumorigenesis of mammary adenocarcinoma in a transgenic mouse model. Cancer Res 2000;60:4362–5.
21. Maroulakou IG, Anver M, Garrett L, Green JE. Prostate and mammary adenocarcinoma in transgenic mice carrying a rat C3(1) simian virus 40 large tumor antigen fusion gene. Proc Natl Acad Sci USA 1994;91:11236–40.
22. Green JE, Shibata MA, Yoshidome K, Liu ML, Jorcyk C, Anver MR, Wigginton J, Wiltrout R, Shibata E, Kaczmarczyk S, Wang W, Liu ZY, et al. The C3(1)/SV40 T-antigen transgenic mouse model of mammary cancer: ductal epithelial cell targeting with multistage progression to carcinoma. Oncogene 2000;19:1020–7.
23. Fueyo J, Gomez-Manzano C, Yung WK, Liu TJ, Alemany R, McDonnell TJ, Shi X, Rao JS, Levin VA, Kyritsis AP. Overexpression of E2F-1 in glioma triggers apoptosis and suppresses tumor growth in vitro and in vivo. Nat Med 1998;6:685–90.
24. Cullinan-Bove K, Koos RD. Vascular endothelial growth factor/ vascular permeability factor expression in the rat uterus: rapid stimulation by estrogen correlates with estrogen-induced increases in uterine capillary permeability and growth. Endocrinology 1993;133: 829–37.
25. Feldman AL, Restifo NP, Alexander HR, Bartlett DL, Hwu P, Seth P, Libutti SK. Antiangiogenic gene therapy of cancer utilizing a recombinant adenovirus to elevate systemic endostatin levels in mice. Cancer Res 2000;60:1503–6.
26. Sacco MG, Caniatti M, Cato EM, Frattini A, Chiesa G, Ceruti R, Adorni F, Zecca L, Scanziani E, Vezzoni P. Liposome-delivered angiostatin strongly inhibits tumor growth and metastatization in a transgenic model of spontaneous breast cancer. Cancer Res 2000;60: 2660–5.
27. Kranz A, Mattfeldt T, Waltenberger J. Molecular mediators of tumor angiogenesis: enhanced expression and activation of vascular endothelial growth factor receptor KDR in primary breast cancer. Int J Cancer 1999;84:293–8.
28. Wellmann S, Taube T, Paal K, Graf V, Einsiedel H, Geilen W, Seifert G, Eckert C, Henze G, Seeger K. Specific reverse transcription-PCR quantification of vascular endothelial growth factor (VEGF) splice variants by LightCycler technology. Clin Chem 2001;47:654–60.
29. Yuan A, Yu CJ, Kuo SH, Chen WJ, Lin FY, Luh KT, Yang PC, Lee YC. Vascular endothelial growth factor 189 mRNA isoform expression specifically correlates with tumor angiogenesis, patient survival, and postoperative relapse in nonsmall-cell lung cancer. J Clin Oncol 2001;19:432–41.
30. Grunstein J, Masbad JJ, Hickey R, Giordano F, Johnson RS. Isoforms of vascular endothelial growth factor act in a coordinate fashion to recruit and expand tumor vasculature Mol Cell Biol 2000;20:7282–91.
31. Shichiri M, Hirata Y. Antiangiogenesis signals by endostatin. FASEB J 2001;15:1044–53.
32. Arap, W., Pasqualini, R., Ruoslahti, E. Cancer treatment by targeted drug delivery to tumor vasculature in a mouse model. Science 1998; 279:377–80.

Carboplatin Selectively Induces the VEGF Stress Response in Endothelial Cells: Synergistic Inhibition of Tumor Growth by Combination Treatment With Antibody to VEGF

Robert Wild[*], Ruud P.M. Dings[*] and S. Ramakrishnan[+*]

Departments of [*]Pharmacology, [+]Obstetrics/Gynecology, Comprehensive Cancer Center

University of Minnesota Medical School, Minneapolis, MN 55455, USA

Running Title: Carboplatin and VEGF Antibody Combination Treatment

Key Words: angiogenesis, Carboplatin, chemotherapy, VEGF, antibody

Address correspondence to: S. Ramakrishnan

Department of Pharmacology

University of Minnesota

6-120 Jackson Hall

321 Church St. SE

Minneapolis, MN 55455

Phone: (612) 626-6461

FAX : (612) 625-8408

E-mail: sunda001@maroon.tc.umn.edu

ABSTRACT

Vascular Endothelial Growth Factor (VEGF) functions as a key regulator in tumor angiogenesis. In addition, VEGF is an important survival factor for endothelial cells under chemical or physical stress. In this report, we show that treatment of endothelial cells with the chemotherapeutic agent, Carboplatin, significantly increased the expression of VEGF. Furthermore, neutralization of secreted VEGF with antibodies sensitized endothelial cells to Carboplatin and increased apoptosis several-fold. Interestingly, Carboplatin treatment did not alter VEGF expression in tumor cells. Similarly, antibody to VEGF did not change the chemosensitivity of tumor cells to the drug. Most importantly, tumor-bearing animals treated with Carboplatin showed an increase in VEGF immunoreactivity in the vasculature, confirming the *in vitro* studies. Based on these observations, we determined whether neutralization of VEGF could enhance the anti-tumor activity of Carboplatin in an *in vivo* model system. A combination therapy consisting of Carboplatin and VEGF antibody synergistically inhibited solid tumor growth and included multiple complete responses. These findings suggest that VEGF is a critical endothelial cell specific survival factor that is induced by Carboplatin and contributes to the protection of tumor vasculature during chemotherapy. Our results provide evidence that a Carboplatin-based treatment regimen can be combined with anti-VEGF antibodies for improved anti-tumor effect. We conclude that this combination therapy should be therapeutically applicable to many types of malignancies since Carboplatin differentially induced VEGF expression in non-tumorigenic cells, i.e. tumor host vasculature.

INTRODUCTION

Ovarian cancer is the leading cause of death among gynecological malignancies (1). The current standard treatment regimen consists of surgical debulking of primary tumors followed by platinum-based chemotherapy. However, major limitations are associated with this approach. Insufficient delivery of drugs to tumor tissues is accompanied by major, intolerable toxicity of current chemotherapeutic agents. In addition, the heterogeneity of cancer tissues and the development of drug resistance complicate cancer therapy. As a consequence, even new combination therapies (i.e. the administration of Carboplatin in combination with Taxol) displayed only marginal improvements in overall response rates in ovarian cancer patients (2, 3). Clearly, there is a need for a better understanding of chemotherapy-induced cancer cell resistance. More importantly, improved treatment modalities are necessary.

Recent studies have shown that tumor angiogenesis may be an alternate target for cancer therapy (4, 5). Angiogenesis, the development of new blood vessels from pre-existing vasculature, is one of the processes linked to tumor growth and its metastatic spread. In the absence of neovascularization tumor cells undergo apoptosis and fail to expand (5). Tumor angiogenesis is mediated by both tumor cells themselves and the host cell microenvironment. Several growth factors have been identified as potential regulators of angiogenesis. However, VEGF and its tyrosine kinase receptors, Flt-1 and KDR/Flk-1, have been implicated as key components in the vascularization of a tumor (6). Direct proof of this hypothesis comes from a multitude of experiments, where the disruption of the VEGF signaling pathway inhibited angiogenesis *in vitro* and solid tumor growth *in vivo* (7-17).

In addition to its central role in regulating tumor angiogenesis, VEGF has been identified to function as an important survival factor for endothelial cells. VEGF expression is induced by hypoxia, which was shown to rescue newly formed endothelial cells in the retina that were exposed to low oxygen environment (18). VEGF is also able to save newly formed tumor vessels from undergoing apoptosis (19, 20). Moreover, VEGF was shown to inhibit endothelial cell apoptosis induced by tumor necrosis factor-alpha (21) and anchorage disruption (22). Therefore, VEGF seems to play an important dual role in the progression of a cancer, which include the direct stimulation of neovascularization and the concomitant protection of tumor vessels.

Various reports have shown that antiangiogenic therapies potentiate cytotoxic anticancer therapies in several *in vivo* model systems (23, 24). Particularly, Carboplatin-based therapies were responsive to combination treatment with the antiangiogenic agent TNP-470, a potent inhibitor of endothelial cell proliferation and migration (25). However, the exact mechanism of action of this combination strategy is not fully understood. In this report, we show that Carboplatin significantly increases the expression of VEGF in endothelial cells *in vitro* and in tumor vessels *in vivo*. Neutralization of VEGF by specific antibodies significantly increased the sensitivity of endothelial cells to Carboplatin. In contrast, antibody to VEGF did not augment the chemosensitivity of tumor cells *in vitro*. We also show that a combination therapy consisting of Carboplatin and VEGF antibody produced a more than additive antitumor effect with multiple complete responses in an ovarian cancer model system. Our findings suggest that Carboplatin treatment induces the VEGF stress response in tumor vessels and by blocking this survival mechanism, synergistic inhibition of tumor growth can be achieved.

MATERIALS AND METHODS

Cell Culture

Early passage Human Umbilical Vein Endothelial Cells (HUVEC), were kindly provided by Dr. G. Vercellotti (University of Minnesota, Minneapolis, MN), and maintained in EGM medium (Clonetics, San Diego, CA) in tissue culture flasks pre-coated with 0.1% gelatin (Sigma, St. Louis, MO). HUVEC cultures were used between the second and fourth passage for experiments. MA148, a human epithelial ovarian carcinoma cell line, was maintained in RPMI 1640 medium (Life Technologies, Grand Island, NY) supplemented with 10% fetal bovine serum (FBS, Cellgro, Mediatech, Washington, DC) and 1% penicillin/streptomycin (Cellgro, Mediatech, Washington, DC). MA148 cultures were split 1:3 every 3-5 days. All cell lines were maintained at 37^0C and 5% CO_2.

Anti-VEGF Antibody

Polyclonal anti-VEGF antiserum was developed in rabbits by a hyperimmunization protocol using recombinant human VEGF165 as previously described (26). The antibodies were purified from the serum by affinity chromatography using a Protein A agarose column (Sigma, St. Louis, MO). Similarly, control antibody was obtained from the serum of non-immunized rabbits and purified by Protein A affinity chromatography. Purified IgG fractions were dialyzed in phosphate buffered saline (PBS, pH 7.6) and concentrated to 20 mg/ml by ultrafiltration using a YM-30 membrane (Millipore, Bedford, MA). Antibody samples were then filter sterilized by a 0.2 μm filter (Millipore, Bedford, MA) and stored in aliquots at -20^0 C. Antibody purity was assessed

by SDS-PAGE. Immunoreactivity with recombinant VEGF165 (R+D Systems, Minneapolis, MN) by ELISA and Western Blot was used to determine specificity of the antibody preparations. Characterization of the antibody has been previously published (26).

Measurement of VEGF Levels

MA148 or HUVEC were plated at a density of 3 x 10^5 cells/well in a 6-well plate, allowed to attach overnight, and exposed to various concentrations of Carboplatin (Sigma, St. Louis, MO). HUVEC were seeded on plates pre-treated with 0.1% gelatin. At 24 and 48 hours time points after Carboplatin treatment, VEGF levels in the conditioned media were measured by ELISA (Cytimmune, College Park, MD) and normalized to viable cell number as determined by Trypan Blue exclusion (Sigma, St. Louis, MO).

Cell Proliferation Assays

Cells (HUVEC or MA148) were seeded at a density of 1x10^4 cells/well into 96-well plates and allowed to attach overnight. Carboplatin and/or antibodies were then prepared in different dilutions using the appropriate culture medium and added to the cells. Forty-eight hours after treatment, cells were treated with MTT (Sigma, St. Louis, MO) at 0.5 mg/ml for four hours. Medium was then removed and the dye was dissolved in 100 µl dimethyl sulfoxide (Sigma, St. Louis, MO). Absorbance was measured at 560 nm with 650 nm background readings subtracted.

Apoptosis Assay

Cells (HUVEC/MA148) were seeded at a density of $3x10^4$ cells/well into 8-well chamber slides (Nalge Nunc, Naperville, IL) and allowed to attach overnight. Carboplatin and/or antibodies were then added to the wells. Samples were incubated for forty-eight hours and then analyzed for apoptosis by TUNEL assay (Boehringer Mannheim, Germany). Digital images were acquired using a fluorescence microscope equipped with an Optronics (TEC 470) single chip cooled camera. Metamorph image analysis software (Image 1, Westchester, PA) was used to store the images as TIFF files. Fields were chosen randomly to ensure objectivity of sampling. The files were then opened in Adobe Photoshop (Adobe Inc., Mountain View, CA) and the apoptotic index was estimated by counting the number of TUNEL positive pixels per field using a histogram analysis.

Tumor Model

Exponentially growing MA148, a human epithelial ovarian carcinoma cell line, was harvested by trypsinization, washed twice with Hanks' balanced salt solution (Cellgro, Mediatech, Washington, DC) and resuspended at 2×10^7 cells/ml in serum free RPMI 1640 medium. One hundred μl of the suspension was then injected subcutaneously into the flanks of 6 – 8 week old female, athymic, nu/nu mice (National Cancer Institute, Bethesda, MD) and the tumors were allowed to establish. On day ten, the animals were randomized and treatment was initiated. Carboplatin (32.5 mg/kg/dose) was administered by i.p. injections once every three days for five doses. Anti-VEGF IgG or pre-immune control IgG treatment (2 mg/dose) was given i.p. once every three days for a total of ten injections. Control animals received equal amounts of sterile PBS. Tumor growth was

monitored by caliper measurements and tumor volumes were calculated by the formula (tumor volume (mm^3) = a x b^2 x $\pi/6$), where 'a' represents the larger diameter and 'b' represents the smaller diameter of the tumor.

For histological examination of the tissues, animals were sacrificed and tumor specimens were harvested at either the conclusion of the Carboplatin treatment regimen (day 22) or anti-VEGF IgG treatment schedule (day 40) as indicated.

Histology and Immunohistochemistry

H&E stainings of paraffin embedded tissue sections were used for general histological examination of the tissue specimens. Frozen sections were prepared for the staining of VEGF and tumor blood vessels in Carboplatin treated specimens versus PBS control animals. Here, harvested tumor tissues were embedded in tissue freezing medium (Miles Inc, Elkhart, IN), snap frozen in liquid nitrogen and subsequently cut into 10 μm thick sections. Next, tissue specimens were slowly brought to room temperature, air dried and subsequently fixed in acetone for ten minutes. The slides were then allowed to air-dry for one hour and washed three times for 5 minutes in PBS, pH 7.5. The samples were then blocked with PBS containing 0.1% bovine serum albumin for thirty minutes at room temperature. The tissue sections were stained for VEGF with a mouse monoclonal anti-VEGF antibody (VEGF Ab-3 (JH121), Neomarkers, Fremont, CA; antibody recognizes both human and mouse VEGF, 1:20 dilution) for one hour at room temperature. Next, the sections were washed in PBS and incubated with FITC-labeled rabbit anti-mouse IgG antibody (Sigma, St. Louis, MO, 1:20 dilution) for one hour at room temperature. In addition, we simultaneously incubated the slides with phycoerythrin (PE) conjugated to a

monoclonal antibody to PECAM-1 (PE conjugated anti-mouse CD-31, 1:50 dilution, Pharmingen, San Diego, CA) to stain for blood vessels. The slides were washed three times with PBS, pH 7.5 and immediately imaged in an Olympus BX-60 fluorescence microscope.

Statistical Analysis

Statistical significance between treatment groups was determined by one-way ANOVA or the Student's t-test.

RESULTS

Differential Sensitivity of Tumor Cells versus Endothelial Cells to Carboplatin

Carboplatin is a potent chemotherapeutic drug used in the treatment of ovarian cancer. In a series of experiments, the *in vitro* sensitivity of ovarian carcinoma cells (MA148) and endothelial cells (HUVEC) to Carboplatin was evaluated. As shown in Fig. 1, MA148 cells were about 100 fold more sensitive to Carboplatin than HUVEC. The tumor cells showed a TCID50 of roughly 0.7 μg/ml compared to a TCID50 of 50-70 μg/ml for HUVEC. Therefore, endothelial cell populations appear to be less sensitive to Carboplatin than tumor cells.

Carboplatin Differentially Up-regulates VEGF Expression in Endothelial Cells

To further elucidate the apparent resistance of endothelial cells to Carboplatin treatment, we investigated the role of Vascular Endothelial Growth Factor (VEGF), a known endothelial cell survival factor, under these conditions. Both ovarian and

endothelial cell cultures were treated with their respective TCID50 concentration of Carboplatin and VEGF levels in the conditioned media were measured by ELISA. As shown in Fig. 2, Carboplatin treatment did not alter the level of VEGF secreted by the tumor cell line at both 24 and 48 hour time points. VEGF concentrations ranged between 47.8 and 58.4 pg/1x10^6 cells. However, treatment of HUVEC with Carboplatin resulted in a five-fold increase of VEGF levels at 24 hours (22.8 pg/1x10^6 cells for control versus 129.4 pg/1x10^6 cells for Carboplatin treated cultures). An even more pronounced effect was seen at the 48 hour time point with a twelve-fold increase in VEGF levels in Carboplatin treated HUVEC (17.9 pg/1x10^6 cells for control cells versus 224.2 pg/1x10^6 cells for Carboplatin treated cells). These values were statistically significant as determined by the Student's t-test ($p < 0.038$). Our results indicate that Carboplatin induced expression of VEGF in endothelial cells could act as an anti-apoptotic factor, which partially rescues these cells from the cytotoxic effects of this drug.

Antibody to VEGF Potentiates the Inhibitory Activity of Carboplatin on Endothelial Cells

To further verify the above-mentioned hypothesis, we next tested whether the addition of specific antibodies to VEGF could neutralize the growth factor dependent rescue. Carboplatin induced cytotoxicity was determined in the presence or absence of anti-VEGF IgG (30 μg/ml). As shown in Fig. 3, the addition of anti-VEGF antibody to Carboplatin-treated HUVEC significantly increased the cytotoxicity of the chemotherapeutic by 12.58% ($p < 0.014$, Student's t-test). This effect was specific since a corresponding pre-immune control IgG treatment (30 μg/ml) did not significantly

increase the inhibitory effect of the drug ($p > 0.34$). In contrast to endothelial cells, anti-VEGF IgG did not influence the chemosensitivity of tumor cells. In fact, the inhibitory activity of Carboplatin was decreased by 10 % with the addition of anti-VEGF IgG and by 3.7 % with the use of pre-immune control IgG. However, these changes were not statistically significant ($p>0.057$ for both points).

We also assessed the effect of exogenous addition of recombinant VEGF165 (27) to Carboplatin-treated HUVEC. VEGF partially rescued endothelial cells at concentrations between 10-100 ng/ml (data not shown). In contrast, the human ovarian carcinoma cell line did not respond to the exogenous addition of VEGF (data not shown). Therefore, VEGF seems to significantly improve the survival of Carboplatin treated endothelial cells selectively. Moreover, the specific neutralization of this growth factor with antibodies potentiates the cytotoxicity of this drug to endothelial cells.

Antibody to VEGF Increases Apoptosis in Carboplatin Treated Endothelial Cells

To determine whether Carboplatin induced expression of VEGF rescues endothelial cells from apoptosis we performed a TUNEL assay. As shown in Fig. 4, addition of the chemotherapeutic drug to HUVEC increased the apoptotic index nine-fold compared to medium control. More importantly, a combination treatment of Carboplatin with anti-VEGF IgG (50 μg/ml) resulted in an additional 1.85-fold increase in apoptotic index versus Carboplatin alone treated samples ($p < 0.03$, Student's t-test). This effect corresponded to a 17.4-fold increase in apoptosis when compared to medium control. Again, the specificity of this effect was verified with the addition of pre-immune IgG (50 μg/ml), which did not augment the apoptotic response to Carboplatin treatment. In

comparison, equal concentrations of anti-VEGF or pre-immune antibodies alone did not change the apoptotic index, which was similar to medium control. Clearly, these results suggest that Carboplatin-induced VEGF, and not basal levels of the growth factor, functions as an important survival factor and partially rescues endothelial cells from apoptosis.

Carboplatin Specifically Up-regulates VEGF Expression in Tumor Vessels *In vivo*

To determine whether Carboplatin could induce VEGF expression *in vivo*, a nude mouse model was employed. MA148 tumor cells, the same carcinoma cell line used for the *in vitro* experiments, were transplanted s.c. into the hind leg of athymic nude mice. After ten days, small palpable tumors were established and treatment was initiated. A low dose of Carboplatin (32.5 mg/kg/dose) was then administered every three days for five doses, at which point the animals were sacrificed and tumor tissues were harvested. Sections were prepared and immunochemically stained for VEGF and CD-31. As shown in Fig. 5A, PBS treated control animals showed a consistent but low expression of VEGF in the tumor tissue. In contrast, Carboplatin treated animals displayed increased expression of VEGF in the vasculature (Fig. 5B). Staining of the tissues with specific antibodies to the endothelial cell marker CD-31 was used to identify vascular structures in the tumor tissue (Fig. 5 C and D). A subsequent overlay of the images showed a clear co-localization of VEGF in the tumor vasculature of Carboplatin treated animals (Fig. 5 F). In contrast, no significant co-localization was seen in the PBS treated control tissue (Fig. 5 E). These results provide evidence that Carboplatin treatment significantly increases the expression of the survival factor VEGF in tumor vessels *in vivo*.

Antibody to VEGF Significantly Improves The Anti-Tumor Effects of Carboplatin

Subsequently, experiments were carried out to determine the therapeutic benefit of anti-VEGF antibodies during Carboplatin chemotherapy. MA148 cells were inoculated s.c. into the hind leg of athymic, nude mice and tumors were allowed to establish for ten days. Animals were then randomized and divided into four treatment groups. Tumor growth was then monitored by caliper measurements and the experiments were terminated once tumor volumes reached about 3,000 mm^3.

Fig. 6 summarizes the results of three independent experiments. In all three trials, administration of low dose Carboplatin slightly inhibited the growth of solid tumors *in vivo*. By the end of the treatment regimen (day 40), effects ranged between 25% inhibition in the first experiment (Fig. 6A, $p<0.37$), 12.7% inhibition in the second trial (Fig. 6B, $p<0.42$) and 52.7% inhibition in the third experiment (Fig. 6C, $p<0.1$) compared to PBS control animals. All p-values were determined by the Student's t-test. Similarly, anti-VEGF antibody alone treated mice displayed either no effect (Fig. 6B) or moderate inhibition of tumor growth (34% inhibition, Fig. 6C; 42.2% inhibition, Fig. 6A). However, these values were not statistically significant as determined by the Student's t-test ($p>0.21$ for all points). In contrast, the administration of Carboplatin in combination with anti-VEGF antibody showed a dramatic improvement in tumor growth inhibition. At day 40, tumor volumes were significantly reduced by 78.7% (Fig. 6C, $p<0.033$), 87.1% (Fig. 6B, $p<0.029$) and 98.3% (Fig. 6A, $p<0.019$) compared to PBS treated control animals. Moreover, in the first and third trial (Fig. 6A and C) combination treatment significantly inhibited solid tumor growth throughout the entire course of the experiment ($p<0.04$ for all time points in experiment one; $p<0.03$ for all time points in experiment

three). In the second trial (Fig. 6B), combination treatment resulted in a significant inhibition up to day 50 of observation ($p<0.04$ for all time points in experiment, all p-values determined by the Student's t-test). Most importantly, 23% of all combination treated animals (cumulative of three experiments) displayed a complete response and remained tumor free for the entire period of observation.

Preliminary statistical analysis indicated that treatment results did not differ between trials. Thus, data from all three experiments were combined and analyzed as one. A one-way ANOVA with treatment as the between-subjects factor with 4 levels was then used to analyze the combined effects of the three individual experiments. On day 22 (end of Carboplatin treatment) both Carboplatin and anti-VEGF IgG did not significantly inhibit tumor growth ($p = 0.0718$ for Carboplatin, $p = 0.6324$ for anti-VEGF IgG), whereas combination therapy showed a significant difference in tumor volume compared to PBS ($p = 0.0016$). Similarly, on day 40 (end of antibody treatment) only the combination treatment of Carboplatin with anti-VEGF IgG displayed a significant inhibition of tumor growth ($p = 0.0003$, $p = 0.1533$ for Carboplatin alone, $p = 0.731$ for anti-VEGF IgG alone). More importantly, tumor volumes from the combination treatment group were also significantly lower than both monotherapies ($p = 0.0229$ compared to Carboplatin, $p = 0.0016$ compared to anti-VEGF IgG).

Treatment of tumor bearing animals with non-specific pre-immune IgG (2 mg/dose every three days for ten injections) did not affect the *in vivo* tumor growth rate of MA148 either alone or in combination with Carboplatin. Fig. 6 D shows a summary of the effects of anti-VEGF IgG or pre-immune control IgG in combination with Carboplatin therapy. Data points are expressed as a mean relative to mean tumor volume

of Carboplatin treated animals ($V/V_{carboplatin}$). Values for anti-VEGF IgG represent the pooled data from the three individual experiments. Values for pre-immune control IgG represent the mean data points from a single experiment (n = 5 mice/group). Again, we chose the two time points of therapy completion for analysis (day 22, end of Carboplatin treatment; day 40, end of antibody treatment). Our results illustrate that the addition of pre-immune control IgG did not significantly alter the inhibitory activity of Carboplatin treatment. However, the addition of specific anti-VEGF IgG showed a statistically significant increase in anti-tumor activity when compared to Carboplatin monotherapy. This outcome clearly demonstrates the specificity of anti-VEGF antibody in potentiating the therapeutic effect of Carboplatin.

To further determine the overall extend of the combined treatment effect of Carboplatin with anti-VEGF IgG, we analyzed the fractional tumor volumes relative to untreated controls after pooling the results of all three individual experiments. As summarized in Table 1, combination therapy showed a multiplicative effect at both day 22 and day 40 of observation. In fact, combination treatment resulted in a more than 2.26-fold higher than expected effect for both time points. All together, these results suggest that Carboplatin and anti-VEGF antibody act in a more than additive, if not synergistic fashion in inhibiting ovarian carcinoma growth *in vivo*.

Carboplatin/Anti-VEGF Antibody Combination Treatment Results in Extensive Tumor Cell Apoptosis and Necrosis

Next, we examined the effects of Carboplatin/Anti-VEGF antibody combination treatment on a microscopic level. Human xenograft tumors were surgically removed from

the animals by the end of the treatment regimen (day 40) and paraffin embedded for the preparation of tissue sections. Histological analysis demonstrated dramatic differences in tumors from Carboplatin/anti-VEGF antibody combination treated animals compared to PBS control or individual drug treatment groups.

A TUNEL assay was used to detect apoptotic cells. Carboplatin or anti-VEGF antibody alone treated animals displayed no difference in apoptosis when compared to PBS treated control tissues (data not shown). In contrast, animals that received a combination treatment regimen presented a marked increase in apoptotic cells (data not shown). Even more striking are the effects seen in H&E stained tissue sections (Fig. 7). Here, Carboplatin (Fig. 7B) or anti-VEGF antibody (Fig. 7C) monotherapy samples displayed a slight increase in apoptotic and necrotic cells (picnotic nuclei) when compared to PBS control (Fig. 7A). However, an enormous decrease in cellularity and large areas of necrosis were observed in tissues from combination treated animals (Fig. 7D). In addition, a marked increase in fibrous tissue was detected in these samples. Most importantly, histological examination of a tumor sample from a complete responder (Fig. 7E) showed that the entire tumor tissue was replaced by fibrous matrix, indicating full remission by combination therapy.

DISCUSSION

Despite significant efforts to produce new and improved treatments, the outcome for patients with ovarian cancer remains poor (3). The application of the chemotherapeutic drug, Carboplatin, either alone or in combination with Paclitaxel, has become the front line therapy for this disease. However, it is still far from being curative

and the development of chemoresistance poses a major challenge. As a consequence, recent efforts have focused on the application of various combination treatment regimens that include cytotoxic and anti-angiogenic agents. Such combinations have shown to significantly improve the overall anti-tumor response *in vivo* (24). However, the mechanism underlying this additive effect has not been fully elucidated.

In this report, we show that tumor cells are by far more sensitive to Carboplatin than endothelial cells. This differential chemosensitivity could be explained by several factors. For instance, the proliferative status of target cells can substantially influence its sensitivity to DNA cross-linking drugs. Tumor cells are actively proliferating as indicated by several-fold higher ^{3}H-thymidine incorporation when compared to endothelial cells[1]. Secondly, drug uptake mechanisms could be differentially regulated in tumor cells versus endothelial cells. In addition, DNA repair mechanisms could be substantially different in these two cell types, which could at least in part contribute to the differential chemosensitivity. Lastly, specific cell survival factors could influence the chemosensitivity of various cell types to this drug therapy.

Here, we provide evidence for the later possibility. Our results demonstrate that Carboplatin substantially induces the expression of VEGF in endothelial cells *in vitro*. VEGF has been shown to function as an important endothelial cell-specific survival factor that prevents apoptotic cell death. As a consequence, up-regulation of VEGF directly increases cell viability and decreases the overall chemosensitivity of endothelial cells to Carboplatin. Proof of principal comes from our experiments where the concomitant neutralization of VEGF by specific antibodies significantly increased the drug-induced cytotoxicity as well as the overall apoptotic response in endothelial cells.

Very interestingly, individual administration of the antibody did not result in any endothelial cell death or increased apoptosis. Therefore, our data suggests that Carboplatin sensitizes the cells to VEGF and illustrates the necessity of this survival factor under such conditions. In contrast, VEGF levels in the tumor cell line were not altered by Carboplatin treatment. In addition, the tumor cells did not respond to either exogenous addition of VEGF or its respective antibodies. As a consequence, the up-regulation of VEGF induced by Carboplatin appears to be unique to the endothelial cell population. This is a novel finding, since the predominant notion in the angiogenesis field was that VEGF functions as a paracrine mediator of endothelial cell activity. However, we report here, that this factor also contributes an important autocrine function to this system. It remains to be seen whether Carboplatin directly influences the expression of VEGF at the transcriptional (i.e. induction of the VEGF promoter) or perhaps at the post-transcriptional level (i.e. increased mRNA stability). Investigations are currently underway to identify such possibilities.

In addition to the implications of Carboplatin induced expression of VEGF *in vitro*, we provide evidence for the potential clinical implications of this phenomenon with our *in vivo* experiments. We show that low dose Carboplatin treatment to tumor bearing mice significantly up-regulates the expression of VEGF in tumor vessels *in vivo*. This experiment provides evidence that even though both tumor cells and blood vessels are exposed to similar concentrations of Carboplatin, a selective increase of VEGF expression was found in the vasculature. Increased levels of this survival factor could potentially save tumor blood vessels from apoptosis, which directly translates into an enhanced overall tumor cell survival. As a consequence, concomitant neutralization of

[1] R. Wild and S. Ramakrishnan unpublished data

this growth factor with specific anti-VEGF antibodies significantly improved the cytotoxic effects of Carboplatin and increased the anti-tumor effect several fold. Previous studies have shown that ionizing radiation combined with VEGF specific antibodies could improve anti-tumor effects *in vivo* (28). However, radiation, unlike Carboplatin, specifically induced the expression of VEGF in tumor cells. It would be interesting to investigate whether radiation stress could also lead to the up-regulation of VEGF in endothelial cells.

Histological analysis of tissue samples provides further evidence for the therapeutic benefit of a Carboplatin/anti-VEGF antibody combination therapy. The complete remission in some of the treated animals and the overall increase in apoptotic activity in tumor tissue clearly support the combination regimen. More importantly, improved anti-tumor effects were possible at significantly lower (sub-optimal) doses of the chemotherapeutic drug, thereby limiting toxicity.

Finally, the role of VEGF as an endothelial cell specific survival factor could have implications that are even more profound in solid tumor therapy in general. Multiple reports have shown that the combination of antiangiogenic drugs with several different cytotoxic therapeutics can significantly increase the antitumor effects *in vivo*. For instance, the addition of the angiogenesis inhibitor TNP-470/Minocycline to the treatment with Paclitaxel and Carboplatin resulted in increased antitumor activity and efficacy in non-small-cell lung cancer and breast cancer (25). Antiangiogenic modulators also markedly increased the cytotoxicity of Cyclophosphamide toward FSaIIC tumor cells (29). Similarly, Minocycline significantly increased the growth delay of Lewis lung carcinoma after treatment with the cytotoxic drugs cis-diamminedichloroplatinum(II),

Melphalan, Cyclophosphamide, Adriamycin and Bleomycin (23). In addition, a recent report showed that the neutralization of VEGF in combination with the cytotoxic agent Doxorubicin resulted in a more than additive inhibition of tumor cell induced angiogenesis in a dorsal skinfold chamber assay (30). Therefore, it is conceivable that other chemotherapeutic drugs act similarly on endothelial cells and induce the expression of VEGF. As a consequence, combining conventional chemotherapeutic drugs with agents that are interfering with the VEGF stress response system could be a widely applicable treatment regimen with immediate clinical implications.

ACKNOWLEDGMENTS

We thank Dr. K. Ghosh for technical support and Dr. C. Le and R.L. Bliss (Biostatistics Core, University of Minnesota Cancer Center) for their advice and assistance in statistical analysis. We want to acknowledge Dr. J Kersey (University of Minnesota Cancer Center) for his comments and suggestions. This work was supported in part by grants from NIH CA 71803, USAMRMC, Gustaves and Louise Pfeiffer Foundation, Sparboe and Women's Health Fund Endowment (to S.R.) and a doctoral dissertation fellowship from the University of Minnesota Graduate School (to R.W.).

REFERENCES

1. Berek, J. S., Bertelsen, K., du Bois, A., Brady, M. F., Carmichael, J., Eisenhauer, E. A., Gore, M., Grenman, S., Hamilton, T. C., Hansen, S. W., Harper, P. G., Horvath, G., Kaye, S. B., Luck, H. J., Lund, B., McGuire, W. P., Neijt, J. P., Ozols, R. F., Parmar, M. K., Piccart-Gebhart, M. J., van Rijswijk, R., Rosenberg,

P., Rustin, G. J., Sessa, C., Willemse, P. H., and et al. Advanced epithelial ovarian cancer: 1998 consensus statements, Ann Oncol. *10 Suppl 1:* 87-92, 1999.

2. Ozols, R. F. Chemotherapy of ovarian cancer, Cancer Treat Res. *95:* 219-34, 1998.

3. Ozols, R. F. Paclitaxel plus carboplatin in the treatment of ovarian cancer, Semin Oncol. *26:* 84-9, 1999.

4. Folkman, J. and Ingber, D. Inhibition of angiogenesis, Semin Cancer Biol. *3:* 89-96, 1992.

5. Folkman, J. Angiogenesis and angiogenesis inhibition: an overview, Exs. *79:* 1-8, 1997.

6. Neufeld, G., Cohen, T., Gengrinovitch, S., and Poltorak, Z. Vascular endothelial growth factor (VEGF) and its receptors, Faseb J. *13:* 9-22, 1999.

7. Kim, K. J., Li, B., Winer, J., Armanini, M., Gillett, N., Phillips, H. S., and Ferrara, N. Inhibition of vascular endothelial growth factor-induced angiogenesis suppresses tumour growth *in vivo*, Nature. *362:* 841-4, 1993.

8. Witte, L., Hicklin, D. J., Zhu, Z., Pytowski, B., Kotanides, H., Rockwell, P., and Bohlen, P. Monoclonal antibodies targeting the VEGF receptor-2 (Flk1/KDR) as an anti-angiogenic therapeutic strategy, Cancer Metastasis Rev. *17:* 155-61, 1998.

9. Prewett, M., Huber, J., Li, Y., Santiago, A., W, O. C., King, K., Overholser, J., Hooper, A., Pytowski, B., Witte, L., Bohlen, P., and Hicklin, D. J. Antivascular endothelial growth factor receptor (fetal liver kinase 1) monoclonal antibody inhibits tumor angiogenesis and growth of several mouse and human tumors, Cancer Res. *59:* 5209-18, 1999.

10. Goldman, C. K., Kendall, R. L., Cabrera, G., Soroceanu, L., Heike, Y., Gillespie, G. Y., Siegal, G. P., Mao, X., Bett, A. J., Huckle, W. R., Thomas, K. A., and Curiel, D. T. Paracrine expression of a native soluble vascular endothelial growth factor receptor inhibits tumor growth, metastasis, and mortality rate, Proc Natl Acad Sci U S A. *95:* 8795-800, 1998.

11. Lin, P., Sankar, S., Shan, S., Dewhirst, M. W., Polverini, P. J., Quinn, T. Q., and Peters, K. G. Inhibition of tumor growth by targeting tumor endothelium using a soluble vascular endothelial growth factor receptor, Cell Growth Differ. *9:* 49-58, 1998.

12. Lin, P., Buxton, J. A., Acheson, A., Radziejewski, C., Maisonpierre, P. C., Yancopoulos, G. D., Channon, K. M., Hale, L. P., Dewhirst, M. W., George, S. E., and Peters, K. G. Antiangiogenic gene therapy targeting the endothelium-specific receptor tyrosine kinase Tie2, Proc Natl Acad Sci U S A. *95:* 8829-34, 1998.

13. Oku, T., Tjuvajev, J. G., Miyagawa, T., Sasajima, T., Joshi, A., Joshi, R., Finn, R., Claffey, K. P., and Blasberg, R. G. Tumor growth modulation by sense and antisense vascular endothelial growth factor gene expression: effects on angiogenesis, vascular permeability, blood volume, blood flow, fluorodeoxyglucose uptake, and proliferation of human melanoma intracerebral xenografts, Cancer Res. *58:* 4185-92, 1998.

14. Im, S. A., Gomez-Manzano, C., Fueyo, J., Liu, T. J., Ke, L. D., Kim, J. S., Lee, H. Y., Steck, P. A., Kyritsis, A. P., and Yung, W. K. Antiangiogenesis treatment for

gliomas: transfer of antisense-vascular endothelial growth factor inhibits tumor growth *in vivo*, Cancer Res. *59:* 895-900, 1999.

15. Fong, T. A., Shawver, L. K., Sun, L., Tang, C., App, H., Powell, T. J., Kim, Y. H., Schreck, R., Wang, X., Risau, W., Ullrich, A., Hirth, K. P., and McMahon, G. SU5416 is a potent and selective inhibitor of the vascular endothelial growth factor receptor (Flk-1/KDR) that inhibits tyrosine kinase catalysis, tumor vascularization, and growth of multiple tumor types, Cancer Res. *59:* 99-106, 1999.

16. Ramakrishnan, S., Olson, T. A., Bautch, V. L., and Mohanraj, D. Vascular endothelial growth factor-toxin conjugate specifically inhibits KDR/flk-1-positive endothelial cell proliferation *in vitro* and angiogenesis *in vivo*, Cancer Res. *56:* 1324-30, 1996.

17. Olson, T. A., Mohanraj, D., Roy, S., and Ramakrishnan, S. Targeting the tumor vasculature: inhibition of tumor growth by a vascular endothelial growth factor-toxin conjugate, Int J Cancer. *73:* 865-70, 1997.

18. Alon, T., Hemo, I., Itin, A., Pe'er, J., Stone, J., and Keshet, E. Vascular endothelial growth factor acts as a survival factor for newly formed retinal vessels and has implications for retinopathy of prematurity, Nat Med. *1:* 1024-8, 1995.

19. Benjamin, L. E. and Keshet, E. Conditional switching of vascular endothelial growth factor (VEGF) expression in tumors: induction of endothelial cell shedding and regression of hemangioblastoma-like vessels by VEGF withdrawal, Proc Natl Acad Sci U S A. *94:* 8761-6, 1997.

20. Jain, R. K., Safabakhsh, N., Sckell, A., Chen, Y., Jiang, P., Benjamin, L., Yuan, F., and Keshet, E. Endothelial cell death, angiogenesis, and microvascular function after castration in an androgen-dependent tumor: role of vascular endothelial growth factor, Proc Natl Acad Sci U S A. *95:* 10820-5, 1998.

21. Spyridopoulos, I., Brogi, E., Kearney, M., Sullivan, A. B., Cetrulo, C., Isner, J. M., and Losordo, D. W. Vascular endothelial growth factor inhibits endothelial cell apoptosis induced by tumor necrosis factor-alpha: balance between growth and death signals, J Mol Cell Cardiol. *29:* 1321-30, 1997.

22. Watanabe, Y. and Dvorak, H. F. Vascular permeability factor/vascular endothelial growth factor inhibits anchorage-disruption-induced apoptosis in microvessel endothelial cells by inducing scaffold formation, Exp Cell Res. *233:* 340-9, 1997.

23. Teicher, B. A., Sotomayor, E. A., and Huang, Z. D. Antiangiogenic agents potentiate cytotoxic cancer therapies against primary and metastatic disease, Cancer Res. *52:* 6702-4, 1992.

24. Teicher, B. A., Emi, Y., Kakeji, Y., and Northey, D. TNP-470/minocycline/cytotoxic therapy: a systems approach to cancer therapy, Eur J Cancer. *32A:* 2461-6, 1996.

25. Herbst, R. S., Takeuchi, H., and Teicher, B. A. Paclitaxel/carboplatin administration along with antiangiogenic therapy in non-small-cell lung and breast carcinoma models, Cancer Chemother Pharmacol. *41:* 497-504, 1998.

26. Olson, T. A., Mohanraj, D., and Ramakrishnan, S. *In vivo* neutralization of vascular endothelial growth factor (VEGF)/vascular permeability factor (VPF)

inhibits ovarian carcinoma-associated ascites formation and tumor growth, Int J Onc. *8:* 505-511, 1996.

27. Mohanraj, D., Olson, T., and Ramakrishnan, S. Expression of biologically active human vascular endothelial growth factor in yeast, Growth Factors. *12:* 17-27, 1995.

28. Gorski, D. H., Beckett, M. A., Jaskowiak, N. T., Calvin, D. P., Mauceri, H. J., Salloum, R. M., Seetharam, S., Koons, A., Hari, D. M., Kufe, D. W., and Weichselbaum, R. R. Blockage of the vascular endothelial growth factor stress response increases the antitumor effects of ionizing radiation, Cancer Res. *59:* 3374-8, 1999.

29. Teicher, B. A., Holden, S. A., Ara, G., and Northey, D. Response of the FSaII fibrosarcoma to antiangiogenic modulators plus cytotoxic agents, Anticancer Res. *13:* 2101-6, 1993.

30. Borgstrom, P., Gold, D. P., Hillan, K. J., and Ferrara, N. Importance of VEGF for breast cancer angiogenesis *in vivo*: implications from intravital microscopy of combination treatments with an anti-VEGF neutralizing monoclonal antibody and doxorubicin, Anticancer Res. *19:* 4203-14, 1999.

Table 1

Carboplatin and Anti-VEGF Antibody Combination Treatment Results in a More than Additive Anti-Tumor Response

	Fractional tumor volume[a]				
Day	Carboplatin	Anti-VEGF	Combined (expected)[b]	Combined (observed)	Expected/ observed[c]
22	0.649	0.879	0.570	0.241	2.363
40	0.598	0.722	0.432	0.190	2.268

[a] fractional tumor volume was obtained by dividing the mean volume of treated tumors by the mean volume of untreated PBS control tumors. All three individual experiments were pooled to determine the overall mean volumes

[b] expected combined effect if treatment modalities have additive activities. Obtained by multiplying the individual fractional tumor volumes of both treatments.

[c] fold increase over additive effect as determined by dividing the combined expected fractional tumor volume by the combined observed fractional tumor volume.

LEGEND

Fig.1

Differential Sensitivity of Tumor Cells versus Endothelial Cells to Carboplatin. The dose response of Carboplatin on endothelial cells (HUVEC) and human ovarian carcinoma cells (MA148) was determined by a non-radioactive cell viability assay (MTT). Values of medium control were considered as 100 % viability. Each point is a mean of triplicate cultures from a representative experiment. Error bars denote S.D. μ HUVEC, λ MA148.

Fig.2

Carboplatin Differentially Up-regulates VEGF Expression in Endothelial Cells. Endothelial cell cultures and human ovarian carcinoma cells were exposed to their respective TCID50 concentration of Carboplatin (0.7 μg/ml for MA148, 50 μg/ml for HUVEC) and conditioned medium was harvested. VEGF levels were measured by ELISA and normalized to cell number. A, 24 hour time point. B, 48 hour time point. □ no Carboplatin (PBS control), ν Carboplatin. Data are presented as means of triplicate cultures with standard deviation as error bars. * statistical significance as determined by the Student's t-test ($p < 0.038$ for all points).

Fig.3

Antibody to VEGF Potentiates the Inhibitory Activity of Carboplatin on Endothelial Cells. Cells were treated with their respective TCID50 concentration of Carboplatin (0.7 μg/ml for MA148, 50 μg/ml for HUVEC) and supplemented with purified anti-VEGF IgG or pre-immune control IgG (30 μg/ml). Forty-eight hours after treatment, cell

viability was measured by MTT assay. Absorbance associated with Carboplatin treatment alone was considered as 100 % inhibition. Results are expressed as % change in inhibition relative to Carboplatin treatment alone. ν anti-VEGF IgG treatment, □ pre-immune IgG treatment. Values represent the mean from the results of three independent experiments with standard errors. * statistical significance as determined by the Student's t-test ($p < 0.014$).

Fig.4

Antibody to VEGF Increases Apoptosis in Carboplatin Treated Endothelial Cells. HUVEC were treated with Carboplatin (50 μg/ml) and/or antibodies (50 μg/ml) and incubated for forty-eight hours. Specimens were then analyzed for apoptosis by a TUNEL assay as described in "Materials and Methods". Values represent the mean of three independent experiments with their respective standard errors. * statistical significance as determined by the Student's t-test ($p < 0.03$).

Fig.5

Carboplatin Specifically Up-regulates VEGF Expression in Tumor Vessels *In vivo*. On day ten after tumor implantation, mice were divided into two groups receiving i.p injections of either Carboplatin (32.5 mg/kg/dose) or PBS every three days for five doses. Animals were then sacrificed and tumor tissues were harvested. Sections were prepared and stained for VEGF and CD31 as described in "Materials and Methods". Shown are representative sections from the PBS control group (A, C and E) and from the Carboplatin treated group (B, D and F). A and B, immunohistochemical localization of

VEGF. C and D, staining for blood vessels with PE conjugated anti-CD31. E and F, co-localization of VEGF and CD-31 by merging respective images. Arrows indicate representative VEGF positive tumor blood vessels. Scale bar, 200 μm.

Fig.6

Antibody to VEGF Significantly Improves The Anti-Tumor Effect of Carboplatin. Human epithelial ovarian carcinoma (MA148) tumors were established by injecting athymic nude mice s.c. in the right flank with 2 x 10^6 tumor cells. Tumors were allowed to establish for ten days and animals were subsequently randomized and divided into treatment groups. Solid tumor growth was then monitored by caliper measurements as described in "Materials and Methods". ν PBS control, μ Carboplatin, λ Carboplatin + anti-VEGF IgG, π anti-VEGF IgG. A-C shows the results of three independent experiments (n = 4-6 animals per group per experiment). Data points show the mean tumor volume with respective standard error bars. D, summary of inhibition of tumor growth with the addition of anti-VEGF IgG or pre-immune control IgG to Carboplatin therapy. Results are expressed as mean tumor volumes relative to mean Carboplatin treated volumes ($V/V_{carboplatin}$). Two time points were chosen for analysis. Day 22 (end of Carboplatin treatment) and day 40 (end of antibody treatment). □ Carboplatin, ν Carboplatin + anti-VEGF IgG, ν Carboplatin + pre-immune IgG. * statistical significance as determined by Student's t-test ($p < 0.033$ for both values compared to Carboplatin alone treatment).

Fig.7

Carboplatin/Anti-VEGF Antibody Combination Treatment Results in Extensive Tumor Necrosis. MA148 tumor tissues were resected at the end of the treatment schedule (day 40), fixed, embedded in paraffin and sectioned onto slides. Representative H&E stained sections are shown. A, PBS control. B, Carboplatin. C, anti-VEGF IgG. D, Carboplatin + anti-VEGF IgG. E, Carboplatin + anti-VEGF IgG complete responder. Scale bar 100 μm for all samples.

Fig. 1

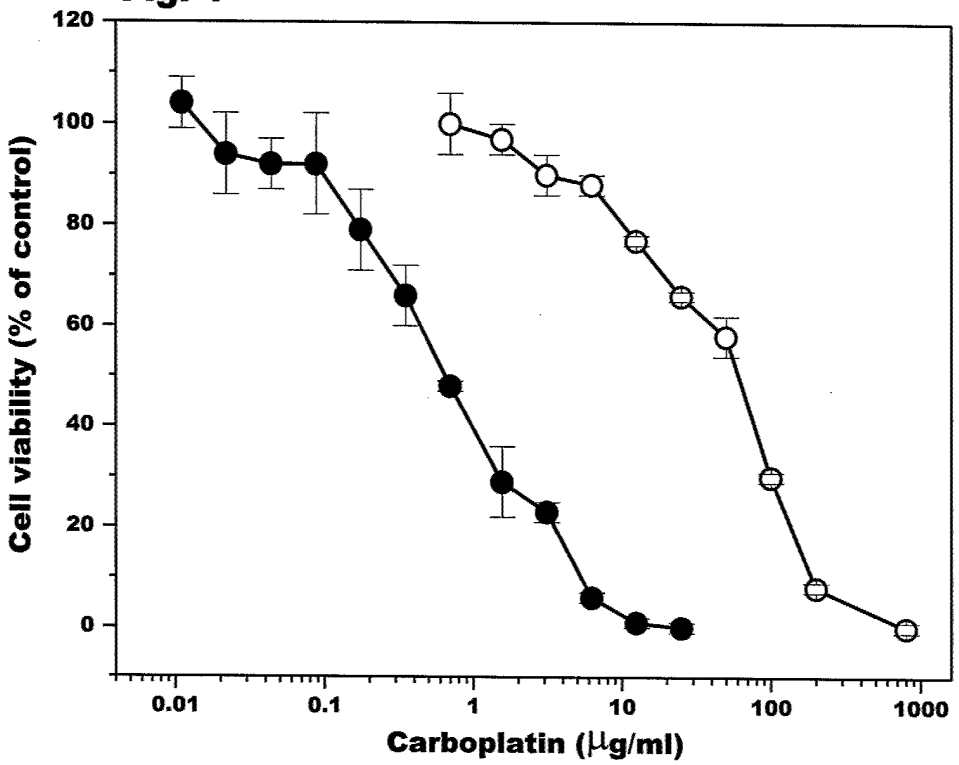
Cell viability (% of control)
120
100
80
60
40
20
0
0.01
0.1
1
10
100
1000
Carboplatin (μg/ml)

Fig. 2

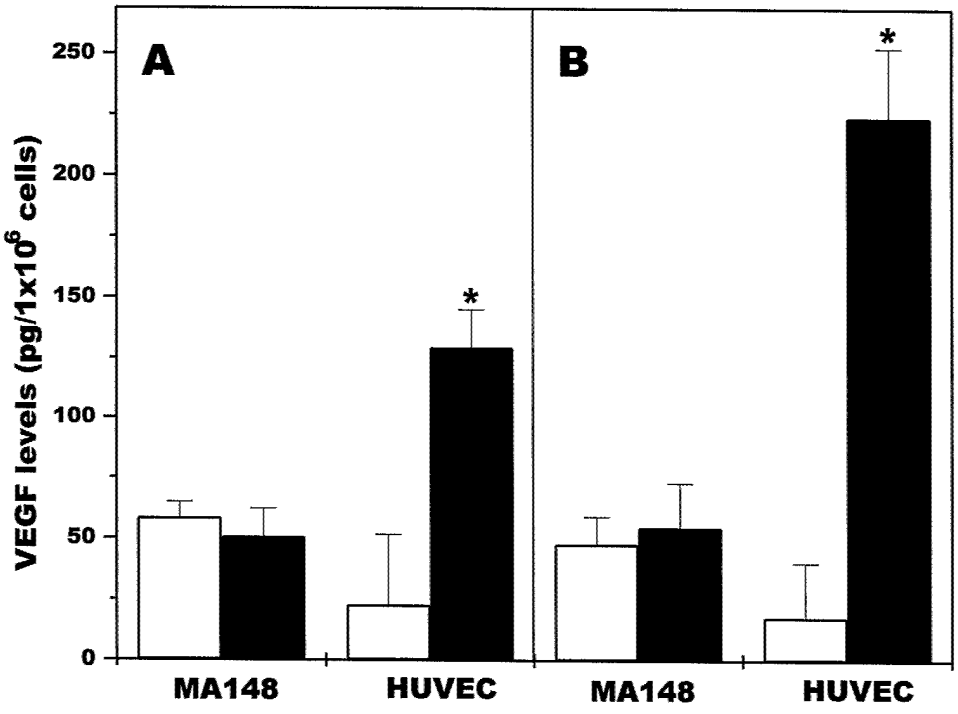
A
B
VEGF levels (pg/1x10^6 cells)
250
200
150
100
50
0
*
*
MA148
HUVEC
MA148
HUVEC

Fig. 3

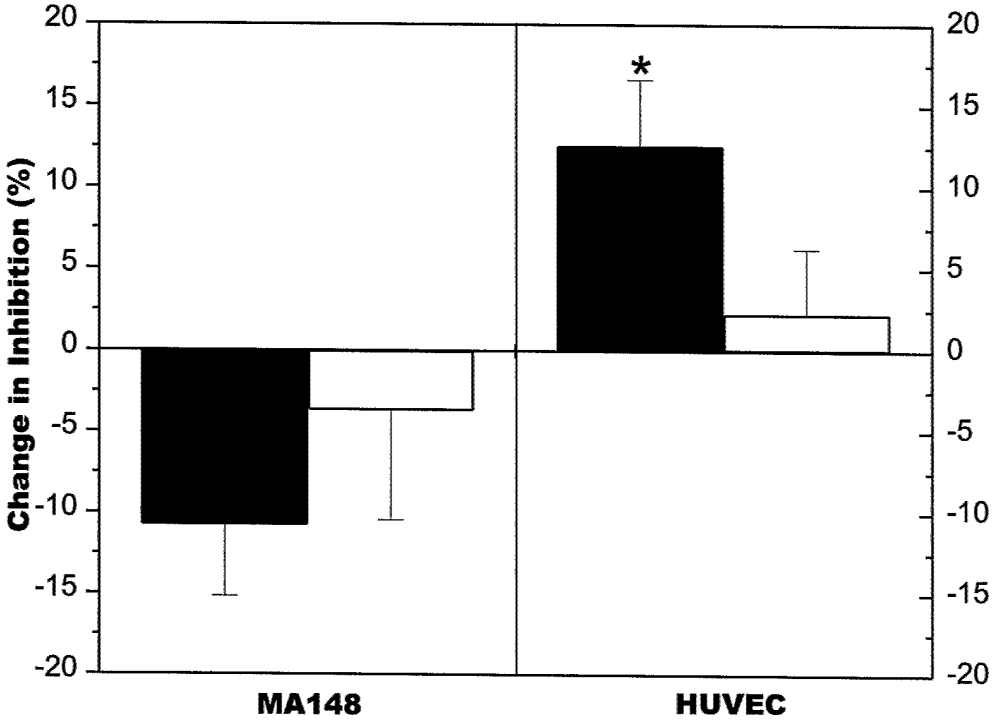

Fig. 4

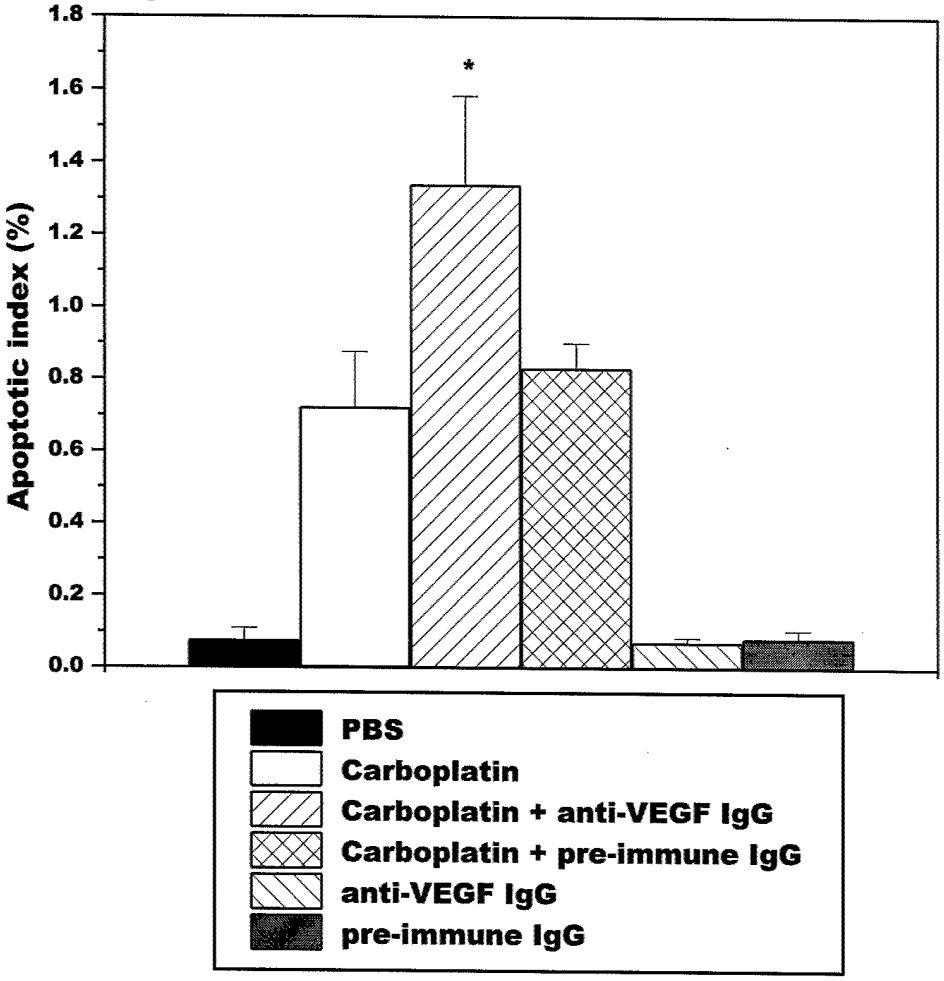
Apoptotic index (%)
1.8
1.6
1.4
1.2
1.0
0.8
0.6
0.4
0.2
0.0
*
PBS
Carboplatin
Carboplatin + anti-VEGF IgG
Carboplatin + pre-immune IgG
anti-VEGF IgG
pre-immune IgG

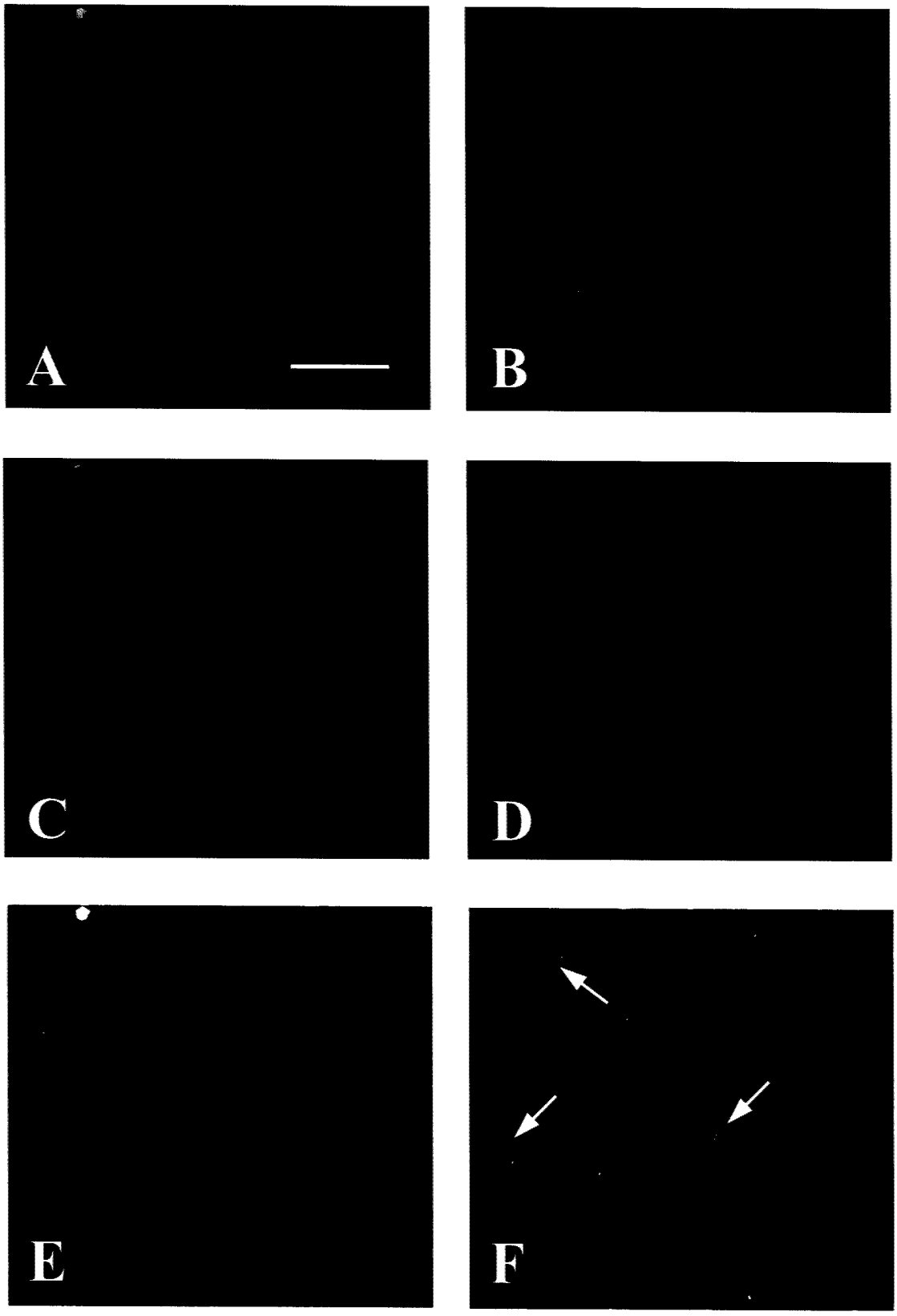

Figure 5

Fig. 6

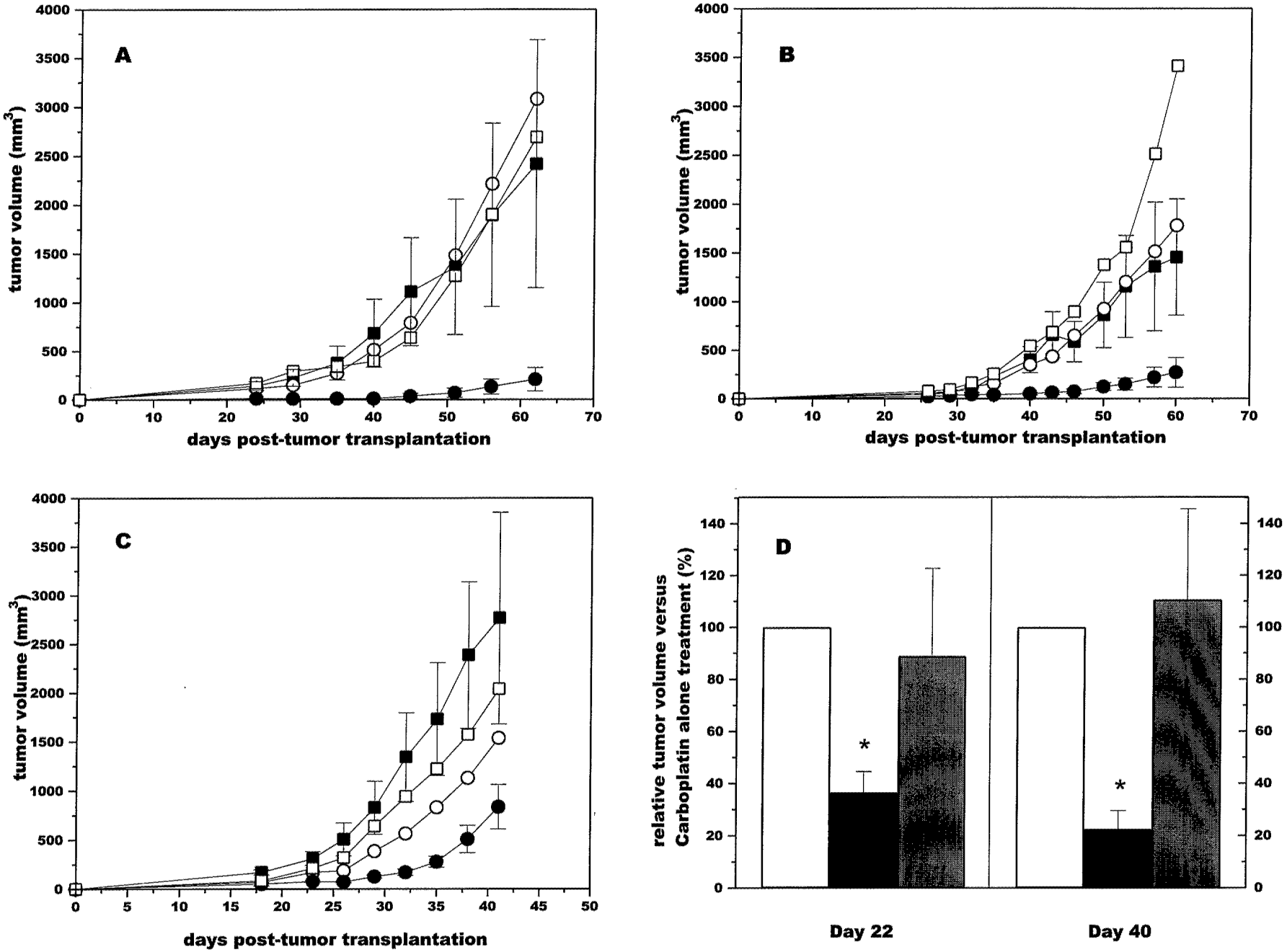
A
B
C
D
tumor volume (mm3)
days post-tumor transplantation
relative tumor volume versus Carboplatin alone treatment (%)
Day 22
Day 40
*

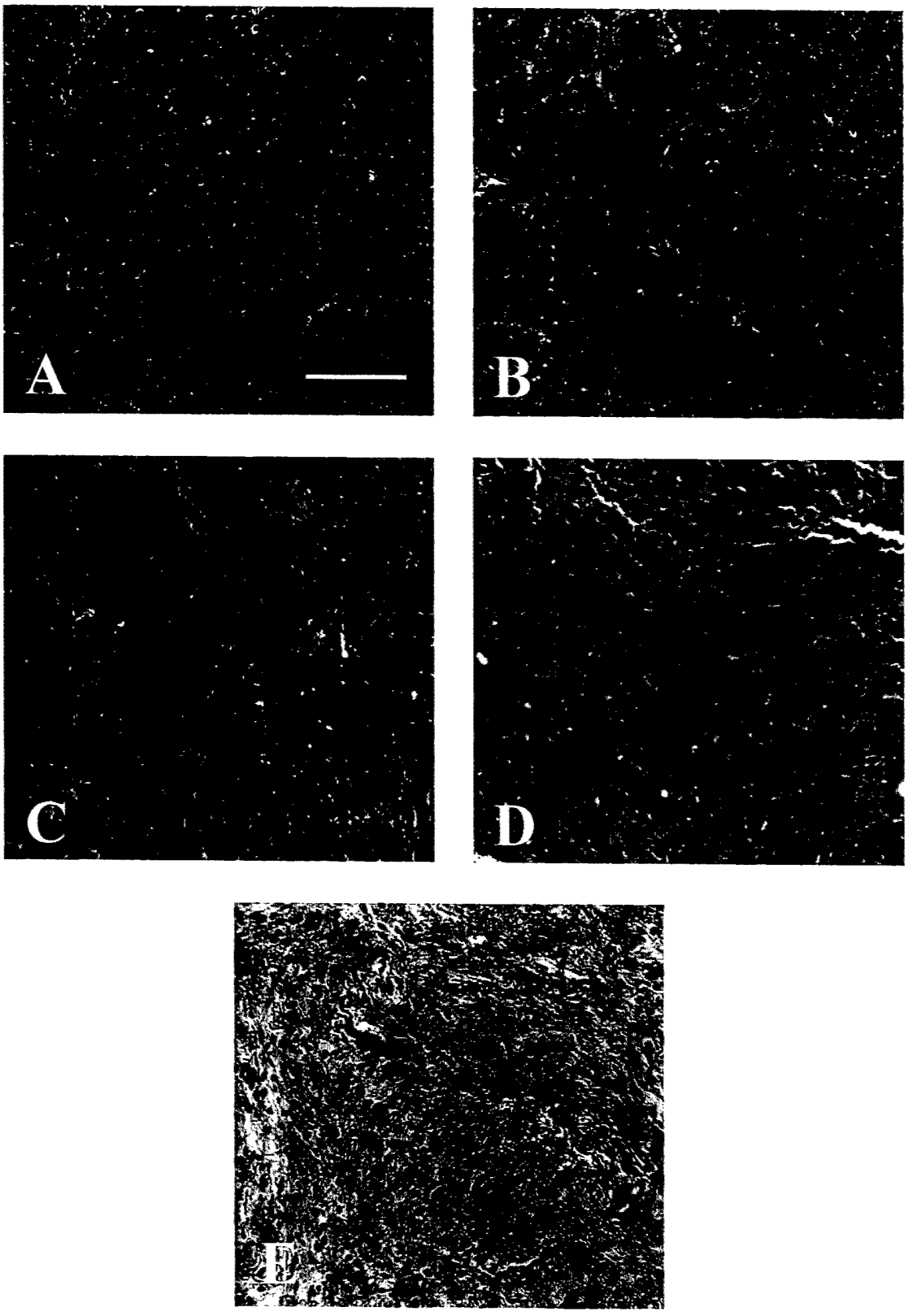

Figure 7

Keystone Meetin on Angiogenesis , Barniff, Alberta, CA 2002.

Substitution of A Single Amino Acid Residue in Human Endostatin Potentiates Inhibition of Ovarian Cancer Growth

Yumi Yokoyama[1] and S. Ramakrishnan[1,2,3]
[1]Department of Pharmacology, [2]Obstetrics and Gynecology, and [3]Comrehensive Cancer Center, University of Minnesota, Minneapolis, MN 55455

Endostatin, a proteolytically cleaved C-terminal fragment of collagen type XVIII, has previously been shown to inhibit tumor neovascularization and consequently, tumor growth.

During expression cloning of human endostatin, a mutant protein containing a substitution of proline to an alanine (P125A) was identified. Proline 125 (P125) is located immediately upstream to Asn-Gly-Arg (NGR) sequence. NGR containing peptides target tumor vasculature and inhibit endothelial membrane associated aminopeptidase N activity. Therefore, P125A endostatin was investigated for changes in its biological activity. P125A endostatin bound to endothelial cells more efficiently. Neither the native protein nor the P125A endostatin inhibited aminopeptidase N. P125A endostatin was more effective than the native endostatin in inhibiting endothelial cell proliferation. Furthermore, P125A mutation substantively improved the inhibition of ovarian cancer growth in athymic mice. These studies suggest that the region around P125 is important for the biological activity of endostatin. (Supported by a grant from DOD. DA/DAMD 17-99-1-9564)

#896 Cryptic proliferative and anti-proliferative domains contained within tissue plasminogen activator. Veronica A. Carroll, Roy Bicknell, Pat Price, and Adrian L. Harris. *Imperial Cancer Research Fund, Oxford, UK, and Hammersmith Hospital, London, UK.*

Isolated kringle domains of plasminogen, prothrombin and hepatocyte growth factor are anti-angiogenic whereas the intact molecules are not. Tissue plasminogen activator (tPA) contains two kringle structures with strong homology to those of plasminogen, as well as a finger (F), epidermal growth factor-like (EGF) and protease (P) domains. We investigated whether the kringle domains of tPA could also influence endothelial cell (EC) growth. We found that monoclonal antibody mediated blocking of the kringle 2 (K2) domain of endogenously secreted tPA increased EC proliferation four fold above control whereas antibodies to the other domains had no effect. Anti-K2 induced EC growth was blocked by both an antibody and a peptide to the finger module of tPA implicating this domain in mediating the EC proliferation observed. To investigate whether the K2 domain itself was inhibitory three types of K2 were obtained: i) recombinant K2 was expressed in the Pichia pastoris yeast expression system and purified by lysine-Sepharose affinity chromatography or ii) was obtained by limited elastase cleavage of a shorter fragment of tPA consisting of only the K2 and protease domains (K2P) followed by lysine-Sepharose purification or iii) K2P was used following protease inactivation with PMSF or PPACK. Exogenous addition of these isolated K2 fragments to human umbilical vein and dermal microvascular ECs resulted in significantly decreased basal growth and inhibited both bFGF and VEGF stimulated cell growth. These data suggest that tPA contains both pro- and anti-proliferative domains.

#897 Improved inhibition of tumor growth by genetic modification of endostatin with an NGR-motif. Yumi Yokoyama and S. Ramakrishnan. *University of Minnesota, Minneapolis, MN.*

Endostatin, a proteolytically cleaved C-terminal fragment of collagen type XVIII, has previously been shown to inhibit tumor neovascularization and consequently tumor growth. Early studies have shown that addition of an RGD (Arg-Gly-Asp) motif enhanced antiangiogenic activities of endostatin and potentiated antitumor activity. In this present study, we investigated additional genetic modification of endostatin with NGR(Asn-Gly-Arg)-motif. NGR motif as well as RGD-motif selectively localizes to tumor neovasculature. Aminopeptidase N (CD13), which is highly expressed on tumor vasculature, has been reported to be a target molecule of NGR peptide. Human endostatin has an internal NGR-motif at position 126-128. However native endostatin did not inhibit aminopeptidase N activity. This result suggests that the internal NGR-site is not accessible to aminopeptidase N. In contrast, construction of an additional NGR-motif to the amino-terminus of endostatin inhibited aminopeptidase N extracted from endothelial cells. NGR-motif enhanced endothelial cell binding to endostatin. NGR-modification resulted in greater inhibition of endothelial cell proliferation. As a consequence, modified endostatin was found to be more effective when compared to the native endostatin in inhibiting growth of human ovarian carcinoma and colon carcinoma transplanted into athymic nude mice. These studies demonstrate that human endostatin can be genetically modified to improve its ability to inhibit tumor growth.

#898 The *in vitro* bioactivity of human endostatin dimer is heparin dependent. Andrew Robert Clamp, Fiona Blackhall, Catherine Merry, Audrey Henrioud, Gordon Jayson, Kashi Javaherian, Judah Folkman, and Jon Gallagher. *CRC Department of Medical Oncology, Christie Hospital, Manchester, UK, and Department of Surgery, Childrens Hospital, Harvard Medical School, Boston, MA.*

Angiogenesis, the formation of new blood vessels is essential for sustained tumor growth and metastasis. Many pro- and anti-angiogenic growth factors require the presence of cell surface heparan sulfate (HS) for their bioactivity. Endostatin is an endogenous inhibitor of angiogenesis that is released by the proteolytic cleavage of the C-terminal domain of collagen XVIII. It has been demonstrated to have heparin affinity and site-directed mutagenesis of its primary heparin-binding epitope significantly reduces its ability to inhibit basic fibroblast growth factor-induced angiogenesis in the chick chorioallantoic membrane assay. (Sasaki et al. 1999 EMBO J 18:6240-8). In this study, we have demonstrated a direct inhibitory effect of heparin on the migratory bioactivity of an artificial dimeric form of endostatin (HED) that closely approximates to the arrangement of endostatin in collagen XVIII (Kuo et al. 2001 J Cell Biol 152:1233-46). When bovine aortic endothelial cells are plated on Matrigel, an extracellular matrix substitute, they spontaneously aggregate into capillary-like tubules. These disaggregate when incubated with HED and the cells acquire a scattered phenotype. Endostatin monomer (HEM) inhibits this disaggregation. The addition of heparin at concentrations above 1μg/ml also prevents disaggregation in a dose-dependent manner and acts synergistically with HEM. Using size- fractionated oligosaccharides derived from tinzaparin, a commercially available low molecular weight heparin preparation, we have shown that although all fragments from dp4 to dp24 have bioactivity, longer oligosaccharides are more potent. Preliminary experiments also show that inhibition of disaggregation is seen with heparan, dermatan and chondroitin sulfates, although none of these glycosaminoglycans are as potent as heparin. HED has also been demonstrated to induce a scattered phenotype in wild-type Chinese Hamster Ovary (CHO) cells plated on Matrigel which is not seen in CHO 745 cells that do not express cell surface HS. Preliminary data indicates that a partial restoration of HED responsiveness in these cells can be obtained by co- incubation with exogenous heparin. In summary, present the first *in vitro* evidence of a biological interaction between heparin a endostatin in endothelial and non-endothelial cells.

#899 Suppression of angiogenesis and tumor growth by K1-5, a nov angiostatin-related inhibitor. Nilna Veitonmäki, Renhai Cao, and Yihai Ca *Karolinska Institute, Stockholm, Sweden.*

Angiostatin is a potent angiogenesis inhibitor, which includes the first fc kringle modules (kringle 1-4) of plasminogen. This angiogenesis inhibitor seems be a potent tumor suppressor. Because it specifically targets the proliferati endothelial cell compartment, angiostatin is less likely to cause side effec including immunosupression, bone marrow suppression and gastrointestir symptoms. However, potential therapeutic application of this angiogenesis inhi itor for a large number of cancer patients can become problematic althou angiostatin has entered into the early phase of clinical trial in a group of sm number of patients. The disadvantages of angiostatin protein therapy incluc administration of large amounts of protein, repeated injections, transmission infectious particles of protein preparations, high costs for manufactures and f patients. In order to overcome these problems, we have identified a more pote endogenous angiogenesis inhibitors, namely kringle 1-5 (K1-5) of plasminoge which displays approximately 100-fold greater effect than angiostatin on su pression of angiogenesis and tumor growth. Our results show that proteolytica released K1-5 from human plasminogen inhibits capillary endothelial cell pro eration, corneal neovascularization in a mouse angiogenesis model, and ne blood vessel growth in the chicken embryo chorioallantoic membrane. In a mou fibrosarcoma tumor model, K1-5 suppresses primary tumor growth by appro mately 60% at a low dose of 2 mg/kg once daily, whereas angiostatin (K1-4) at t same dose does not inhibit tumor growth. Thus, K1-5 is more potent angioge esis inhibitor than angiostatin and may become more useful and realistic th angiostatin for potential clinical treatment of cancer patients and other angioger diseases including diabetic retinopathy.

#900 Development of recombinant human endostatin in SOS to suppo clinical subcutaneous administration. William E. Fogler, Zachary Yim, To Chen, Beth Chen, Nilima Leffers, Carolyn Sidor, Anne H. Fortier, David Jacksc Stacy M. Plum, Emily Kough, and B. Kim. Lee Sim. *EntreMed, Inc, Rockville, M.*

To facilitate the studies of rhEndostatin protein in the clinic, beyond curre levels, a new formulation of rhEndostatin protein has been developed that allo for concentrations that are approximately 16 fold greater (130 mg/mL) than t current clinical formulation (8 mg/mL). The new formulation uses sucrose oct sulfate (SOS) as the excipient. The SOS formulation of rhEndostatin was th compared with the citrate-phosphate formulation that is currently used in clinic trials, for potency, pharmacokinetics, and safety. The biological activity ar relative potency of rhEndostatin protein formulated as SOS was statistica indistinguishable from the current formulation of rhEndostatin protein as a sessed by inhibition of experimental metastases in mice. The nonclinical pha macokinetic behavior of rhEndostatin protein formulated as SOS following su cutaneous injection to cynomolgus monkeys was found to be similar to th current clinical formulation of rhEndostatin protein, with an approximate bioava ability of 100%. A study was conducted in cynomolgus monkeys to evaluate th safety of rhEndostatin protein SOS formulation after subcutaneous administra tion. This study concluded that rhEndostatin protein formulated in SOS was we tolerated when administered subcutaneously as high as 600 mg/m²/day for 2 days. The single notable histologic observation in this study was a local irritatic at the injection site consistent with chronic-active inflammation and manifestin as hemorrhage, inflammation of the subcutis, and perivasculitis. Although th study did not have a subcutaneous SOS control group, these findings we similar to those in previous toxicologic assessments of rhEndostatin protein in th current clinical formulation. The NOAEL of rhEndostatin protein in SOS of rhE dostatin protein after subcutaneous injection was 600 mg/m² daily. Results fro these studies demonstrate the biologic equivalence of rhEndostatin protein fo mulated as SOS to the rhEndostatin protein formulated in citrate-phospha buffer. The results also support the introduction of this formulation into clinic studies as a subcutaneous injection.

#901 2-Methoxyestradiol sulfamates are potent anti-cancer agents. Mik John Reed, Simon Newman, Atul Purohit, Bindu Malini, Mat Leese, Bertrar LeBlond, David Bennetto, Lawrence Woo, and Barry Potter. *Imperial College, S Mary's Hospital, London, UK, and University of Bath, Bath, UK.*

The endogenous estrogen metabolite 2-methoxy-estradiol (2-MeOE2) inhibi the proliferation of a wide range of malignant cells as well as angiogenesis. In th study we have synthesized the 3-O-monosulfamate (2-MeOE2MATE) and 17-O-bis-sulfamate (2-MeOE2bisMATE) derivatives of 2-MeOE2 and compare their potencies as inhibitors of breast cancer cell growth *in vitro* and angiogenesis In human MDA-MB-231 breast cancer cells IC_{50}s for the inhibition of cell growt were 4.5μM, 0.8μM and 0.3μM for 2-MeOE2, 2-MeOE2MATE an 2-MeOE2bisMATE respectively. Flow cytometric analysis of propidium iodid stained cells revealed that the ability of the sulfamoylated derivatives, at 1μM, t induce irreversible G_2/M arrest of the cell cycle, and subsequent cell death, wa much greater than for 2-MeOE2. The anti-angiogenic potential of these com pounds was examined by testing their ability to inhibit the proliferation of huma vascular umbilical endothelial cells (HUVECs) and the growth of tubules in

#4572 Patterns of gene expression in ovarian cancer cells treated with Epothilone B. Dineo Khabele, Weija Zhang, Sima Solaimanzadeh, Susan Horwitz, Carolyn Runowicz, and Raju Kucherlapati. *Albert Einstein College of Medicine, Bronx, NY, and Harvard Medical School, Partners, Boston, MA.*

Epothilone B (EpoB) is a non-taxane chemotherapeutic agent that binds to microtubules and induces cell cycle arrest and apoptosis. Mechanistically, it is similar to Taxol, but it has the advantage of being active in Taxol-resistant cells expressing p-glycoprotein, the multidrug resistance transporter. Our goal was to investigate mechanisms of sensitivity to EpoB in an ovarian cancer cell line, SKOV3. We utilized cDNA microarrays encompassing 9,216 human sequences. We treated SKOV3 cells with EpoB, or with media minus drug as a control (C), and harvested cells at time points over a 24-hour period. Each time point was analyzed in 4 independent experiments. Statistical and cluster analyses were used to evaluate the results. Genes altered in expression by EpoB were also characterized as to function. There was a recruitment of 70 genes into the EpoB response by 8 hours, which expanded to 133 genes by 24 hours. Most genes were related to apoptosis, signal transduction and cellular transport. Selected genes such as cytochrome c oxidase, caspases, STAT5B and several unknown ESTs are being examined in detail using real-time, quantitative RT-PCR. Cluster analysis demonstrated unique patterns of gene expression at each time point. Our data suggest that clusters of similarly expressed genes may be potential molecular markers of EpoB treatment leading to cell death. Additional evaluation may reveal novel mechanisms of drug resistance to epothilones.

#4573 An aminoglycoside antibiotic, Geneticin, can inhibit the growth of a HER-2 positive ovarian cancer in SCID mice model. Timothy T. C. Yip, C. S. Kwok, F. F. So, W. H. Lau, K. L. Leung, W. K. Cheung, W. S. Ma, and R. K. K. Ngan. *Clinical Oncology Department, Queen Elizabeth Hospital, Kowloon, Hong Kong, and Department of Optometry and Radiography, Hong Kong Polytechnic University, Kowloon, Hong Kong.*

Tetracycline is a safe and inexpensive antibiotic (less than US$1 per capsule) that has been used for decades. Recent findings of this antibiotic in preventing bone metastasis of breast and prostate cancers in mice probably through the inhibition of matrix metalloproteinase activity (Duivenvoorden et al., Invasion metastasis, 17(6): 312-322, 1997) has rekindled its interest for cancer treatment. Tetracycline can inhibit protein synthesis by binding to 30S ribosomal RNA. Using an aminoglycoside antibiotic, Geneticin (G418), which is commonly used for DNA transfection study and has the same mechanism of action as tetracycline, we reported in this paper its *in vivo* growth inhibition effect in a HER-2 positive ovarian cancer cell line, SKOV-3 in SCID mice model. In the first series of experiments, Geneticin at a concentration of 30, 125 and 500 micrograms/ml or saline were concurrently injected intramuscularly onto the trunk of the SCID mice together with 2 millions SKOV-3 cells. Tumor growth was completely inhibited in mice by 125 and 500 micrograms/ml of Geneticin at day 45 after injection. There was 83% reduction of tumor mass (or a growth delay of 32 days) at 30 micrograms/ml when compared with the saline control. In contrast, only injection of Tetracycline at a concentration of 500 micrograms/ml but not at 30 or 125 micrograms/ml resulted in significant tumor mass reduction. To further investigate the cytotoxic effect of Geneticin, SKOV-3 tumor was grown to an average size of 76 mm3 (SD 42 mm3) before Geneticin was injected. Reduction of tumor mass of 30%, 42% and 67% in a concentration dependent manner were respectively found at 30, 125 and 500 micrograms/ml when compared with the saline control. Further findings in the extent of apoptosis and the inhibition on distant spread of the tumor will be discussed. The tumor growth inhibition effect exerted by this antibiotic opens up an advantageous possibility in making use of this inexpensive agent at a cost even affordable in the developing countries as adjuvant for treating ovary, breast and prostate cancers in conjunction with other conventional treatment modalities.

#4574 Transfection of ovarian cancer cells with mutated human endostatins suppresses tumor growth. Indira V. Subramanian, Yumi Yokoyama, Rahel Ghebre, Blair Harkness, and S. Ramakrishnan. *University of Minnesota, Minneapolis, MN.*

The inhibitory effect of ovarian cancer cells transfected with mutated endostatins was evaluated in-vivo in a mouse model. Previous studies in our laboratory have shown that a point mutation (Pro to Ala) at position 125 (P125A) has improved antiangiogenic activities compared to the native protein. Pro125 precedes Asn-Gly-Arg (NGR) sequence in human endostatin, which is known to bind endothelial aminopeptidase-N. P125A endostatin was further modified to incorporate an Arg-Gly-Asp sequence at the carboxyl terminus. Mutated endostatin cDNAs were cloned into eukaryotic expression vectors with IgG kappa light chain signal sequence. MA-148, human ovarian cancer cells were transfected with mutated endostatin constructs using DOTAP liposomes. Clones of MA-148 cells expressing endostatin at 0.5 to 10 ng/ml as measured by ELISA and confirmed by western blotting were selected for further studies. Conditioned media collected from endostatin secreting cells inhibited HUVEC proliferation very efficiently. Transfected MA-148 cells were then injected into athymic nude mice subcutaneously. Tumor cells transfected with vector alone served as a control. All the transfected clones had near identical growth curve *in vitro*. Vector transfected cells formed tumors readily. In contrast, MA 148 cells expressing either the P125A endostatin or endostatin-RGD showed suppression of tumor growth for about 50 days. At this time point the vector control showed a mean tumor volume of 300 mm3. By day 64, control mice showed a mean tumor volume of 1600 mm3 wher as the mutant endostatin transfected cells showed a mean tumor volume of 20 mm3. Ovarian tumor cells harvested from mice on day sixty-seven showe continued secretion endostatin albeit at a lower levels when compared to th original clone. Serum samples collected from mice on day 64 showed presenc of endostatin. Histopathological and immunocytochemical localization of CD-3 showed lower vessel density in the mutated endostatin secreting tumors whic are surgically removed at the end of the experiment. Finally, real-time PCR wa used to determine whether compensatory secretion of proangiogenic facto such as VEGF could play a role in overcoming the inhibitory effects of mutate endostatin *in vivo*.

#4575 The establishment of xenograft models from osteosarcoma san ples and their growth inhibition by ET-743. Bethanne D. Mazza, Rui Yan Rebecca S. Sowers, Paul A. Meyers, John H. Healey, Andrew G. Huvos, Glynn Faircloth, Jose Jimeno, and Richard G. Gorlick. *Memorial Sloan Kettering Canc Center, New York, NY, PharmaMar USA, Inc, Cambridge, MA, and PharmaMa S.A., Madrid, Spain.*

Several high-grade osteosarcoma patient-derived tumors have been esta lished as xenograft models in SCID mice. Both cultured and fresh tissue sampl were subcutaneously injected into mice. Each tumor was passaged in serial mi until its growth was reproducible. Cytogenetics and comparative genomic hybr ization, as well as, routine staining were performed to further characterize t tumors. Prior to and following passage in SCID mice, the tumors were capable proliferation in cell culture. *In vitro* cytotoxicity assays were completed for each the agents being tested. An estimation of the maximum tolerated dose of ea drug was made. Three different osteosarcoma xenografts were used. For ea tumor, four groups consisting of six mice each were treated with Phosph Buffered Saline (PBS) (as a control), Trimetrexate with simultaneous Leucovc (TMTX/LV)(40mg/kg, twice daily for 10 days), Trastuzumab (20mg/kg, tw weekly for 3 weeks) or Ecteinascidin-743 (ET-743)(0.1mg/kg twice week fo doses). Drug treatment was begun one week after tumor implantation or when t tumors reached approximately 0.5cm in diameter. Each animal was weighed a the tumor measured before, during and following treatment. Of the agents test the greatest growth inhibition was observed with ET-743. At approximately th weeks the PBS control averaged 1.2cm in size versus Trastuzumab at 1c TMTX/LV at 0.95cm, and ET-743 at 0.7cm. At the doses used, ET-743 was a associated with the greatest animal weight loss. PBS treated animals weighed average of 20g while the Trastuzumab weighed 19.5g; TMTX/LV 18g and ET-7 was 15g. Further experiments are being conducted to determine if reduced dos of ET- 743 can still result in marked tumor growth inhibition without toxic Additional xenograft models for preclinical evaluation of new agents for oste sarcoma have been developed and the results obtained thus far suggest ET-7 has activity against osteosarcoma. Further preclinical and clinical studies warranted.

#4576 Specific inhibition of MLL fusion gene leukemias by the heat sho protein inhibitors Herbimycin A and 17-allylamino-17-demethoxygeldanar cin. Qing Yao, Wendy Hudson, Marnie Taylor, and John H. Kersey. *Universit Minnesota Cancer Center, Minneapolis, MN.*

MLL fusion gene leukemias, especially infant MLL-AF4, are resistant to st dard chemotherapy and candidates for novel therapies. A screen of poss novel agents was undertaken of several benzoquinone ansamycins, incluc Herbimycin A (HA) and 17-allylamino-17-demethoxygeldanamycin (17-A These agents are known to specifically bind to heat shock protein 90, inh activity and result in the decreased activity of signal transduction proteins, ste receptors, cell cycle kinases, transcription factors and p53. We have designe *vitro* cell proliferation studies to evaluate these agents in human and murine M fusion gene leukemia cell lines. The 50% inhibitory concentration (IC50) determined in a Cell-Titer96 assay. Extensive studies were done with the prc type agent, HA. Human MLL-AF4 leukemia cell lines had IC50 of 40nM (SEM and 65nM (RS 4:11) with HA; phenotype-matched control cell lines KM3 and B were about 11 times less sensitive (IC50 of 390nM and 1000nM respectively). human MLL-AF9 leukemia cell line, Molm13, had an IC50 of 25nM with HA; phenotype matched control cell line, U937, was 300 times less sensitive with IC50 of 7800nM. A murine MLL-AF9 leukemia cell line, 4166, that we h recently established was sensitive to HA with IC50 of 57nM while phenot matched control cell lines were 6 times less sensitive with 350nM for Baf3 1000nM for 32Dc13. Extensive studies were also carried out with the clinic better tolerated 17-AAG, now in clinical trials in solid tumors. Both MLL-AF4 MLL-AF9 cell lines were very sensitive to 17-AAG (RS 4:11, 700nM; SEM 350nM; Molm13, 31nM; 4166, 60nM) compared to control cell lines (K 2200nM; TE8, 2100nM; U937, 4500nM; Baf3, 430nM; 32Dc13, 350nM). Th results show that HA and 17-AAG specifically inhibit proliferation of MLL-AF4 MLL-AF9 fusion gene leukemias with IC50's that are potentially useful for ther for MLL fusion gene leukemias. 17-AAG will be tested further in pre-clinical *in* and mechanistic studies of human leukemia.

ence in cytotoxic activity of NK-92 and transduced NK-92-scFv(FRP5)−ζ cells towards ErbB2 negative targets was found. In contrast, even at low effector to target ratios NK-92-scFv(FRP5)−ζ cells specifically and efficiently lysed Er bB 2 expressing tumor cells of various origin that were completely resistant to cytolytic activity of parental NK-92. Similarly, ErbB2-positive primary breast cancer cells isolated from pleural effusions of patients with recurrent disease were selectively killed by NK-92-scFv(FRP5)−ζ cells. Our results demonstrate that efficient retargeting of NK-cell cytotoxicity can be achieved, and might allow the generation of potent cell-based therapeutics for the treatment of ErbB2 expressing malignancies.

#4797 Murine monoclonal anti-idiotype antibodies as surrogate antigens for 19A211, a sialylated carbohydrate antigen associated with superficial bladder cancer. Nancy Frenette, Alain Bergeron, Helene Larue, and Yves Fradet. *Centre de recherche, Hotel-Dieu de Quebec, CHUQ, Quebec, QC, Canada.*

Bladder cancer offers a unique opportunity to investigate cancer vaccines. Up to 75% of primary bladder tumors are superficial and, although treated effectively by transurethral surgery, recurrences occur in 60% of patients. Moreover, these tumors respond well to non-specific immunotherapy using BCG. Vaccines based on bladder tumor-associated antigens could be used to prevent recurrence of this disease. Monoclonal antibody (mAb) 19A211 reacts with an antigen that is expressed on about 70% of superficial bladder tumors. We previously showed that mAb 19A211 reacts with a bladder cancer-associated sialylated carbohydrate epitope present on a group of protein including a glycoform of CEA. Its expression is restricted to tumor cells with the exception of superficial umbrella cells of normal bladder in 25% of individuals. The aim of this study was to produce a murine monoclonal anti-idiotype antibody. BALB/C mice were immunized with mAb 19A211 conjugated to Keyhole Limpet Hemocyanin in presence of QUIL-A adjuvant. Hybridoma production resulted in 1478 clones of which 26 reacted with 19A211 and no other control antibodies. In inhibition assays, 14 of the 26 clones inhibited the binding of mAb 19A211 to its antigen expressed on MGH-U3 bladder cancer cells. This suggests that these antibodies can mimic the natural 19A211 antigen. The potential of these surrogate antigens to induce, in allogeneic mice and rabbits, a response against superficial bladder tumors will be discussed.

#4798 Comparison of bispecific antibodies for pretargeted delivery of small molecules to tumors. Marianne K. Hayes, Hong Ma, Kim J. Consolino, Richard P. Tomko, Ching Y. Wang, Hans J. Hansen, David M. Goldenberg, and Zhengxing Qu. *Immunomedics Inc, Morris Plains, NJ.*

Bispecific antibodies (bsAbs) with one specificity for a tumor associated antigen and another for a hapten are employed in a versatile two-step pretargeting system for radioimmunodetection (RAID) and radioimmunotherapy (RAIT). In this system, the radionuclides are directed to the tumor sites by high-affinity binding of divalent hapten molecules to the tumor bound bsAbs. The radiolabeled hapten molecules by themselves, usually low molecular weight peptides, are rapidly cleared from the blood and almost exclusively excreted in the urine, resulting in little, if any, cytotoxicity to normal tissues. The efficacy of this system is dependent on the pharmacokinetics of the bsAbs, including tumor penetration, non-tumor tissue retention and blood clearance. These properties are influenced by the structure and binding properties of the bsAbs. To determine the optimal configuration of bsAbs for RAID and RAIT, various forms of anti-CEA and anti-In-DTPA bsAbs were constructed by genetic engineering and transfection. These bsAbs differ in their sizes, valencies to CEA and/or In-DTPA, and the ability to interact with Fc receptors. Their *in vivo* biodistribution and pretargeting properties were investigated. All of the bsAbs showed specific tumor targeting in mice bearing human colonic tumors. The time needed for blood clearance (to a level lower than ~0.1% ID/g) was proportional to the size of bsAbs, i.e. Fab-scFv (~75 kDa) < Fab-$(scFv)_2$ (~100 kDa) < IgG-$(scFv)_2$ (~200 kDa), at about 2, 3, and 7 days, respectively. A point mutation in the Fc domain that diminishes the interaction with FcnR significantly accelerated the blood clearance of IgG-$(scFv)_2$ to 3-4 days. Tumor uptake of the bsAbs with two binding sites for CEA was generally higher than that of monovalent bsAbs. In the pretargeting system, ^{99m}Tc-In-DTPA peptide was administered when a pre-set tumor-to-blood ratio of the pretargeted bsAb had been achieved (5-10 or higher). The radiolabeled peptide was specifically directed to tumor sites. BsAbs with two binding sites for In-DTPA directed more radiolabeled peptide to the tumor sites. However, trace amount of IgG-$(scFv)_2$ in the circulation trapped the In-DTPA peptide, resulting in poor tumor-to-non tumor ratios. The mutation in the Fc domain minimized the trapping and improved peptide targeting. Further studies are in progress to optimize the configuration of the bsAbs for tumor localization and peptide targeting. (Supported in part by SBIR grant CA81760 from the NIH to HJH.)

#4799 Single chain antibodies (scFv) isolated from a phage display library as a tool to identify unique gp96 associated peptide antigens. Ashok T. Badithe, Yuangen Chen, Abraham Mittelman, and Raj Tiwari. *New York Medical College, Valhalla, NY.*

Protective immunity by purified preparations of the heat shock protein, gp96, is attributed to associated peptides. Isolation of these peptides has been a challenge, although tumor rejection property has been linked to the gp96-peptide complex as neither the peptides nor gp96 alone can confer protective immunity. We have been developing scFv reagents from a synthetic combinatorial phage display library that can identify the unique species of tumor associated gp96-peptide complexes in a complex pool of non-tumor and tumor specific gp96-peptide complexes. We utilized the VSV8 peptide, RGYVYQGL, and gp96 purified from a rat tumor to validate our hypothesis. The peptides at 1:50 molar ratio of gp96 to peptide were loaded on to purified preparation of gp96. In our experiments purified gp96 was not stripped of their tissue specific peptides. VSV8 peptide loaded gp96 and unloaded gp96 were used to differentially pan a synthetic combinatorial phage display antibody library. After four rounds of successive panning and amplification, we screened the soluble scFvs for reactivity to VSV peptide alone, VSV-peptide-gp96 complexes and gp96 alone. We isolated scFvs that reacted specifically to gp96-VSV peptide complexes and did not react to gp96 or peptide alone. These scFvs had distinct CDR3 sequences suggesting that different groups of antibodies can be generated that recognize specific sub-species of gp96-peptide complexes. We are currently extending these preliminary feasibility studies to utilize the scFvs from phage display antibody libraries to identify and better define the immunogenic subspecies of tumor specific gp96-peptide complexes.

#4800 Construction and characterization of bispecific minibody structures to enhance anti-tumor immune response. Lillian S. Shahied, Eva M. Horak, Heidi H. Simmons, and Louis M. Weiner. *Fox Chase Cancer Center, Philadelphia, PA.*

In recent years monoclonal antibody therapy has become a more popular and widely accepted treatment for a variety of diseases such as cancer. Antibody-dependent cellular cytotoxicity (ADCC) may be one of the mechanisms by which clinically effective antibodies such as rituximab and trastuzumab exert their therapeutic effects. In order to improve this anti-tumor mechanism of action, a series of bispecific antibodies was constructed in which two single-chain antibody fragments (scFvs) with different targets (the tumor antigen HER2/*neu* and the leukocyte FcγRIII receptor) were joined by a fifteen amino acid linker. Several mutants were created with varying affinities for HER2/*neu* while linked to the same anti-FcγRIII scFv. The results from these studies indicated that an increased affinity for HER2/*neu* correlated with an increased ability of the bispecific antibody to potentiate ADCC. It was also confirmed that activation of leukocytes did not occur in the absence of tumor cell engagement; this property minimizes unwanted leukocyte activation, and attendant host toxicity, in the absence of tumor engagement. However, the level of tumor cell lysis observed using these novel scFv-based reagents was attenuated when compared with the cytotoxicity seen with a full-length bispecific antibody. This diminution in activity could be due to the reduced wingspan or flexibility of the $(scFv)_2$ molecules in comparison to a full-length IgG. Accordingly, we are creating bispecific antibodies that are larger and possess an increased flexibility but still retain the same specificity. A bispecific minibody was constructed in which the IgG1 CH3 constant domain serves as the oligomerization domain and is attached to the anti-FcγRIII and the anti-HER2/*neu* scFvs via 19 and 29 amino acid linkers, respectively. This molecule can be expressed in mammalian cells from a dicistronic vector and has been purified using sequential affinity purification techniques. Analysis by surface plasmon resonance shows that the bispecific minibody can bind to HER2/*neu* and FcγRIII, both individually and simultaneously. Furthermore, cytotoxicity studies show that the minibody can induce tumor cell lysis at 40 nM concentration to the same extent as a related IgG bispecific antibody. A trimeric, bispecific minibody has also been expressed using a strategy similar to the one employed to make the bispecific minibody. This construct is dimeric for binding to HER2/*neu* but binds monomerically to FcγRIII. The cytotoxic potential of this new construct is being compared to that of the bispecific minibody, bispecific $(scFv)_2$ and bispecific IgG.

#4801 Isolation and *in vitro* and *in vivo* characterization of human anti-human VEGF scFv fragments. Xinhui Wang, Jianming Hong, Yumi Yokoyama, Sunda Ramakrishnan, and Soldano Ferrone. *Roswell Park Cancer Institute, Buffalo, NY, University of Minnesota, Minneapolis, MN, and Roswell Park Cancer Institute, Buffalo, NY.*

Vascular endothelial growth factor (VEGF) stimulates proliferation of endothelial cells and contributes to the development of solid tumors by promoting tumor angiogenesis. Anti—VEGF monoclonal antibodies (mAb) have been shown to inhibit the functional activity of VEGF *in vitro* and in nude mice transplanted with human tumors. These findings have provided the background to implement clinical trials with anti—VEGF mAb in patients with malignant diseases. Potential limitations of the clinical application of anti—VEGF mAb are the poor diffusion from the vasculature into the tumor and normal organ antibody accumulation associated toxicity. These limitations may be overcome by the application of single chain fragments of variable regions (scFv) of antibodies. The latter offer also the advantage that they can be easily modified genetically to increase their specific targeting to malignant lesions. Therefore, we have isolated VEGF binding scFv fragments and assessed their functional properties *in vitro* and *in vivo*. Panning of a semi-synthetic phage display human—derived scFv library with recombinant human VEGF165 resulted in the isolation of 56 clones. Testing in a binding assay with VEGF165 of the 56 clones identified 14 positive clones. DNA sequencing of these 14 positive clones identified the same sequence in 13 clones and a different one in the remaining one. The latter clone, named JH2, and one of the 13 clones, named JH1, were selected for additional studies. Soluble scFv JH1 and JH2 reacted specifically in a standard sandwich assay with VEGF165 and VEGF121, which are the predominant isoforms of VEGF. Moreover, soluble scFv JH1 markedly neutralized VEGF165 and VEGF121 induced *in vitro* proliferation of

human endothelial cells HUVEC. Lastly, four intraperitoneal injections of scFv JH1 (100μg/injection) on day 9, 13, 17 and 19 following transplant of human ovarian carcinoma cells MA148 to nude mice ($2x10^6$ cells/mouse) significantly inhibited tumor growth. These results suggest that anti-VEGF scFv JH1 may be a useful reagent to develop anti-angiogenic therapy of solid tumors.

#4802 Surface plasmon resonance-based competition assay to assess the sera reactivity of variants of humanized antibodies. Noreen R. Gonzales, Peter Schuck, Jeffrey Schlom, and Syed V. S. Kashmiri. *LTIB, CCR, NCI, NIH, Bethesda, MD, and MIR, DBEPS, ORS, NIH, Bethesda, MD.*

To evaluate the relative potential immunogenicity of variants to the parental humanized antibody (Ab), we have taken the approach of comparing the reactivities of the humanized Ab and its variants to patients' sera containing anti-idiotypic antibodies (anti-Ids) to the parental Ab. Sera reactivity is measured by the ability of a humanized Ab variant to compete with the parental Ab for binding to patients' sera. We developed a Surface Plasmon Resonance-based assay to monitor the binding of the sera anti-Ids to the parental Ab and the inhibition of this binding by the variants. This new assay requires no radiolabeling, is relatively less time-consuming, and uses only small amounts of serum through an innovative sample application technique. To validate the assay, we have tested the relative reactivities of the CDR-grafted anti-carcinoma Ab, HuCC49, and two variants, designated V5 and V10, to the sera of two patients, who were earlier administered radiolabeled murine CC49 in a clinical trial. IC_{50}s, the concentrations of the competitor antibody required for 50% inhibition of the binding of the serum to HuCC49, showed a 9.6-fold reactivity difference between HuCC49 and V10 to one serum, and a 164-fold difference in their reactivities to the other serum. The results may indicate the difference between the potential immunogenicities of the variants and the parental humanized Ab. Furthermore, the assay can be adapted to allow a comparison of relative amounts of anti-Ids present in sera of different patients without removing the circulating antigen. This can facilitate the rapid screening of the sera of patients involved in clinical trials for the presence of anti-Ids.

#4803 Characterization of five new fully human monoclonal IgM antibodies isolated from carcinoma patients. Stephanie Braendlein, Frank Hensel, Judith Lorenz, Matthias Eck, Bertram Illert, Justus Mueller, Hans Konrad Mueller-Hermelink, and H. Peter Vollmers. *Pathology, Univ. Wuerzburg, Wuerzburg, Germany, and Surgery, Univ. Wuerzburg, Wuerzburg, Germany.*

Monoclonal antibodies are accepted to be ideal adjuvant therapeutical reagents for all kinds of diseases. Polyvalent (crosslinking) and low mutated IgM antibodies (less immunogenic) are believed to be the most effective weapons against cancer. The best source for these types of antibodies is the cancer patient itself. Using conventional hybridoma technique, not only fully human monoclonal IgM antibodies are isolated, but also new targets are identified by the same experimental approach. The resulting antibodies can be used directly for therapeutical purposes without further modulation and manipulation. B-cells from patients with carcinomas of colon, pancreas and lung were isolated from lymph nodes and immortalized by fusion to the heteromyeloma HAB-1/X. Resulting human monoclonal antibodies were tested initially on autologous tumor tissue and tumor reacting antibodies were further tested on panels of malignant and healthy tissues to determine the specificity. Antibodies were blotted on cell extracts to characterize the targets and tested in functional assays for cytostatic/toxic activities. We have generated and characterized five new human monoclonal IgMs. The mainly germ-line coded IgM antibodies CM-1 and CM-2 (colon), PM-1 and PM-2 (pancreas) and LM-1 (lung) are specific for malignant tissues and show only restricted reactivity with healthy cells. Biochemical analysis to determine the corresponding receptors are underway. Tested for functional *in vitro* activity, human antibody CM-1 inhibits tumor cell proliferation by inducing apoptosis. Adjuvant treatment of cancer with monoclonal antibodies requires new antibodies and new targets. By using classical human hybridoma technique we have established five new human monoclonal IgM antibodies from patients with different cancers. All five antibodies show a tumor restricted reactivity pattern and at least one antibody (CM-1) induces apoptosis. This shows that carcinoma patients have an anti tumor B-cell immunity and manifest tumors are not a matter of quality but most likely of quantity of humoral immunity.

#4804 Granulocyte-colony stimulating factor enhances chimeric antibody Nd2 dependent cytotoxicity against pancreatic cancer mediated by polymorphonuclear neutrophils. Yutaka Tamamori, Tetsuji Sawada, Tamahiro Nishihara, Yoshito Yamashita, Masaichi Ohira, and Kosei Hirakawa. *Department of Surgical Oncology, Osaka City University Graduate School of Medicine, Osaka, Japan.*

Nd2 is a monoclonal antibodiy against pancreatic cancer. We have previously reported that human/mouse chimeric antibody Nd2 (c-Nd2) can induce antibody-dependent cell-mediated cytotoxicity (ADCC) with peripheral blood mononuclear cells (PBMs) as effectors. In this study, we investigated c-Nd2 induced ADCC by polymorphonuclear neutrophils (PMNs) as effector cells and the effects of G-CSF in enhancing this cytotoxicity. Cytotoxicities for pancreatic cancer cell line SW1990 were dose-dependently increased during mixed PMN and tumor cell culture with c-Nd2, and these cytotoxicities were significantly suppressed by neutralizing antibodies against CD16, which were Fcγ receptors expressed on PMN membranes. Furthermore, the treatment of PMNs with G-CSF was significantly enhanced. *In vitro* c-Nd2 induced ADCC activity with these PMN
tumor growth of SW1990 subcutaneously transplanted nude mouse tendec
suppressed by i.p. administration of c-Nd2 or G-CSF. In addition, the co
tion of c-Nd2 and G-CSF significantly inhibited this *in vivo* tumor growth,
was accompanied by a strong infiltration of PMNs into and around the
planted tumor, as confirmed by immunohistochemical study with anti-
neutrophil elastase antibody. These results suggest that PMNs play an im
role in c-Nd2 induced ADCC and that combination immunotherapy of c-Nc
G-CSF may be beneficial in clinical applications against pancreatic can
enhancing ADCC induced by PMNs.

**#4805 Development of a single chain Fv from a human anti-ID mor
nal antibody that mimics the GD2 antigen: A vaccine candidate for c
immunotherapy.** Pradip K. Maiti, Joycelyn Entwistle, Darren Fast, anc
MacDonald. *Viventia Biotech Inc, Winnipeg, MB, Canada.*

We have generated a human anti-id antibody namely 4B5, that mimics th
ganglioside, a tumor antigen that is overexpressed on melanoma, neurobla
and small cell lung cancers. In addition to an intact IgG antibody, we hav
developed a single chain Fv form. The specificity of the 4B5 scFv was de
strated by its ability to bind to 14G2a, an anti-GD2 MAb, and to inhibit the b
of 14G2a to a GD2-positive melanoma cell line SK-MEL-5. To explore the p
tial of 4B5 as an anti-id cancer vaccine, we have assessed and compar
immunogenicity of both the scFv and the intact IgG forms of 4B5 in
Immunization with either form of 4B5 resulted in the induction of both hu
and cell-mediated immune responses. However, mice immunized with th
scFv demonstrated a stronger humoral immune response. This was indica
a higher 4B5-specific antibody titer, a stronger anti-anti-id response,
stronger anti-GD2 antibody (Ab3) response. A somewhat stronger cell-me
immune response was induced in mice immunized with the 4B5 scFv, as
onstrated by the production of IL-2, IL-13 and IFN γ in the primary cult
spleen cells. These results indicate that the scFv form induces a stronger
response than the IgG. Thus, the 4B5 scFv has potential as an anti-id vacc
cancer immunotherapy.

**#4806 Cancer autoantigens are cleaved by granzyme B: A pot
mechanism for revelation of cryptic epitopes.** Danielle Ulanet, Amy Cox,
Dang, Livia Casciola-Rosen, and Antony Rosen. *Johns Hopkins University S
of Medicine, Baltimore, MD.*

The ongoing identification of tumor antigens has begun to elucidate th
majority of these proteins are non-mutated and thus immune responses a
them represent an autoimmune phenomenon. Unlike in autoimmune dis
where the immune response against self proteins is detrimental to the
immune responses against self proteins in tumors have been associated
more favorable prognosis. Thus, the identification of a common mech
responsible for rendering such self proteins immunogenic, may greatly bene
field of tumor immunology. The recent finding that the majority of autoan
targeted across the spectrum of systemic autoimmune diseases are sele
cleaved by the cytotoxic lymphocyte granule protease granzyme B to ger
unique fragments, implies that altered cleavage of these molecules, during
toxic lymphocyte-granule induced cell death, may play a role in spec
breaking tolerance to them. We demonstrate here that susceptibility to sp
cleavage by granzyme B is also a feature shared by cancer autoantigens
molecules examined (tyrosinase, c-myc, nucleophosmin/B23, UBF/NOR-9
fibrillarin) included autoantigens of diverse function and sub-cellular locali
and were targeted by autoantibodies in various different malignancies. W
pose that altered cleavage of these molecules in the pro-immune sett
cytotoxic lymphocyte induced cell death, combined with increased express
tumors, may play a role in inciting the specific adaptive immune respor
cancer.

#4807 Mutagenesis of human RNase for immunotoxin therapy. He
Erickson, Michelle Jund, and Christopher A. Pennell. *University of Minn
Minneapolis, MN.*

An immunotoxin is a chimeric molecule consisting of a targeting molety
toxin moiety. In the treatment of T cell acute lymphoblastic leukemia (T
immunotoxins directed against CD7, an antigen highly expressed on leuke
cells, have been con structed. Historically, the toxin moiety has been pl
bacterially derived; however, their efficacy in an immunotoxin is limited by i
nogenecity and non-specific toxicity. An appealing alternative to such toxin
use a human toxin such as ri bonuclease (hRNase) in an immunotoxin cons
RNases are efficient enzymes that digest RNA, prohibiting protein synt
thereby leading to apoptosis. Normally, they are efficiently inhibited by rib
clease inhibitor (RI), a cytosolic protein found in abundance in most ce
hRNase was mutated such that it was bound less effectively by RI, it cou
used to derive a potent, less immunogenic immunotoxin. To this end, a ser
mutations were made within key regions in the RI/RNase interfac e. T
mutants will be examined for their ability to evade RI binding and linkec
targeting moiety directed against CD7.

Project 2: Angiogenesis Inhibitors in the Malignant Transformation of Ovarian Surface Epithelium

ABSTRACT

Etiology of ovarian cancer is not completely understood. Previous studies have shown that both genetic and epigenetic factors could contribute to ovarian tumorigenesis. Epidemiological studies suggest that number of ovulation and ovulation related gonadotropic hormones could play a role in the malignant transformation of surface epithelium. In this project, we will investigate how the normal ovarian epithelium acquires tumorigenic phenotype. Specifically, the effect of angiogenic growth factors in the etiology of ovarian cancer is studied using a model system.

Table of Contents

Cover.....67

SF 298.....68

Table of Contents.....69

Introduction.....70

Body.....70

Key Research Accomplishments.....72

Reportable Outcomes.....72

Conclusions.....73

References.....73

Appendices.....73

(4) INTRODUCTION:

The vast majority of ovarian cancers arise from the surface epithelium. Only a small percent of ovarian cancers are genetically linked . Epidemiological data clearly suggest that ovulation related events can be associated with ovarian cancer development. Recurrent process of wounding and repair during repeated ovulation is implicated in transformation of surface epithelium. Transformed cells are then selected in vivo for their ability to attract new blood vessels, angiogenesis, one of the necessary steps involved in the establishment of tumors. Secretion of angiogenic factors is prognostically significant. Furthermore, gonadotropic hormones can induce angiogenic factors in cell cultures. These studies lead to a possible relationship between, ovulation, ovulatory hormones and angiogenic phenotype. Based on these data, the present proposal is designed to investigate the role of angiogenic factors in the development of ovarian cancer.

(5) BODY :

In our " Statement of Work" we proposed to perform Task # 1 and #2 during the first 36 months. Task 1 and 2 are related the expression of angiogenic growth factor in surface epithelium of the ovary . To evaluate whether angiogenic growth factor play a role in the development of ovarian cancer.

In the Year 2 report (2001) we described the establishment of rat ovarian surface epithelial cells secreting VEGF stably. These cells were characterized for their ability to induce angiogenesis in vivo using a matrigel assay. Results showed that VEGF secretion was accompanied by increased angiogenesis. Interestingly, exogenous expression of VEGF provided a survival advantage to these cells to establish as tumors.

Results related to Task 1 and 2 in Year 3 : We continued to characterize the tumorigenic potential of VEGF expression in rat ovarian surface epithelial cell line, ROSE199. Intraperitoneal injection of VEGF-ROSE cells induced the formation of malignant ascites. An average of 9 ml of ascitic fluid was found in VEGF-ROSE injected mice. VEGF-ROSE injected mice survived shortly, and all the mice died due to tumor burden by day 56. Control mice injected with similar number of vector transfected ROSE cells survived for more than 100 days. These results are summarized in the manuscript included in the Appendix.

Since VEGF secretion provided in vivo survival advantage and converted the non-tumorigenic ROSE199 cells into a tumorigenic phenotype, we carried out studies to determine whether one can reverse this phenomenon by intervening VEGF mediated signaling. VEGF-ROSE cells were injected into groups of athymic mice and one group was treated with a recombinant human single chain antibody to VEGF. Antibodies will neutralize the VEGF outside the cell and prevent angiogenic signaling. In another set of experiment, a specific inhibitor of VEGF-Receptor 2, SU 5416 was used. SU5416

inhibits the tyrosine kinase activity of flk-1. Both external neutralization and inhibition of VEGF-receptor mediated signaling significantly inhibited the growth of VEGF-ROSE cells in athymic mice. These studies suggest that angiogenic growth factor secretion is a necessary component in ovarian cancer development and that inhibition of angiogenic signaling can inhibit ovarian cancer growth.

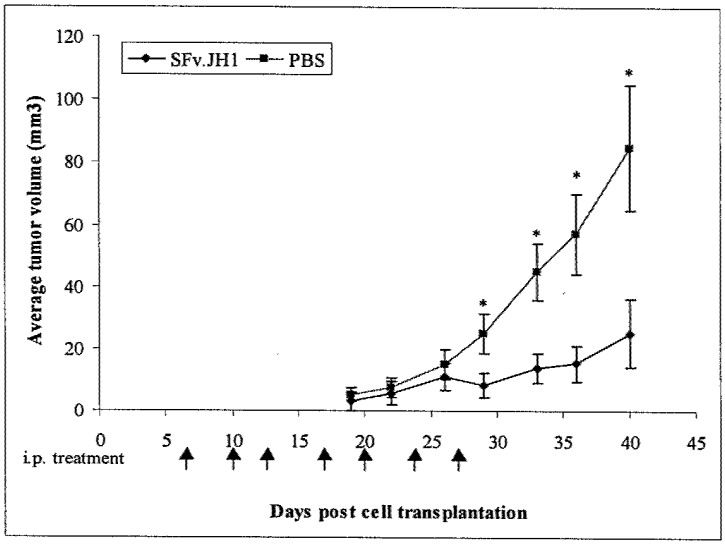

Fig. 1 : Effect of a single chain antibody to VEGF on the growth of VEGF secreting rat ovarian surface epithelial cell line. Solid squares show PBS treated control mice. Each group contained 10 mice . Antibody treatment is indicated as arrows. Each mouse was injected with 100 ug of the antibody.

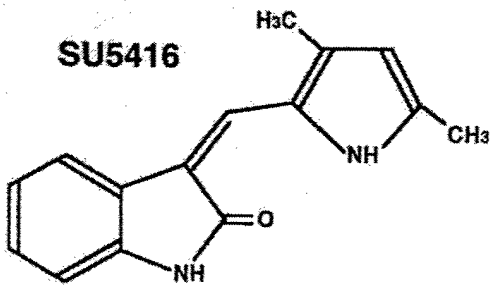

Fig. 2 : Structure of SU 5416, a selective inhibitor of flk-1 receptor tyrosine kinase

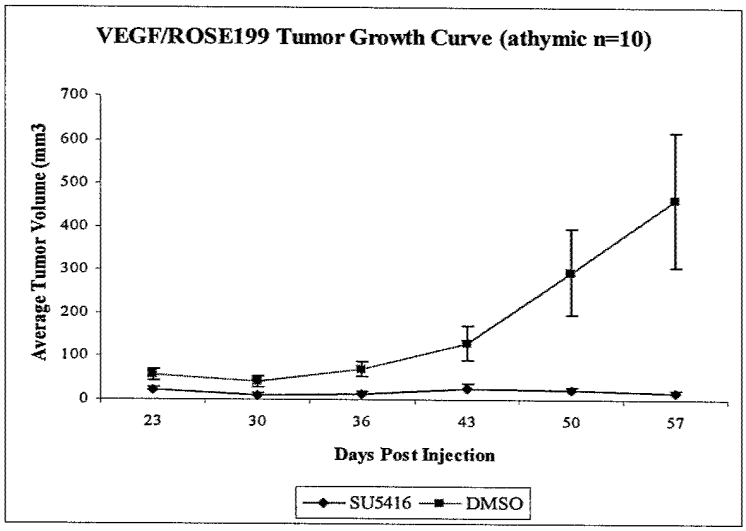

Fig. 3. Effect of SU5416 on the growth of VEF-ROSE cells. Each value is a mean of 10 animals. SU5416 was dissolved in DMSO and given at a dose of 15 mg/kg/d every day for a period of two weeks. Treatment started on day 7 after the transplantation of VEGF-ROSE cells.

Future studies will focus on switching the angiogenic balance by trensfecting the VEGF-ROSE cells with an angiogenesis inhibitor. Outcome of this experiment will prove that reversing angiogenic phenotype can prevent ovarian cancer growth.

(6) KEY RESEARCH ACCOMPLISHMENTS :

VEGF-secreting ROSE 199 cells formed solid tumors when injected s.c. and malignant ascites when injected intraperitoneally.

Tumor incidence is 100 %.

VEGF seems to confer survival advantage in vivo and confer tumorigenic phenotype.

Neutralization of VEGF by a single chain antibody inhibited the growth of VEGF-ROSE cells in athymic mice.

Inhibition of VEGF mediated signaling at the endothelial cells by SU5416 prevented the growth of VEGF-ROSE cells.

(7) REPORTABLE OUTCOMES :

Manuscripts: **VEGF Overexpression in Normal Ovarian surface epithelial cell line leads to tumorigenesis and ascites formation**

Jennifer J. Schumacher, J. Cosin, N. Auersperg and S. Ramakrishnan. (communicated).

(9) **CONCLUSIONS** : Secretion of VEGF gives a selective advantage for non-tumorigenic ovarian surface epithelial cell line to become tumorigenic. Formation of malignant ascites is clearly associated with VEGF secretion, which is a characteristic of ovarian cancer. Neutralizing VEGF extracellularly inhibits ovarian cancer growth. Similarly, inhibition of VEGF mediated signaling by a kinase inhibitor, SU5416, can also prevent tumorigenesis of VEGF-ROSE cells.

(10) REFERENCES : None

(11) APPENDIX :

Manuscripts: VEGF Overexpression in Normal Ovarian surface epithelial cell line leads to tumorigenesis and ascites formation

Jennifer J. Schumacher, J. Cosin, N. Auersperg and S. Ramakrishnan. (communicated).

APPENDIX

Project 2

VEGF Over-expression in a Normal Ovarian Surface Epithelial Cell Line Leads to Tumorigenesis and Ascites Formation

Jennifer J. Schumacher[1], J. Cosin[2], N. Auersperg[3] and S. Ramakrishnan[1*]

[1]Department of Pharmacology
[2]Department of Obstetrics and Gynecology,
University of Minnesota,
Minneapolis, MN 55445.
[3]Department of Obstetrics and Gynaecology,
University of British Columbia,
Vancouver, Canada

Short Title: Effects of VEGF Over-Expression on Ovarian Surface Epithelium

Keywords: Vascular Endothelial Growth Factor, Angiogenesis, Ovarian Surface Epithelium

Abbreviations: ROSE, rat ovarian surface epithelial; VEGF, vascular endothelial growth factor; OSE, ovarian surface epithelium; OEC, ovarian epithelial cancer

Journal Category: Cancer Cell Biology

*Address correspondence to:

[1]S. Ramakrishnan, Ph.D.
University of Minnesota,
6-120 Jackson Hall
321 Church St. S.E.,
Minneapolis, MN 55445
Ph. 612.626.6461

FAX: 612.625.8408
E-mail: sunda001@tc.umn.edu

Summary

Vascular endothelial growth factor (VEGF) is a potent angiogenic factor that is upregulated in malignancies such as ovarian cancer. To determine the functional role of VEGF in development of ovarian tumors, we transduced human *VEGF165* into a normal rat ovarian surface epithelial cell line, ROSE199. A number of highly secreting VEGF/ROSE199 clones was established. As a positive control, ROSE199 cells were transfected with the *neu* oncogene which is over-expressed in >30% of ovarian cancers. *Neu* transfected ROSE199 cells showed phenotypic characteristics of transformation *in vitro* with an abundance of focal forming units in monolayer cultures and colony growth in soft agar. In contrast, VEGF secreting ROSE199 cells did not show characteristic changes of transformation. Transfection of ROSE199 cells with *VEGF165* or vector alone did not alter *in vitro* proliferation rate of these cells compared to parental ROSE199 cells. *Neu* transfected ROSE199 cells formed solid tumors in >90% of mice injected and interestingly 85% of mice injected with VEGF/ROSE199 cells developed vascularized tumors. Intraperitoneal injection of VEGF/ROSE199 cells lead to malignant ascites formation in 100% of injected mice whereas, control transfected ROSE199 cells failed to produce tumors under similar conditions. Furthermore, blocking VEGF mediated signaling by the receptor specific kinase inhibitor SU5416 reduced the growth of VEGF/ROSE199 tumors. These studies demonstrate that VEGF expression may play an important role in the etiology of ovarian cancer and blocking VEGF mediated signaling may be useful in the treatment of epithelial ovarian cancer.

Introduction

The most common form of ovarian cancer results from the malignant transformation of the ovarian surface epithelium, a single layer of cells that surround the ovaries. Ovarian epithelial cells secrete lysosomal proteases to aid in follicular rupture during ovulation then proliferate and migrate to heal the resultant wound. The etiology of ovarian surface epithelial cancer; however, remains poorly understood. Epidemiological evidence supports two main theories: the 'incessant ovulation' hypothesis (Fathalla, 1971) and the 'gonadotropin hypothesis' (Stadel, 1975). The 'incessant ovulation' hypothesis suggests that the risk of ovarian cancer increases with increased number of ovulation's [1]. A decrease in occurrence of epithelial ovarian cancer (OEC) is found in women with reduced ovulatory cycles due to pregnancy, oral contraceptive use, lactation, etc. It is therefore suggested that repeated wounding and healing of the ovarian surface epithelium (OSE) increases the susceptibility for malignant transformation of OSE. Growth factors and cytokines influence post-ovulatory repair of the OSE, and impaired regulation of these factors may also be involved in the development of ovarian cancer [2, 3]. The 'gonadotropin' hypothesis predicts that high levels of pituitary gonadotropins increase cancer risk by stimulation of the ovarian surface epithelium [4]. Recent studies have shown that gonadotropins stimulate OSE proliferation and induce expression of growth factors such as hepatocyte growth factor (HGF), keratinocyte growth factor (KGF) [5], and vascular endothelial growth factor (VEGF) [6] which may also play a role in the onset of ovarian epithelial cancer. It is likely that the etiology of ovarian cancer is multifactorial with genetic, hormonal, and environmental factors playing a role; however,

a common feature of these hypotheses is high level expression of growth factors surrounding the OSE.

It is widely accepted that solid tumors require new blood supply in order to survive and grow beyond a critical size of 2 mm in diameter. Many studies have shown that VEGF, a potent angiogenic growth factor, is up-regulated in ovarian tumors and that high levels of VEGF are found in associated ascites fluid in ovarian cancer patients [7-10]. Furthermore, neutralization of VEGF with a monoclonal antibody inhibits ovarian tumor growth and ascites formation in athymic mouse models [11]. We therefore hypothesized that acquisition of an angiogenic phenotype by OSE may be an important initial step in the development of epithelial ovarian cancer. Utilizing a normal rat ovarian surface epithelial (ROSE199) cell line, we induced high level expression of human $VEGF_{165}$ similar to that in ovarian cancer physiology and characterized its effects on OSE both *in vitro* and *in vivo*.

Material and Methods

Cell Culture

Parental ROSE199 cells were kindly provided by Dr. N. Auersperg (University of British Columbia, Vancouver, Canada). ROSE199, Neu/ROSE199 and pINA/ROSE199 cells were grown in M199 medium (GibcoBRL) with high glucose (4.5 g/liter) containing 10% fetal bovine serum and supplemented with 100 IU ml^{-1} penicillin and 100 ug ml^{-1} streptomycin (Cellgro). Selection and maintenance of Neu/ROSE199 cells was accomplished by growing cells in the presence of 0.8 mg/ml G418 (Calbiochem). $VEGF_{165}$ and vector (pSecTag C) transfected ROSE199 cells were grown in Dulbecco's

Modified Eagle Medium (GibcoBRL) with low sodium chloride (4.7 g/liter) supplemented with 10% fetal bovine serum and 100 IU ml^{-1} penicillin and 100 ug ml^{-1} streptomycin. VEGF/ROSE199 and control vector clones were selected and maintained in DMEM in the presence of 50 ug/ml Zeocin (Invitrogen).

Generation of transfected cell lines

Human $VEGF_{165}$ cDNA was cloned into the CMV promoter-driven mammalian expression vector pSecTag C (Invitrogen). The full-length VEGF165 cDNA (498 bp) was inserted directly between the EcoRI and NotI sites downstream of the murine IgG kappa-chain signal peptide (VEGF165/ROSE199). Transfection of VEGF165/ROSE199 or vector alone (Empty/ROSE199) was performed by calcium phosphate method [12]. Zeocin resistant colonies were selected with optimized concentrations of Zeocin (50 ug/ml) and culture supernatants were assayed for VEGF165. The oncogenic Neu/ROSE199 cell line was generated using a retrovirus containing the coding sequence for rat transforming *neu* inserted into retroviral vector pINA. The retroviral plasmid is a derivative of pgagneoSRV in which the rat beta actin promoter replaced the SV40 promoter as previously described by Edwards *et al.* 1993 [13]. Both the pINA and p*neu*INA vector DNA were kindly provided by Dr. A.W. Edwards (University of Cambridge, Cambridge, UK). ROSE199 cells were serially infected with either p*neu*INA or pINA retrovirus and G418 resistant clones were characterized.

Measurement of hVEGF165 protein expression

Secretion of human $VEGF_{165}$ protein from VEGF/pSecTag C or vector only transfected ROSE199 cells *in vitro* was determined using a human VEGF enzyme-linked immunosorbent assay (ELISA) kit according to the manufacturer's protocol (R & D Systems). Briefly, 1 x 10^5 zeocin resistant VEGF or control transfected cells were seeded into 6-well plates in 2 mls of respective medium. After 48 hours, culture supernatants were harvested, centrifuged at 1,000 rpm for 5 min. and assayed by ELISA to determine protein expression.

Proliferation rate of ROSE199 cell lines

Cell proliferation *in vitro*, was determined by MTT assay [14]. Briefly, 1 x 10^3/well were seeded in a 96-well culture plate in 0.2 ml of respective culture medium. Briefly, 20 ul MTT (Sigma) stock solution (2.5 mg MTT/ml of PBS) was added to each well and incubated at 37 °C for 4 h, the medium was aspirated and 100 ul of DMSO was added to each well. Conversion of MTT to formazan by metabolically viable cells was monitored by a Dynatech MR 5000 fluorescence microplate reader at a wavelength of 450 nm. Results were analyzed by regression analysis. Results were further confirmed by seeding 1.0 x 10^4 of each cell line into 6-well tissue culture plates in their respective medium and counting viable cells by trypan blue exclusion.

Characterization of transfected ROSE199 cells in vitro

The propensity for foci formation was assessed *in vitro*. As a positive control, ROSE199 cells expressing the mutant rat *neu* oncogene were used. Briefly, 3.0 x 10^5 *neu* transfected

ROSE199, VEGF/ROSE199 or Empty/ROSE199 cells were seeded into 10-cm tissue culture dishes and allowed to grow to 100% confluence. The cells were allowed to incubate at 37 °C + 5% CO_2 for an additional 2-4 days before assessing foci (colony) formation. Focal units equal to or greater than 0.1mm were counted.

The potential for cells to form colonies in semi-solid medium was measured by suspending 4 x 10^4 VEGF/ROSE199, Empty/ROSE199 or Neu/ROSE199 cells in 1 ml of top agar consisting of 0.36% Bacto-agar in DMEM media with 10% FBS. The top agar was plated onto 1.5 mls of solidified bottom agar, consisting of 0.5% Bacto-agar in DMEM. After 21 days, the dishes were examined and colonies containing more than approximately 50 cells were counted. Cloning efficiencies were determined by the ratio: number of colonies counted / number of cells seeded.

In vivo matrigel assay

In vivo matrigel assay has previously been described [15], [16]. Briefly, matrigel (Sigma E-1270) containing 2 x 10^6 VEGF/ROSE199, Emtpy/ROSE199, Neu/ROSE199, or pINA/ROSE199 cells were implanted s.c. into the right hind flanks of athymic mice. 7 days after transplantation, mice were euthanized and matrigel plugs removed for histological examination.

Tumorigenicity assays

Female athymic mice, 6 to 8 weeks old, were obtained from NCI (National Cancer Institute. 2 x 10^6 VEGF/ROSE199 (clone 4) or Empty/ROSE199 cells were suspended in 200 ul of sterile saline and injected either i.p. or s.c. into the right hind flank of the

animal. All animals were monitored for general health status and tumor formation. The date of the first indication of tumor growth (or ascites development) was noted, and the animals were euthanized when they became moribund or if subcutaneous tumors reached a size larger than 1 cm^3 if neither of these criteria were reached, animals were sacrificed 5 months after the initial injection. The extent of tumor burden was evaluated by caliper measurements of s.c. tumors or by gross examination of all organs within the peritoneal cavity. Resected tumor tissues were either fixed in 10% buffered formalin, embedded in paraffin, sectioned and stained with hematoxylin and eosin, or snap frozen for immunohistochemical staining with anti-CD31-PE conjugate. To ascertain that the tumors (s.c. or i.p.) were derived from the injected cells, parts of the tumor tissues were minced, treated with collagenase and cultured in M199 (Neu/ROSE199) or DMEM (VEGF/ROSE199) plus 10% FBS and 0.8 mg/ml G418 or 50 ug/ml Zeocin, respectively to verify maintenance of antibiotic resistance.

Immunohistochemistry

Harvested tumor tissues or matrigel plugs were embedded in tissue freezing medium (Miles Inc., Elkhart, IN) and snap frozen in liquid nitrogen. The samples were then cut into 10-μm thick sections and stored at -80^0C until further use. For immunohistochemical analysis, tissue specimens were air dried and subsequently fixed in acetone at room temperature for ten minutes. The slides were then allowed to air-dry for one hour and washed three times in phosphate buffered saline (PBS, pH 7.4) for 5 minutes each. The samples were then blocked with PBS containing 5% bovine serum albumin for 30 minutes at room temperature and subsequently incubated with a

phycoerythrin (PE) conjugated monoclonal antibody to PECAM-1 (PE conjugated anti-mouse CD31, 1:50 dilution, PharMingen, San Diego, CA) for 1 hour at room temperature in a humidified chamber. The slides were washed three times in PBS and immediately imaged in an Olympus BX-60 fluorescence microscope at 200X magnification.

Quantitative real-time PCR assays

Steady-state levels of specific VEGF receptors Flk-1/KDR and Flt-1 mRNA transcripts were analyzed using a specific QRT-PCR assay for each gene. These quantitative RT-PCR assays have previously been described in detail (Perkin Elmer Applied Biosystems). The primers used in our analysis were synthesized based on rat Flk-1 and Flt-1 sequences respectively. These same sets of primers are also able to amplify human KDR and Flt-1 receptor transcripts. We utilized these primers to compare receptor levels in human vascular endothelial cells and rat epithelial cells. The primers used in this comparative quantitative analysis of Flk-1/KDR and Flt-1 were: Flk-1/KDR, 5' -CTC AGG TTT TGT GGA GGA GAA ATC C- 3' (5' primer, 25-mer) and 5' -GCC AAT GTC CAA CAG GAT GGT AAA G- 3' (3' primer, 25-mer) that generated a specific 123-bp Flk-1/KDR PCR product and Flt-1, 5' -GCC AAT GTC CAA CAG GAT GGT AAA G- 3' (5' primer, 25-mer) and 5' -TGA GAA GGT GGG GAC TGA GTA TGT G- 3' (3' primer, 25-mer) that generated a specific 92-bp product from all cell types, demonstrating the integrity of the RNA samples.

Effect of Flk-1/KDR receptor tyrosine kinase inhibition on VEGF/ROSE199 tumor growth

VEGF/ROSE199 cells (2×10^6) were implanted subcutaneously in the hind-flank region of BALB/c *nu/nu* female mice 6 - 8 weeks of age. Animals were treated once daily with a 50-µl i.p. bolus injection of SU5416 at 15 mg/kg per day, a selective inhibitor of the Flk-1/KDR receptor tyrosine kinase (Sugen Inc., San Francisco, CA) in DMSO or DMSO alone for fourteen days beginning 3 days after implantation. Tumor growth was monitored by measuring s.c. tumor mass using venier calipers. Tumor volume was calculated as the product of $(a \times b^2 \times \pi)/6$ where a = greatest diameter, b = perpendicular to a. Statistical analysis was carried out using Student's *t*-test. Toxicity profile was assessed by measuring mean weight change and hematocrit levels (% PCV) of mice on days 1, 7, and 14. Tumor specimens were surgically removed and processed for histochemical analysis as described previously.

Results

Expression of hVEGF165 in ROSE199 cells

ROSE199 cells were transfected with pSecTag C containing the entire coding sequence for *hVEGF165* (VEGF/ROSE199) or pSecTag C vector only (Empty/ROSE199). After selection in zeocin, supernatant from resistant clones was assayed for the presence of secreted hVEGF165 using a human specific VEGF ELISA. Clones transfected with VEGF165 secreted hVEGF protein ranging from 300 pg/ml up to 3200 pg/ml (Fig. 1). Expression of neu in p*neu*INA transfected ROSE199 cells was verified by immunohistochemical staining of G418 resistant cells using a rat specific anti-neu antibody (Oncogene Research Products) (data not shown).

Proliferation rate of ROSE199 cells in vitro

The ability of hVEGF165 to influence the growth of ROSE199 cells *in vitro* was investigated. Viable cell counts were performed on parental ROSE199, VEGF/ROSE199, and Empty/ROSE199 cells at 24 hr., 48 hr., and 72 hr. time points. Viable cell counts by trypan blue exclusion reveal no significant difference in cell proliferation rate between the different ROSE199 cell lines *in vitro*. This data was further confirmed by determining viable cells by MTT assays. There was no significant difference in cell doubling time between the cell lines. Parental ROSE199 cells had a doubling time of 16 hours, Empty/ROSE199 17.4 hrs. and VEGF/ROSE199 cells showed a doubling time of 18.2 hrs. The marginal differences seen in doubling times were not statistically significant (Table 1).

In vitro phenotypes of transfected ROSE199 cells

Anchorage independence (growth in soft agar) and loss of contact inhibition (foci formation) are generally considered phenotypic markers of transformation. Parental ROSE199 cells have previously been shown to retain non-transformed characteristics of normal epithelium. We assayed VEGF/ROSE199, Empty/ROSE199, Neu/ROSE199 and pINA/ROSE199 cells for foci formation in monolayer cultures and anchorage independent growth in soft agar. Results summarized in Table 1 show the oncogenic *neu* transfected ROSE199 cells formed foci in monolayer cultures but neither VEGF/ROSE199, Empty/ROSE199 nor pINA/ROSE199 cells were able to form foci after reaching confluence. Similar results were observed in anchorage independent growth assays where the Neu/ROSE199 cells were able to form multiple large colonies in

soft agar with a cloning efficiency of approximately 70% while parental ROSE199 and Empty/ROSE199 cells produced no colonies at any of the cell densities tested. VEGF/ROSE199 cells; however, did form a small number of colonies in soft agar with an average cloning efficiency of 5%.

Angiogenesis induced by ROSE199 transfectants

In order to assess angiogenic stimulation by the different ROSE199 cell lines *in vivo*, 2 million, a) VEGF/ROSE199 b) Empty/ROSE199 c) Neu/ROSE199 or d) pINA/ROSE199 cells were mixed in matrigel and injected s.c. into athymic nude mice. Seven days after implantation animals were euthanized and matrigel specimens resected for histological examination (Fig. 2*a*). H & E staining of paraffin embedded sections reveal microvessels dispersed throughout matrigels containing VEGF/ROSE199 and Neu/ROSE199 cells compared to nearly avascular matrigels containing Empty/ROSE199 and pINA/ROSE199 cells (Fig. 2*b*). Frozen sections of gels were stained with a PE-conjugated antibody against mouse CD-31 and vessels were directly visualized by fluorescence microscopy (Fig. 2*c*). A traditional estimation of microvessel density was performed by a manual count of tumor blood vessels per high power field (200X magnification) as well as evaluation using computer assisted image analysis as described by Wild *et al.* [17]. As shown in figure 2*d*, *VEGF* and *Neu* transfected ROSE199 implanted matrigels had a 4 to 5 fold higher vessel count than matrigels containing control ROSE199 cells ($p < 0.01$).

Quantification of VEGF receptor mRNA expression by real-time PCR

Flk-1/KDR and Flt-1 are two VEGF specific receptors highly expressed by vascular endothelial cells. To assess if these receptors are also expressed by ROSE199 cells we utilized primer sets that are capable of amplifying both human and rat Flk-1/KDR and Flt-1 transcripts. Steady state levels of both the Flk-1/KDR and Flt-1 mRNA were examined in parental ROSE199, VEGF and Empty vector transfected ROSE199 cells in comparison to human umbilical vein endothelial (HUVE) cells. As expected, Flk-1/KDR and Flt-1 transcript levels were highly expressed in the endothelial cell line HUVE, and though significantly lower (approximately 3% - 8% of the HUVE) both receptor transcripts were expressed in all three ROSE199 cell lines (Fig. 4). Our data reveals for the first time the presence of Flk-1/KDR and Flt-1 receptor mRNA in ovarian surface epithelial cells.

Tumorigenicity of VEGF transfected ROSE199 cells

In parallel experiments, athymic mice were injected with 2 million VEGF/ROSE199 or Empty/ROSE199 cells either s.c. or i.p. Tumor incidence was 20/20 (100%) in mice injected i.p. with VEGF/ROSE199 cells and 17/20 (85%) in mice injected s.c. with VEGF/ROSE199 within 2 months of cell transplantation. In contrast, no tumors (0/20) developed in any of the mice injected with Empty/ROSE199 cells in either s.c. or i.p. models (Table 2). The animals injected i.p. with VEGF/ROSE199 cells necessitated culling within two months after injection due to extensive ascites formation and animals becoming moribund (Fig 3 *a* and *c*). Examination of the peritoneum revealed widespread intra-abdominal tumor mass and up to 11 mls of ascites fluid per mouse. Animals injected s.c. with VEGF/ROSE199 cells developed palpable, vascularized tumors which

reached an average size of 2500 mm^3 in volume (Fig. 3 *b* and *d*). Tumors were locally invasive into muscle and adipose tissue but no distant metastasis were found. Animals were euthanized and tumors harvested for histological examination.

Flk-1 kinase inhibition suppresses VEGF/ROSE199 induced tumor growth in athymic mice

Our data reveal low-level expression of the VEGF specific receptor Flk-1 in ROSE199 cell lines. In order to assess whether the specific Flk-1/KDR tyrosine kinase inhibitor SU5416 (SUGEN) had an effect on VEGF/ROSE199 tumor development, we treated athymic mice transplanted s.c. with VEGF/ROSE199 cells with 15 mg/kg/day SU5416 or DMSO alone (control). Figure 5 shows the tumor growth in control and treated mice. Our results show a significant inhibition of tumor growth in the mice treated with SU5416 compared to control animals with an average tumor volume in mice receiving SU5416 of 200 mm^3 compared to 1200 mm^3 in control mice at the end of experiment. This data suggests that Flk-1 specific receptor tyrosine kinase inhibitors can be used in the treatment of epithelial ovarian cancer.

Discussion

VEGF expression is implicated in the pathology of ovarian cancer. High level expression of VEGF is associated with poor prognosis yet the molecular basis of ovarian cancer and the role of VEGF remains relatively unknown. A number of oncogenes have been implicated in the pathology of ovarian cancer including *BRCA-1/-2*, *p53*, and *neu/c-erbB2*. A high frequency of allele loss in the BRCA-1 (17q) and BRCA-2 (13q) loci has

been observed in both familial and sporadic ovarian tumors [18] and p53 gene mutations resulting in over-expression of the p53 protein has been suggested as an important prognostic factor for epithelial ovarian cancer [Ozalp, 2000 #47. Studies have also shown that the *neu*/c-*erb*B2 gene is frequently amplified and/or over-expressed in human epithelial ovarian cancers (OEC) [19]. A study by Davies *et al.* showed that when ROSE199 cells were transduced by retrovirus expressing mutated rat *neu*, the neu expressing ROSE199 cells had an altered morphology and expressed characteristic malignant phenotypes such as loss of contact inhibition, anchorage independent growth, and tumor formation in athymic mice [20]. Recently, Yen *et al.* demonstrated activation of the neu receptor induced VEGF expression in tumor cells [21]. In order to identify if over-expression of VEGF resulted in similar tumorigenic phenotypes, we compared *in vitro* and *in vivo* growth characteristics of parental ROSE199 (negative control) and Neu/ROSE199 (positive control) cells to VEGF and vector only transfected ROSE199 cells. Injection of either Neu/ROSE199 cells or VEGF/ROSE199 cells s.c. or i.p. into female nude mice resulted in tumor formation. None of the mice injected with Empty/ROSE199 cells developed tumors. This study shows that over-expression of the potent angiogenic stimulator VEGF confers a tumorigenic phenotype to normal ROSE199 cells. Similarly, previous studies have also suggested a more functional role for VEGF in cancer development. Lee *et al.* studied the use of VEGF for therapeutic angiogenesis in ischemic myocardium. Their results showed that unregulated and continuous expression of VEGF in murine myoblasts lead to formation of endothelial cell-derived vascular tumors in immunodeficient mice [22]. Furthermore, Arbriser *et al.* showed that over-expression of VEGF121 in MS1 endothelial cells resulted in

development of slowly growing endothelial tumors in nude mice [23]. Our studies along with others suggest that factors in addition to known oncogenes and tumor-suppressors may play a significant role in tumor formation.

In our study, mice injected i.p. with VEGF/ROSE199 and Neu/ROSE199 cells but not Empty/ROSE199 cells developed extensive abdominal ascites fluid. These studies suggest the importance of VEGF in ascites development. Accumulation of ascites is thought to be due to blockage of lymphatics and by increased influx of fluid. VEGF is implicated in ascites development by increasing permeability of peritoneal microvessels. Ascites development by VEGF/ROSE199 cells provides distinct evidence for the role of VEGF in ascites formation in ovarian cancer. Further characterization of the VEGF/ROSE199 cells revealed that compared to the Neu/ROSE199 cells, VEGF expression did not alter ROSE199 cell growth *in vitro*. Foci formation assays revealed Neu/ROSE199 cells continued to grow in monolayer cultures forming multiple foci whereas the VEGF/ROSE199 and Empty/ROSE199 cells did not grow beyond confluence and no visible colonies formed. Furthermore, Neu/ROSE199 cells acquired the ability to form multiple, large foci when plated in soft agar. Interestingly, VEGF/ROSE199 cells formed colonies in soft agar at a very low efficiency compared to Neu/ROSE199 cells but consistently formed small numbers of colonies in separate experiments.

It is possible that epithelial cells are capable of an autocrine-signaling pathway via VEGF and its receptors Flk-1/KDR or Flt-1. Abu-Jawdeh *et al.* showed expression of VEGF mRNA and protein in malignant and borderline tumors of the ovary but low to no expression in normal ovarian cortex or surface epithelium [7]. This was further

confirmed by Boocock *et al.* who showed expression of mRNAs encoding VEGF, Flt-1 and Flk-1/KDR in primary ascitic cells and in multiple ovarian carcinoma cell lines [24]. This may explain the slight growth advantage acquired by the VEGF/ROSE199 cells seen in anchorage independent growth assays. To ascertain if autocrine stimulation was possible we analyzed the different ROSE199 cell lines for VEGF receptor mRNA expression by real-time PCR and found low-level expression of both Flk-1 and Flt-1 receptor transcripts. However, when we analyzed the proliferation rate of the VEGF transfected cells compared to parental ROSE199 and vector only transfected cells, with and without exogenous VEGF administration (100 ηg/ml), we observed no change in growth rate compared to parental ROSE199 cells (data not shown). Therefore, VEGF does not seem to act as an autocrine growth factor for ROSE199 cells *in vitro*; however, VEGF expression provides a survival advantage *in vivo* by attracting new blood supply to tumor tissue.

Attempts to interfere with the angiogenic process have involved inhibition of VEGF production, neutralization of VEGF with antibodies, and interference with VEGF signaling and receptor activation. Olson *et al.* showed significant reduction in solid tumor growth and ascites fluid development in mice treated with neutralizing antiserum to VEGF [25]. A later study by Lin *et al.* showed a 75% inhibition of tumor growth and 50% reduction in vascular density in carcinoma transplant models using a recombinant soluble VEGF receptor [26]. More recently, synthetic compounds that act to inhibit the enzymatic activity of VEGF receptors have been developed. SU5416 is a potent and selective inhibitor of Flk-1/KDR receptor tyrosine kinase activity, which has been shown to be effective in limiting tumor growth in a variety of tumor types [27]. Our studies

reveal that inhibition of Flk-1/KDR receptor-mediated signaling significantly reduced VEGF/ROSE199 tumor growth suggesting a use in treatment of OECs and since SU5416 targets host endothelial cells, this treatment may be effective in escaping development of drug resistance common to many chemotherapeutic agents.

Future studies will test the effects of VEGF over-expression in other cell lines, specifically human ovarian surface epithelium. We would also like to investigate the effects other angiogenic growth factors such as endocrine-gland-derived vascular endothelial growth factor (EG-VEGF) recently identified by Ferrara *et al.*, which may be a useful target of therapeutics to increase efficacy and decrease possible side effects of antiangiogenic therapies [28]. The results described in this paper demonstrate a functional role for VEGF165 in formation of ovarian surface epithelial tumors and suggests that acquisition of an angiogenic phenotype may be an earlier step in tumorigenesis than previously thought. These studies clearly demonstrate a use for antiangiogenic therapy in ovarian epithelial cancer treatment.

Acknowledgements

This study was supported in part from grants from the United States Department of Defense (DAMD-17-99-1-9564), and the Sparboe Endowment. We thank Dr. Nelly Auersperg for providing the ROSE199 cell line. Also Lisa Dauffenbach, Jeremy Trass, and Robert Wild for their helpful suggestions and assistance during this study.

References

1. Fathalla, MF. Incessant ovulation--a factor in ovarian neoplasia? *Lancet* 1971, **2**, 163.

2. Berchuck, A, Olt GJ, Everitt L, Soisson AP, Bast RC, Jr., Boyer CM. The role of peptide growth factors in epithelial ovarian cancer. *Obstet Gynecol* 1990, **75**, 255-62.

3. Malik, S, Balkwill F. Epithelial ovarian cancer: a cytokine propelled disease? *Br J Cancer* 1991, **64**, 617-20.

4. Stadel, BV. Letter: The etiology and prevention of ovarian cancer. *Am J Obstet Gynecol* 1975, **123**, 772-4.

5. Parrott, JA, Doraiswamy V, Kim G, Mosher R, Skinner MK. Expression and actions of both the follicle stimulating hormone receptor and the luteinizing hormone receptor in normal ovarian surface epithelium and ovarian cancer. *Mol Cell Endocrinol* 2001, **172**, 213-22.

6. Wang, J, Luo F, Lu JJ, Chen PK, Liu P, Zheng W. VEGF expression and enhanced production by gonadotropins in ovarian epithelial tumors. *Int J Cancer* 2002, **97**, 163-7.

7. Abu-Jawdeh, GM, Faix JD, Niloff J, Tognazzi K, Manseau E, Dvorak HF, *et al.* Strong expression of vascular permeability factor (vascular endothelial growth factor) and its receptors in ovarian borderline and malignant neoplasms. *Lab Invest* 1996, **74**, 1105-15.

8. Barton, DP, Cai A, Wendt K, Young M, Gamero A, De Cesare S. Angiogenic protein expression in advanced epithelial ovarian cancer. *Clin Cancer Res* 1997, **3**, 1579-86.

9. Yamamoto, S, Konishi I, Mandai M, Kuroda H, Komatsu T, Nanbu K, *et al.* Expression of vascular endothelial growth factor (VEGF) in epithelial ovarian neoplasms: correlation with clinicopathology and patient survival, and analysis of serum VEGF levels. *Br J Cancer* 1997, **76**, 1221-7.

10. Orre, M, Rogers PA. VEGF, VEGFR-1, VEGFR-2, microvessel density and endothelial cell proliferation in tumours of the ovary. *Int J Cancer* 1999, **84**, 101-8.

11. Olson, TA, Mohanraj D, Carson LF, Ramakrishnan S. Vascular permeability factor gene expression in normal and neoplastic human ovaries. *Cancer Res* 1994, **54**, 276-80.

12. Chen, CA, Okayama H. Calcium phosphate-mediated gene transfer: a highly efficient transfection system for stably transforming cells with plasmid DNA. *Biotechniques* 1988, **6**, 632-8.

13. Bradbury, JM, Arno J, Edwards PA. Induction of epithelial abnormalities that resemble human breast lesions by the expression of the neu/erbB-2 oncogene in reconstituted mouse mammary gland. *Oncogene* 1993, **8**, 1551-8.

14. Carmichael, J, DeGraff WG, Gazdar AF, Minna JD, Mitchell JB. Evaluation of a tetrazolium-based semiautomated colorimetric assay: assessment of chemosensitivity testing. *Cancer Res* 1987, **47**, 936-42.

15. Schumacher, JJ, Upadhyaya P, Ramakrishnan S. Inhibition of vascular endothelial cells by 1,4-phenylenebis (methylene)selenocyanate--a novel chemopreventive organoselenium compound. *Anticancer Res* 2001, **21**, 1945-51.

16. Wild, R, Dhanabal M, Olson TA, Ramakrishnan S. Inhibition of angiogenesis and tumour growth by VEGF121-toxin conjugate: differential effect on proliferating endothelial cells. *Br J Cancer* 2000, **83**, 1077-83.

17. Wild, R, Ramakrishnan S, Sedgewick J, Griffioen AW. Quantitative assessment of angiogenesis and tumor vessel architecture by computer-assisted digital image analysis: effects of VEGF-toxin conjugate on tumor microvessel density. *Microvasc Res* 2000, **59**, 368-76.

18. Matias-Guiu, X, Prat J. Molecular pathology of ovarian carcinomas. *Virchows Arch* 1998, **433**, 103-11.

19. King, BL, Carter D, Foellmer HG, Kacinski BM. Neu proto-oncogene amplification and expression in ovarian adenocarcinoma cell lines. *Am J Pathol* 1992, **140**, 23-31.

20. Davies, BR, Auersperg N, Worsley SD, Ponder BA. Transfection of rat ovarian surface epithelium with erb-B2/neu induces transformed phenotypes in vitro and the tumorigenic phenotype in vivo. *Am J Pathol* 1998, **152**, 297-306.

21. Yen, L, You XL, Al Moustafa AE, Batist G, Hynes NE, Mader S, *et al.* Heregulin selectively upregulates vascular endothelial growth factor secretion in cancer cells and stimulates angiogenesis. *Oncogene* 2000, **19**, 3460-9.

22. Lee, RJ, Springer ML, Blanco-Bose WE, Shaw R, Ursell PC, Blau HM. VEGF gene delivery to myocardium: deleterious effects of unregulated expression. *Circulation* 2000, **102**, 898-901.

23. Arbiser, JL, Larsson H, Claesson-Welsh L, Bai X, LaMontagne K, Weiss SW, *et al.* Overexpression of VEGF 121 in immortalized endothelial cells causes conversion to

slowly growing angiosarcoma and high level expression of the VEGF receptors VEGFR-1 and VEGFR-2 in vivo. *Am J Pathol* 2000, **156**, 1469-76.

24. Boocock, CA, Charnock-Jones DS, Sharkey AM, McLaren J, Barker PJ, Wright KA, *et al.* Expression of vascular endothelial growth factor and its receptors flt and KDR in ovarian carcinoma. *J Natl Cancer Inst* 1995, **87**, 506-16.

25. Olson, DMaSR. In vivo neutralization of vascular endothelial growth factor (VEGF)/vascular permeability factor (VPF) inhibits ovarian carcinoma-associated ascites formation and tumor growth. *International Journal of Oncology* 1996, **8**, 1-7.

26. Lin, P, Sankar S, Shan S, Dewhirst MW, Polverini PJ, Quinn TQ, *et al.* Inhibition of tumor growth by targeting tumor endothelium using a soluble vascular endothelial growth factor receptor. *Cell Growth Differ* 1998, **9**, 49-58.

27. Fong, TA, Shawver LK, Sun L, Tang C, App H, Powell TJ, *et al.* SU5416 is a potent and selective inhibitor of the vascular endothelial growth factor receptor (Flk-1/KDR) that inhibits tyrosine kinase catalysis, tumor vascularization, and growth of multiple tumor types. *Cancer Res* 1999, **59**, 99-106.

28. LeCouter, J, Kowalski J, Foster J, Hass P, Zhang Z, Ferrara N *et al.* Identification of an angiogenic mitogen selective for endocrine gland endothelium. *Nature* 2001, **412**, 877-84.

TABLE 1 – Tumor Formation in Athymic Mice Injected With VEGF/ROSE199 and Empty/ROSE199 Cells

Cell type	Site of injection	Tumor Incidence	Termination (weeks post injection)	Average tumor volume (mm^3)/ascites (mls)
VEGF/ROSE199	s.c.	17/20 (85%)	14	2500
	i.p.	20/20 (100%)	7-8	11
Control/ROSE199	s.c.	0/20	35	N/S
	i.p.	0/20	35	N/S

N/S, no symptoms.

TABLE 2 - Characteristics of rat ovarian surface epithelial cells

Cell Line	Foci formation[a]	Growth in soft agar[b]	Doubling time[c]
ROSE199	N/A	<0.01	16.0
VEGF/ROSE199	---	0.05	18.2
Empty/ROSE199	---	<0.01	17.4
Neu/ROSE199	+++	0.7	13.5
pINA/ROSE199	---	N/A	N/A

[a] cultures displaying focal units ≥0.1 mm in diameter qualified as positive for foci formation.
[b] colonies consisting of approximately 50 cells or more were counted. Results are expressed as ratio of colonies to total number of cells seeded.
[c] population doubling times were determined by counting viable cells at 24 h intervals for 72 hours and are expressed as mean hours for triplicate cultures.
N/A, not applicable

Legends

Figure 1.

VEGF165 protein expression levels in conditioned medium from ROSE199 transfected clones. Individual culture medium from independent clones was assayed for hVEGF165 protein expression using a human specific VEGF ELISA. Numbered bars represent individual VEGF transfected ROSE199 clones, control bars represent vector only transfected ROSE199 clones.

Figure 2.

Induction of angiogenesis by transfected ROSE199 cells in matrigel. Matrigel plugs containing transfected ROSE199 cells were resected 7 days after implantation into nude mice (n=2). **A:** Representative phase contrast photomicrographs of matrigel plugs immediately after resection. **B:** H & E staining of paraffin embedded sections (arrows show blood vessels) **C:** Representative sections of frozen matrigels stained with endothelial cell specific anti-CD-31-PE showing vessel density. **D:** Quantification of vessel density as measured by CD-31 positive pixels. Statistical significance ($p < 0.05$) as determined by Student's t-test. The data shown in B and C are representative of more than 15 images taken per section at X200 magnification. Bar, 10.0 μm.

Figure 3.

Tumor development in nude mice injected with VEGF or vector only transfected ROSE199 cells in s.c. and i.p. models. **A:** Ascites development following i.p. transplantation of VEGF/ROSE199 cells. Observation time point 6-weeks after

transplantation. **B:** Gross appearance of s.c. tumors overexpressing hVEGF165. Mice were injected with VEGF/ROSE199 cells in right hind flank. Picture was taken 45 days after cell transplantation. **C:** Survival of athymic mice injected i.p. with either VEGF/ROSE199 or Empty/ROSE199 cells (n=10). 20/20 mice injected with VEGF/ROSE199 cells i.p. developed ascites compared to 0/20 mice injected with Empty/ROSE199 cells. **D:** Average tumor volume in mice injected s.c. with either VEGF/ROSE199 or Empty/ROSE199 cells (n = 10). Data are presented as the mean tumor volume +/- SE.

Figure 4.

Quantitation of Flk-1/KDR and Flt-1 receptor mRNA in ROSE199 cells. Parental ROSE199, Neu, VEGF, and vector only transfected ROSE199 cells were grown in monolayer cultures and total RNA was extracted from cultured cells. Steady-state levels of Flk-1/KDR and Flt-1 mRNA were determined using quantitative real-time PCR as described in *Materials and Methods*. Levels of Flk-1/KDR and Flt-1 mRNA were determined and normalized to levels of GAPDH mRNA. Data are presented as percent Flk-1/KDR (or Flt-1) mRNA in individual cell lines compared to HUVE cells and are shown as the mean $\pm$ SEM of duplicate determinations from 3 different sets of RNA from each cell type.

Figure 5.

Inhibition of VEGF/ROSE199 tumor growth by SU5416. Female, athymic nude mice were transplanted s.c. with 2 x 10^6 VEGF/ROSE199 cells in a volume of 250 µls PBS.

After 3 days, mice were treated with SU5416 (15 mg/kg i.p.) or DMSO daily for 2 weeks. Tumor growth was followed by caliper measurements. Each value is a mean of 10 animals with respective standard errors. ν DMSO control. υ SU5416 treated. * shows statistical significance ($p < 0.05$) as determined by Student's t-test.

Figure 1 – Schumacher

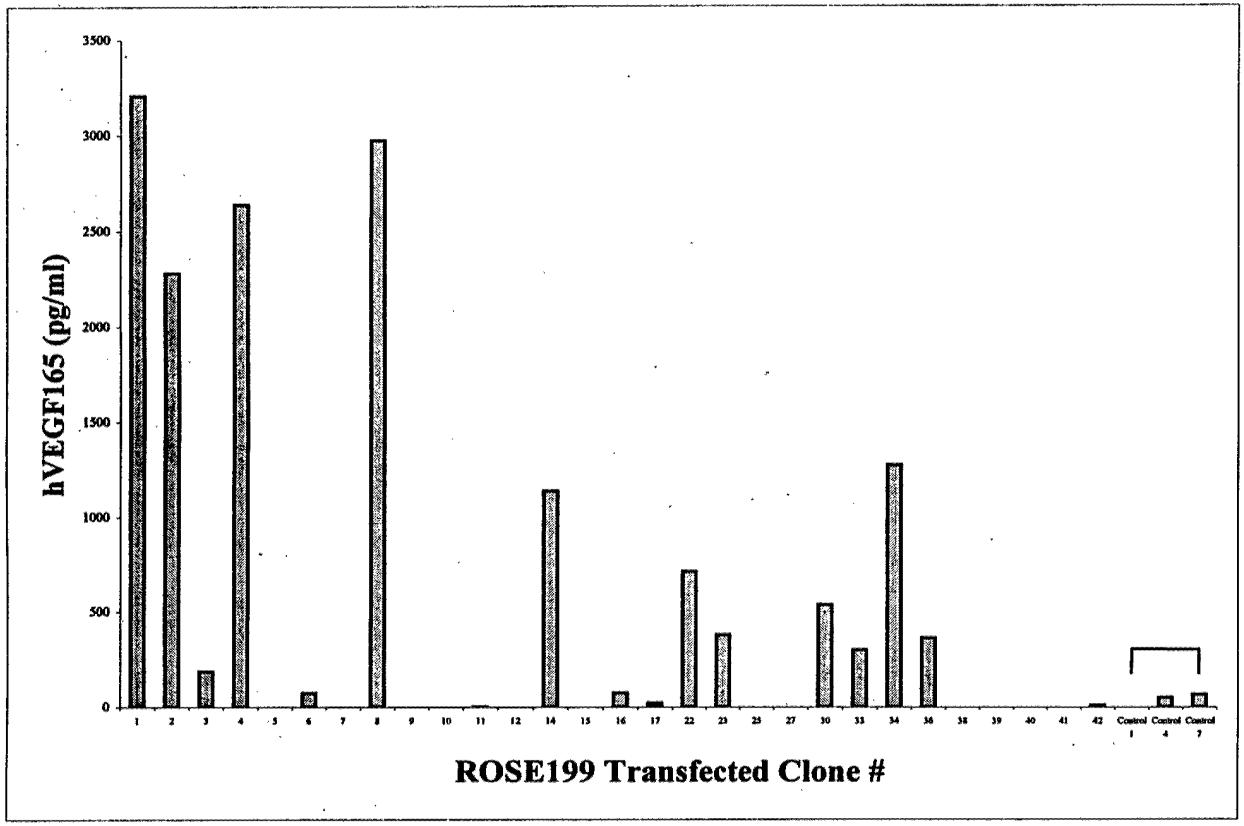

Figure 2 - Schumacher

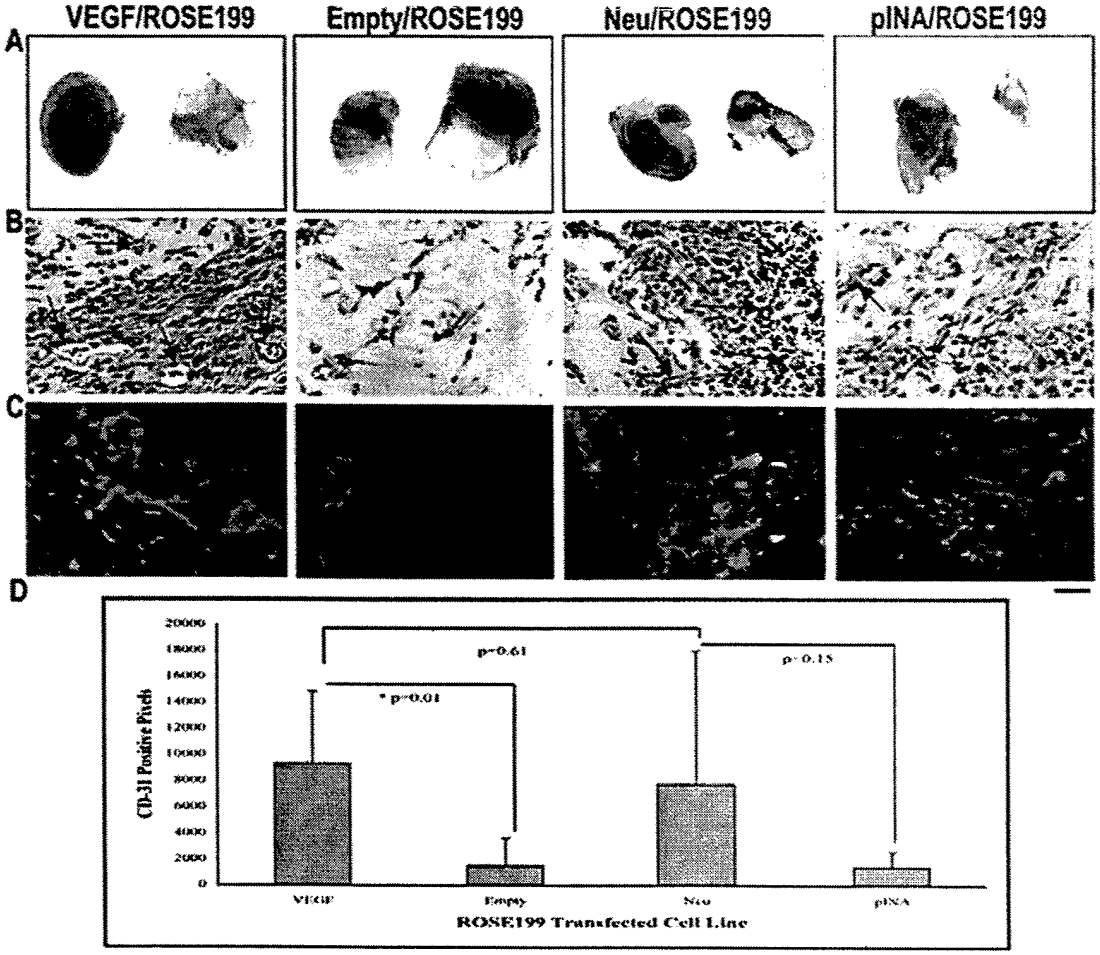

Figure 3 – Schumacher

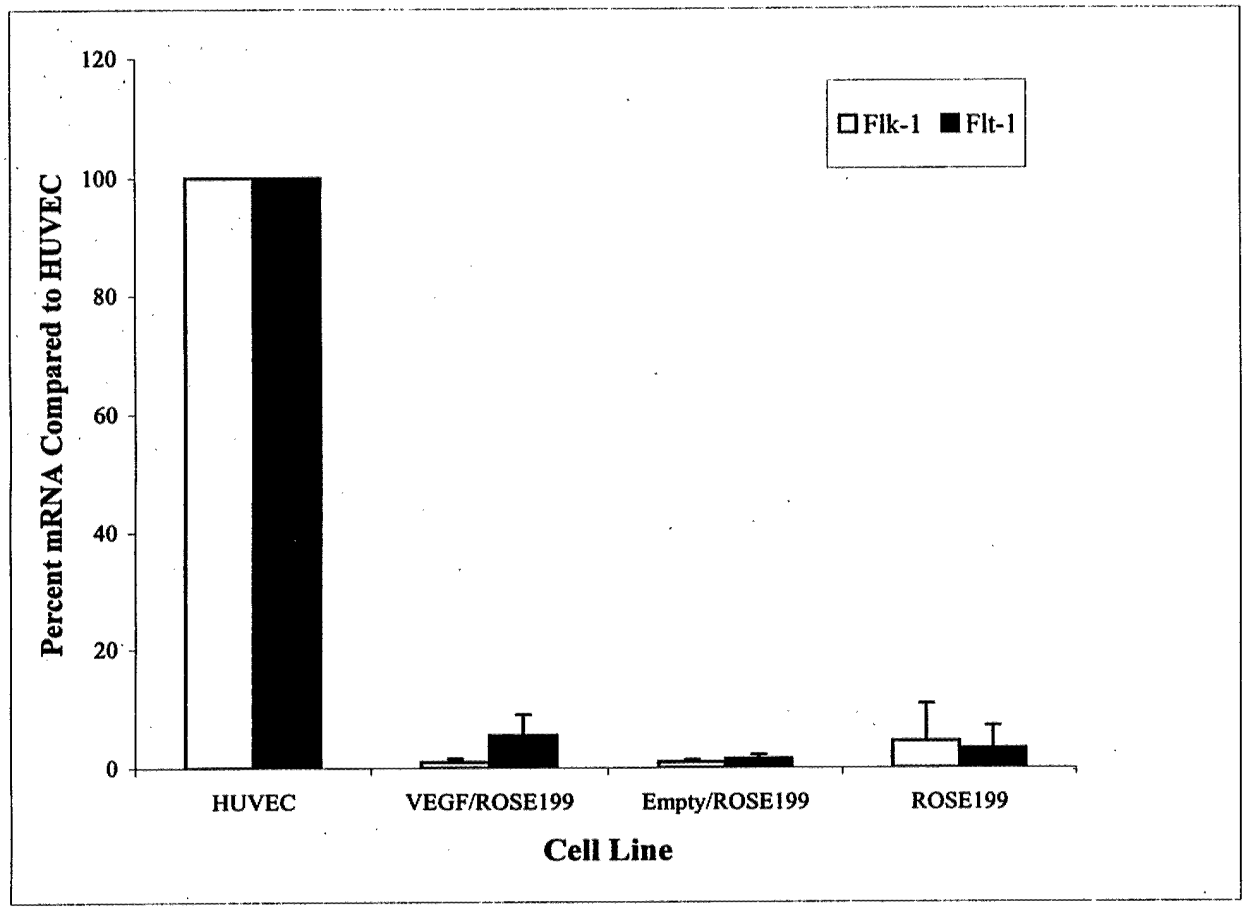

Figure 4 - Schumacher

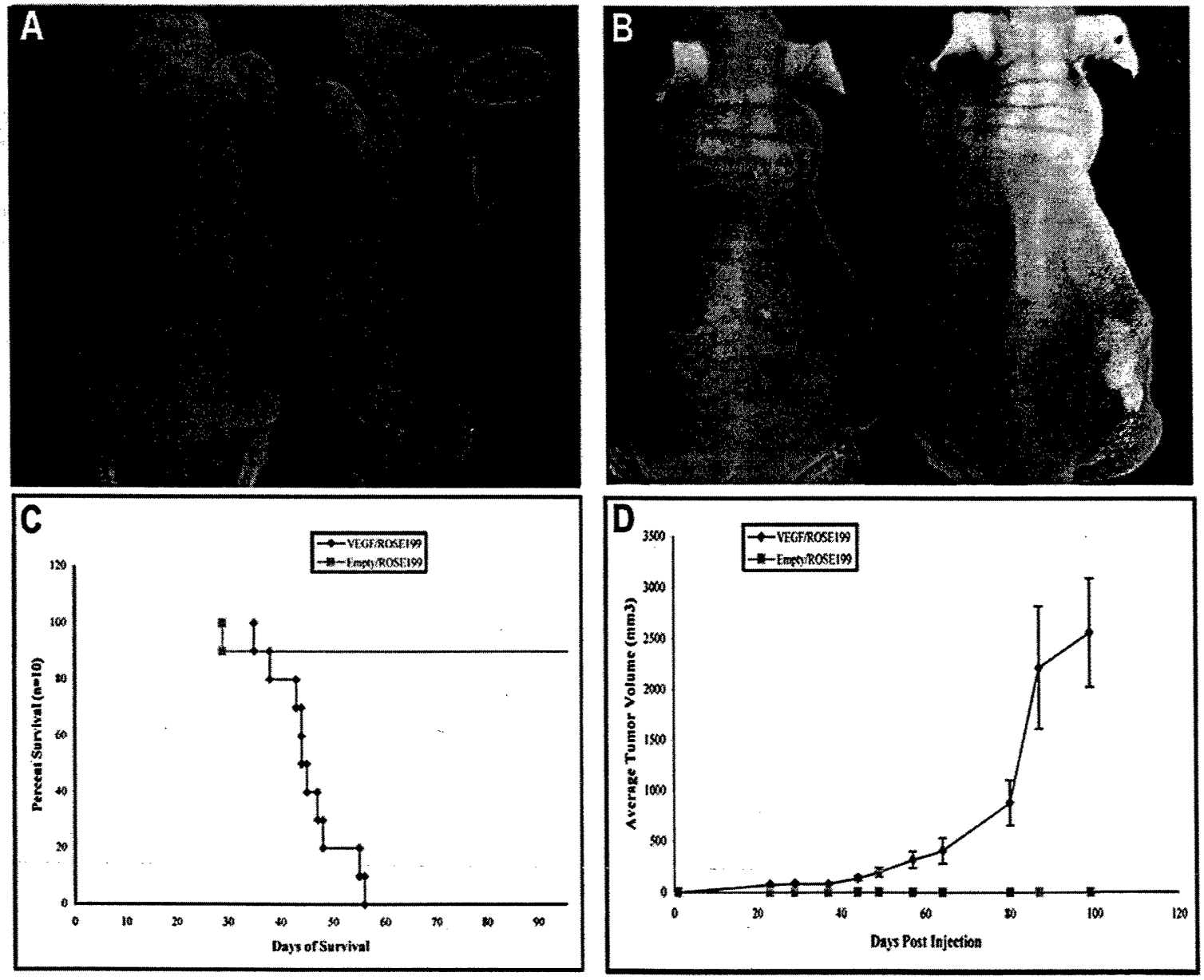

Figure 5 - Schumacher

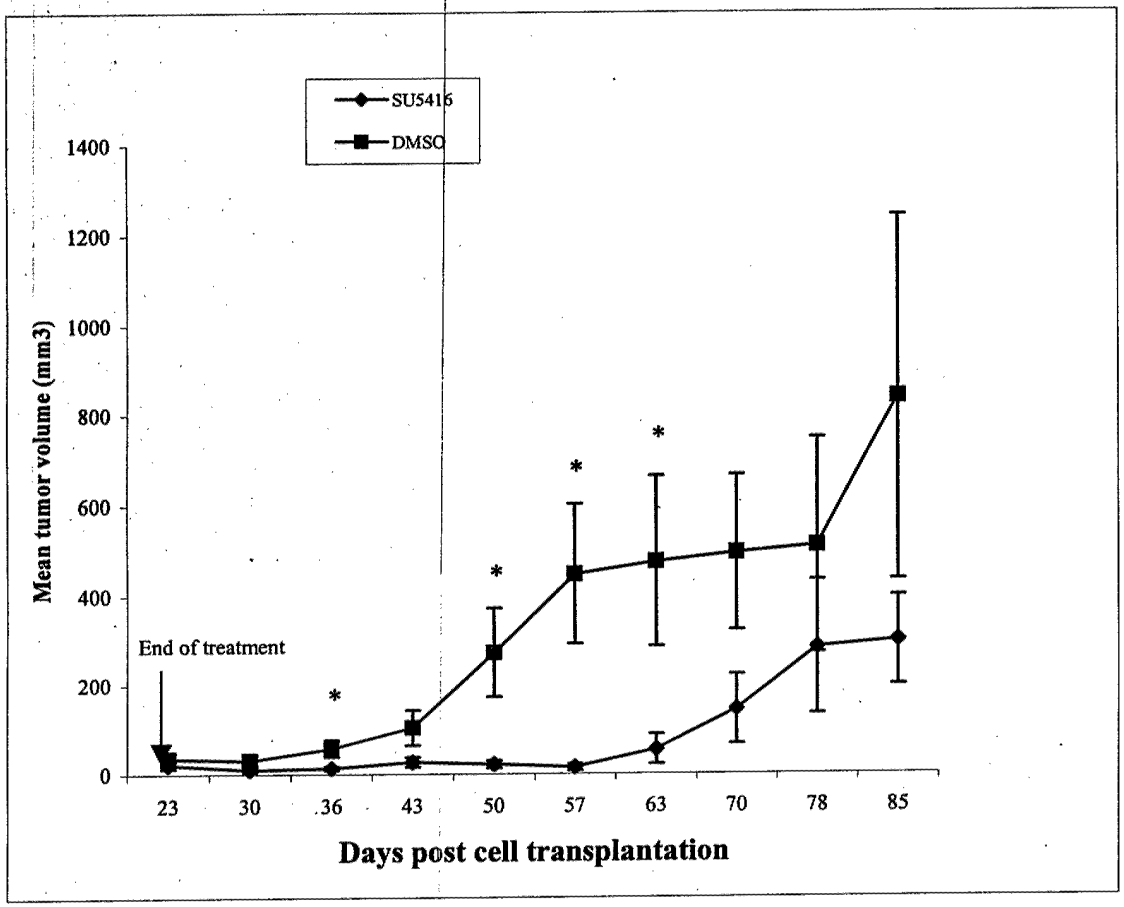

Project 3: Rational Angiogenesis in the Etiology and Prevention of Ovarian Cancer

ABSTRACT

The purpose of this project to evaluate de novo synthesis of a short polypeptides, which is capable of inhibiting tumor angiogenesis. As tumor growth in general and ovarian cancer in particular is associated with angiogenesis, the synthetic peptide can be used to inhibit growth and peritoneal seeding of ovarian cancer.

Table of Contents

Cover.....106

SF 298.....107

Table of Contents.....108

Introduction.....109

Body.....109

Key Research Accomplishments.....111

Reportable Outcomes.....111

Conclusions.....111

References.....111

Appendices.... 111

Annual Report for Project 3 -- October 2001 - September 2002
"Rational Antiangiogenic Peptide Design - Effect on Ovarian Cancer Growth"
K.H. Mayo, PI.

INTRODUCTION

Achievements in the prevention of metastasis and solid tumor growth in ovarian cancer and in cancer in general, have been limited over the last decade. Current available anti-cancer strategies, which are all aimed at directly killing tumor cells, badly need improvement. A very promising, alternative prevention to cancer is anti-angiogenic therapy. Sprouting of new microvasculature from pre-existing blood vessels is a prerequisite for outgrowth of tumors beyond a certain size and the development of metastases. Negative regulation of angiogenesis can be effected in various ways by an ever-growing number of endogenous inhibitors such as platelet factor-4 (PF4), interferon-γ inducible protein-10 (IP-10), interferon-γ, angiostatin and endostatin as well as by synthetic agents (e.gs., thalidomide, TNP-470, metalloproteinase inhibitors and bFGF-binding oligosaccharides). Blockade of angiogenesis or the tumor's blood supply, has recently been demonstrated to be effective ways to treat tumors in animal models. It is expected that combining anti-angiogenesis therapy with conventional chemotherapy will result in a significant improvement of cancer prevention and treatment. The advantage of these novel anti-angiogenic strategies is the better accessibility of molecules to be targeted compared with direct tumor targets. Moreover, these strategies interfer at the level of the powerful control that the endothelial compartment exerts over the growth of tumor cells. Finally, it is likely that tumor endothelial cells are genetically more stable than tumor cells and that they are therefore not expected to develop resistance against the therapies applied. Recently, the P.I. designed a novel peptide, βpep-25, with potent angiostatic activity. Of direct health-relatedness in this project is that βpep peptides define a novel class of non-endogenous cytokines which are active angiostatic agents capable of abrogating tumor growth. Structurally, βpep peptides form β-sheets in a tetrameric array. The significance and novelty of this project lie in understanding the angiostatic mechanism of action of βpep peptides and in designing an angiostatic βpep peptide, as well as analogs, capable of preventing or suppressing tumor growth in ovarian cancer.

BODY

Hypothesis/Objective

βpep-25 and its designed analogs can be used to abrogate tumor growth in vivo and potentiate the action of chemotherapy, making use of lower, less toxic, doses of chemotherapeutics possible. The objectives are to preform in vitro and tumor model studies in mice using MA148 ovarian cancer cell line in the absence and presence of chemotherapeutic agents and to modify the amino acid sequence of the peptide to improve its own efficacy. Given the angiostatic potential of βpep-25 and its analogs, the overall aim of this research is to develop βpep-25 or an analog into a preventative therapeutic anti-tumor agent against ovarian cancer.

Relevance to Ovarian Cancer

The tumor model studies mentioned above will be performed using an ovarian cancer cell line, MA148. In this regard, studies will be performed to specifically assess the efficacy of treatment on ovarian carcinoma.

Methodology and Design

<u>Specific Aim 1:</u> define structure-activity relationships in βpep-25 and design new, more potent βpep sequences. The βpep-25 peptide sequence will be modified by substituting individual amino acid residues and by alanine scanning. Walk-through peptides will also be generated. Peptides

will then be screened for various *in vitro* bioactivities relating to angiostatic potential: endothelial cell (EC) proliferation and collagen gel-based tube formation assay. Proper folding of peptides will be assessed by using CD and NMR in order to differentiate direct and indirect (conformational) effects. The initial round of amino acid substitutions will naturally lead into multiple substitutions and designing in conformational constraints [rationally placed S-S bond(s) or specific turn sequences]. Residues from sequences of other angiostatic agents like endostatin and angiostatin, will also be built into the basic βpep design. Designing and bioassaying will be applied iteratively with the intent of improving angiostatic potential.

Results for Aim 1 in year 3: In years 1 and 2, alanine scanning and walk-through βpep-25 peptides were synthesized and analyzed in *in vitro* assays, and structure-function relationships were derived. From this information, key amino acids were identified that led to the design and synthesis of the CF series in year 2. This series uses a biphenylfuran scaffold onto which are covalently attached short, key amino acid sequences derived from βpep-25. CF analogs maintain the bioactive β-sheet fold found in the parent peptide, βpep-25. In *in vitro* assays, we originally found that CF-8, as analog having 18 of the original 33 residues, maintained relatively good potency compared to βpep-25. CF-8 inhibits completely the growth of endothelial cells at a concentration of about 10 micromolar. Since that time, it was discovered that CF-8 is as potent as βpep-25 *in vivo*. We continued reducing the number of residues in CF-8 and found that an analog with only 8 residues (CF-4) was nearly as active in vitro as CF-8 or βpep-25. This analog was then tested in vivo (see below).

Specific Aim 2: elucidate the molecular mechanism of action of βpep-25 by which angiostatic effects are mediated. This includes identifying the angiostatic pathway, the receptor(s) involved, internalization pathway and the like.

Results for Aim 2 in year 3: From year 1, we knew the essentials of the molecular mechanism of anti-angiogenic action of βpep-25. The peptide interacts with a receptor, CD36, on the surface of EC, becomes internalized and triggers the apoptotic cascade. This process is specific for angiogenically-activated EC where CD36 is upregulated, and does not affect resting EC or other cell types. Last year, we discovered that βpep-25 may also be interacting with the TNF-α receptor. We have extended this understanding of the molecular mechanism to include the CF series. Both CF-8 and CF-4 (as well as other Cf analogs) are highly cytostatic like βpep-25.

Specific Aim 3: study effectivity to inhibit angiogenesis and tumor growth *in vivo*. For this aim, we have focused on performing nude mouse tumor growth models and have basically decided that the chicken ovarian cancer model will not presently be used for these investigations. In nude mice studies, the ovarian cancer cell line MA148 will be used. In these models, all preclinical research can be performed to prepare the research line for phase I clinical trials. Pharmacokinetics and tissue distribution of peptides in animals will then be studied with the use of anti-peptide mAbs, polyclonals and mass spectrometry.

Results for Aim 3 in year 3: The ovarian cancer cell line MA148 has been used in nude mice tumor studies with βpep-25 and mimetics CF-8 and CF-4. For these studies, MA148 cancer cells have been injected SC into the hind flank of nude mice and tumors have been allowed to grow to the size of 50 mm^3 to 100 mm^3 prior to administering the drug. The best route for administration is systemic s.c. using osmosis-based mini-pumps. Mini-pumps were implanted 48 hours prior to innoculation with MA148 cells. Results indicate a good dose response and high level of effectivity for the peptide and its CF analogs. At the optimal dose of 0.2 mg/day/animal over a four week period, tumor size was reduced by about 70%, somewhat greater than that of angiostatin in the same model (in this model, endostatin is essentially ineffective). In this model, CF-8 and CF-4 both function better than parent peptide βpep-25, by reducing tumor volume to about 90% at the same dose of 0.2 mg/day/animal given over a four week period. Because these CF analogs are more effective in vivo

and somewhat less effective in vitro, this suggests that we have essentially improved bioavailability in the CF series. Pharmacokinetics and tissue distribution of these peptides in animals have begun. The half-life is about 50 minutes for βpep-25, and tissue distribution is such that much of the peptide is found in the kidney (filtered out) and in the tumor, but the other tissues are essentially clear. In this regard, the peptide is specific for tumor tissue.

Specific Aim 4. investigate combined angiogenesis and chemotherapy *in vivo*. Additional animal studies will be performed to investigate whether conventional chemotherapy can be improved by co-administration with anti-angiogenic agents.

Results for Aim 4 in year 3: In vivo studies were performed with combination therapy of βpep-25 with carboplatin and angiostatin. In both cases, synergistic effects were observed and tumors were found to regress. The final year of the grant will investigate effects from combination therapy using CF-4 and CF-8 with carboplatin and angiostatin.

KEY RESEARCH ACCOMPLISHMENTS

-- βpep-25 inhibits the growth of ovarian tumors by about 70%.

-- Using info derived from identification of functionally key residues in βpep-25, a series of partly non-peptide mimetics of βpep-25 have been designed and synthesized. The most efficacious of these is CF-8.

-- CF-8 and the shorter mimetic, CF-4, inhibit the growth of ovarian tumors in athymic mice by about 90%, an improvement over βpep-25.

REPORTABLE OUTCOMES

Five papers have been published from this work so far, and others are in preparation.

1. Griffioen, A.W., van der Schaft, D., Barandsz-Janson, A., Cox, A., Hillen, H.F.P., & MAYO, K.H. "Anginex (βpep-25), a designed Peptide that Inhibits Angiogenesis," Biochem. J. 354, 233-242 (2001).
2. Cox, A., Arroyo, M. & MAYO, K.H. "Effects on Folding and Self-Association from Substitution of Hydrophobic Residues at the β-Sheet Sandwich Interface of βpep-4," Biochem. J. 357, 739-747 (2001).
3. MAYO, K.H., van der Schaft, D., & Griffioen, A.W. "Designed β-sheet peptides that inhibit proliferation and induce apoptosis in endothelial cells" Angiogenesis 4, 45-51 (2001).
4. Dings, R.P.M., Yokoyama, Y., Ramakrishnan, S., Griffioen, A.W. and MAYO, K.H. 'The designed angiostatic peptide anginex synergistically improves chemotherapy and anti-angiogenesis therapy with angiostatin," Cancer Res. (in the Press) (2002).
5. Dings, R.P.M., Hargittai, B., Haseman, J., Griffioen, A.W. and MAYO, K.H. "Anti-tumor activity of the novel angiogenesis inhibitor anginex," Cancer Letters (submitted) (2002).

CONCLUSIONS

Peptide βpep-25, and next generation CF analogs, are effective anti-angiogenic, anti-tumor agents with reasonably high potential for effectivity against ovarian carcinoma in humans.

REFERENCES

None.

APPENDICES

Final two papers listed under 'Reportable Outcomes'.

APPENDIX

Project 3

Journal: Cancer Research
Article Type: regular article
File: revised canres1021

The designed angiostatic peptide anginex synergistically improves chemotherapy and anti-angiogenesis therapy with angiostatin.

Ruud P.M. Dings[*$], Yumi Yokoyama[#], S. Ramakrishnan[#],
Arjan W. Griffioen*, Kevin H. Mayo[$].

[$]*Departments of Biochemistry and* [#]*Pharmacology University of Minnesota Health Sciences Center, 435 Delaware Street, Minneapolis, MN 55455.*
[*]*Tumor Angiogenesis Laboratory, Department of Internal Medicine, University Hospital Maastricht, P.O. Box 5800, 6202 AZ Maastricht,The Netherlands.*

running title: **Anginex, a potent *in vivo* tumor growth inhibitor.**

[+] correspondence to:
Dr. Mayo, [$]*Department of Biochemistry, Molecular Biology and Biophysics. University of Minnesota Health Sciences Center, 312 Church Street, Minneapolis, MN 55455. Phone: 612-6259968* Fax:612-6245121 E-mail: mayox001@tc.umn.edu

Abbreviations: EC, endothelial cell; HUVEC, human umbilical vein EC; PBS, phosphate buffered saline; BSA, bovine serum albumin.

Key words: Anginex, angiogenesis, angiostatin, chemotherapy, and ovarian carcinoma.

Abstract

Recently, we demonstrated that the designed peptide anginex displays potent anti-angiogenic activity. The aim of the present study was to investigate anginex-treatment as a single-agent therapy and to test its ability to improve conventional chemo- and anti-angiogenesis therapy. In a human ovarian carcinoma mouse model, anginex inhibited tumor growth by 70%. When anginex was combined with a sub-optimal dose of carboplatin, tumors regressed to an impalpable state. Anginex plus angiostatin worked synergistically to inhibit tumor growth. Assessment of microvessel density suggested that the anti-tumor activity of anginex is mediated by angiogenesis inhibition. In any of the experiments, no sign of anginex-induced toxicity was observed.

Introduction

Neo-vascularization or angiogenesis is the process of new capillary outgrowth from pre-existing blood vessels. Sustained angiogenesis is one of the essential alterations in cell physiology that collectively dictate malignant growth (1). Angiogenesis is required for solid tumors to grow beyond the size of approximately of 1-2 mm^3. A highly vascularized tumor is associated with poor clinical prognosis, not only because of the potential for exponential tumor growth, but also because of the increased access capacity to the capillaries (2), which supposedly facilitates metastasis formation (3). Consequently, methods to inhibit angiogenic sprouting provide a unique opportunity to arrest tumor growth and prevent metastasis, either alone or in combination with conventional therapies. Combination of angiogenic inhibitors with radiation (4, 5), gene therapy (6) or chemotherapy (7) has been show to be successful. Recently, we reported the design of anginex, a β-sheet forming peptide 33mer, with potent *in vitro* anti-angiogenesis activity (8). The aims of the present study were to investigate anginex treatment *in vivo* as a single-agent therapy and in combination with conventional chemotherapy and the structurally unrelated anti-angiogenic angiostatin. Here, we show that while anginex alone significantly inhibits tumor growth, treatment in combination with a sub-optimal dose of carboplatin, results in tumor remissions to microscopic disease and in combination with angiostatin demonstrates a synergistic effect at inhibiting tumor growth. The present data warrant further development of anginex for clinical use.

Materials and Methods

Reagents. Anginex and control peptide, ßpep28 were synthesized as described earlier (8). ßpep28 is 91% homologous and 67% identical peptide compared to anginex but has no anti-angiogenic activity (8). Carboplatin (Sigma Diagnostics; St Louis, MO) was dissolved in PBS (32.5 mg/kg) and administered once every three days i.p.. Angiostatin (20 mg/kg) was administered daily s.c. in the neck, as described earlier (11).

Culture. MA148, a human epithelial ovarian carcinoma cell line, was cultured on non-coated flasks using 10% FBS, 1% penicillin/streptomycin in RPMI 1640. Cultures were split 1:3 every 3 days. Mouse angiostatin (kringle 1-4) was cloned and expressed in *Pichia pastoris* (9), with culturing, elution and purification being done as described previously (10, 11).

Ovarian Carcinoma Mouse Model. Female athymic nude mice (nu/nu, 5-6 weeks old) were purchased from the National Cancer Institute and allowed to acclimatize for one week. Human ovarian MA-148 epithelial carcinoma cells were cultured, harvested and inoculated subcutaneously into the right flank of the mouse as described previously (11). In the initial experiment, treatment was initiated after randomization of mice, and implanting osmotic mini-pumps (Durect; Cupertino, CA) into the left flank. The pumps had a treatment span of 28 days, which started on the same day as the inoculation of the ovarian carcinoma cells. Subsequently, studies were carried out in a therapeutic intervention model with established tumors to test the capacity of anginex to inhibit tumor growth and to test it in conjunction with angiostatin. In this latter model, treatment was initiated 7 days post-inoculation with

the MA148 cells. To test anginex's ability to enhance conventional chemotherapy, carboplatin was used in combination with anginex, in the same intervention model.

Tumor volume was determined by measuring the size of the tumors on the flanks of the mice. The diameters of tumors were measured using callipers (Scienceware; Pequannock, NJ) and the volume was calculated using the equation to determine the volume of a spheroid: $(a^2 \times b \times \Pi) / 6$, where 'a' is the width and 'b' is the length of the tumor.

Immunohistochemistry. Tumor tissues were embedded in tissue freezing medium (Miles Inc.; Elkart, IN) and snap frozen in liquid nitrogen. Preparation and procedures were done as described earlier (12). Samples were subsequently incubated in a 1:50 dilution with phycoerytrin (PE)-conjugated monoclonal antibody to mouse CD-31 (PECAM-1) (Pharmigen; San Diego, CA) or a fluorescien isothiocyanate (FITC)-conjugated PCNA (Ab-1) (Oncogene; San Diego, CA) to stain for microvessel density (MVD) or proliferation, respectively. After a 1-hour incubation at room temperature, slides were washed with PBS and immediately imaged in an Olympus BX-60 fluorescence microscope at 200X magnification. Sections were also stained for cell death using a TUNEL (terminal deoxyribonucleotidyl transferase-mediated dUTP-nick-end labelling) assay carried out according to the manufacturer's instructions (*in situ* cell death detection kit, fluorescein; TUNEL, Roche). Although the TUNEL assay detects apoptosis, it can not be ruled out that TUNEL will also stain for necrosis, where extensive DNA fragmentation may occur. Digital images were acquired and processed using Adobe Photoshop (Adobe Inc., Mountain View, CA). Vessel density was quantified as described earlier (12). Statistical analysis was performed using the Student's *t* test.

Toxicity assays. As an indirect measurement of general toxicity, body weights of mice were monitored twice weekly, using a digital balance (Ohaus Florham, NJ). To determine hematocrit and creatinine levels, blood samples were extracted by tail vein bleedings one day after terminating treatment and blood was collected in heparinized micro-hematocrit capillary tubes (Fisher; Pittsburgh, PA). For hematocrit levels, samples were spun down for 10 minutes in a micro-hematocrit centrifuge (Clay-Adams; NY), and the amount of hematocrit was determined using an international microcapillary reader (IEC; Needham, Mass). To obtain creatinine levels, a kit was purchased from Sigma (Sigma Diagnostics; St Louis, MO) and used according to the manufacturer's instructions.

Results

Anginex inhibits tumor growth *in vivo*. Mice, inoculated with MA148 ovarian carcinoma cells, were randomized and treated systemically with anginex for 28 days using osmotic mini-pumps starting at the day of inoculation. A control peptide, βpep-28, that is 91% sequentially homologous and 67% identical to anginex, was used to control for peptide content. Another set of animals was treated with vehicle containing BSA to control for protein content. As illustrated in Figure 1, treatment with anginex resulted in a dose-dependent inhibition of tumor growth that was maximal at 10 mg/kg/day as compared with vehicle-treated animals. At this dose, anginex inhibited about 70% of tumor growth. At half this dose, tumor growth was inhibited only by 50%, while a higher dose (20 mg/kg/day) did not result in enhanced efficacy (Figure 1). Tumors from control peptide βpep-28 treated mice did not differ in size from tumors in the BSA vehicle treated animals. Moreover, treatment with

BSA or βpep-28 did not result in altered tumor growth as compared to treatment with saline alone (not shown).

Anginex inhibits tumor growth of established tumors and improves conventional chemotherapy. Since initial animal experiments were performed using an experimental set-up where treatment was started at the time of tumor inoculation (a system that models treatment of minimal residual disease), anginex was also tested using the MA148 model in an intervention set-up where treatment was initiated after tumor establishment. In these experiments, anginex inhibited tumor growth by approximately 50% (Figure 2B).

In an attempt to improve the efficacy of platinum-based chemotherapy, anginex was administered to tumor-bearing mice that were concurrently treated with a sub-optimal dose of carboplatin. Carboplatin treatment resulted in an effective reduction of tumor growth; however when it was combined with anginex, no tumor mass could be palpated in these mice (Figure 2A). One week after termination of treatment the tumor reestablished.

Anginex and angiostatin act synergistically to inhibit tumor growth. Using optimized treatment regimes for angiostatin (11), and anginex, we found that both anginex and angiostatin, administered separately, inhibited tumor growth comparably by approximately 50%, in the same ovarian tumor model. Based on those findings the interaction between angiostatin an anginex was examined. Combination therapy of angiostatin with anginex, resulted in enhanced tumor growth inhibition (80%) (Figure 2B), which was deemed to be synergistic (Table 1).

Toxicity. Animals treated with anginex (alone or in combination regimens) did not show any sign of toxicity as assessed by unaltered behaviour, weight gain during experiments, normal hematocrit and creatinine levels, and macro- and microscopic morphology of internal organs on autopsy. Body weights of mice were monitored as an indirect measurement of general toxicity. In experiments where carboplatin was administered, the weights of mice actually fell initially and subsequently increased on termination of exposure to carboplatin. This was taken as a sign of mild reversible toxicity. Anginex did not augment this toxicity. One day after the termination of treatment, blood was drawn and hematocrit and creatinine levels were determined as a measure of bone marrow and kidney toxicity, respectively. Hematocrit levels reported as a percentage of red blood cells (vehicle 50.2 ± 2.9, anginex 51.3 ± 2.5, carboplatin 49.3 ± 2.8, and combination 47.2 ± 2.4) and creatinine levels reported in μmoles/l (vehicle 46.8 ± 8, anginex 48 ± 1.4, carboplatin 55.5 ± 12.6, and combination 42 ± 5.3) showed no significant difference in the study involving carboplatin. The study combining anginex and angiostatin treatment showed similar hematocrit levels (vehicle 49 ± 1.7, anginex 49.2 ± 2.6, angiostatin 47.8 ± 2.1, and combination 48.3 ± 1.9 in percentage red blood cells) and creatinine levels (vehicle 46.8 ± 6.4, anginex 48 ± 1.4, angiostatin 41 ± 0.4, and combination 39.2 ± 5.9 in μmoles/l).

Histological analysis of microvessel density, cell death and proliferation. Anginex treatment resulted in a decrease of tumor microvessel density (MVD), suggesting that the anti-tumor activity of anginex is the result of angiogenesis inhibition. Angiostatin demonstrated a similar result. Although anginex and angiostatin acted synergistically on tumor growth inhibition, this was not reflected in

the MVD assessment (Figure 3B). Aside from vessel density (including number, size and length (12)), the digital approach discriminates branch points, end points and vessel lengths. Some of these architectural parameters did change upon combination treatment relative to single agent treatment. For example, combination treatment revealed a synergistic reduction in the number of branch points (not shown). Tumors from anginex-treated animals showed a convincing MVD reduction ($p < 0.01$), whereas tumors from carboplatin-treated animals showed a smaller, albeit significant ($p < 0.05$), reduction in MVD (Figure 3A). Tumors treated with the combination of anginex and carboplatin could not be stained because all tumors disappeared three weeks after initiation of treatment.

Although combination of anginex and angiostatin also showed a synergistic effect in the increased amount of cell death ($p < 0.03$), as determined by TUNEL analysis, angiostatin by itself did not trigger increased cell death compared to the vehicle group (Figure 3D). As expected, carboplatin did show an increase in the amount of cells undergoing cell death ($p < 0.01$). A down regulation in proliferation, as determined by PCNA staining, was revealed in all treated groups compared to controls, significant for anginex and combination treated groups ($p< 0.01$, Figures 3E and F).

Discussion

Induction of angiogenesis by malignant cells has been shown to play a pivotal role in the process of tumor proliferation and metastasis (13). Inhibition of angiogenesis is, therefore, a promising way to arrest tumor growth and prevent metastasis. Due to the need for new anti-tumor agents with improved potency, stability, selectivity and ease of delivery, we used a novel approach in designing the β-sheet-forming anginex peptide (8). Anginex acts specifically on activated endothelial cells (EC) to trigger apoptosis, presumably by preventing cell adhesion and subsequent induction of anoikis (8). Here, we demonstrate that anginex is an anti-angiogenic compound with anti-tumor activity when administered systemically as a single-agent therapeutic.

Because anti-angiogenic agents can potentiate cytotoxic cancer therapies (7), anginex was tested in combination with the chemotherapeutic carboplatin. Platinum agents are the most widely used drugs in the first-line of defense against ovarian cancer (14, 15). In a recent study, single-agent carboplatin proved to be just as effective as carboplatin plus paclitaxel in women requiring chemotherapy for ovarian cancer. The favorable toxicity profile of carboplatin alone suggested that this is a reasonable option as a single-agent chemotherapeutic (16). An additional advantage of carboplatin is that, in contrast to other agents such as taxanes, cyclophosphamide and vincristine, it is not an anti-angiogenic by itself. Because carboplatin has been shown to be a very powerful anti-cancer drug in the model used here, a sub-optimal dose was employed. Both anginex and carboplatin inhibited tumor growth, but the combination blocked tumor growth completely, and palpable tumors regressed to undetectable sizes in all animals. Moreover, tumors remained undetectable until at least one week after termination of the treatment, after which tumors re-established

themselves, indicating continued presence of microscopic disease, which was unresponsive to carboplatin and apparently independent of angiogenesis.

Whereas numerous investigators have focused on the anti-cancer effects from endostatin in their tumor model studies, we chose to use angiostatin because in the same MA148 tumor mouse model, Yumi et al. (11) found that angiostatin was considerably more effective at inhibiting tumor growth than endostatin. Here, we found that although treatment with angiostatin or anginex showed essentially the same capacity to inhibit tumor growth, combination of the two produced a dramatically enhanced inhibitory effect. This synergy between angiostatin and anginex suggests that their mechanisms of action are different and that they can augment each other as anti-angiogenic agents. These data, therefore, provide a validation for combination therapy, if not for cocktails of angiogenesis inhibitors, to improve the treatment of cancer.

Immunohistochemical assessment of MVD indicated that tumor growth inhibition by anginex is explained by its anti-angiogenic activity. Angiostatin showed the same trend. Combination therapy, however, did not yield an increased MVD reduction. This may be explained by the fact that differences in architecture are not represented in the MVD value assessed either digitally or manually. The digital approach discriminates for architectural parameters, some of which did change upon combination treatment relative to single agent treatment. For example, combination treatment revealed a synergistic reduction in the number of branch points (not shown).

This study adds credence to the proposal that cancer treatment using anti-angiogenesis agents is more effective when performed in combination with other agents. However, it might be that only cocktails of anti-angiogenic compounds would

provide sufficient potency to be evaluated properly in early clinical trials. Currently, clinical evaluation of anti-angiogenic compounds is in its infancy, and while a stand-alone approach using an anti-angiogenic agent shows promise, combination therapy may provide for the best evaluation of these agents and, in the end, may be more beneficial. Present results suggest that combination of anti-angiogenics with chemotherapeutics will produce a greater effect than combinations of anti-angiogenic agents alone. At the very least, this study indicates that combining the anti-angiogenic compound anginex with conventional chemotherapy allows dosage of the chemotherapeutic to be reduced, while still being able to effect tumor growth reduction.

Acknowledgements

This research was supported by grants from the Department of Defense (DA/DAMD 17-99-1-9564) to K.H.M. and S.R. and from the National Institutes of Health (NIH CA-96090) to K.H.M.. We would like to thank V.P. Sukhatme for providing us with the angiostatin clone.

References

1. Hanahan, D. and Weinberg, R. A. The hallmarks of cancer, Cell. *100:* 57-70, 2000.
2. Williams, S. G., Buscarini, M., and Stein, J. P. Molecular markers for diagnosis, staging, and prognosis of bladder cancer, Oncology (Huntingt). *15:* 1469-70, 1473-4, 1476; discussion 1476-1484, 2001.
3. Weidner, N. Angiogenesis as a predictor of clinical outcome in cancer patients, Hum Pathol. *31:* 403-405, 2000.
4. Gorski, D. H., Mauceri, H. J., Salloum, R. M., Gately, S., Hellman, S., Beckett, M. A., Sukhatme, V. P., Soff, G. A., Kufe, D. W., and Weichselbaum, R. R. Potentiation of the antitumor effect of ionizing radiation by brief concomitant exposures to angiostatin, Cancer Res. *58:* 5686-5689, 1998.
5. Mauceri, H. J., Hanna, N. N., Beckett, M. A., Gorski, D. H., Staba, M. J., Stellato, K. A., Bigelow, K., Heimann, R., Gately, S., Dhanabal, M., Soff, G. A., Sukhatme, V. P., Kufe, D. W., and Weichselbaum, R. R. Combined effects of angiostatin and ionizing radiation in antitumour therapy, Nature. *394:* 287-291, 1998.
6. Wilczynska, U., Kucharska, A., Szary, J., and Szala, S. Combined delivery of an antiangiogenic protein (angiostatin) and an immunomodulatory gene (interleukin-12) in the treatment of murine cancer, Acta Biochim Pol. *48:* 1077-1084, 2001.
7. Teicher, B. A., Sotomayor, E. A., and Huang, Z. D. Antiangiogenic agents potentiate cytotoxic cancer therapies against primary and metastatic disease, Cancer Res. *52:* 6702-6704, 1992.

8. Griffioen, A. W., van der Schaft, D. W., Barendsz-Janson, A. F., Cox, A., Struijker Boudier, H. A., Hillen, H. F., and Mayo, K. H. Anginex, a designed peptide that inhibits angiogenesis, Biochem J. *354:* 233-242, 2001.

9. Dhanabal, M., Ramchandran, R., Volk, R., Stillman, I. E., Lombardo, M., Iruela-Arispe, M. L., Simons, M., and Sukhatme, V. P. Endostatin: yeast production, mutants, and antitumor effect in renal cell carcinoma, Cancer Res. *59:* 189-197, 1999.

10. Mohanraj, D., Olson, T., and Ramakrishnan, S. Expression of biologically active human vascular endothelial growth factor in yeast, Growth Factors. *12:* 17-27, 1995.

11. Yokoyama, Y., Dhanabal, M., Griffioen, A. W., Sukhatme, V. P., and Ramakrishnan, S. Synergy between angiostatin and endostatin: inhibition of ovarian cancer growth, Cancer Res. *60:* 2190-2196, 2000.

12. Wild, R., Ramakrishnan, S., Sedgewick, J., and Griffioen, A. W. Quantitative assessment of angiogenesis and tumor vessel architecture by computer-assisted digital image analysis: effects of VEGF-toxin conjugate on tumor microvessel density, Microvasc Res. *59:* 368-376, 2000.

13. Alvarez, A. A., Krigman, H. R., Whitaker, R. S., Dodge, R. K., and Rodriguez, G. C. The prognostic significance of angiogenesis in epithelial ovarian carcinoma, Clin Cancer Res. *5:* 587-591, 1999.

14. Harries, M. and Kaye, S. B. Recent advances in the treatment of epithelial ovarian cancer, Expert Opin Investig Drugs. *10:* 1715-1724, 2001.

15. Tattersall, M. H. N. Ovarian cancer chemotherapy: carboplatin as standard, The Lancet. *360:* 500-501, 2002.

16. ICON. Paclitaxel plus carboplatin versus standard chemotherapy with either single-agent carboplatin or cyclophosphamide, doxorubicin, and cisplatin in women with ovarian cancer: the ICON3 randomised trial, The Lancet. *360:* 505-515, 2002.

Figure Legends

Fig. 1. Anginex causes significant tumor growth inhibition. The mean tumor growth of human MA148 ovarian carcinoma is shown in athymic mice treated with a dose-range of anginex [(-▼-) 5 mg/kg/day, n=14; (-●-) 10 mg/kg/day, n=16, or (-▲-) 20 mg/kg/day, n=8)] administered by mini-pumps implanted in the left flank of animals. Controls (-□-) contained PBS with BSA (n=13) and PBS with ßpep28 5 mg/kg/day (-O-; n=8) and 10 mg/kg/day (-△-; n=4), which did not differ from each other. The treatment period was initiated on the day of tumor inoculation (day 0) and lasted for 28 days as indicated by the vertical arrow in the figure. Data from three independent studies are shown and represent the mean tumor volume in mm^3 (± SE).

Fig. 2. The mean tumor growth curves in a human ovarian carcinoma model treated with anginex, carboplatin, angiostatin or a combination treatment. In panel 2A groups are shown defined as follows, vehicle containing BSA (-□-, n=11), anginex (-●-; 10 mg/kg/day, n=11), carboplatin (-X-; n=12) and a combination group (-◆-; n=12). Carboplatin was given in a sub-optimal dosage (32.5 mg/kg) once every three days in an intra-peritoneal matter. In panel 2B groups are defined as vehicle containing BSA (-□-, n=11), angiostatin (-▲-; 20 mg/kg/d, n=11), anginex (-●-; 10 mg/kg/day, n=11) or combination (-▼-; n=12) of angiostatin and anginex in an ovarian carcinoma xenograft model. In both experiments treatment was given for 28 days starting on day 7 post-inoculation. The vehicle and anginex were given by osmotic mini-pump implanted subcutaneously in the flank, and angiostatin was given daily by injections subcutaneously in the neck (11). The data are shown as means of tumor burden; bars: SE. The tumor volumes were determined three times a week. The insets in both panels show body weights of mice during treatment as an indirect measurement of toxicity.

Fig. 3. Immunohistochemistry analyses. After snap freezing tumor tissues, 10 μm sections were made and stained for microvessel density by using anti-CD-31 antibodies (panel A and B), cell death by TUNEL (panel C and D) and proliferation by PCNA (panel E and F), all expressed in number of white pixels. The procedure and

quantification were described earlier (12). Panel A, C, and E show quantifications of the studies involving anginex and carboplatin. Panels B, D and F show quantification of studies involving anginex, angiostatin or combination therapy. As determined by using the student's *t* test relative to the vehicle group, * $p < 0.05$, ** < 0.03, *** $p < 0.01$.

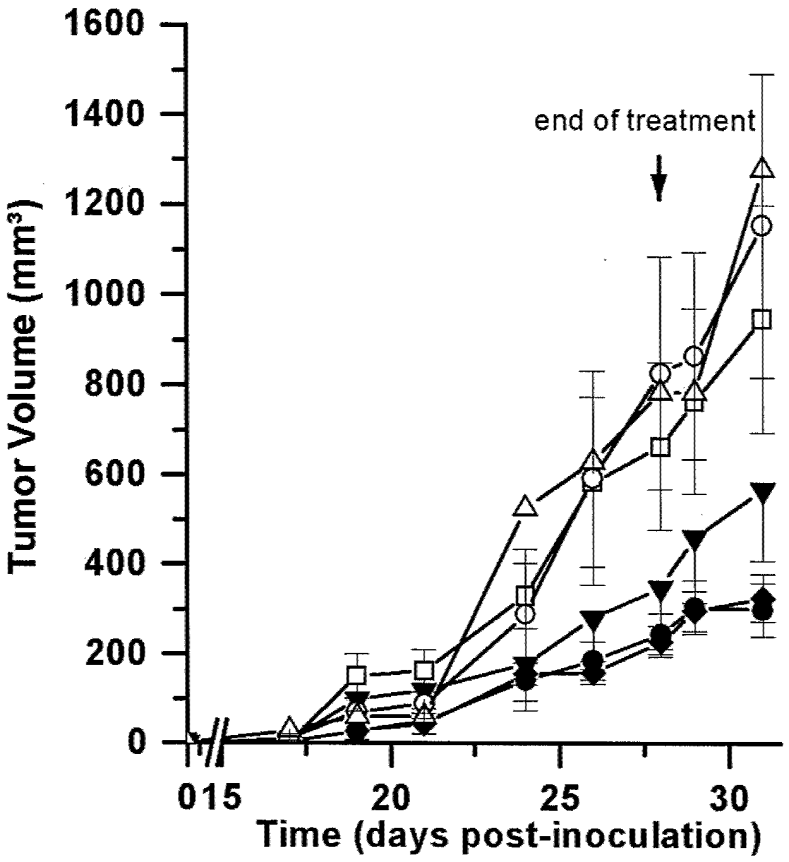

Figure 1
Dings et al. Top ⇑

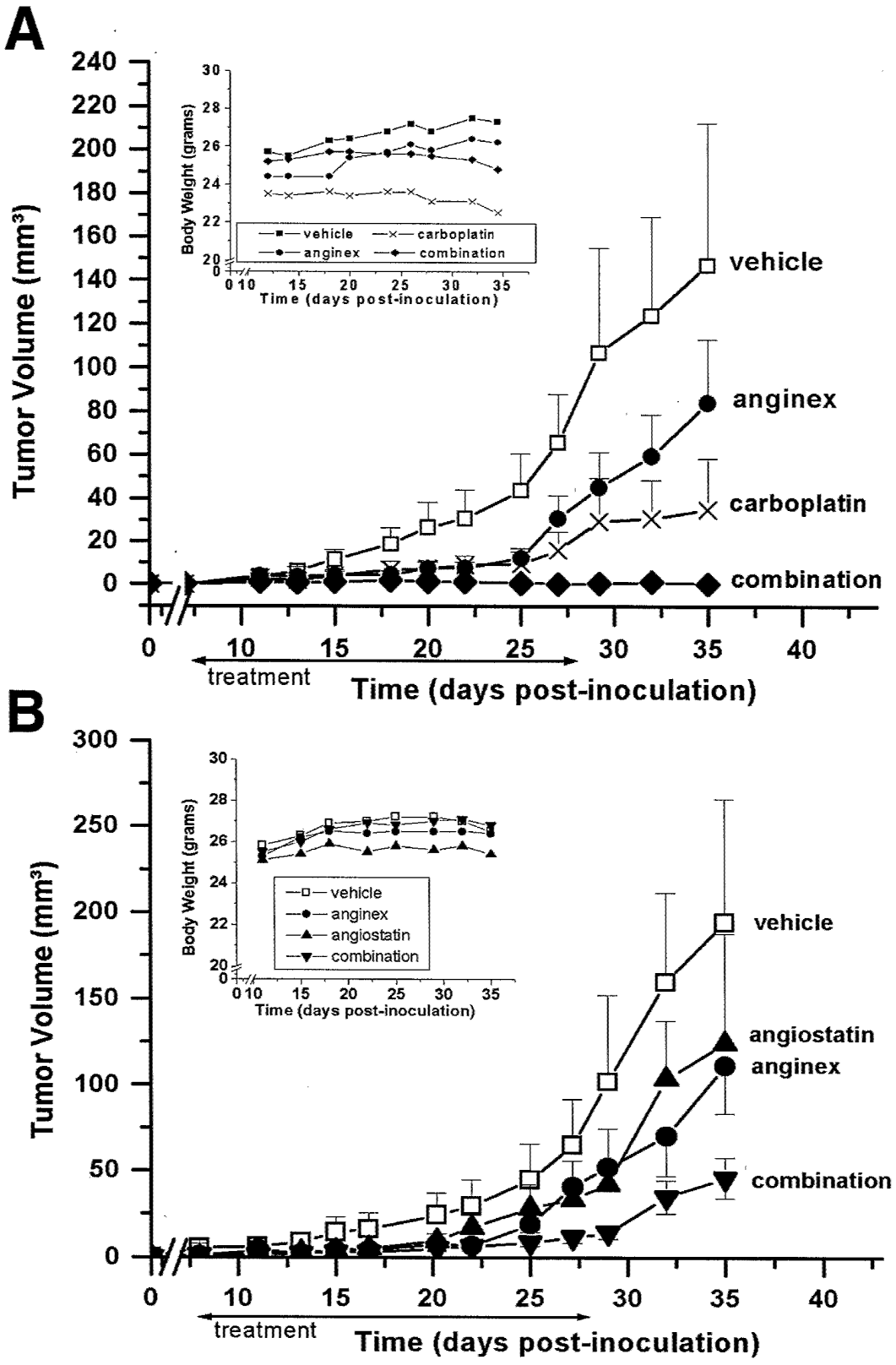

Figure 2
Dings et al. Top ⇑

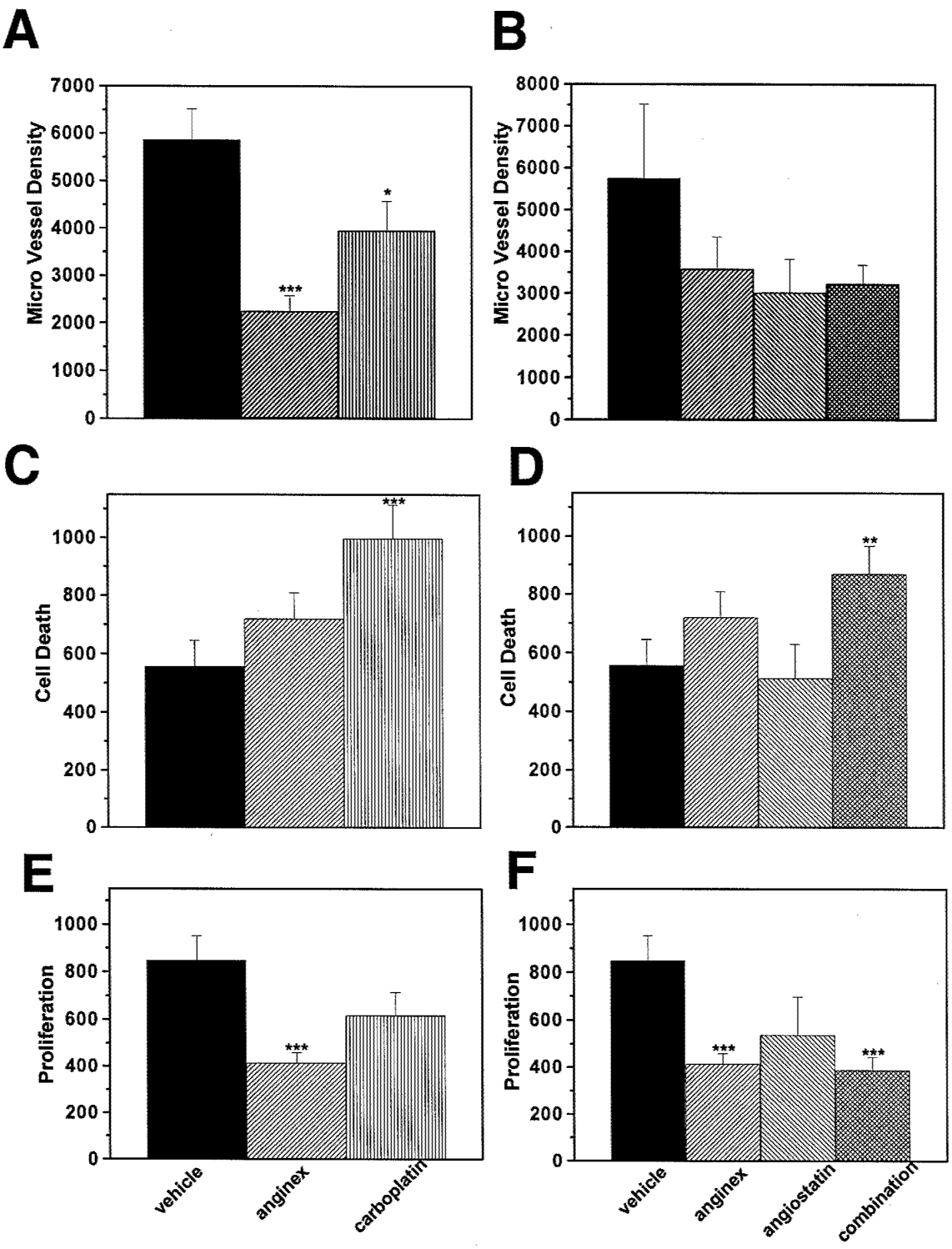

Figure 3
Dings et al. Top ⇑

Table 1 *Combination therapy of anginex with carboplatin and angiostatin*

Fractional tumor volume (FTV) relative to untreated controls [a]

			Combination treatment		*Ratio* [d]
Day [b]	*Anginex*	*Carboplatin*	*Expected* [c]	*Observed*	*Expected FTV/ Observed FTV*
20	0.28	0.28	0.08	0.05	1.6
25	0.28	0.22	0.06	0.01	6
32	0.48	0.25	0.12	0.01	12.4
35	0.57	0.24	0.13	0	∞

			Combination treatment		*Ratio* [d]
Day [b]	*Anginex*	*Angiostatin*	*Expected* [c]	*Observed*	*Expected FTV/ Observed FTV*
25	0.42	0.64	0.27	0.19	1.4
29	0.51	0.41	0.21	0.14	1.5
32	0.44	0.65	0.29	0.22	1.3
35	0.57	0.64	0.37	0.24	1.6

[a] FTV (mean tumor volume experimental)/(mean tumor volume control).

[b] Day after tumor cell transplantation.

[c] (Mean FTV of anginex) X (mean FTV of other experimental group).

[d] Obtained by dividing the expected FTV by the observed FTV. A ratio of >1 indicates a synergistic effect, a ratio of <1 indicates a less then additive effect.

Version: 17 September 2002
For: Cancer Letters
Experimental Therapeutics
File: canlet0917

Anti-tumor Activity of the Novel Angiogenesis Inhibitor Anginex

Ruud P. M. Dings[*$], Daisy W. J. van der Schaft[*], Balazs Hargittai[$#], Judy Haseman[$], Arjan W. Griffioen*, and Kevin H. Mayo[$+]

[$]*Department of Biochemistry, Molecular Biology & Biophysics, University of Minnesota Health Sciences Center, 321 Church Street, Minneapolis, MN 55455, USA*

[*]*Angiogenesis Laboratory, Research Institute for Growth and Development (GROW), Depts of Internal Medicine & Pathology, University Hospital & Maastricht University, P.O. Box 5800, 6202 AZ Maastricht,The Netherlands*

running title: anti-tumor agent anginex

[+] Corresponding autor. Tel.: 612-625-9968; fax: 612-624-5121 (612-625-2163).
E-mail address: mayox001@tc.umn.edu

[#] Present address: Department of Chemistry, Mathematics and Physical Sciences, St. Francis University, Loretto, PA

Abstract

Anginex is a novel cytokine-like peptide with potent anti-angiogenic activity, which operates specifically against angiogenically-activated endothelial cells via prevention of cell adhesion/migration on the extracellular matrix and subsequent induction of apoptosis. Here, we demonstrate that anginex inhibits tumor growth *in vivo* in mouse xenograft models. In the MA148 ovarian carcinoma model, tumor growth was inhibited dose-dependently by up to 80% when systemically administered via osmotic mini-pumps starting at the time of tumor cell inoculation. The optimal dose was found to be 10 mg/kg/day. When tested against established tumors, mini-pump-administered anginex demonstrated essentially the same effectivity at this optimal dose, whereas once or twice-daily injections were only half as effective. When anginex was conjugated to human serum albumin, effectivity was significantly improved, most likely due to increased bioavailability of the conjugate. Immunohistochemical analysis of microvessel density indicated that the anti-tumor activity of anginex is mediated by angiogenesis inhibition. This was confirmed in an *in vitro* angiogenesis assay based on tube formation in a collagen gel. Animals demonstrated no signs of toxicity as judged by unaltered behaviour, normal weight gain, blood markers and macro- and microscopic morphology of internal organs upon autopsy. Overall, these *in vivo* studies indicate that anginex is an effective anti-tumor agent.

Keywords: Angiogenesis; Anginex; Bioavailability; Microvessel density; Conjugation; Systemic treatment

1. Introduction

Angiogenesis or neovascularization is the process through which new blood vessels develop from pre-existing vasculature [1]. The growth of solid tumors is dependent on angiogenesis, as tumors generally can not grow beyond the size of 1-2 mm in diameter without formation of new blood vessels to supply nutrition and oxygen and remove waste products. Most tumors release angiogenesis-regulating factors, and neovasculatization occurs only when there are more positive than negative regulators of angiogenesis [2,3]. The dependency of tumors on angiogenesis is non-tumor-type specific and allows the therapeutic treatment of tumors to be based, at least in part, on the inhibition of angiogenesis.

A highly vascularized tumor is correlated with a poor clinical prognosis, not only because of the potential for uncontrolled tumor growth, but also because of the increased access of the tumor to capillaries, which contributes to increased metastatic potential [4,5]. Consequently, methods that inhibit angiogenic sprouting provide a unique opportunity to arrest tumor growth and prevent metastasis formation. Many endogenous and exogenous anti-angiogenic agents have been identified, such as angiostatin [6], endostatin [7], thrombospondin [8], TNP-470 [9], platelet factor-4 [10], thalidomide [11], squalamine [12], bactericidal/permeability-increasing protein [13] and carboxyamino-imidazole [14].

Although preclinical testing of anti-angiogenic agents shows promise, the need for more and better angiogenesis inhibitors is driven by the absence of any major clinical breakthroughs (e.g. SU5416, BB2516, AG3340, Bay 12-9566, IM-862 [15]). The most successful angiostatic agents have been those that directly act by inhibiting endothelial cell proliferation. Anginex, a designed ß-sheet-forming cytokine-like 33-mer peptide, which potently inhibits multiple steps in the angiogenesis process, is a member of this class of angiogenesis inhibitors [16]. The angiostatic activity of anginex is based primarily on apoptosis-induction via prevention of adhesion on and migration through the extracellular matrix of angiogenically-activated endothelial cells [16].

The aim of the present study was to test and to optimize the *in vivo* efficacy of anginex as an anti-cancer agent in mouse models. Various treatment regiments, i.e., dose response, mode and frequency of administration, were investigated. For other angiogenesis inhibitors, the literature reports that continuous, systemic administration of, for example endostatin [17], results in more effective tumor growth suppression at significantly reduced doses compared with bolus

administration. Continuous systemic administration of anginex in a 10 mg/kg/day dose provided optimal efficacy. Efficacy was significantly improved by conjugating anginex to human serum albumin to improve its bioavailability. These results demonstrate that anginex is a promising pharmacological anti-cancer agent that should be developed for clinical testing.

2. Materials and Methods

2.1. Cell Culture

The human epithelial ovarian carcinoma cell line, MA148, was kindly provided by Prof. Dr. Ramakrishnan. MA148 cells were cultured at 37 °C in RPMI 1640 medium (Life Technologies, Grand Island, NY) supplemented with 10% fetal bovine serum (Cellgro, Mediatech, Washington, DC) and 1% penicillin/streptomycin (Cellgro, Mediatech). Cultures were grown in the presence of 5% CO_2 and split 1:3 every 3 days. The human SK-OV-3 carcinoma cell line was kindly provided by Dr. Rebecca Bagley (Genzyme).

2.2. Proliferation assay

Human umbilical vein derived EC were harvested from normal human umbilical cords by perfusion as described earlier [16]. HUVEC were seeded in a 96 wells culture plate coated with 1 mg/ml fibronectin (2 hours at 20°C) at a concentration of 3,000 cells per well in a volume of 50 µl. The cells were allowed to adhere for 3 hours at 37°C at 5% CO_2 and subsequently 50 µl of culture medium with 20 ng/ml basic Fibroblast Growth Factor (bFGF), with or without anginex or conjugated anginex was added. The cells were cultured for 72 hours. During the last 6 hours of the assay, the culture was pulsed with 0.5 µCi [methyl-^{3}H]-thymidine(Amersham Life Science)/well. Activity was measured using liquid scintillation. Measurements were done in triplicate.

2.3. In vitro Angiogenesis

Sprouting and tube formation of EC were studied using cytodex-3 beads overgrown with EC in a 3-dimensional gel. Bovine capillary EC (BCE) were mixed with gelatin coated cytodex-3 microcarrier beads (Sigma, The Netherlands) at a concentration of 25 cells per bead and cultured for 72 hours in a tissue culture plate in RPMI-1640, supplemented with 20% HS, 2 mM L-glutamine, 50 ng/ml streptomycin, and 50 U/ml penicillin. The beads were spun down and resuspended, in a concentration of 25 beads per 100 µl, in 8 volumes of vitrogen-100 (Collagen

Corporation, Fermont, CA, USA), 1 volume 10x concentrated α-MEM (Life Technologies, Breda, The Netherlands), 1 volume 11.76 mg/ml sodium bicarbonate and 20 ng/ml bFGF. 100 µl of this mixture was suspended to each well of a 96 wells culture plate, after which gelation was allowed to take place at 37°C. After gellation medium was applied on top of the gel containing 20 ng/ml bFGF, with or without anginex at concentrations as indicated. After 24 hours photographs were made. For quantification these images were analyzed using NIH image computer software. Statistical analysis was done using the Mann-Whitney U test.

2.4. Animals

In all studies, female athymic nude mice (nu/nu, 5-6 weeks old) were used. These mice were purchased from the National Cancer Institute and allowed to acclimatize to local conditions for at least one week. Animals were given water and standard chow ad libitum, and were kept on a 12-hour light/dark cycle. All experiments were approved by the University of Minnesota Research Animal Resources ethical committee.

2.5. Xenograft Mouse Models

MA148 cells, growing in exponential phase, were harvested by trypsinization, washed with Hanks' balanced salt solution (Cellgro, Mediatech) and resuspended at 2 x 10^7 cells/ml in serum-free RPMI-1640 medium. 100 µl of the suspension was injected subcutaneously into the right flank of the mouse. For mice with minimal residual disease, treatment was initiated at the time of inoculation with MA148 cells. As a therapeutic intervention variant, tumors were allowed to grow to an average size of 50 mm^3 (day 17 post-inoculation) before treatment was initiated.

Another therapeutic intervention model was performed with a more aggressive carcinoma, human SK-OV-3, where tumors were allowed to establish themselves to an average size of approximately 75 mm^3 before treatment was initiated. In either case, animals were randomized prior to the initiation of treatment.

2.6. Treatment Variations

Three variations in treatment administration were employed: loco-regional injections, alginate beads and osmotic mini-pumps. Loco-regional administration was performed by injecting agents subcutaneously in the right flank within 1 cm of the tumor, rather than directly into the tumor mass. Single and double daily injections were performed. Double daily injections were administered at 12-hour intervals. Alginate beads and osmotic mini-pumps were both used in order to compare two different continuous and systemic modes of treatment. Alginate beads, a simple, mild, aqueous-based gel formation of sodium alginate in the presence of divalent cations such as Ca^{2+}, were made using alginic acid (Sigma Chemical Co.), with some modifications from the method previously described [18]. Briefly, the peptide anginex was dissolved in 2% w/v sodium alginate solution, which was then extruded through a 30-G needle into a 0.1 M calcium chloride solution while stirring. Alginate beads were stored overnight at 4°C and subsequently washed three times in sterile distilled H_2O. Each week, these beads were made fresh and placed subcutaneously in the left flank of the animals, achieving a dose of 10 mg/kg/day. In studies using osmotic mini-pumps (Durect, Cupertino, CA), mini-pumps were implanted subcutaneously in the left flank of mice. Concentrated solutions of anginex were formulated such that the 28-day treatment period would be covered by implantation of a single pump.

For each route of administration, control groups of animals were given either PBS, PBS containing human serum albumin, or PBS containing a negative control peptide ßpep-28 that is 91% sequentially homologous and 67% identical to anginex [16]. Tumor growth curves were found to be virtually identical in any of these control cases.

2.7. Tumor Volume Measurements

Tumor volume was determined by measuring the diameters of tumors using calipers (Scienceware, Pequannock, NJ) and calculated by the equation for the volume of a spheroid: $(a^2 \times b \times \pi) / 6$, where 'a' is the width and 'b' is the length of the tumor. Measurements were performed two or three times per week. At the conclusion of an experiment, tumor weights were also taken following excision of the tumors from euthanized animals.

2.8. Anginex-HSA conjugate

Given that small peptides like anginex are subject to rapid clearance via the kidney, a study was performed in which anginex was coupled to a larger carrier protein, human serum albumin (HSA). To produce this conjugate, five milligrams of HSA (Aldrich Chemicals, Milwaukee, WI) was dissolved in 1 ml of 50 mM $NaPO_4$ buffer, pH 7.5, containing 1 mM EDTA. Freshly dissolved *S*-acetylthioacetic acid (SATA, 65 mM in dimethyl sulfoxide) was then added and stirred at 25 °C for 1 hour [19]. The resulting derivatized protein was separated from smaller molecules by gel filtration using Sephacryl S-200HR (Amersham Pharmacia Biotechnology). To the collected and combined fractions, a 0.5 M aqueous solution of hydroxylamine hydrochloride (in PO_4 buffer containing 25 mM EDTA; pH 7.5) was added and stirred at 25 °C for 1.5 hours in order to remove the acetyl-protecting group [20]. The amount of free sulfhydryl was measured using dinitrothiobenzoic acid (Ellman's reagent) [21]. There were, on average, five free sulfhydryls per HSA molecule.

Following gel purification, the derivatized protein was treated with succinimidyl 4-(*N*-maleimidomethyl)cyclohexane-1-carboxylate (47 mM in dioxane) that acted as the cross-linker. The reagent was added in nine aliquots of 4 μl/ml at 5-minutes intervals under gentle agitation, and gently shaken overnight at 32 °C. The resulting protein was purified by gel filtration, lyophilized and redissolved in H_2O (1 ml). 1 mg anginex, dissolved in H_2O (0.25 ml), was then added to the protein solution. The resulting cloudy solution was stirred at 25 °C overnight, centrifuged to remove any precipitate, purified using gel filtration, and finally dialyzed and lyophilized to give the desired conjugate. The protein was characterized by HPLC and Mass Spectrometry. From Mass Spectrometry, it was estimated that there was an average of 5 anginex molecules per HSA molecule. An EC proliferation assay (incorporation of [^{3}H]thymidine) showed no enhanced activity of conjugated anginex compared to its molecular equivalent of free anginex.

2.9. Immunohistochemistry

Immunohistochemistry was used to assess microvessel density and the extent of total cell death. Tumor tissue was embedded in tissue freezing medium (Miles Inc, Elkart, IN) and shock

frozen in liquid nitrogen. 10 μm thick sections of tissue were prepared for immuno-histochemical analysis. For this, tissue sections were brought to room temperature, air dried overnight, and then fixed in acetone for 10 minutes. Slides were allowed to air dry for at least 30 minutes and were washed three times for 5 minutes each in phosphate-buffered saline (PBS, pH 7.4). Samples were then blocked with PBS containing 0.1% bovine serum albumin and 3% human serum albumin for at least 30 minutes at room temperature in a humidified box. Samples were subsequently incubated with phycoerytrin (PE)-conjugated monoclonal antibody to CD-31 (PECAM-1) in a 1:50 dilution (Pharmigen, San Diego, CA) to stain for microvessel density. After 1-hour incubation at room temperature, slides were washed with PBS and immediately imaged using an Olympus BX-60 fluorescence microscope at 200X magnification. Digital images were stored and processed using Adobe Photoshop (Adobe Inc., Mountain View CA).

To assess the extent of total cell death, tissue sections were stained by using the TUNEL (terminal deoxyribonucleotidyl transferase-mediated dUTP-nick-end labeling) assay, which was performed according to the manufacturer's instructions (*in situ* cell death detection kit, fluorescein; TUNEL, Roche). Although the TUNEL assay detects apoptosis, it can not be ruled out that TUNEL will also stain for necrosis, where extensive DNA fragmentation may occur. Stainings were imaged using an Olympus BX-60 fluorescence microscope at 200X magnification, and the digital images were stored and processed using Adobe Photoshop (Adobe Inc., Mountain View CA).

Quantification of microvessel density and the rate of total cell death were determined as described earlier [22]. Statistical analysis was performed using the Student's *t* test.

2.10. Toxicity assessment

As an indirect measure of toxicity, body weights of mice were monitored three times per week using a digital balance (Ohaus Florham, NJ). Hematacrit levels were determined in blood samples extracted by tail vein bleedings prior to treatment, ten days after the initiation and on the last day of treatment. Blood samples were collected using heparinized micro-hematocrit capillary tubes (Fisher; Pittsburgh, PA). Samples were spun down for 10 minutes in a micro-hematocrit centrifuge (Clay-Adams; NY) and hematocrit levels were calculated using an international microcapillary reader (IEC; Needham, Mass). To obtain creatinine levels blood was

withdrawn on the last day of treatment. Creatinine was determined according manufacturer's instructions (Sigma Diagnostics; St Louis, MO).

3. Results

3.1. Anginex inhibits tumor growth dose dependently

The dose dependency of anginex was assessed in the MA148 human ovarian carcinoma xenograft model, whereby anginex was administered at 5 mg/kg/day, 10 mg/kg/day, and 20 mg/kg/day via osmotic mini-pumps. For this study, there were three control groups: one given PBS containing BSA and the other two given PBS containing homologous peptide βpep-28 (5 mg/kg/day or 10 mg/kg/day). As a model for minimal residual disease, treatment was initiated immediately after inoculation of animals with tumor cells. Anginex was observed to inhibit tumor growth dose dependently with the optimal dose being 10 mg/kg/day (Fig. 1). At this dose, anginex inhibited tumor growth by 80% relative to control groups. Whereas greater effectivity was not observed at the higher dose of 20 mg/kg/day, tumor growth was inhibited by only 50% on average at half the optimal dose (5 mg/kg/day). Tumors in all control groups were essentially of the same size. Data, taken from three independent studies, are shown as average tumor volumes in $mm^3 \pm SE$ (Fig.1).

3.2. Anginex inhibits growth of established tumors

Having demonstrated its *in vivo* efficacy, anginex was then tested in mice with established MA148 tumors (approximately 50 to 75 mm^3). The optimal dose of 10 mg/kg/day was administered via mini-pumps, which resulted in a 70% to 80% inhibition of tumor growth (Fig. 2A). The efficacy of anginex against MA-148 tumors was comparable to that observed against tumors produced using another ovarian carcinoma cell line, SKOV-3 (data not shown). As an alternative to continuous systemic administration by osmotic mini-pumps, anginex was encapsulated in alginate beads. Delivery of anginex via alginate beads was less pronounced compared to mini-pumps, producing only about a 50% reduction in tumor volume (Fig. 2A). Lower efficacy was also observed when anginex was administered loco-regional by daily subcutaneous injections. At the sub-optimal dose of 5 mg/kg/day, tumor growth in these experiments was inhibited by only 30%. Giving the same dose of anginex by twice daily injections did not improve efficacy of the peptide (Fig. 2B).

3.3. Anginex conjugation to HSA enhances inhibition of tumor growth

Since anginex is a small peptide that may be cleared rapidly via filtration through the kidney, an attempt to improve bioavailability was made by conjugating anginex to human serum albumin (HSA-anginex, HSA:anginex molecule ratio of 1:5). Activity of the conjugate was first measured in the EC proliferation assay. On a molar basis, the activity of conjugated and unconjugated anginex, in this *in vitro* assay, was found to be essentially the same (Fig. 3A). *In vivo* activity of the conjugate was then tested in the MA148 xenograft tumor model along with unconjugated anginex. Molar equivalent doses (anginex at 2.5 mg/kg/day and the HSA-anginex conjugate at 41.5 mg/kg/day) were subcutaneously administered via osmotic mini-pumps. Data in Figure 3B show averages of three independent experiments. A significant improvement in tumor growth inhibition was observed when animals were treated with the conjugate. 30 days post-treatment (day 58), tumors in animals treated with HSA-conjugated anginex remained significantly smaller than those in control animals treated with free HSA. At this time point, the mean tumor volume in HSA-conjugate treated animals was approximately 75% less than in control treated animals. Results from tumor volume measurements were virtually the same as those derived from wet weights of post-mortem excised tumors (vehicle 2875±1404 mg; conjugate 767±267 mg).

3.4. Toxicity Assessment

In vivo toxicity of anginex and its conjugate was assessed by observing animal behavior, determining body weight, measuring hematocrit and creatinine blood levels, and examining macro- and microscopic morphology of internal organs upon autopsy at the end of each study. By any of these criteria, neither anginex nor its HSA-conjugate appeared to be toxic. Treated and untreated mice behaved and ate normally. Body weights of treated and untreated mice were the same among any of the groups studied. Each mouse gained on average approximately 3 grams during the course of the studies. In addition, prior to the start of treatment, ten days after the initiation of treatment, and the last day of treatment, blood was drawn and hematocrit levels were determined as measurement for bone marrow toxicity. Prior to treatment, the average percentage of red blood cells was 54.3% ± 4.7%. Ten days after initiating treatment, red blood cells

accounted for 51.0% ± 3%, 51.0% ± 2% and 46.3% ± 6.6% for control, anginex and conjugate treated groups, respectively. On the last day of treatment red blood cells accounted for 50.3% ± 1.1%, 50.0% ± 2.6% and 50.0 ± 1.0% for control, anginex and HSA-conjugate treated groups, respectively. Creatinine levels, which were determined on the last day of treatment, showed amounts of 49.6 μmoles/l ± 2.5 μmoles/l, 46.6 μmoles/l ± 4.5 μmoles/l, and 42.1 μmoles/l ± 3.0 μmoles/l for control, anginex and conjugated treated groups, respectively. At the termination of all studies, macro- and microscopic morphology of internal showed no abnormalities among all groups of animals.

3.5. Aspects of the mechanism of action

To demonstrate that anginex functions by inhibition of blood vessel formation, microvessel density (MVD) and the extent of total cell death (Fig. 4 and Table 1) in cross sections from tumor tissues were determined. Results show that anginex inhibits the number of microvessels by up to 50%, whereas the conjugate inhibited MVD by approximately 80%. Not only was the number of microvessels reduced in anginex treated animals, but vessel length was also reduced by a similar extent. This, together with an increase in the number of endpoints, is indicative of a change in vessel architecture. In all parameters (Table 1), the HSA-conjugate demonstrated greater anti-angiogenic effectivity compared to free anginex. The TUNEL assay, which reveals the extent of total cell death within tumors (Fig. 4D-F), showed that cell death was greatest in animals treated with the HSA-anginex conjugate, consistent with results from microvessel staining (Fig. 4H). These results were supported by the inhibition of tube formation in the *in vitro* angiogenesis assay. In this assay, sprout formation was measured in a 3D collagen gel (Fig. 5), and anginex was found to inhibit tube formation by 50% at 800 nM.

4. Discussion

Anginex is a rationally designed, cytokine-like peptide 33-mer, which has been shown *in vitro* to induce apoptosis specifically in angiogenically-activated endothelial cells (EC) by inhibiting EC from adhering to and migrating on the extracellular matrix [16]. The present paper reports the *in vivo* efficacy of this small peptide and its development as a therapeutic anti-cancer agent. We have shown here that anginex significantly inhibits the growth of ovarian carcinoma-derived tumors in athymic mice. Of the three administrative routes used (daily loco-regional bolus injections, continuous systemic delivery via osmotic mini-pumps, and suspension in alginate beads implanted subcutaneously), continuous systemic administration of the peptide worked best. Inhibition of tumor growth was observed to be dose dependent and optimal at 10 mg/kg, with a maximum reduction in tumor size of about 80% relative to control. When anginex was administered loco-regionally by once or twice daily injections, tumor growth was inhibited by only about 50%. This reduction in efficacy is consistent with the previous observation that continuous administration of endostatin resulted in sustained systemic concentrations of the protein leading to increased efficacy, which was manifested as increased tumor regression compared to single daily bolus administration [17]. Nevertheless, it was somewhat surprising to find that twice-daily injection of the same total dose did not lead to enhanced efficacy over single daily injections as was demonstrated with other angiogenesis inhibitors, e.g., Matrix Metallo Proteinase Inhibitor AG3340 [23]. AG3340 was able to inhibit tumor growth at the same rate as when it was administered in only 1/8 of the dose, but injected multiple times a day. The plasma levels of the proteinase inhibitor explained this effect. Apparently, single or double daily injections of anginex did not produce appropriate threshold or steady state levels of the drug in the serum to be as effective.

As a third route of administration, we also investigated the use of alginate beads in which anginex was suspended. This non-toxic and biodegradable method is an established method drug delivery [24] and was also reported to be an effective means of delivery by others in the anti-angiogenesis field [25]. However, with anginex this slow-release approach was less effective than administration via osmotic mini-pumps. At best, tumor growth was inhibited by about 60% when delivered via alginate beads. The problem with the use of alginate beads stems from the

fact that the percentage of encapsulated compound can differ and that administration, i.e., release, is not well regulated [26].

Because anginex has a relatively low molecular weight (3.9 kDa) and may, therefore, be rapidly excreted via the kidney, we thought that its *in vivo* efficacy could be improved by conjugating the peptide to a larger 'carrier' protein, i.e., human serum albumin (HSA; 67 kDa). Molecular weight-dependent tissue accumulation and clearance has been systematically investigated for dextrans [27] and polyethyleneglycols (PEGs) [28]. For PEGs it was found that the circulatory half-life of PEG increased from 18 min to 1 day as the PEG molecular weight increased from 6 kDa to 190 kDa. However, although renal clearance decreased, hepatic clearance increased with increasing PEG molecular weight. For dextrans in a molecular-weight range of 4 kDa to 150 kDa, renal clearance decreased with increasing molecular weight, whereas hepatic clearance was maximal at 70 kDa and a further increase in molecular weight resulted in a decrease of liver uptake. Conjugation of smaller molecules to larger carrier molecules, e.g. HSA, has been shown to be effective in increasing bioavialablity for reasons, beyond an increase in size, e.g., changes the molecular hydrophobicity. For instance this was demonstrated by conjugating the well-known and hydrophobic chemotherapeutic agent paclitaxel to HSA [29]. Because anginex is readily soluble in water [16], this latter point is moot with regards to explaining *in vivo* effects from the HSA-anginex conjugate. The HSA-anginex conjugate shows a substantial improvement in efficacy. Whereas a sub-optimal dose of free anginex proved to be ineffective, a molar equivalent dose of anginex conjugated to HSA inhibited tumor growth by about 65%. Although we did not measure serum levels of anginex or of the HSA-anginex conjugate, treatment with the conjugate presumably led to prolonged circulation in the serum merely due to the increase in size. This, in turn, relates to improved bioavailability of the drug.

Mechanistically, anginex functions *in vitro* as an anti-angiogenic agent [16]. Immunohistochemical results on cross-sections of exercised tumors from anginex-treated and untreated animals, demonstrate that tumor growth inhibition by anginex is indeed mediated by its ability to inhibit angiogenesis. Here, this has been quantified by microvessel density and digital analysis of vessel architecture. Microvessel density in tumors, but not in other tissues, is significantly decreased in anginex-treated animals compared to control tumors. In addition, anginex-treated tumors have smaller vessels and the analysis of vessel architecture reveals decreased branching and less differentiation of the vascular bed. Furthermore, TUNEL analysis

shows an increased amount of cell death within tumors exposed to anginex. This increased cell death most likely results from a reduction in angiogenesis, i.e., vessel density reduction, because *in vitro* data demonstrate that anginex only affects angiogenically-activated endothelial cells [16]. Therefore, apoptosis of tumor cells is not a direct effect of anginex treatment, but rather it is an indirect effect due to a reduction in the number of endothelial cells in the tumor. In studies with other anti-angiogenics, similar observations were made. For example, treatment with C225, an antibody to the EGF receptor showed that inhibition of tumor-induced angiogenesis led to tumor cell apoptosis and regression which, in turn, led to a significant antitumor effect against human pancreatic carcinoma in nude mice [30].

For several reasons, anginex shows promise for clinical use as a therapy against cancer. Anginex is a potent anti-tumor agent that demonstrates no signs of toxicity in mice. Moreover, the peptide is synthetically produced and has a very long shelf-life either as a powder or in solution. Currently, we are using the NMR structure of anginex and derived structure-function relationships to design a small molecule mimetic of the peptide.

Acknowledgements

This research was supported by grants from the Department of Defense (DA/DAMD 17-99-1-9564) and the National Institutes of Health (R01 CA-96090) to K. H. Mayo.

References

[1] A.W. Griffioen, G. Molema, Angiogenesis: potentials for pharmacologic intervention in the treatment of cancer, cardiovascular diseases, and chronic inflammation, Pharmacol Rev 52 (2000) 237-268.

[2] J. Folkman, M. Klagsbrun, Angiogenic factors, Science 235 (1987) 442-447.

[3] D. Hanahan, J. Folkman, Patterns and emerging mechanisms of the angiogenic switch during tumorigenesis, Cell 86 (1996) 353-364.

[4] S.G. Williams, M. Buscarini, J.P. Stein, Molecular markers for diagnosis, staging, and prognosis of bladder cancer, Oncology (Huntingt) 15 (2001) 1469-70, 73-4, 76; discussion 76-84.

[5] N. Weidner, Angiogenesis as a predictor of clinical outcome in cancer patients, Hum Pathol 31 (2000) 403-405.

[6] M.S. O'Reilly, L. Holmgren, Y. Shing, C. Chen, R.A. Rosenthal, M. Moses, W.S. Lane, Y. Cao, E.H. Sage, J. Folkman, Angiostatin: a novel angiogenesis inhibitor that mediates the suppression of metastases by a Lewis lung carcinoma, Cell 79 (1994) 315-328.

[7] M.S. O'Reilly, T. Boehm, Y. Shing, N. Fukai, G. Vasios, W.S. Lane, E. Flynn, J.R. Birkhead, B.R. Olsen, J. Folkman, Endostatin: an endogenous inhibitor of angiogenesis and tumor growth, Cell 88 (1997) 277-285.

[8] F. Rastinejad, P.J. Polverini, N.P. Bouck, Regulation of the activity of a new inhibitor of angiogenesis by a cancer suppressor gene, Cell 56 (1989) 345-355.

[9] M. Kusaka, K. Sudo, T. Fujita, S. Marui, F. Itoh, D. Ingber, J. Folkman, Potent anti-angiogenic action of AGM-1470: comparison to the fumagillin parent, Biochem Biophys Res Commun 174 (1991) 1070-1076.

[10] S.K. Gupta, J.P. Singh, Inhibition of endothelial cell proliferation by platelet factor-4 involves a unique action on S phase progression, J Cell Biol 127 (1994) 1121-1127.

[11] A. Onn, J.E. Tseng, R.S. Herbst, Thalidomide, cyclooxygenase-2, and angiogenesis: potential for therapy, Clin Cancer Res 7 (2001) 3311-3313.

[12] A.K. Sills, Jr., J.I. Williams, B.M. Tyler, D.S. Epstein, E.P. Sipos, J.D. Davis, M.P. McLane, S. Pitchford, K. Cheshire, F.H. Gannon, W.A. Kinney, T.L. Chao, M. Donowitz, J. Laterra, M. Zasloff, H. Brem, Squalamine inhibits angiogenesis and solid tumor growth in vivo and perturbs embryonic vasculature, Cancer Res 58 (1998) 2784-2792.

[13] D.W. van der Schaft, E.A. Toebes, J.R. Haseman, K.H. Mayo, A.W. Griffioen, Bactericidal/permeability-increasing protein (BPI) inhibits angiogenesis via induction of apoptosis in vascular endothelial cells, Blood 96 (2000) 176-181.

[14] R.S. Kerbel, Tumor angiogenesis: past, present and the near future, Carcinogenesis 21 (2000) 505-515.

[15] M. Fogarty, Learning from Angiogenesis Trial Failures, The Scientist 16 (2002) 33-35.

[16] A.W. Griffioen, D.W. van der Schaft, A.F. Barendsz-Janson, A. Cox, H.A. Struijker Boudier, H.F. Hillen, K.H. Mayo, Anginex, a designed peptide that inhibits angiogenesis, Biochem J 354 (2001) 233-242.

[17] O. Kisker, C.M. Becker, D. Prox, M. Fannon, R. D'Amato, E. Flynn, W.E. Fogler, B.K. Sim, E.N. Allred, S.R. Pirie-Shepherd, J. Folkman, Continuous administration of endostatin by intraperitoneally implanted osmotic pump improves the efficacy and potency of therapy in a mouse xenograft tumor model, Cancer Res 61 (2001) 7669-7674.

[18] M.K. Majumdar, E. Wang, E.A. Morris, BMP-2 and BMP-9 promotes chondrogenic differentiation of human multipotential mesenchymal cells and overcomes the inhibitory effect of IL-1, J Cell Physiol 189 (2001) 275-284.

[19] R.J. Duncan, P.D. Weston, R. Wrigglesworth, A new reagent which may be used to introduce sulfhydryl groups into proteins, and its use in the preparation of conjugates for immunoassay, Anal Biochem 132 (1983) 68-73.

[20] I.M. Klotz, R.E. Heiney, Introduction of sulfhydryl groups into proteins using acetylmercapto succinic anhydride, Arch. Biochem. Biophys 96 (1962) 605-612.

[21] G.L. Elman, Tissue sulfhydryl groups, Arch. Biochem. Biophys 82 (1959) 70-77.

[22] R. Wild, S. Ramakrishnan, J. Sedgewick, A.W. Griffioen, Quantitative assessment of angiogenesis and tumor vessel architecture by computer-assisted digital image analysis: effects of VEGF-toxin conjugate on tumor microvessel density, Microvasc Res 59 (2000) 368-376.

[23] D.R. Shalinsky, J. Brekken, H. Zou, C.D. McDermott, P. Forsyth, D. Edwards, S. Margosiak, S. Bender, G. Truitt, A. Wood, N.M. Varki, K. Appelt, Broad antitumor and antiangiogenic activities of AG3340, a potent and selective MMP inhibitor undergoing advanced oncology clinical trials, Ann N Y Acad Sci 878 (1999) 236-270.

[24] S. Takka, O.H. Ocak, F. Acarturk, Formulation and investigation of nicardipine HCl-alginate gel beads with factorial design-based studies, Eur J Pharm Sci 6 (1998) 241-246.

[25] T.A. Read, D.R. Sorensen, R. Mahesparan, P.O. Enger, R. Timpl, B.R. Olsen, M.H. Hjelstuen, O. Haraldseth, R. Bjerkvig, Local endostatin treatment of gliomas administered by microencapsulated producer cells, Nat Biotechnol 19 (2001) 29-34.

[26] B. Arica, S. Calis, H. Kas, M. Sargon, A. Hincal, 5-Fluorouracil encapsulated alginate beads for the treatment of breast cancer, Int J Pharm 242 (2002) 267-269.

[27] R. Mehvar, M.A. Robinson, J.M. Reynolds, Molecular weight dependent tissue accumulation of dextrans: in vivo studies in rats, J Pharm Sci 83 (1994) 1495-1499.

[28] T. Yamaoka, Y. Tabata, Y. Ikada, Distribution and tissue uptake of poly(ethylene glycol) with different molecular weights after intravenous administration to mice, J Pharm Sci 83 (1994) 601-606.

[29] F. Dosi, P. Brusa, P. Crosasso, S. Arpicco, L. Cattel, Preparation, characterization and properties in vitro and in vivo of a paclitaxel-albumin conjugate, J. Controlled Release 47 (1997) 293-304.

[30] C.J. Bruns, M.T. Harbison, D.W. Davis, C.A. Portera, R. Tsan, D.J. McConkey, D.B. Evans, J.L. Abbruzzese, D.J. Hicklin, R. Radinsky, Epidermal growth factor receptor blockade with C225 plus gemcitabine results in regression of human pancreatic carcinoma growing orthotopically in nude mice by antiangiogenic mechanisms, Clin Cancer Res 6 (2000) 1936-1948.

Table 1.
Vessel density quantification and related parameters

	Vessel Density[a]	End Points[b]	Branch Points[c]	Vessel Length[d]
Vehicle	56785 ± 23790	20.3 ± 10.2	17.1 ± 9.9	22.7 ± 7.4
Anginex	27576 ± 13304[e]	41.2 ± 14.0	13.0 ± 8.9[e]	7.2 ± 3.0[e]
Conjugate	9875 ± 3638[e,f]	30.4 ± 16.6	3.2 ± 2.3[e,f]	5.7 ± 2.7[e,f]

[a] Following binarization of images, microvessel density was estimated by scoring the total number of white pixels per field. Results show the mean white pixel count per image ± standard deviation.
[b] Mean number of vessel end points □ standard deviation as determined after skeletonization of the images.
[c] Mean number of vessel branch points/nodes per image in pixels ± standard deviation as determined after skeletonization of the images.
[d] Mean total vessel length per image in pixels ± standard deviation as determined after skeletonization of the images.
[e] $p < 0.05$. Experimental group compared to vehicle, using the student t test.
[f] $p < 0.01$. Experimental group compared to anginex, using the student t test.

Figure legends

Fig. 1. Anginex causes significant tumor growth inhibition. The mean tumor growth of human MA148 ovarian carcinoma is shown for athymic mice treated with a dose-range of anginex (-▼-: 5 mg/kg/day, $n = 14$; -●-: 10 mg/kg/day, $n = 16$; -◆-: 20 mg/kg/day, $n = 8$) administered via mini-pumps implanted in the left flank of animals. Controls contained PBS with BSA (-□-; $n = 13$) and PBS with ßpep-28 5 mg/kg/day (-○-; $n = 8$) and 10 mg/kg/day (-△-; $n = 4$). The treatment period was initiated on the day of tumor inoculation (day 0) and lasted for 28 days as indicated by the horizontal arrow in the figure. Data were taken from three independent studies and represent the mean tumor volume in mm^3 (± SE).

Fig. 2. Effect of different routes of administration for anginex. (A) Tumor growth of human MA148 ovarian carcinoma in athymic mice treated with anginex (10 mg/kg/day) that was administered in alginate beads (-●-; $n = 10$) or via osmotic mini-pumps (-▼-; $n = 9$) implanted in the left flank of animals. Tumors grew on the right flank of animals. The alginate control group (-□-) used 4 mice, whereas the mini-pump control group used 5 mice (-△-). (B) The mean tumor growth of human MA148 tumors in athymic mice treated with anginex (-▼-: 5 mg/kg/day or -●-: 2.5 mg/kg/day b.i.d.) that was administered by daily loco-regional injection near the site of the tumor. Controls were performed using PBS with BSA (-□-) and PBS with ßpep-28 (-◊-: 5 mg/kg/day). 10 mice were present in all groups except controls, which used 9 mice. Horizontal arrows in both panels indicate the treatment period, which was initiated on day 17 post-inoculation when palpable tumors were present and lasted until day 45. Data have been taken from two independent studies and represent mean tumor volume in mm^3 ± SE.

Fig. 3. Enhanced tumor growth inhibition using HSA-conjugated anginex. (A) Proliferation data is shown which was measured after 72 hours of culture in the presence of free anginex or conjugate anginex in different concentrations by analysis of [^{3}H]-thymidine incorporation. (B) The mean tumor growth plotted for human MA148 ovarian carcinoma in athymic mice. Treatment consisted of anginex (-●-; 2.5 mg/kg/day; $n = 11$) or HSA-conjugated anginex (-▼-; 41.5 mg/kg/d; $n = 18$) that was administered via osmotic mini-pumps implanted in the left flank of animals. Tumors grew on the right flank of animals. Control animals were treated with free HSA in PBS (-○-; $n = 17$). The horizontal arrow indicates the treatment period,

which was initiated on the same day as inoculation (day 0) and lasted for 28 days (prevention model). Data were pooled from three independent studies and represent mean tumor volume in $mm^3 \pm SE$.

Fig. 4. Histochemical analysis. Tumor cross-sections were stained for vessel density (panels A, B, C) and for apoptosis (panels D, E, F). Microvessel density (MVD) is revealed by PE-labelled anti-CD31 antibody staining. Apoptosis staining is revealed by using the TUNEL assay. Panels A and D exemplify tumor tissue cross-sections taken from control-treated mice; B and E exemplify tumor tissue cross-sections taken from anginex-treated mice, and C and F exemplify tumor tissue cross-sections taken from HSA-conjugate-treated mice. Data in panels G and H show the mean of white pixels per image (± SE), MVD and apoptosis, respectively. Black bars represent results from control tumors; right diagonal striped and the left diagonal striped bars represent tumors treated with anginex (respectively 2.5 mg/kg/day and 10 mg/kg/day), and horizontal striped bars represent tumors treated with HSA-conjugated anginex at 41.5 mg/kg/day. Statistical analysis was performed using the student-t-test, where the asterix indicates $P < 0.05$ vs. control-treated tumors and the symbol # indicates $P < 0.01$ vs. anginex-treated (2.5 mg/kg) tumors. Original magnification X200; scale bar = 50 μm.

Fig. 5. Anginex inhibits *in vitro* angiogenesis in a collagen matrix. BCE were cultured on gelatin coated Cytodex-3 beads in a collagen matrix. Sprouting was induced by addition of 20 ng/ml bFGF (A). (B) Sprouting of BCE in the presence of 20 ng/ml bFGF and 25 μM anginex. Quantification of results (C) was performed by NIH-image software ($n = 3$, *$p<0.013$).

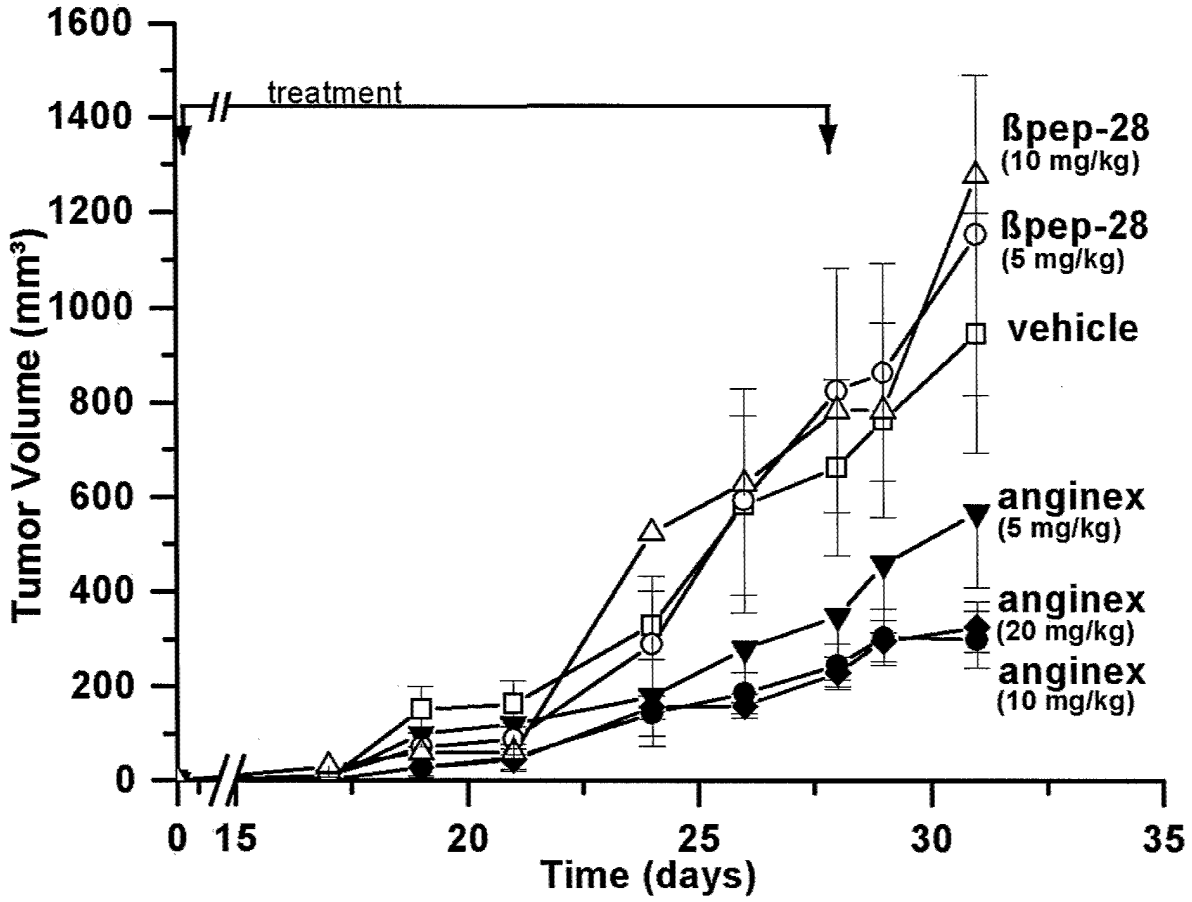

Figure 1
Dings et al. top ⇑

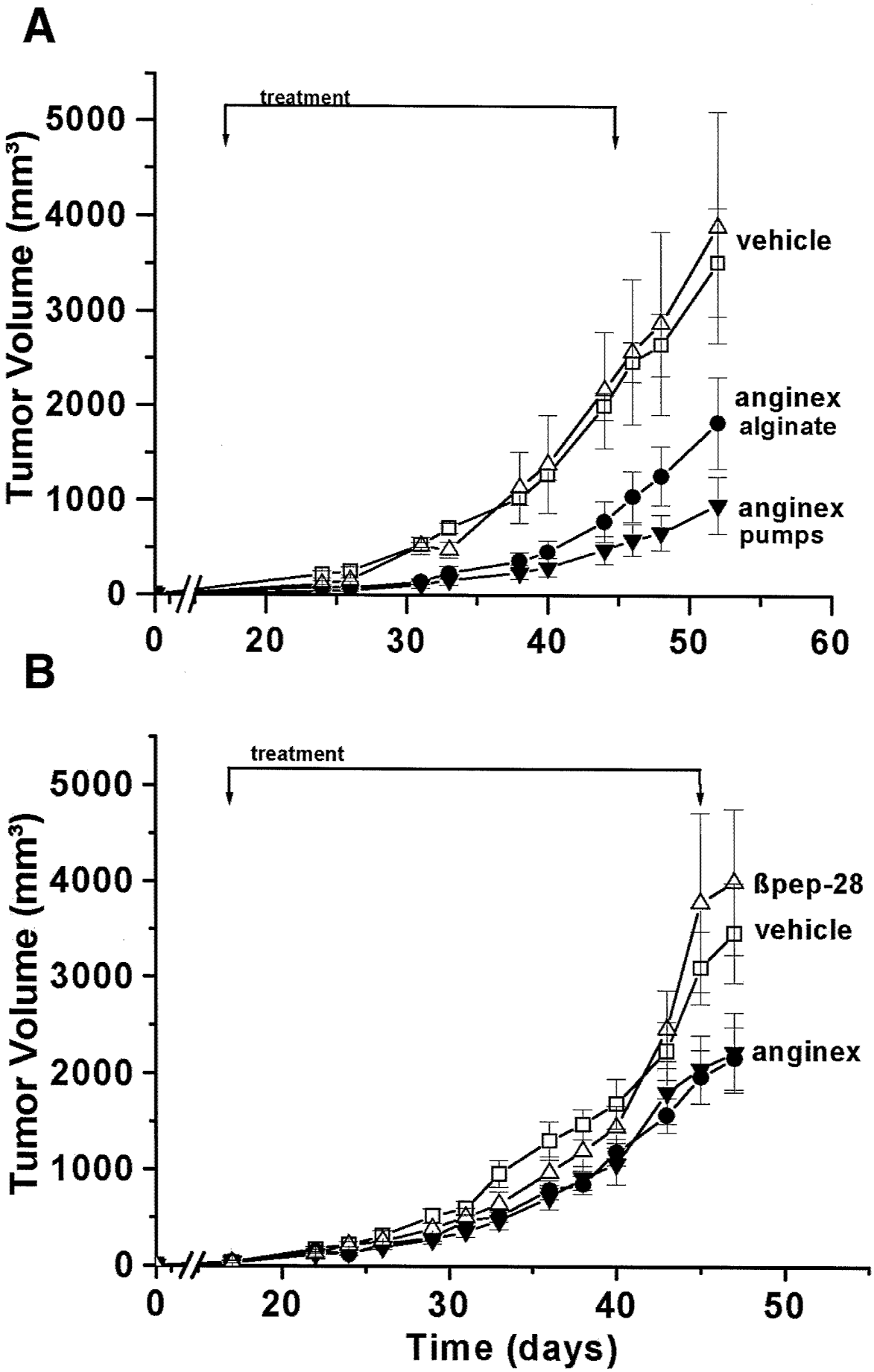

Figure 2
Dings et al. top ⇑

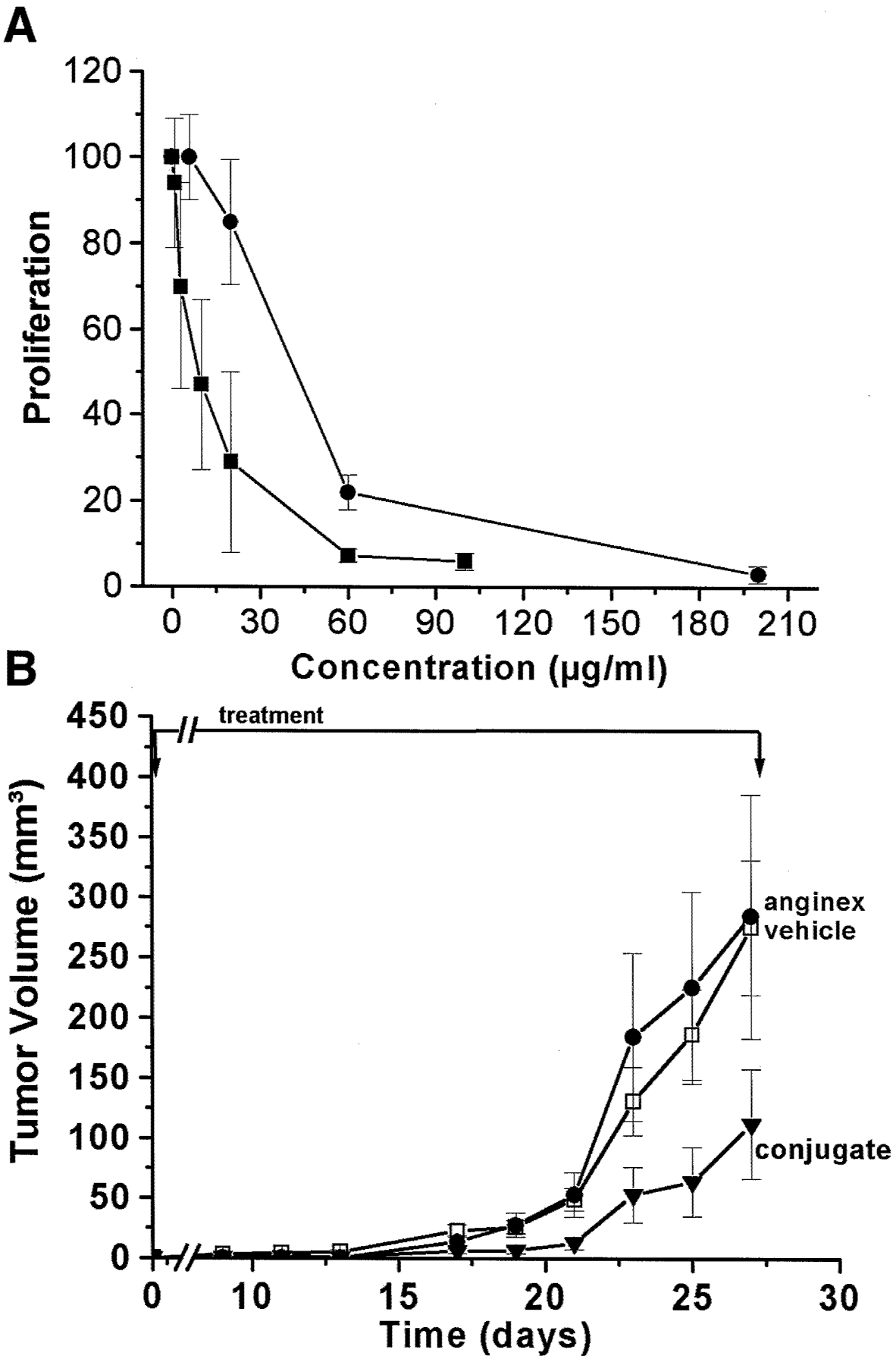

Figure 3
Dings et al. top ⇑

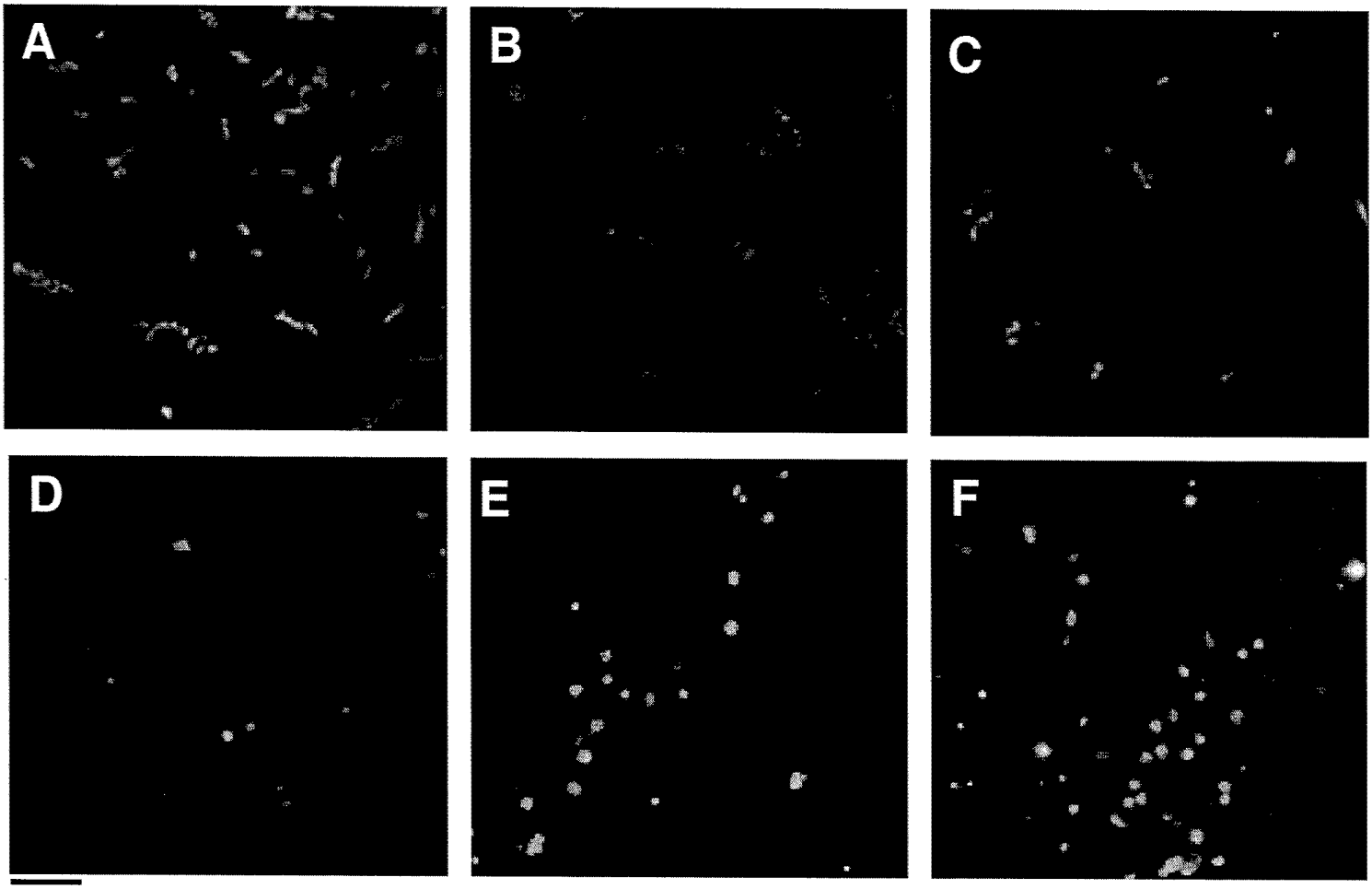

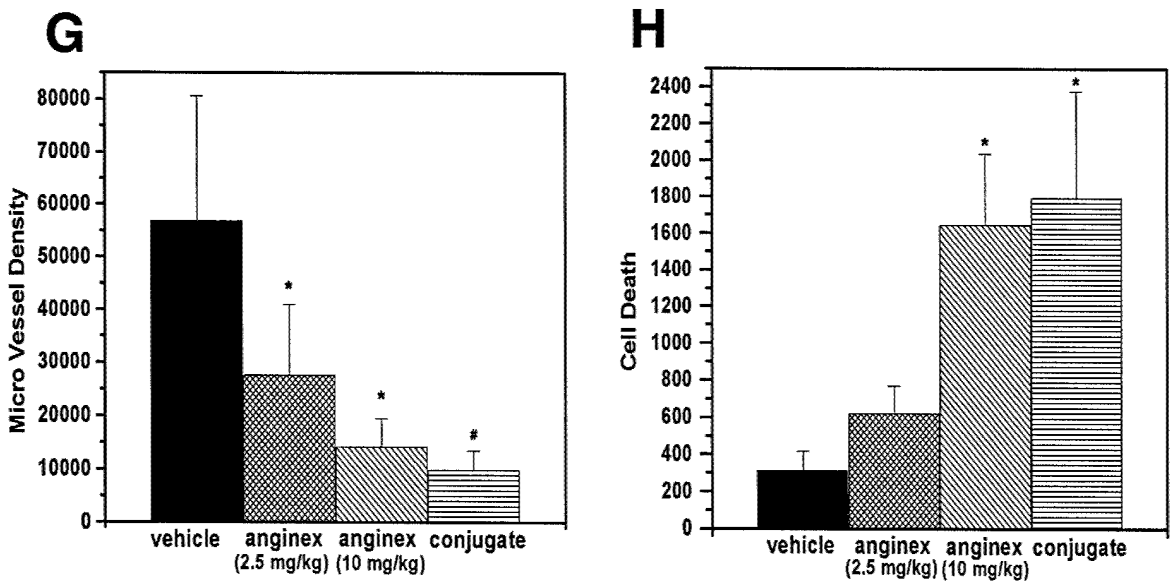

Figure 4
Dings et al. top ⇑

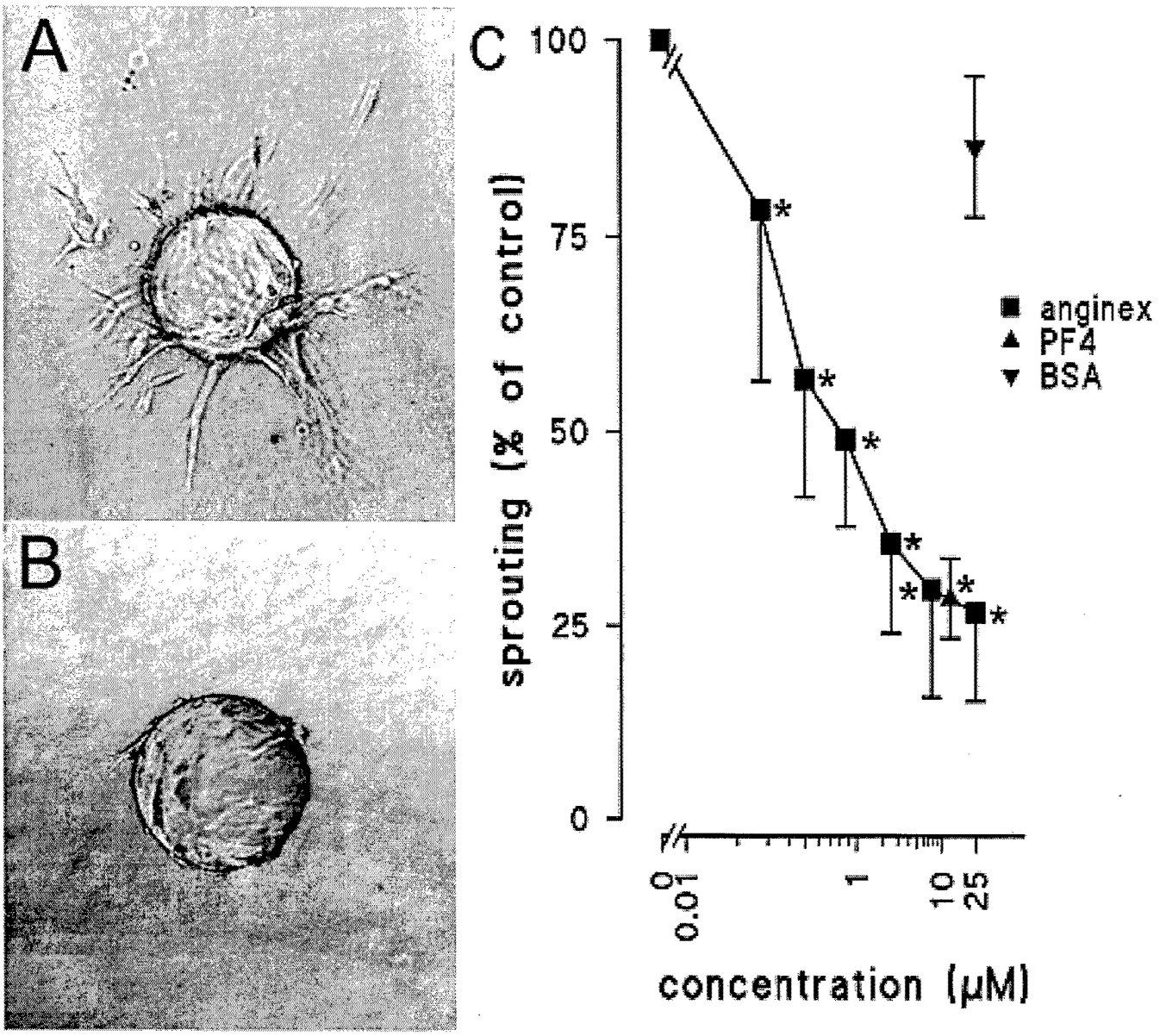

Figure 5
Dings et al. top ⇑

Project 4: Prevention of Ovarian Carcinoma Dissemination by Inhibiting Cell Adhesion

ABSTRACT

The purpose of this project to evaluate the mechanism by which ovarian cancer cell spread with in the peritoneal cavity. Ovarian cancer cells adhere to mesothelial cells and their extracellular matrix lining the peritoneum. Characterizing the cell surface molecules involved in this interaction will facilitate development of methods to inhibit ovarian cancer spread and perhaps limit their growth as well.

Table of Contents

Cover.....164

SF 298.....165

Table of Contents.....166

Introduction.....167

Body.....167

Key Research Accomplishments.....170

Reportable Outcomes.....171

Conclusions.....173

References.....173

Appendices.....174

(4) INTRODUCTION:

Epithelial cancer of the ovary spreads by implantation of tumor cells onto the mesothelial cells and their associated extracellular matrix lining the peritoneal cavity. Our earlier data indicated that ovarian carcinoma cells adhere to mesothelial cells and their associated extracellular matrix (ECM) by use of CD44 and the β1 integrin subunit [1]. We hypothesized that CD44 and the β1 integrin subunit play a fundamental role in the formation of secondary tumor growths in ovarian carcinoma by promoting the adhesion, migration, and invasion of the ovarian carcinoma cells to the mesothelial cells that line the peritoneal cavity. By inhibiting these steps of secondary tumor growth, we will attempt to prevent the dissemination of ovarian carcinoma to organs within the peritoneal cavity. During the past year, we have addressed the following aims: (i) determine the role of CD44 and the β1 integrin subunit in the adhesion, migration, and invasion of primary ovarian carcinoma cells, specifically spheroids, toward mesothelial cells and their associated ECM; (ii) evaluate the role of CD44 and the β1 integrin subunit in ovarian carcinoma cell adhesion, migration, and invasion using both ovarian carcinoma cell lines and populations of ascites cells isolated from patients with ovarian carcinoma; and (iii) determine whether ovarian carcinoma cells isolated as "floaters" from ascites fluid have different levels of expression of CD44 and the β1 integrin subunit, growth properties, or levels of apoptosis.

(5) BODY:

Task #1: Determine the role of CD44 and the β1 integrin subunit in the adhesion and invasion of ovarian carcinoma cell lines toward mesothelial cells and their associated extracellular matrix. This task has essentially been completed. However, since we have shown that CD44 affects ovarian carcinoma cell adhesion [1] and migration [2, 3], and others have reported that the carbohydrate moieties on CD44 regulate cell adhesion, [4, 5] we expanded these studies to examine the role of cell membrane glycosylation in ovarian carcinoma metastasis.

Task #1a: Evaluate reagents for their ability to inhibit the adhesion of ovarian carcinoma cells to extracellular matrix components and/or monolayers of mesothelial cells.

- NIH:OVCAR5 cell membrane glycosylation mediated cell adhesion to ECM components [Appendix 1, Figures 1, 2]. NIH:OVCAR5 ovarian carcinoma cells were enzymatically treated with glycosidases to remove chondroitin sulfate chains, sialic acid residues, or hyaluronan from the cells' surface prior to their addition to adhesion assays. The removal of chondroitin sulfate chains inhibited cell adhesion to fibronectin, collagen type IV, and laminin, but augmented cell adhesion to hyaluronan. The removal of cell surface hyaluronan augmented cell adhesion to fibronectin and laminin, while the removal of sialic acid residues had no effect on cell adhesion to ECM proteins. It is important to note that the enzymatic treatment did not alter the cells' viability.
- NIH:OVCAR5 ovarian carcinoma cell adhesion to live mesothelial monolayers was augmented by the removal of chondroitin sulfate chains, but was unaffected by the removal of hyaluronan or sialic acid residues [Appendix 1, Figure 3]. This suggests that chondroitin sulfate proteoglycans may inhibit ovarian carcinoma cell adhesion to mesothelial cells *in vivo*.

Task #1b: Evaluate reagents for their ability to inhibit the migration of ovarian carcinoma cells through extracellular matrix components.

- NIH:OVCAR5 cell migration toward fibronectin was increased by the removal of chondroitin sulfate chains, but was decreased by the removal of sialic acid residues [Appendix 1, Figure 4]. Ovarian carcinoma cell migration toward collagen type IV and laminin was increased by the removal of chondroitin sulfate chains, but not by the removal of hyaluronan or sialic acid residues. Multiple interactions mediated by proteoglycans may affect the migratory abilities of ovarian carcinoma cells.

Task #1c: Evaluate reagents for their ability to inhibit the invasion of ovarian carcinoma cells through a monolayer of mesothelial cells.

- NIH:OVCAR5 ovarian carcinoma cell invasion through Matrigel toward fibronectin, collagen type IV, and laminin was inhibited by the removal of sialic acid residues from the cells' surface [Appendix 1, Figure 5]. The removal of chondroitin sulfate chains or hyaluronan had no effect on cell invasion through Matrigel.
- We designed a cell-based invasion assay in which LP9 peritoneal mesothelial cells were grown to confluence in tissue culture wells, and then fixed to the plates with dimethyl sulfoxide. NIH:OVCAR5 ovarian carcinoma cells were added atop the fixed mesothelial cell monolayers. Ovarian carcinoma cell invasion through the mesothelial cells was monitored daily for up to 7 days. The extent of invasion was visualized with trypan blue dye, which imparted a blue color to the dead, fixed mesothelial cells. Live NIH:OVCAR5 cells, which excluded the dye, were easily distinguished as unstained patches of cells. Single cell suspensions of NIH:OVCAR5 cells required 3-4 days to establish initial foci of invasion through the mesothelial cell monolayers, and widespread invasion was observed by 7 days [Appendix 2, Figure 1].
- Putative inhibitors of invasion were added to the single cell suspensions of NIH:OVCAR5 ovarian carcinoma cells in the cell-based invasion assay described above [Appendix 2, Figures 2, 3]. Ovarian carcinoma cell invasion through fixed mesothelial cell monolayers was inhibited by the addition of RGD peptides or a blocking mAb against the β1 integrin subunit. This suggests that β1 integrins may participate in ovarian carcinoma invasion *in vivo*. Blocking mAbs against the α2, α3, α4, α5, or α6 integrin subunits had no effect on invasion, suggesting that β1 integrin-mediated signal transduction is required for invasion, rather than interactions between particular integrins and ligands. Invasion was also blocked by GM6001, a broad-spectrum inhibitor of matrix metalloproteinases (MMPs). Taken together, this data suggests that β1 integrin signal transduction may mediate ovarian carcinoma cell invasion by regulating the expression and/or activity of MMPs.

Task #2: Test whether reagents that cause *in vitro* inhibition in Task #1 can inhibit *in vivo* ovarian carcinoma, intraperitoneal tumor nodule formation, tumor burden, and/or ascites formation in chickens.

- As a Program Project, we have not been able to conduct the chicken model experiments.

Task #3: Evaluate the role of CD44 and the β1 integrin subunit in ovarian carcinoma cell adhesion and invasion using populations of ascites cells isolated from patients with ovarian carcinoma that express either high levels or nondetectable levels of CD44 and/or and the β1 integrin subunit.

Task #3a: By fluorescent-activated cell sorting (FACS), sort ascites cells into populations of cells with high or nondetectable levels of expression of CD44 and/or the β1 integrin subunit.

- Because ovarian carcinoma cells are present in the ascites fluid of patients as aggregates or clumps of cells that do not readily disperse into a single cell suspension, we could not separate the cells by FACS analysis. We have performed subsequent experiments using all of the ovarian carcinoma cells that we isolated from the patient ascites fluid.

Task #3b: Determine whether differences in adhesion and/or invasion to ECM components and/or mesothelial cells are observed depending upon the expression of CD44 and/or β1 integrins on ascites cells.

- By immunohistochemistry, we have observed that both CD44 and β1 integrins are expressed on the surface of patients' ascites tumor cells.
- We confirmed our preliminary observations that spheroids obtained from ovarian carcinoma patient ascites samples adhered to chamber slides coated with laminin, fibronectin, collagen type I, and type IV collagen (Appendices #4,5). The patient samples separated into three groups: highly adherent (30-70% adhesion); moderately adherent (10-20% adhesion); or non-adherent (0-5% adhesion). We also observed that in all the adherent samples, patient spheroid adhesion to fibronectin was typically higher than to the other ECM proteins. Maximum adhesion of patient spheroids to ECM proteins was observed at 2 hours, with a. partial loss of adhesion at 4 hours. The initial adhesion of these spheroids may require further stimuli *in vivo* (i.e., cell-cell interactions with target tissues) to continue the metastatic process. Taken together, these results imply that the spheroids found in patients' ascites fluid can demonstrate an adhesive capability, though not as great as those of single cells.
- Win preliminary studies, we determined the ability of ovarian carcinoma spheroids to adhere to glycosaminoglycans commonly found in cell ECMs: hyaluronan, hyaluronan fragments, and chondroitin sulfate. Patient ascites spheroids demonstrated variable adhesive abilities: a highly adherent group (30-60% adhesion); a moderately adherent group (10-20% adhesion); and a non-adherent group (0-5% adhesion). Patient ascites spheroids may adhere to secondary tumor sites via interactions with glycosaminoglycans or proteoglycans. Carbohydrate moieties present upon the ovarian carcinoma cells may provide an alternative mechanism of cell adhesion; alternatively, spheroids may bind to at secondary tumor site in a nonspecific manner.
- We previously reported that blocking mAbs against integrin subunits inhibited NIH:OVCAR5 spheroid adhesion to ECM proteins [6, 7]. In preliminary studies, we observed that blocking monoclonal antibodies against the β1, α2, α5, and α6 integrin subunits partially inhibited patient ascites spheroids adhesion to fibronectin, laminin, and collagen type IV (Appendices #4,5). This implies ovarian carcinoma spheroid adhesion to ECM proteins is partially mediated by integrins.
- We have observed that a blocking mAb against CD44, used either alone or in conjunction with the blocking mAb against the β1-integrin subunit, had no significant effect on patient ascites spheroid adhesion to laminin, fibronectin, or collagen type IV.

Task #4: Determine whether ovarian carcinoma cells that are isolated from tumor nodules present in the peritoneal cavity have different levels of expression of CD44 and β1 integrin, growth properties, or levels of apoptosis compared to ovarian carcinoma cells isolated as "floaters" from the ascites fluid of patients.

Task #4a. Determine the levels of CD44 and β1 integrins on primary ovarian carcinoma cells.

- Ovarian carcinoma tumor cells isolated from the ascites of patients diagnosed with stage III or IV ovarian carcinoma were analyzed by immunohistochemistry. Our continuing studies show that both CD44 and β1 integrins are expressed on the surfaces of ovarian carcinoma cells.

Task #4b. Quantitate the growth of ovarian carcinoma cells on ECM components

- NIH:OVCAR5 cell adhesion to 96-well plates coated with fibronectin, laminin, collagen type IV, or hyaluronan did not affect cell proliferation, suggesting that ovarian carcinoma cell proliferation is dependent upon the general phenomenon of cell adhesion to a substrata, rather than a requirement for adhesion to a particular ECM component [Appendix 1, Figure 4].

Task #4c. Quantitate the growth of ovarian carcinoma cells on mesothelial cells.

- We developed a novel cell-based assay to study ovarian carcinoma cell invasion described in Task #1c. We have observed that the ovarian carcinoma cells adhered to and invaded through the fixed mesothelial cell monolayers. In some cases, the ovarian carcinoma cells grew to confluence, displacing the mesothelial cell monolayers [Appendix 1, Figure 1].

Task #4f. Determine whether the subpopulation of ovarian carcinoma cells isolated from ascites fluid and/or solid tumors that are not undergoing apoptosis will survive when they are maintained in suspension.

- We have confirmed our preliminary observations that spheroids isolated from the ascites of ovarian carcinoma patients remained viable for up to 1 month when cultured in tissue culture-treated flasks or in suspension. We have observed that both adherent and nonadherent spheroids remained viable for up to 1 month.

Status of Project Schedule:

Task #1 (months 1-18): This task has been completed, but successful results have prompted us to expand the studies initially proposed for this task.
Task #2 (months 1-48): This task has proven to be unfeasible and will not be completed.
Task #3 (months 6-48): Tasks 3a and 3b have been completed. Task 3c will not be completed.
Task #4 (months 24-48): Tasks 4a, 4b, and 4f have been completed, although the constant influx of additional primary patient samples will result in periodic updating of our results. Tasks 4c, 4d, and 4e remain to be completed.

(6) KEY RESEARCH ACCOMPLISHMENTS:

- We confirmed our preliminary observations that spheroids obtained from ovarian carcinoma patient ascites samples adhered to ECM components (laminin, fibronectin, collagen type I, type IV collagen, hyaluronan, hyaluronan fragments, and chondroitin sulfate), with maximum adhesion to fibronectin. We observed that patient samples exhibited heterogeneous range of adhesive ability. Since spheroids exhibit resistance to radio- and chemotherapies [8, 9], our results suggest that they may comprise a source of metastasis that is not effectively eradicated by current treatment strategies.

- We determined that adhesion to ECM proteins by spheroids obtained from ovarian carcinoma patients was partially mediated by β1 integrins, but not by CD44.
- In preliminary studies, we have observed that both NIH:OVCAR5 and patient ascites spheroids adhered to confluent monolayers of live mesothelial cells. Interestingly, the spheroids adhered to the mesothelial cell monolayers at a higher rate than to ECM components. Also, the patient samples adhered to live, but not fixed, mesothelial cell monolayers, indicating that either receptor conformation or signaling between the mesothelial and tumor cells is necessary for optimal adhesion.
- NIH:OVCAR5 cell adhesion to 96-well plates coated with ECM components did not affect cell proliferation, suggesting that ovarian carcinoma cell proliferation occurs independently of the substrata to which the cells adhere.
- Cell membrane glycosylation mediates metastatic events in ovarian carcinoma. The enzymatic removal of carbohydrate moieties from the surface of NIH:OVCAR5 ovarian carcinoma cells partially affected the cells' ability to adhere, migrate, and invade. However, cell viability was not affected by enzymatic treatment.
- We developed a novel cell-based assay to study ovarian carcinoma cell invasion. Briefly, human mesothelial cells were grown to confluence in tissue culture plates and fixed with dimethyl sulfoxide. Single cell suspensions of NIH:OVCAR5 cells were cultured atop the fixed mesothelial cell monolayers for up to 7 days. Trypan blue dye was used to visualize the. fixed mesothelial cell monolayers. Live, invading ovarian carcinoma cells excluded the stain and were easily identified with a light microscope.
- We confirmed preliminary studies in which we observed that NIH:OVCAR5 invasion through fixed mesothelial monolayers was inhibited by RGD peptide and a blocking mAb against the β1 integrin subunit, but not mAbs against the α2, α3, α4, α5, or α6 integrin subunits or CD44. β1 integrin-mediated signal transduction may be required for ovarian carcinoma cell invasion, rather than interactions between particular integrins and ligands.

(7) REPORTABLE OUTCOMES:

Manuscripts:

1. Casey RC, Burleson KM, Pambuccian S, Skubitz K, Oegema T, Skubitz APNS. (2001) β1 integrins regulate the formation and adhesion of ovarian carcinoma multicellular spheroids. The American Journal of Pathology 159:2071-2080.
2. Casey RC, Oegema TR, Skubitz KM, Pambuccian SE, Skubitz APN. Cell membrane glycosylation mediates the adhesion and migration of ovarian carcinoma cells toward extracellular matrix components and mesothelial cell monolayers. [Submitted]
3. Casey RC, Koch K, Oegema TR, Skubitz KM, Pambuccian SE, Grindle SM, Skubitz APN. (2002) Establishment of an *in vitro* assay to measure the invasion of ovarian carcinoma cells through mesothelial cell monolayers. [Submitted]
4. A fourth manuscript describing potential biomarkers of ovarian cancer: Skubitz APN, Grindle SM, Pambuccian S, Casey RC, Burleson KM, Hibbs KA, Skubitz KM. Gene expression in ovarian cancer. [In preparation].
5. A fifth manuscript describing the results that we have observed with the metastatic properties of multicellular spheroids obtained from ovarian carcinoma patient primary ascites: Burleson KM, Skubitz APN [In preparation].

Abstracts and Presentations:

1. Burleson KM, Casey RC, Oegema TR, Skubitz KM, Pambuccian S, and Skubitz APN. The metastatic potential of ovarian carcinoma spheroids. The Molecular, Cellular, Developmental Biology and Genetics Fall 2001 Poster Session and Retreat. The results from this study were presented as a poster presentation in Minneapolis, MN on **October 12, 2001**.
2. Burleson, K.M., Casey, R.C., and Skubitz, A.P.N. (2001) The metastatic potential of ovarian carcinoma spheroids. Presented at the Biomedical Genomics Center Conference, "Crossing Washington Avenue Both Ways: A Mixer for Biologists, Chemists, Chemical Engineers, Physicists, Computer Scientists, and Biostatisticians", **October 24, 2001**, Minneapolis, MN.
3. Burleson KM. "The metastatic potential of ovarian carcinoma spheroids". Molecular, Cellular, Developmental Biology & Genetics Interactive Television seminar. The results from these studies were presented as a televised seminar in Minneapolis and St. Paul, MN on **March 6, 2002**.
4. Casey RC, Oegema TR, Skubitz KM, Pambuccian SE, Skubitz APN. (2002) "Cell membrane glycosylation mediates the adhesion and migration of ovarian carcinoma cells toward extracellular matrix components and mesothelial cell monolayers." 93rd Annual Meeting of the American Association for Cancer Research. The results from this study were published in the Proceedings of the American Association Cancer Research, 43:368, and presented as a poster presentation at the 93rd Annual Meeting of the American Association for Cancer Research in San Francisco, CA on **April 6-10, 2002**.
5. Casey RC, Oegema TR, Skubitz KM, Pambuccian SE, Skubitz APN. (2002) "Cell membrane glycosylation mediates the adhesion, migration, and invasion of ovarian carcinoma cells toward extracellular matrix components and mesothelial cell monolayers." 3rd Annual University of Minnesota Cancer Center Spring Poster Session & Symposium. The results from these studies were presented as a poster session in Minneapolis, MN on **May 16-19, 2002.**
6. Burleson KM, Casey RC, Pambuccian SE, Skubitz KM, Oegema TR, Skubitz APN. (2002) "Comparisons of ovarian carcinoma multicellular spheroids from cell lines and patient ascites: Do spheroids have metastatic potential?" 3rd Annual University of Minnesota Cancer Center Spring Poster Session & Symposium. The results from these studies were presented as a poster session in Minneapolis, MN on **May 16-19, 2002**.
7. Burleson KM, Casey RC, Pambuccian S, Skubitz KM, Oegema TR, and Skubitz APN. Comparison of ovarian carcinoma multicellular spheroids from cell lines and patient ascites: Do spheroids have metastatic potential?" American Association for Cancer Research Pathobiology of Cancer Workshop. The results from this study were presented as a poster presentation on **July 14-21, 2002**.
8. Burleson KM, Casey RC, Grindle S, Pambuccian SE, Skubitz KM, Oegema TR, Skubitz, APN. Ovarian carcinoma ascites spheroids are capable of adhesion to extracellular matrix proteins and mesothelial monolayers. To be presented at the AACR special conference in Cancer Research, "Proteases, Extracellular Matrix, and Cancer" at Hilton Head Island, SC on **October 9-13, 2002**.

Graduate student theses

1. Jeannine Thiele: "Identification of genes up-regulated in ovarian cancer by large-scale gene expression analysis." Master's degree thesis, May, 2002.

2. Kathleen Hibbs: "Immunohistochemical staining of ovarian carcinoma tumors with antibodies against proteins shown to be upregulated by gene expression array analysis." Master's degree thesis, August 2002.

Awards

1. Rachael C. Casey: American Association for Cancer Research Minority Scholar, 2002. Competitive award to present data at 93rd Annual AACR meeting.
2. Kathryn M. Burleson: American Association for Cancer Research "Pathobiology of Cancer" Workshop trainee, Keystone, CO, July, 2002. Trainee positions were awarded by competitive selection of applicants.
3. Kathryn M. Burleson: Mary Haga Travel Award from the Graduate Women in Sciences: Sigma Delta Epsilon Society. Competitive award to defray costs of attending "Pathobiology of Cancer" Workshop.
4. Kathryn M. Burleson. $1000 from the Masonic/Dietz Family Award for Educational Travel through the University of Minnesota Cancer Center to defray costs of attending the AACR special conference in Cancer Research, "Proteases, Extracellular Matrix, and Cancer" at Hilton Head Island, SC on October 9-13, 2002.
5. Kathryn M. Burleson. $1000 AACR Scholar-in-Training Award to defray costs of attending the AACR special conference in Cancer Research, "Proteases, Extracellular Matrix, and Cancer" at Hilton Head Island, SC on October 9-13, 2002.

(8) CONCLUSIONS: We report that ovarian carcinoma cell membrane glycosylation, may mediate the adhesion, migration, and invasion of ovarian carcinoma cells toward mesothelial cells and their associated ECM components. Our results suggest that ovarian carcinoma spheroids adhere to mesothelial cells via interactions with fibronectin, and that additional cell-cell interactions may be involved. Finally, we have designed a cell-based invasion assay that can serve as an *in vitro* model to examine the invasion of ovarian carcinoma cells into monolayers of mesothelial cells and identified potential inhibitors of invasion assay with this new assay. These studies may lead to the identification and development of reagents that can prevent the further spread of ovarian carcinoma *in vivo*.

(9) REFERENCES:

1. Lessan, K., Aguiar, D.J., Oegema, T., Siebenson, L., and Skubitz, A.P.N. (1999) CD44 and the β1 integrin mediate ovarian carcinoma cell adhesion to peritoneal mesothelial cells. American Journal of Pathology 154:1525-1537.
2. Casey, R.C. and Skubitz, A.P.N. (2000) CD44 and β1 integrins mediate ovarian carcinoma cell migration toward extracellular matrix proteins. Clinical & Experimental Metastasis 18:67-750.
3. Casey, R.C. and Skubitz, A.P.N. (2000) Ovarian carcinoma cell chemotaxis toward extracellular matrix proteins is mediated by CD44 and β1 integrin. Late-Breaking Abstracts at the 91st Annual Meeting of the American Association for Cancer Research, San Francisco, CA, pp. 5.
4. Catterall J.B., Jones L.M., Turner G.A. (1999) Membrane protein glycosylation and CD44 content in the adhesion of human ovarian cancer cells to hyaluronan. Clinical & Experimental Metastasis 17:583-91.

5. Knutson J.R., Iida J, Fields G.B., McCarthy JB. (1996) CD44/chondroitin sulfate proteoglycan and $\alpha 2\beta 1$ integrin mediate human melanoma cell migration on type IV collagen and invasion of basement membranes. Molecular Biology of the Cell. 7:383-396.
6. Casey, R.C., Burleson, K.M., Skubitz, K.M., Pambuccian, S.E., Oegema, T.R., Ruff, L.E., and Skubitz, A.P.N. (2001) $\beta 1$ integrins mediate the formation and adhesion of ovarian carcinoma spheroids. American Journal of Pathology 159:2071-2080.
7. Casey, R.C., Burleson, K.M., Pambuccian, S.E., Skubitz, K.M., Oegema, T.R., and Skubitz, A.P.N. (2001) The formation, growth, and adhesion of ovarian carcinoma multicellular spheroids. 92nd Proceedings of the American Association for Cancer Research, 42:147.
8. Filippovich I.V., Sorokina N.I., Robillard N., Chatal J.F. (1997) Radiation-induced apoptosis in human ovarian carcinoma cells growing as a monolayer and as multicell spheroids. International Journal of Cancer 72:851-859.
9. Makhija S., Taylor D.D., Gibb R.K., Gercel-Taylor C. (1999) Taxol-induced bcl-2 phosphorylation in ovarian cancer cell monolayer and spheroids. International Journal of Oncology 14:515-521.

(10) APPENDICES:

1. Casey RC, Oegema TR, Skubitz KM, Pambuccian SE, Skubitz APN. (2002) Cell membrane glycosylation mediates the adhesion and migration of ovarian carcinoma cells toward extracellular matrix components and mesothelial cell monolayers. [Submitted]
2. Casey RC, Koch K, Oegema TR, Skubitz KM, Pambuccian SE, Grindle SM, Skubitz APN. (2002) Establishment of an *in vitro* assay to measure the invasion of ovarian carcinoma cells through mesothelial cell monolayers. [Submitted].
3. Casey RC, Oegema TR, Skubitz KM, Pambuccian SE, Skubitz APN. (2002) "Cell membrane glycosylation mediates the adhesion and migration of ovarian carcinoma cells toward extracellular matrix components and mesothelial cell monolayers." Proceedings of the American Association Cancer Research, 43:368.
4. Burleson KM, Casey RC, Pambuccian S, Skubitz KM, Oegema TR, and Skubitz APN. Comparison of ovarian carcinoma multicellular spheroids from cell lines and patient ascites: Do spheroids have metastatic potential?" American Association for Cancer Research Pathobiology of Cancer Workshop. The results from this study were presented as a poster presentation on July 14-21, 2002.
5. Burleson KM, Casey RC, Grindle S, Pambuccian SE, Skubitz KM, Oegema TR, Skubitz, APN. Ovarian carcinoma ascites spheroids are capable of adhesion to extracellular matrix proteins and mesothelial monolayers. To be presented at the AACR special conference in Cancer Research, "Proteases, Extracellular Matrix, and Cancer" at Hilton Head Island, SC on October 9-13, 2002.
6. Casey RC, Burleson KM, Pambuccian S, Skubitz K, Oegema T, Skubitz APNS. (2001) $\beta 1$ integrins regulate the formation and adhesion of ovarian carcinoma multicellular spheroids. The American Journal of Pathology 159:2071-2080.

APPENDIX

Project 4

Cell membrane glycosylation mediates the adhesion, migration, and invasion of ovarian carcinoma cells.

Rachael C. Casey*, Theodore R. Oegema Jr.‡, Keith M. Skubitz†, Stefan E. Pambuccian*, Suzanne M. Grindle§, and Amy P.N. Skubitz*

Departments of *Laboratory Medicine and Pathology, ‡Orthopaedic Surgery, and †Medicine, and the §Tissue Procurement Facility, University of Minnesota, Minneapolis, MN 55455, USA

Number of Text Pages: 31; **Number of Tables:** 2; **Number of Figures:** 6

Running Title: Glycosylation affects ovarian carcinoma cell function

Sources of Support: Supported by grants from the National Institute of Health/National Cancer Institute (CA0913825), Department of the Army (DA/DAMD17-99-1-9564), Minnesota Medical Foundation (SMF-2078-99), Graduate School Grant-in-Aid of Research (#18118), and the Biomedical Genomics Center, University of Minnesota.

Correspondence and Reprint Requests to: Dr. Amy P.N. Skubitz, Department of Laboratory Medicine and Pathology, University of Minnesota, MMC 609, 420 Delaware St. S.E., Minneapolis, MN 55455, USA. Tel: 612-625-5920; Fax: 612-625-1121, email: skubi002@umn.edu

Keywords: Cell adhesion, cell invasion, cell migration, cell membrane glycosylation, ovarian carcinoma, proteoglycans

Abbreviations: ECM: extracellular matrix; EHS: Engelbreth-Holm-Swarm; FBS: fetal bovine serum; PBS: phosphate buffered saline.

Abstract

We have previously shown that ovarian carcinoma cell adhesion to mesothelial cell monolayers and migration toward fibronectin, collagen type IV, and laminin is partially mediated by CD44, a proteoglycan known to affect the functional abilities of tumor cells. The purpose of this study was to determine the role of cell membrane glycosylation in the metastatic abilities of ovarian carcinoma cells. NIH:OVCAR5 cells were treated with glycosidases to remove carbohydrate moieties from molecules on the cells' surface. The ability of the treated cells to adhere to extracellular matrix components or mesothelial cell monolayers, migrate toward extracellular matrix proteins, and invade through Matrigel was assessed. We observed that the loss of different carbohydrate moieties resulted in altered ovarian carcinoma cell adhesion, migration, and/or invasion toward extracellular matrix components or mesothelial cell monolayers. Glycosidase treatment did not alter the molecular weight of CD44 in NIH:OVCAR5 cells in Western blots, suggesting that CD44 did not contain the carbohydrate residues responsible for the phenomena observed. Gene array analysis of NIH:OVCAR5 cells revealed the expression of several proteoglycans, including syndecan 4, decorin, and perlecan. In tissue samples obtained from patients, altered proteoglycan gene expression was observed in primary ovarian carcinoma tumors and secondary metastases, compared to normal ovaries. Taken together, these results suggest that ovarian carcinoma cell proteoglycans affect the cells' ability to adhere, migrate, and invade toward extracellular matrix components and mesothelial cell monolayers. Thus, the carbohydrate modifications of several proteoglycans may mediate the formation and spread of secondary tumor growth in ovarian carcinoma.

Introduction

Proteoglycans are major components of the extracellular matrix (ECM) that mediate interactions with other ECM and cellular components. Proteoglycans have been shown to regulate cell adhesion,[1] cell signaling,[2] and apoptosis[3]. In cancer, altered glycosylation is a common feature of malignancy, and some of these alterations contribute to metastatic processes, including cell adhesion, migration, and invasion.

CD44, a proteoglycan found on ovarian carcinoma cells,[4-6] binds the ECM glycosaminoglycan hyaluronan with high affinity[7] and also has a weak affinity for fibronectin, type IV collagen, and laminin.[8] Hyaluronan is a high molecular weight glycosaminoglycan that is present in the ECM of the mesothelial cells that line the peritoneum.[9] We have previously reported that ovarian carcinoma cell adhesion to mesothelial cell monolayers and migration toward the extracellular matrix proteins fibronectin, type IV collagen, and laminin is partially mediated by interactions between CD44 and hyaluronan.[6, 7] Interactions between CD44 and hyaluronan affect cell adhesion,[6] migration,[5, 7] and tumor growth[10] in ovarian carcinoma cells. In some ovarian carcinoma cell lines, CD44 is heavily glycosylated, and the removal of carbohydrate moieties from the cells' surfaces resulted in altered cell adhesion to hyaluronan.[11]

Other proteoglycans have also been implicated in cancer cell functions. Syndecan-1, a heparan sulfate proteoglycan, has been shown to mediate the invasion of myeloma cells.[12] Ovarian carcinoma cell adhesion to fibronectin and collagen type I is mediated by heparan sulfate and chondroitin sulfate proteoglycans synthesized by the cells.[13] Versican, a chondroitin sulfate proteoglycan, contains a hyaluronan-binding domain,[14] stimulates cell growth, and inhibits human melanoma cell adhesion to fibronectin and collagen type I,[15] possibly facilitating

tumor cell detachment and proliferation. Decorin, another chondroitin sulfate proteoglycan that binds collagen fibrils, has been shown to inhibit the growth of ovarian cancer cells.[16] Clearly, proteoglycans and their carbohydrate residues mediate many tumor cell functions; however, their exact roles in cancer metastasis are poorly understood.

The purpose of this study was to examine the roles of cell membrane glycosylation upon the adhesive, migratory, and invasive abilities of ovarian carcinoma cells. Our results suggest that proteoglycans, particularly those with chondroitin sulfate or sialic acid moieties, may affect the ability of ovarian carcinoma cells to interact with mesothelial cells and proteins found in their ECMs, and thus may affect the ability of ovarian carcinoma tumor cells to metastasize.

Methods

Unless otherwise stated, all standard reagents and materials were obtained from Sigma Chemical Company (St. Louis, MO). Unless otherwise specified, all experiments were performed a minimum of three times.

Cell culture. The human ovarian carcinoma cell line NIH:OVCAR5, which mimics the progression of ovarian carcinoma when injected into *in vivo* mouse models,[17] was maintained in RPMI 1640 medium, 10% fetal bovine serum (FBS), 2 mM glutamine, 0.2 U/ml insulin, and 50 U/ml penicillin G/streptomycin. The ovarian carcinoma cell line NIH:OVCAR5 was originally established by Dr. Thomas Hamilton (Fox Chase Cancer Center)[18] and obtained from Dr. Judah Folkman, Harvard Medical School. The human peritoneal mesothelial cell line LP9 (Coriell Cell Repositories, Camden, NJ) was maintained in a medium containing a 1:1 ratio of M199 and MCDB 10 media, 15% FBS, 2 mM glutamine, 5 ng/ml epidermal growth factor, 0.4 μg/ml hydrocortisone, and 50 U/ml penicillin G/streptomycin. Both cell lines were maintained in 75-mm^2 tissue culture flasks in a humidified incubator with 5% CO_2 at 37°C.

Human tissue samples. Tissue samples from 50 normal ovaries, 20 primary ovarian carcinomas, 17 secondary omental metastases, and 7 normal omentas were obtained from the Tissue Procurement Facility of the University of Minnesota Cancer Center. Samples were obtained using protocols approved by the University of Minnesota Institutional Review Board. All samples were identified, dissected, and snap frozen in liquid nitrogen within 30 min of removal from the patient. Tissue sections of each sample were prepared before freezing, and were

examined by a pathologist by light microscopy after H&E staining to confirm the pathologic nature of the sample. None of the samples were necrotic.

ECM Molecules. Collagen type IV, isolated from mouse Engelbreth-Holm-Swarm (EHS) tumor, was purchased from Trevigen, Gaithersburg, MD. Mouse EHS laminin, prepared as previously described,[19] was provided by Dr. Leo Furcht, University of Minnesota. Human plasma fibronectin, purified as described,[20] was provided by Dr. James McCarthy, University of Minnesota. Human umbilical cord hyaluronan, chondroitin sulfate A, and ovalbumin were purchased from Sigma. Matrigel was purchased from Becton Dickinson, Bedford, MA.

Glycosidase treatment. Chondroitinase ABC from *P. vulgaris*, hyaluronidase from bovine testes, and neuraminidase from *C. perfringens* were purchased from Sigma Chemical Company. NIH:OVCAR5 cells were grown in monolayer cultures, released with 0.5% trypsin, 2 mM ethylenediaminetetraacetic acid as previously described,[21] and resuspended in base medium at a concentration of 10^6 cells/ml. The cells were incubated in the presence of chondroitinase ABC (0.5 U/ml), hyaluronidase (200 U/ml), or neuraminidase (10 mU/ml) in base medium for 30 min at 37°C prior to their use in further assays. Chondroitinase ABC was used to remove chondroitin sulfate resides and neuraminidase was used to remove terminal sialic acid residues. Bovine testicular hyaluronidase primarily cleaves hyaluronan, but also may cleave chondroitin sulfate residues. Heat-inactivated enzymes had no effect on cell adhesion, migration, or invasion (results not shown).

Cell-ECM adhesion assay. The ability of the glycosidase-treated ovarian carcinoma cells to adhere to ECM components was quantified as previously described.[5] Clear-bottom 96-well plates were coated with 5 μg/ml fibronectin, collagen type IV, or laminin, or with 1 mg/ml ovalbumin, chondroitin sulfate A, or hyaluronan in phosphate buffered saline (PBS) for 16 hr at 37°C. Nonspecific binding sites were blocked with 2% ovalbumin in PBS. NIH:OVCAR5 cells were radiolabeled with L-[^{35}S]methionine for 24 hr, trypsinized, washed, and subjected to glycosidase treatment. The cells (10^5 cells/100 μl) were added to the coated 96-well plates and incubated for 30 min. Nonadherent cells were removed by washing and the radioactivity was counted. These experiments were performed three times each in eight replicates.

Cell-cell adhesion assay. The ability of glycosidase-treated ovarian carcinoma cells to adhere to monolayers of the human mesothelial LP9 cell line was determined as previously described.[5] The assays were performed as described above in the cell-ECM assay, except that the clear-bottom 96-well microtiter plates were coated with LP9 cells grown to confluence for 48 hr in complete medium. Prior to the addition of ovarian carcinoma cells, the mesothelial cell monolayers were rinsed twice with RPMI 1640 medium. These experiments were performed three times each in eight replicates.

Cell migration assay. Chemotaxis of glycosidase-treated ovarian carcinoma cells in response to ECM molecules was quantitated in modified Boyden chambers, using 8 μm pore size polycarbonate polyvinylpyrrolidine-free filters (Fisher Scientific, Itasca, IL) determined as previously described.[6] Base medium containing fibronectin (5 μg/ml), type IV collagen (2.5 μg/ml), or laminin (5 μg/ml) was added to the lower compartments. Glycosidase-treated

NIH:OVCAR5 cells (10,000 cells/50 µl) were added to the upper chamber compartments. After a 5-hr incubation at 37°C, the filters were stained with Diff-Quik (Dade Behring, Newark, DE) and nonmigratory cells were removed from the tops of the filters. The number of migrating cells is expressed as the sum of cells counted in five fields at a 40x magnification.

Cell invasion assay. The ability of glycosidase-treated ovarian carcinoma cells to invade through Matrigel was assessed. Glycosidase-treated cells were washed, resuspended at 10^5 cells/100 µl in base medium containing 1% FBS, and were applied atop Transwells® (Corning Inc., Bloomington, MN) coated with 1 mg/ml Matrigel®. The bottom chambers were filled with 10 µg/ml fibronectin, collagen type IV, or laminin in base medium. After a 20-hr incubation at 37°C, the filters were stained with Diff-Quik and noninvasive cells were removed from the tops of the filters. The number of invading cells is expressed as the sum of cells counted in five fields at a 40x magnification.

Gene expression analysis of NIH:OVCAR5 cells. The gene expression of NIH:OVCAR5 cells was determined using protocols described in the Affymetrix GeneChip® Expression Analysis Manual. Briefly, total RNA was isolated from NIH:OVCAR5 cells using the RNeasy Total RNA Isolation kit (Qiagen Inc., Valencia, CA). Double-stranded cDNA was synthesized from 8 µg of total RNA using the Superscript Choice system (Gibco BRL, Gaithersburg, MD). First-strand cDNA synthesis was primed with a T7-(dT_{24}) oligonucleotide primer (Genset Corp., La Jolla). The cDNA was then extracted with phenol/chloroform and precipitated with ethanol. From 10 µg of cDNA, cRNA was synthesized and biotinylated using the BioArray™ HighYield™ RNA Transcript Labeling kit (Affymetrix). The resulting cRNA was purified according to the RNeasy

Mini kit protocol (Qiagen) and then fragmented in 40 mM Tris-Acetate, pH 8.1, 30 mM magnesium acetate, and 100 mM potassium acetate for 35 min at 94°C. The fragmented cRNA was applied to Affymetrix GeneChip® U_133 arrays representing more than 39,000 transcripts derived from approximately 33,000 well-substantiated human genes or EST sequences. The subsequent processing, scanning, and quality control of the fragmented cRNA were performed by the Biomedical Genomics Center, University of Minnesota, according to Affymetrix protocols. The data was analyzed using Microarray Suite, version 5.0 (Affymetrix), and GeneData Analyst, version 3.1 (GeneData AG, Basel, Switzerland). This experiment was performed in quadruplicate.

Gene expression analysis of human tissues. RNA was prepared and gene expression was determined at Gene Logic Inc. (Gaithersburg, MD) using Affymetrix GeneChip® U_95 arrays (Santa Clara, CA) containing approximately 12,000 known genes and 48,000 ESTs. Gene expression analysis utilized the Gene Logic Gene Express® Software System.

Statistical Analysis. Student's t-test was performed as a test of significance with the use of Microsoft Excel 1997 (Microsoft Co., Redmond, WA). P values of < 0.01 were considered to indicate statistically significant differences.

Results

Ovarian carcinoma cell adhesion to ECM components is altered by glycosidase treatment.

The effect of cell membrane glycosylation upon the ability of ovarian carcinoma cells to adhere to ECM proteins was measured in an *in vitro* adhesion assay (Fig. 1). Pretreatment with chondroitinase ABC inhibited cell adhesion to fibronectin, collagen type IV, and laminin. This suggests that proteoglycans that contain chondroitin sulfate residues may augment ovarian carcinoma cell adhesion to ECM proteins. Hyaluronidase pretreatment augmented cell adhesion to fibronectin and laminin, suggesting that the presence of cell-surface hyaluronan may inhibit cell adhesion to fibronectin and laminin, but not collagen type IV. Neuraminidase treatment had no effect on cell adhesion to ECM proteins, suggesting that sialic acid residues may not affect ovarian carcinoma cell adhesion to ECM proteins.

The ability of glycosidase-treated ovarian carcinoma cells to adhere to the glycosaminoglycans chondroitin sulfate A or hyaluronan was also determined (Fig. 2). Chondroitinase ABC pretreatment augmented cell adhesion to hyaluronan, which suggests that chondroitin sulfate proteoglycans may partially inhibit ovarian carcinoma cell adhesion to hyaluronan, which has been shown to coat mesothelial cells.[9] The other glycosidases had no effect on ovarian carcinoma adhesion to chondroitin sulfate A or hyaluronan.

To ensure that glycosidase treatment did not induce cell death, aliquots of each enzymatically treated cell population were stained with trypan blue following both enzymatic treatment and the completion of the assays. In all cases, the cells excluded trypan blue stain, indicating that alterations in cell function were not attributable to the induction of cell death.

Ovarian carcinoma cell adhesion to mesothelial cells is partially mediated by chondroitin sulfate moieties.

The role of cell membrane glycosylation on ovarian carcinoma cell adhesion to mesothelial cells was determined (Fig. 3). The adhesion of ovarian carcinoma cells was inhibited by chondroitinase ABC pretreatment, but not by pretreatment with hyaluronidase or neuraminidase. This suggests that chondroitin sulfate proteoglycans may facilitate ovarian carcinoma cell adhesion to mesothelial cells.

Ovarian carcinoma cell migration toward ECM proteins is altered by glycosidase treatment.

The role of cell membrane glycosylation on ovarian carcinoma cell migration toward fibronectin, collagen type IV, and laminin was determined (Fig. 4). Ovarian carcinoma cell migration toward all three ECM proteins was increased by pretreatment with chondroitinase ABC. This suggests that the presence of chondroitin sulfate proteoglycans on the surface of ovarian carcinoma cells may impede cell migration toward ECM proteins, possibly by increasing their adhesion to ECM molecules (Fig. 1 and Fig. 3). Neuraminidase pretreatment resulted in decreased cell migration toward fibronectin, but had no effect on cell migration toward collagen type IV and laminin. These results suggest that sialic acid-modified proteoglycans may specifically mediate cell migration toward fibronectin. Hyaluronidase pretreatment had no effect upon ovarian carcinoma cell migration toward ECM proteins.

Ovarian carcinoma cell invasion is altered by glycosidase treatment.

Ovarian carcinoma cells were treated with glycosidases before their addition to the invasion assays. Pretreatment with neuraminidase inhibited cell invasion through Matrigel toward fibronectin, collagen type IV, and laminin (Figure 5). This suggests that sialic acid-modified glycoproteins may mediate ovarian carcinoma cell invasion. Chondroitinase ABC and hyaluronidase treatment had no effect on cell invasion through Matrigel.

Many proteoglycans are differentially expressed in normal ovary cells and ovarian carcinoma cells.

The relative expression of proteoglycan gene transcripts in NIH:OVCAR5 cells are listed in Figure 6. Proteoglycan transcripts that were detected in high amounts in NIH:OVCAR5 cells included syndecan 4, decorin, perlecan, and bamacan. Also expressed, although in lower amounts, were transcripts of the proteoglycans CD44, glypican 1, syndecan 1, secretory granule proteoglycan (PG) 1, glypican 4, versican, and syndecan 2.

We also examined the gene expression of proteoglycan transcripts in relevant human samples: normal ovaries, primary ovarian carcinoma tumors, secondary ovarian carcinoma metastases found in the omentum, and normal omentum. Almost all of the proteoglycans detected in NIH:OVCAR5 cells were also expressed in both primary and secondary ovarian carcinoma tumor tissues (Table I), except for syndecan 2 and syndecan 4. Syndecan 2, which was detected a very low levels in NIH:OVCAR5 cells, was expressed also at very low levels in normal ovaries and omenta; however, syndecan 2 was not detected in primary ovarian carcinoma

or secondary omental metastatic tumor samples. Expression of the syndecan 4 transcript was detected at high levels by the Affymetrix U_133 gene chips used to screen NIH:OVCAR5 cells, but we were not able to quantitate the expression of syndecan 4 in the human tissues since this probes for this gene transcript were not present on the Affymetrix U_95 gene chips used to screen them.

The relative expression of some proteoglycan transcripts underwent significant alterations in normal ovarian tissue compared to primary ovarian tumors. Versican and neuroglycan C, which contain chondroitin sulfate modifications, and the heparan sulfate proteoglycan syndecan 1 and biglycan were significantly up-regulated in primary ovarian tumors, compared to normal ovaries (Table I). The expression of glypican 3 decreased 4.2-fold and lumican expression decreased 2.7-fold. Although syndecan 2 transcript expression was absent from both primary ovarian carcinoma tumors and secondary omental metastases, it was detected in both normal ovaries and normal omenta, suggesting that the transformation of ovarian epithelial cells may result in termination of the expression of syndecan 2 gene products. The expression of all other proteoglycan transcripts listed in Table I were altered by 2-fold or less, as indicated by NC for "no change".

Alterations of the relative expression of proteoglycan transcripts in normal omenta and omental metastases were also observed. Significant increases in the expression of syndecan 1, biglycan, versican, and neuroglycan C were observed in secondary omental tumors, compared to normal omentum tissues. In constrast, the expression of glypican 3 and secretory granule PG1 was significantly lower in the secondary omental metastases compared to the normal omenta (Table I). As in normal ovaries and primary ovarian carcinoma tumors, the expression of syndecan 2 was low in normal omentum, but completely absent from secondary omental

metastases. The alterations in gene expression of these proteoglycans may reflect the ECM rearrangement frequently observed in tumor cells. They may also indicate responses to tumor cells or may identify effectors of ovarian carcinoma metastatic behavior.

Discussion

In this study, we attempted to elucidate the role of cell membrane glycosylation in cellular functions that mediate ovarian carcinoma secondary tumor growth. The effects of glycosidase treatment upon the functional abilities of NIH:OVCAR5 cells to adhere to ECM components and mesothelial cell monolayers, migrate toward ECM proteins, and invade through Matrigel are summarized in Table II. In short, glycosidase treatment alters ovarian carcinoma cell adhesion, migration, and invasion. This suggests that proteoglycans, or to be more precise carbohydrate modifications of proteoglycans, may contribute to the activation or suppression of these metastatic processes. Different carbohydrate moieties may mediate different cellular functions in ovarian carcinoma cells. Several proteoglycans and their glycosyl modifications may contribute to or inhibit the formation of secondary tumor growths in ovarian carcinoma.

Many studies specifically describe roles for the proteoglycan CD44, and its ligand hyaluronan, in ovarian carcinoma cell adhesion and migration. Cell-cell adhesion between ovarian carcinoma cells and mesothelial cells are mediated by CD44-hyaluronan interactions.[5, 9] The removal of cell membrane-associated carbohydrate residues resulted in altered cell adhesion to hyaluronan in some ovarian carcinoma cell lines.[11] CD44-hyaluronan interactions have been shown to mediate ovarian carcinoma cell migration via signal transduction through c-src kinase, Ras, and Rac 1.[22, 23] Disruptions of the CD44-hyaluronan interactions altered the ability of ovarian carcinoma cells to migrate toward ECM proteins.[6] For these reasons, we considered the proteoglycan CD44 a likely candidate as a carbohydrate-mediated modifier of cell functions. However, in the NIH:OVCAR5 cell line, CD44 was not extensively modified with sialic acid or chondroitin sulfate groups, as shown by Western blot analysis. This suggests that other

proteoglycans present in the NIH:OVCAR5 cells' ECM may be responsible for the altered cellular functions that we described here.

Proteoglycans are mediators of cell function in both normal and cancer cells. In normal cells, the chondroitin sulfate proteoglycan versican enhances cell proliferation, at least in part through binding to the EGF receptor.[24] Versican also inhibits cell adhesion in astrocytoma cells.[25] The chondroitin sulfate proteoglycan decorin can inhibit growth in ovarian carcinoma cells[16] and syndecans, a family of heparan sulfate proteoglycans, mediate cell adhesion[26] and invasion[12] in myeloma cells. Syndecans also bind and modulate activity of fibroblast growth factor[27, 28] and promote oligomerization of bound ligands, which enhances activation of primary signaling receptors.[29] Overexpression of the chondroitin sulfate proteoglycan bamacan resulted in the transformation of normal mouse fibroblasts.[30] Ovarian carcinoma cells synthesize both chondroitin sulfate and heparan sulfate proteoglycans that mediate cell adhesion to fibronectin, collagen type I, and collagen type III.[13] Here we report that cell surface proteoglycans with chondroitin sulfate or sialic acid residues mediate the adhesion, migration, and invasion of ovarian carcinoma cells.

In particular, the loss of chondroitin sulfate residues resulted in decreased cell adhesion to the ECM proteins fibronectin, collagen type IV, and laminin and to mesothelial cell monolayers. Coupled with our observation that the removal of chondroitin sulfate residues resulted in increased cell migration, our results suggest that chondroitin sulfate proteoglycans promote ovarian carcinoma cell adhesion toward mesothelial cells and their associated ECM proteins. This is consistent with reports that the melanoma chondroitin sulfate proteoglycan modulates the adhesive abilities of integrin $\alpha_4\beta_1$[31] and matrix metalloproteinase-dependent invasion into collagen type I in melanoma cell lines.[32] Ovarian carcinoma cell adhesion to hyaluronan

increased after the digestion of chondroitin sulfate residues. This suggests that some chondroitin sulfate proteoglycans may act as negative effectors of cell adhesion. We observed gene expression of versican, which contains chondroitin sulfate residues and a hyaluronan-binding domain,[14] in the NIH:OVCAR5 cell line. Taken together, these results suggest that ovarian carcinoma cell adhesion may be inhibited by versican- hyaluronan interactions. We also report that versican expression is significantly up-regulated in primary and secondary ovarian carcinoma tumors, which suggests that ovarian carcinoma cell interactions with mesothelial cell hyaluronan may mediate secondary tumor growth. Further studies are required to determine the contributions of individual chondroitin sulfate proteoglycans that result in their net effect upon ovarian carcinoma cell adhesion and migration.

The removal of sialic acid residues from the surface of NIH:OVCAR5 cells resulted in decreased cell migration toward fibronectin and decreased invasion through Matrigel. Taken together, these results suggest that proteoglycans with sialic acid residues may promote a more invasive phenotype in ovarian carcinoma.

The removal of hyaluronan resulted in increased adhesion to ECM proteins and mesothelial cell monolayers, but did not affect cell migration or invasion. We have previously shown that the NIH:OVCAR5 cells have a hyaluronan-rich pericellular matrix that can be cleared by hyaluronidase treatment.[5] The clearance of hyaluronan from these tumor cells may unmask the integrins that are present on the cells' surfaces,[6] thus facilitating the increased adhesion to ECM proteins and mesothelial cell monolayers that we observed. However, bovine testicular hyaluronidase can also cleave chondroitin sulfate residues. Our data suggests that the net increased cell adhesion that resulted from hyaluronan digestion was greater than the decreased cell adhesion that may have resulted from the concurrent removal of chondroitin

sulfate residues, thus indicating that few chondroitin sulfate residues were cleaved during treatment with hyaluronidase.

To identify proteoglycans potentially responsible for the altered cellular functions that were reported here, gene expression analysis of the NIH:OVCAR5 cell line was performed. The expression of several proteoglycan transcripts, including syndecans, glypicans, decorin, perlecan, and bamacan was detected. We also screened patient samples for the expression of proteoglycan genes in primary ovarian carcinoma tumors and secondary omental metastases, a common site of metastasis in ovarian carcinoma. These values were compared to those of samples obtained from normal ovary and omental tissues. Except for syndecan 4, whose expression was not measured in the Affymetrix gene chips used to screen the human tissues, and syndecan 2, all of the proteoglycan transcripts detected in the NIH:OVCAR5 cell line were detected in primary ovarian carcinoma cell lines. These data suggest that this cell line expresses proteoglycan transcripts in a fashion similar to that of primary ovarian carcinoma tumors. Syndecan 2 gene expression was absent from normal ovaries and omenta, but was expressed in both primary and secondary ovarian carcinoma tumors.

In addition to their detection in NIH:OVCAR5 cells, versican, syndecan 1, and biglycan, gene expression values increased more than 2-fold in primary and secondary ovarian tumors compared to normal ovarian and omental tissues. These alterations in gene expression may indicate roles for these proteoglycans in ovarian carcinoma metastasis. In human ovarian tumors, we also observed significant decreases in the gene expression of glypican 3 and lumican, compared to normal ovaries. Glypican 3 expression was also significantly down-regulated in secondary omental metastases, suggesting that its loss may be a general feature of ovarian carcinoma. Interestingly, decreased lumican expression was noted only in primary ovarian

carcinoma tumors, but not in secondary metastases. The loss of lumican expression in primary ovarian carcinoma tumors may reflect early-stage events in the development of the disease, rather than events associated with secondary tumor growth.

The gene expression of CD44 was unchanged in primary ovarian tumors, compared to normal ovaries, but glycosyl residues of CD44 have been implicated in tumor cell adhesion.[11] CD44 from both NIH:OVCAR5 cells incubated in base medium alone or glycosidase-digested cells was immunoprecipitated and subjected to Western blotting. In all cases, CD44 exhibited a relative mobility of approximately 90 kDa, which is consistent with the standard isoform of CD44 (not shown). The failure of all three glycosidase treatments to alter the relative mobility of CD44 suggests that the CD44 present on NIH:OVCAR5 cells was not extensively glycosylated with carbohydrate residues sensitive to these enzymes. This does not, however, preclude the possibility that CD44 on the surface of NIH:OVCAR5 cells may contain small amounts of sialic acid or chondroitin sulfate groups, below the detection limits of this assay.

We observed no significant change in the gene expression of other proteoglycans in ovarian carcinoma tumors compared to normal ovaries. These findings contradict another study that reported significantly decreased gene expression of decorin in ovarian carcinoma tumors, compared to the pooled brushings of ovary epithelial cells from patients without cancer.[33] However, alterations of gene expression observed in several proteoglycan transcripts suggest that the modulation of ovarian carcinoma metastasis is a complex phenomenon mediated by several proteoglycans. Here, we identify several proteoglycans that may be involved in secondary tumor growth. They may reflect alterations in tumor cell ECM or may mediate the formation of secondary tumor growths in ovarian carcinoma. Further study is required to determine whether

alterations of the proteins encoded by these transcripts are also altered in ovarian carcinoma tumors and cell lines.

Many of the cellular functions attributed to proteoglycans are due to post-translational modifications. Both syndecans and glypicans bind fibroblast growth factor via their heparan sulfate moieties.[34, 35] The ability of glypicans to target apical surfaces is partially dependent upon the extent of their glycosylation.[36] In healing wounds and several carcinomas, antigenic epitopes of decorin were masked by the addition of chondroitin sulfate chains.[37] Further studies are required to elucidate the roles of carbohydrate moieties in the cellular functions of proteoglycans.

In this study, we report that cell membrane glycosylation mediates cellular functions associated with ovarian carcinoma secondary tumor growth. Glycosidase treatment altered the functional abilities of NIH:OVCAR5 cells to adhere to ECM components and mesothelial cell monolayers, migrate toward ECM proteins, and invade through Matrigel. This suggests that the carbohydrate residues of several proteoglycans contribute to the activation or suppression of cell adhesion, migration, and invasion in ovarian carcinoma cells. Further study is required to identify the roles of individual proteoglycans that may participate in the formation of secondary tumor growths in ovarian carcinoma.

Acknowledgements

We thank the staff of Gene Logic Inc, Gaithersburg, MD, for performing the gene expression experiments with the human tissue samples, the staff of the Biomedical Genomics Center, University of Minnesota, for performing gene expression experiments on NIH:OVCAR5 cells, and the staff of the University of Minnesota Tissue Procurement Facility for assistance in collecting and processing the human tissue samples. We thank Dr. James McCarthy for providing fibronectin, Dr. Leo Furcht for providing laminin and the monoclonal antibody P5D2 against the β1 integrin subunit, and Drs. Thomas Hamilton and Judah Folkman for providing the NIH:OVCAR5 cell line.

References

1. Knox P, Wells P. Cell adhesion and proteoglycans I. The effect of exogenous proteoglycans on the attachment of chick embryo fibroblasts to tissue culture plastic and collagen. J Cell Sci 1979; 40:77-88.
2. Baciu PC, Goetinck PF. Protein kinase C regulates the recruitment of syndecan-4 into focal contacts. Mol Biol Cell 1995; 6:1503-1513.
3. Dhodapkar MV, Abe E, Theus A et al. Syndecan-1 is a multifunctional regulator of myeloma pathobiology: control of tumor cell survival, growth, and bone cell differentiation. Blood 1998; 91:2679-2688.
4. Cannistra SA, Abu-Jawdeh G, Niloff J et al. CD44 variant expression is a common feature of epithelial ovarian cancer: lack of association with standard prognostic factors. J Clin Oncol 1995; 13:1912-21.
5. Lessan K, Aguiar DJ, Oegema T et al. CD44 and β1 integrin mediate ovarian carcinoma cell adhesion to peritoneal mesothelial cells. Am J Pathol 1999; 154:1525-1537.
6. Casey RC, Skubitz APN. CD44 and β1 integrins mediate ovarian carcinoma cell migration toward extracellular matrix proteins. Clin Exp Metastasis 2000; 18:67-75.
7. Aruffo A, Stamenkovic I, Melnick M, Underhill CB. CD44 is the principal cell surface receptor for hyaluronate. Cell 1990; 61:1303-1313.
8. Jalkanen S, Jalkanen M. Lymphocyte CD44 binds the COOH-terminal heparin-binding domain of fibronectin. J Cell Biol 1992; 116:817-825.

9. Gardner MJ, Catterall, JB, Jones LM, Turner GA. Human ovarian tumour cells can bind hyaluronic acid via membrane CD44: a possible step in peritoneal metastasis. Clin Exp Metastasis 1996; 14:325-334.

10. Strobel T, Swanson L, Cannistra SA. In vivo inhibition of CD44 limits intra-abdominal spread of a human ovarian cancer xenograft in nude mice: a novel role for CD44 in the process of peritoneal implantation. Cancer Res 1997; 57:1228-1232.

11. Catterall JB, Jones LMH, Turner GA. Membrane glycosylation and CD44 content in the adhesion of human ovarian cancer cells to hyaluronan. Clin Exp Metastasis 1999; 17:583-591.

12. Liebersbach BF, Sanderson RD. Expression of syndecan-1 inhibits cell invasion into type I collagen. J Biol Chem 1994; 269:20013-20019.

13. Kokenyesi R. Ovarian carcinoma cells synthesize both chondroitin sulfate and heparan sulfate cell surface proteoglycans that mediate cell adhesion to interstitial matrix. J Cell Biochem 2001; 83:259-270.

14. LeBaron RG, Zimmermann DR, Ruoslahti E. Hyaluronate binding properties of versican. J Biol Chem 1992; 267:10003-10010.

15. Touab M, Villena J, Barranco C et al. Versican is differentially expressed in human melanoma and may play a role in tumor development. Am J Pathol 2002; 160:549-557.

16. Nash MA, Loercher AE, Freedman RS. *In vitro* growth inhibition of ovarian cancer cells by decorin: synergism of action between decorin and carboplatin. Cancer Res 1999; 59:6192-6196.

17. Molpus KL, Koelliker D, Atkins L et al. Characterization of a xenograft model of human ovarian carcinoma which produces intraperitoneal carcinomatosis and metastases in mice. Int J Cancer 1996; 68:588-595.

18. Hamilton TC, Young RC, Ozols RF. Experimental model systems of ovarian cancer: applications to the design and evaluation of new treatment approaches. Semin Oncol 1984; 11:285-298.

19. McCarthy JB, Skubitz APN, Palm SL, Furcht LT. Metastasis inhibition of different tumor types by purified laminin fragments and a heparin-binding fragment of fibronectin. J Natl Cancer Inst 1988; 80:108-116.

20. Smith DE, Mosher DF, Johnson RB, Furcht LT. Immunological identification of two sulfhydryl-containing fragments of human plasma fibronectin. J Biol Chem 1982; 257:5831-5838.

21. Pattaramalai S, Skubitz KM, Skubitz APN. A novel recognition site on laminin for $\alpha 3\beta 1$ integrin. Exp Cell Res 1996; 222:281-290.

22. Bourguignon LYW, Zhu H, Shao L, Chen Y. CD44 interactions with c-Src kinase promotes cortactin-mediated cytoskeleton function and hyaluronic acid-dependent ovarian tumor cell migration. J Biol Chem 2001; 276:7327-7336.

23. Bourguignon LYW, Zhu H, Zhou B et al. Hyaluronan promotes CD44v3-Vav2 interaction with Grb2-p185HER2 and induces Rac1 and Ras signaling during ovarian tumor cell migration and growth. J Biol Chem 2001; 276:48679-48692.

24. Yang BL, Zhang Y, Cao L, Yang BB. Cell adhesion and proliferation mediated through the G1 domain of versican. J Cell Biochem 1999; 72:210-220.

25. Ang LC, Zhang Y, Cao L et al. Versican enhances locomotion of astrocytoma cells and reduces cell adhesion through its G1 domain. J Neuropathol Exp Neurol 1999; 58:597-605.

26. Ridley RC, Xiao H, Hata H et al. Expression of syndecan regulates human myeloma plasma cell adhesion to type I collagen. Blood 1993; 8:767-774.

27. Feyzi E, Saldeen T, Larsson E et al. Age-dependent modulation of heparan sulfate structure and function. J Biol Chem 1998; 273:13395-13398.

28. Asundi VK. Carey DJ. Self-association of N-syndecan (syndecan-3) core protein is mediated by a novel structural motif in the transmembrane domain and ectodomain flanking region. J Biol Chem. 1995; 270:26404-26410.

29. Johnson GR. Wong L. Heparan sulfate is essential to amphiregulin-induced mitogenic signaling by the epidermal growth factor receptor. J Biol Chem 1994; 269:27149-27154.

30. Ghiselli G, Iozzo RV. Overexpression of bamacan/SMC3 causes transformation. J Biol Chem 2000; 275:20235-20238.

31. Iida J, Pei D, Kang T et al. Melanoma chondroitin sulfate proteoglycan regulates matrix metalloproteinase-dependent human melanoma invasion into type I collagen. J Biol Chem 2001; 276:18786-18794.

32. Iida J, Meijne AML, Oegema TR et al. A role of chondroitin sulfate proteoglycosaminoglycan binding site in $\alpha 4\beta 1$ integrin-mediated melanoma cell adhesion. J Biol Chem 1998; 273:5955-5962.

33. Shridhar V, Sen A, Chien J et al. Identification of underexpressed genes in early- and late-stage primary ovarian tumors by suppression subtraction hybridization. Cancer Res 2002; 62:262-270.

34. Zhou FY, Owens R, Hermonen J et al. Sensitivity of cells for FGF-1 and FGF-2 is regulated by cell surface heparan sulfate proteoglycans. Eur J Cell Biol 1997; 73:166-174.

35. Aviezer D, Levy E, Safran M et al. Differential structural requirements of heparin and heparan sulfate proteoglycans that promote binding of basic fibroblast growth factor to its receptor. J Biol Chem 1994; 269:114-121.

36. Mertens G, Van der Schueren B, Van den Berghe H, David G. Heparan sulfate expression in polarized epithelial cells: The apical sorting of glypican (GPI – anchored proteoglycan) is inversely related to its heparan sulfate content. J Cell Biol 1996; 132:487-497.

37. Yeo TK, Brown L, Dvorak HF. Alterations in proteoglycan synthesis common to healing wounds and tumors. Am J Pathol 1991; 138:1437-1450.

Figure Legends

Figure 1. Ovarian carcinoma cell adhesion to ECM proteins is altered by glycosidase treatment. Untreated ovarian carcinoma cells (open bars) were incubated with glycosidases (solid bars) before their addition to the adhesion assays. Pretreatment with chondroitinase ABC inhibited cell adhesion to fibronectin, collagen type IV, and laminin, while hyaluronidase pretreatment augmented cell adhesion to fibronectin and laminin. Neuraminidase treatment had no effect on cell adhesion to ECM proteins. * $P < 0.001$ and ‡ $P < 0.01$.

Figure 2. Ovarian carcinoma cell adhesion to hyaluronan is augmented by removal of chondroitin sulfate chains. Untreated ovarian carcinoma cells (open bars) were incubated with glycosidases (solid bars) before their addition to the adhesion assay. Chondroitinase ABC pretreatment augmented cell adhesion to hyaluronan. ‡ $P < 0.01$.

Figure 3. Ovarian carcinoma cell adhesion to mesothelial cells is inhibited by the removal of chondroitin sulfate chains. Ovarian carcinoma cells were untreated (open bar) or treated with chondroitinase ABC (dotted bar), hyaluronidase (striped bar), or neuraminidase (solid bar) before their addition to the adhesion assays. Adhesion of ovarian carcinoma cells was inhibited by chondroitinase ABC pretreatment, but not by pretreatment with hyaluronidase or neuraminidase. ‡ $P < 0.01$ compared to untreated controls.

Figure 4. Ovarian carcinoma cell migration toward ECM proteins is altered by glycosidase treatment. Ovarian carcinoma cells were treated with chondroitinase ABC, neuraminidase, or

hyaluronidase, then allowed to migrate toward ovalbumin (circles), fibronectin (triangles), collagen type IV (diamonds), or laminin (squares). Ovarian carcinoma cell migration toward fibronectin was increased by pretreatment with chondroitinase ABC and was inhibited by pretreatment with neuraminidase. Chondroitinase ABC pretreatment resulted in increased cell migration toward collagen type IV and laminin. * $P < 0.001$, ‡ $P < 0.01$, and § $P < 0.05$.

Figure 5. Ovarian carcinoma cell invasion through Matrigel is altered by glycosidase treatment. Ovarian carcinoma cells were untreated (open bar) or treated with chondroitinase ABC (dotted bar), hyaluronidase (striped bar), or neuraminidase (solid bar) before their addition to the invasion assays. Pretreatment with neuraminidase inhibited cell invasion through Matrigel toward fibronectin, collagen type IV, and laminin. Chondroitinase ABC and hyaluronidase treatment had no effect on cell invasion through Matrigel. ‡ $P < 0.01$, and § $P < 0.05$.

Figure 6. Gene expression of proteoglycans in ovarian carcinoma cells. Mean intensity values of proteoglycan transcripts that were present in NIH:OVCAR5 cells. For each transcript, the intensity values are expressed as the mean and standard deviation of quadruplicate samples, each performed in duplicate.

Table I. Many proteoglycan genes are differentially expressed in ovarian carcinoma.

Gene expressed	Ovarian carcinoma tumor vs. normal ovary Mean Fold Change	Secondary omental metastases vs. normal omenta Mean Fold Change
versican	4.9 ↑	2.7 ↑
syndecan 1	2.6 ↑	4.4 ↑
biglycan	2.3 ↑	4.4 ↑
neuroglycan C	2.1 ↑	1.7 ↑
glypican 4	NC	NC
CD44	NC	2.1 ↓
perlecan	NC	1.9 ↓
decorin	NC	NC
glypican 3	4.2 ↓	6.4 ↓
lumican	2.7 ↓	NC
bamacan	NC	NC
glypican 1	NC	NC
secretory granule PG1	NC	2.2 ↓
syndecan 2	*	*

The mean fold change ratio differences between tumor and normal samples are listed in Table I. Unchanged tumor:normal mean fold changes are denoted as NC. *Because syndecan 2 gene expression was not detected in ovarian carcinoma tumors or omental metastases, the tumor:normal mean fold change could not be computed.

Table II. Effects of glycosidase treatment on ovarian carcinoma cell metastasis.

	Enzyme treatment	Fibronectin	Collagen type IV	Laminin	Hyaluronan	Mesothelial monolayer
Adhesion	Chondroitinase ABC	↓↓↓	↓↓↓	↓	↑	↓
	Hyaluronidase	↑	--	↑↑↑	--	--
	Neuraminidase	--	--	--	--	--
Migration	Chondroitinase ABC	↑↑↑	↑	↑↑		
	Hyaluronidase	--	--	--		
	Neuraminidase	↓↓	--	--		
Invasion	Chondroitinase ABC	--	--	--		
	Hyaluronidase	--	--	--		
	Neuraminidase	↓↓	↓↓↓	↓↓↓		

This table summarizes the changes observed in NIH:OVCAR5 cell adhesion, migration, and invasion toward fibronectin, collagen type IV, laminin, hyaluronan, and mesothelial cell monolayers after glycosidase treatment. Increased cellular function is denoted by upward arrows (↑) and decreased cellular function is denoted by downward arrows (↓). The arrows denote significant alterations in cellular function caused by pretreatment with the indicated glycosidases: one arrow ($P < 0.05$), two arrows ($P < 0.01$), three arrows ($P < 0.001$), and – (no effect).

Figure 1

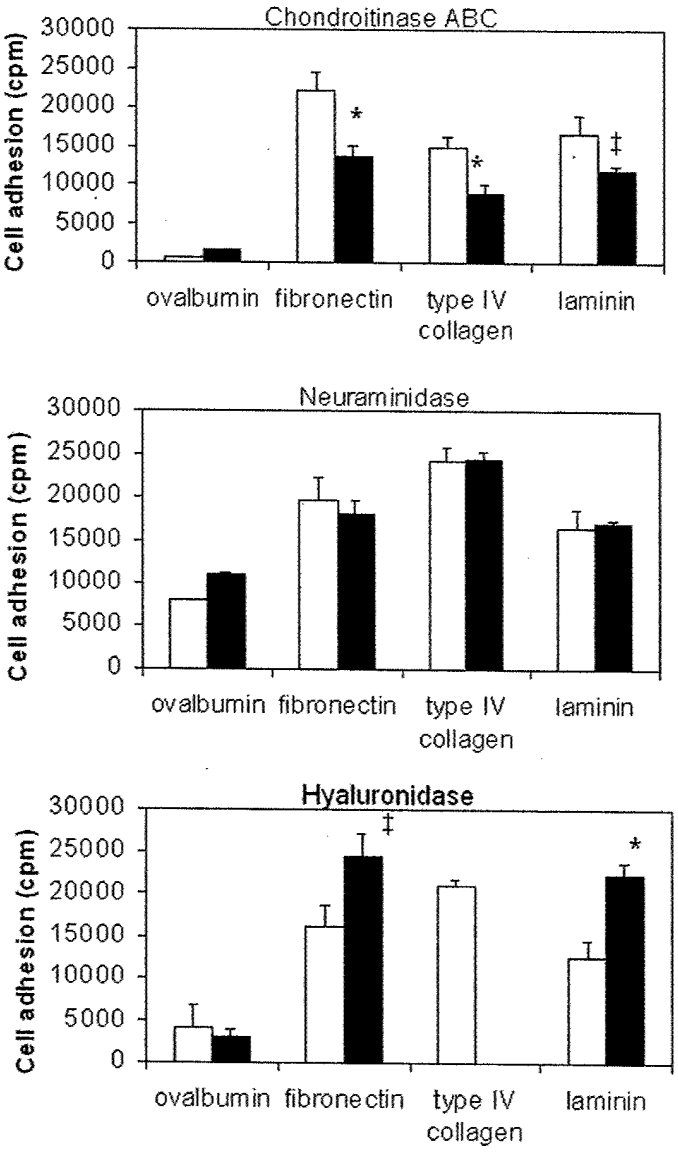
Chondroitinase ABC
Cell adhesion (cpm)
30000
25000
20000
15000
10000
5000
0
*
*
‡
ovalbumin
fibronectin
type IV collagen
laminin
Neuraminidase
Cell adhesion (cpm)
30000
25000
20000
15000
10000
5000
0
ovalbumin
fibronectin
type IV collagen
laminin
Hyaluronidase
Cell adhesion (cpm)
30000
25000
20000
15000
10000
5000
0
‡
*
ovalbumin
fibronectin
type IV collagen
laminin

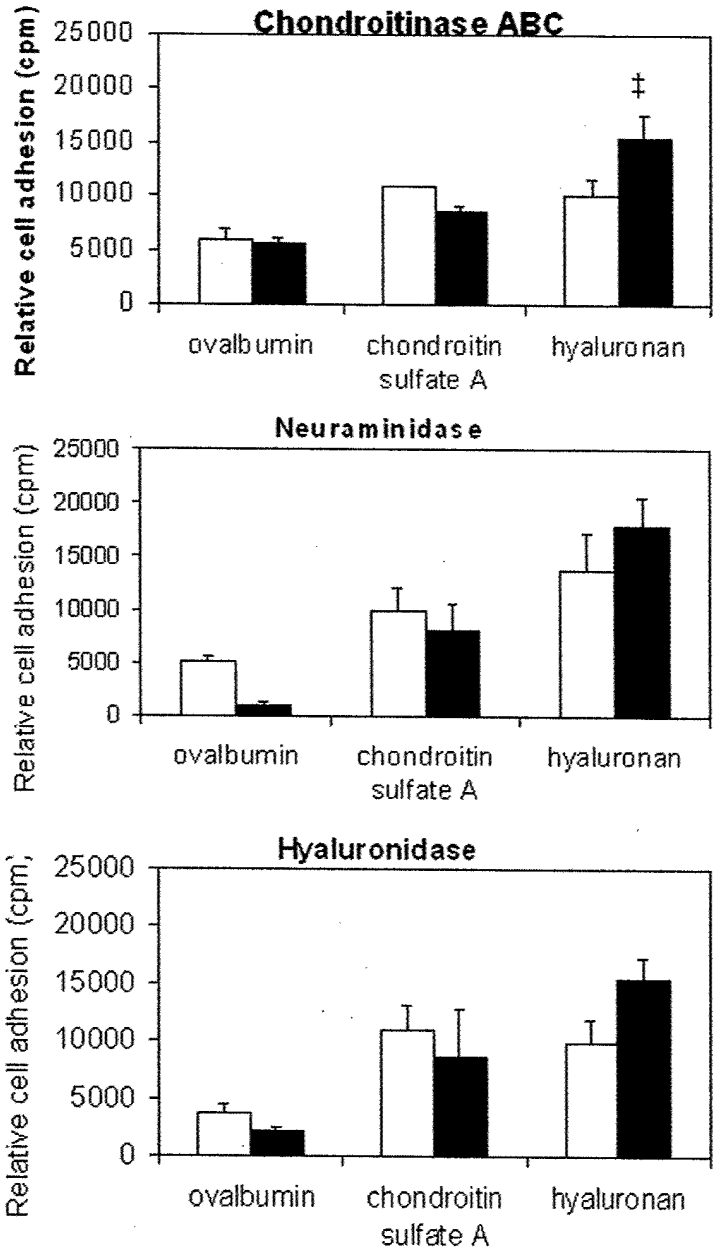
Chondroitinase ABC
Relative cell adhesion (cpm)
25000
20000
15000
10000
5000
0
‡
ovalbumin
chondroitin sulfate A
hyaluronan
Neuraminidase
Relative cell adhesion (cpm)
25000
20000
15000
10000
5000
0
ovalbumin
chondroitin sulfate A
hyaluronan
Hyaluronidase
Relative cell adhesion (cpm)
25000
20000
15000
10000
5000
0
ovalbumin
chondroitin sulfate A
hyaluronan

Figure 3

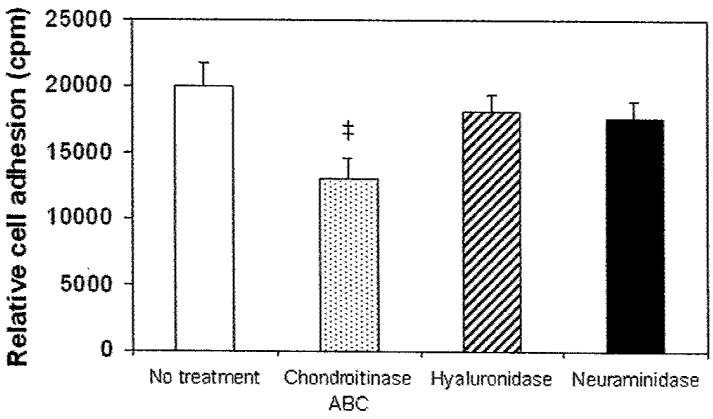
Relative cell adhesion (cpm)
25000
20000
15000
10000
5000
0
‡
No treatment
Chondroitinase ABC
Hyaluronidase
Neuraminidase

Figure 4

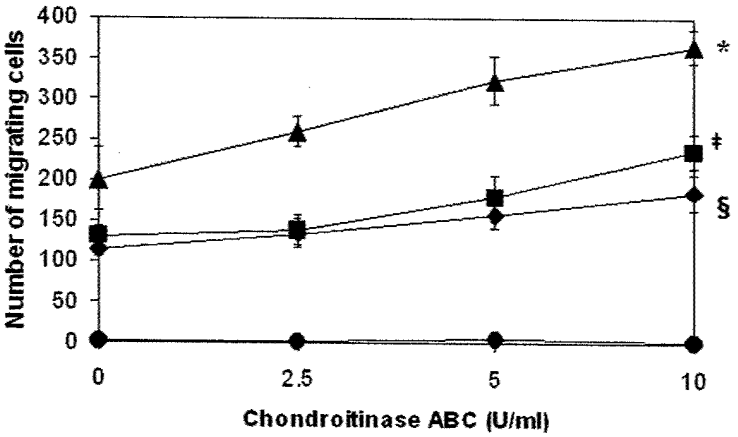
Number of migrating cells
400
350
300
250
200
150
100
50
0
0
2.5
5
10
Chondroitinase ABC (U/ml)
*
‡
§

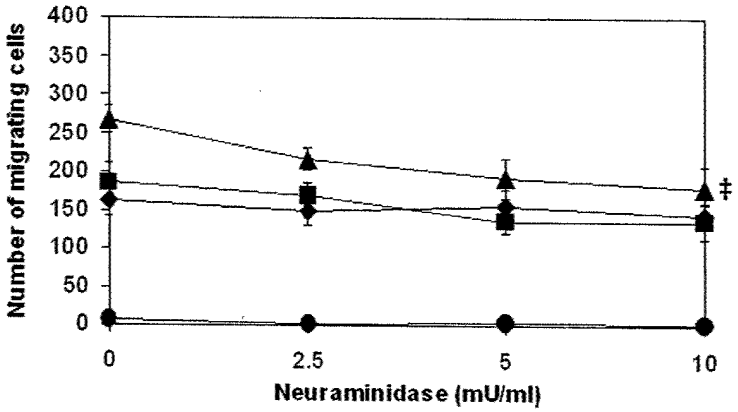
Number of migrating cells
400
350
300
250
200
150
100
50
0
0
2.5
5
10
Neuraminidase (mU/ml)
‡

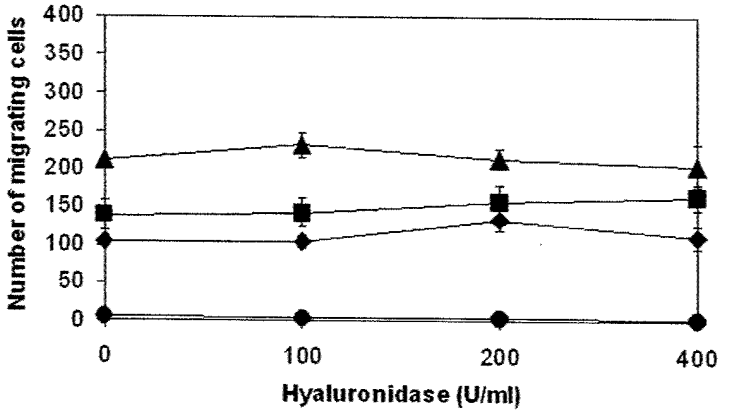
Number of migrating cells
400
350
300
250
200
150
100
50
0
0
100
200
400
Hyaluronidase (U/ml)

Figure 5

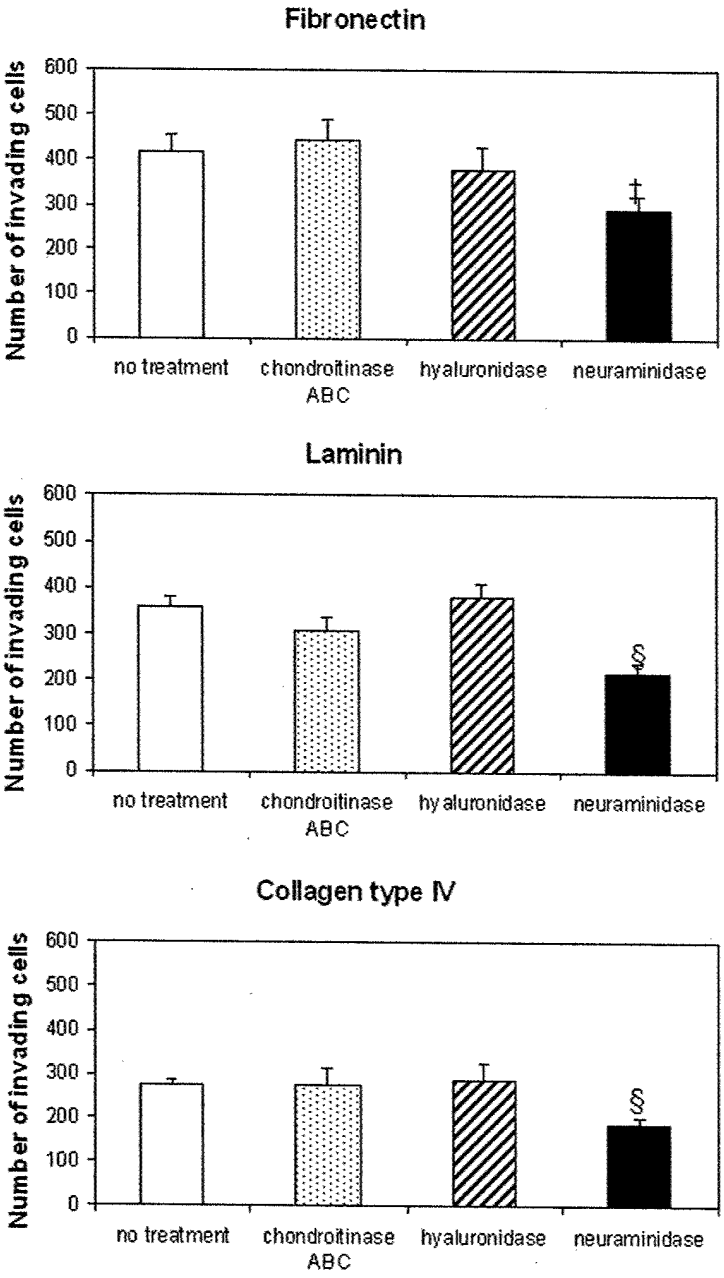
Fibronectin
Number of invading cells
600
500
400
300
200
100
0
‡
no treatment
chondroitinase ABC
hyaluronidase
neuraminidase
Laminin
Number of invading cells
600
500
400
300
200
100
0
§
no treatment
chondroitinase ABC
hyaluronidase
neuraminidase
Collagen type IV
Number of invading cells
600
500
400
300
200
100
0
§
no treatment
chondroitinase ABC
hyaluronidase
neuraminidase

Figure 6

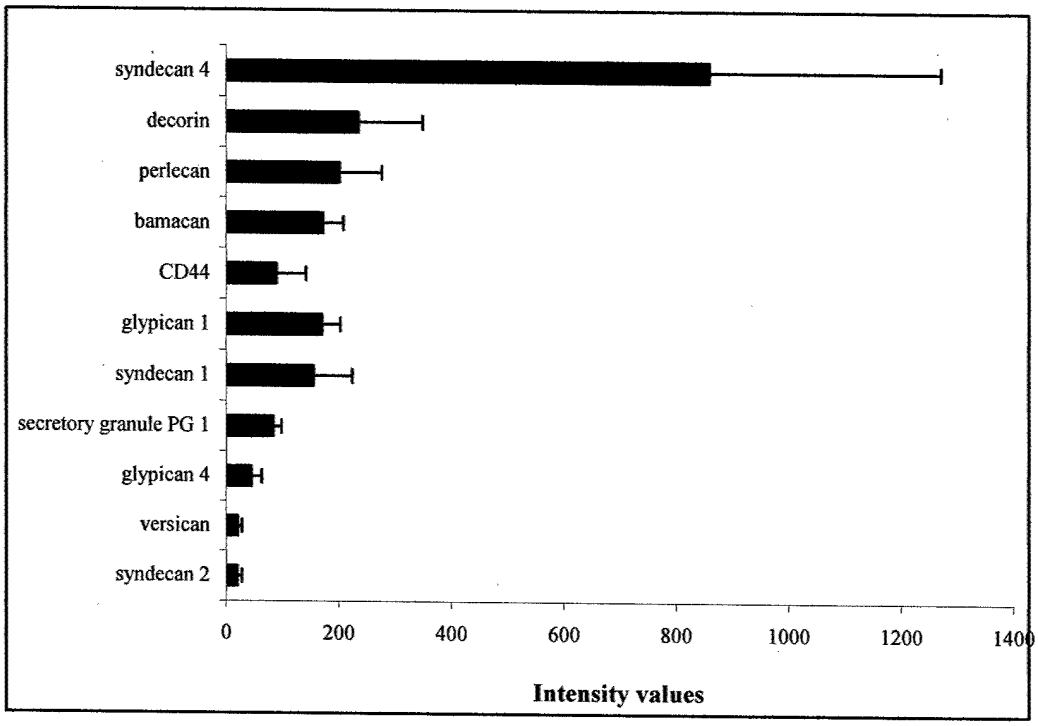
syndecan 4
decorin
perlecan
bamacan
CD44
glypican 1
syndecan 1
secretory granule PG 1
glypican 4
versican
syndecan 2
0
200
400
600
800
1000
1200
1400
Intensity values

Appendix #2
Amy P.N. Skubitz

Establishment of an *in vitro* assay to measure the invasion of ovarian carcinoma cells through mesothelial cell monolayers.

Rachael C. Casey*, Kim Koch,* Theodore R. Oegema Jr.‡, Keith M. Skubitz†, Stefan E. Pambuccian*, Suzanne M. Grindle§, and Amy P.N. Skubitz*

Departments of *Laboratory Medicine and Pathology, ‡Orthopaedic Surgery, and †Medicine, and the §Tissue Procurement Facility, University of Minnesota, Minneapolis, MN 55455, USA

Number of Text Pages: 29; Number of Figures: 5

Running Title: *In vitro* ovarian carcinoma cell invasion assay

Sources of Support: Supported by grants from the National Institute of Health/National Cancer Institute (CA0913825), Department of the Army (DA/DAMD17-99-1-9564), Minnesota Medical Foundation (SMF-2078-99), and Graduate School Grant-in-Aid of Research (#18118).

Correspondence and Reprint Requests to: Dr. Amy P.N. Skubitz, Department of Laboratory Medicine and Pathology, University of Minnesota, MMC 609, 420 Delaware St. S.E., Minneapolis, MN 55455, USA. Tel: 612-625-5920; Fax: 612-625-1121, email: skubi002@umn.edu

Keywords: Cell invasion, integrins, mesothelial cells, ovarian carcinoma

Abbreviations: ADAM: a disintegrin and metalloprotease; ADAMTS: a disintegrin and metalloprotease with thrombospondin type I repeat; ECM: extracellular matrix; EHS: Engelbreth-Holm-Swarm; FBS: fetal bovine serum; IgG: immunoglobulin; mAb: monoclonal antibody; MMP: matrix metalloproteinase; PBS: phosphate buffered saline; TIMP: tissue inhibitor of metalloproteinase

Abstract

Ovarian carcinoma is the leading cause of gynecological cancer deaths in the United States. Secondary tumor growths form by tumor cell invasion through the mesothelial lining of the peritoneal cavity and peritoneal organs. To study this interaction, we developed an *in vitro* cell-based model system in which mesothelial cells were cultured as monolayers and fixed, and then ovarian carcinoma cells were added. The cultures were stained with trypan blue dye, which enabled the visualization of ovarian carcinoma cell invasion through fixed monolayers of mesothelial cells. Ovarian carcinoma cell invasion was inhibited for up to 7 days by the addition of RGD peptides or a blocking monoclonal antibody against the β1 integrin subunit. Cell invasion was also inhibited by GM6001, a chemical inhibitor of matrix metalloproteinases. Differential gene expression of matrix metalloproteinases, tissue inhibitors of matrix metalloproteinases, and disintegrins were observed in primary ovarian carcinoma tumors and secondary metastases, compared to normal ovaries. Taken together, these results suggest that complex interactions between integrins, disintegrins, matrix metalloproteinases, and tissue inhibitors of matrix metalloproteinases may mediate ovarian carcinoma cell invasion, and that the novel assay described here is a suitable tool for its study.

Introduction

Ovarian cancer is the leading cause of gynecologic malignancy and the fifth leading cause of cancer death among women in the United States[1]. In ovarian carcinoma, cancer cells detach from the surface of the tumor into the peritoneal cavity. Subsequent peritoneal implants are characterized by the invasion of the tumor cells through the mesothelial cells that line the peritoneum and underlying organs. However, the mechanisms that contribute to ovarian carcinoma invasion are not well understood.

Currently, cancer cell invasion is studied with Matrigel invasion assays[2]. Matrigel is comprised of extracellular matrix (ECM) extracted from mouse Engelbreth-Holm-Swarm (EHS) sarcoma cells, and is believed to mimic the basement membrane through which tumor cells invade[3]. Several factors make this procedure a less than ideal method to study ovarian carcinoma cell invasion. Matrigel is murine in origin, not human. It is made by tumor cells, which synthesize and organize their ECMs differently than normal cells. Most importantly, the Matrigel invasion assay measures only cell-ECM interactions, and can not be used to examine cell-cell interactions between the tumor cells and target cells. Finally, Matrigel is synthesized by sarcoma cells, which are not typical targets of ovarian carcinoma metastasis. The Matrigel invasion assay provides only an approximation of the *in vivo* conditions found at sites of metastasis.

Ovarian carcinoma metastasis is mediated by interactions between ovarian cancer cells and ECM components of the mesothelial cells at sites of secondary tumor growth. It has previously been shown that ovarian carcinoma cell adhesion and migration are mediated by interactions between β1 integrins and fibronectin, collagens, and laminin,[4, 5] and interactions between CD44 and hyaluronan.[6, 7] Pretreatment of lung adenocarcinoma cells with blocking

monoclonal antibodies against β1 integrins inhibited the formation of lung metastases in murine models.[8] Up-regulation of β1 integrin expression promoted matrix metalloproteinase-dependent cell invasion in ovarian carcinoma cells.[9] Perturbation of CD44-hyaluronan interactions decreased the invasive ability of human breast cancer cells [10] and inhibited murine mammary carcinoma cell growth.[11] The addition of hyaluronan into Matrigel resulted in increased glioma cell invasion in Matrigel invasion assays.[12] Together, these studies suggest that β1 integrin- and CD44-mediated cell-ECM interactions may contribute to ovarian carcinoma cell invasion.

Cancer cell invasion is mediated by a complex balance between degradative enzymes, including matrix metalloproteinases (MMPs), tissue inhibitors of matrix metalloproteinases (TIMPs), and ADAMs (a disintegrin and metalloprotease). MMPs are proteolytic enzymes that play an important role in cancer cell invasion through the degradation of ECM proteins, such as fibronectin and collagens.[13, 14] Increased activity of MMPs has been linked to the invasive potential of tumor cells.[15, 16] In ovarian carcinoma, increased secretion and activity of MMP 2, MMP 9, and MT1-MMP have been reported.[17, 18] However, the expression of TIMP 1 was shown not to be altered in ovarian carcinoma.[19, 20] These studies suggest that elevation of MMP secretion, relative to the concentrations of MMP inhibitors, can facilitate ovarian cancer cell invasion. The ADAMs are a recently discovered family of cell adhesion receptors, most of which are composed of pro-, metalloprotease, disintegrin-like, cysteine-rich, EGF-like repeat, transmembrane and cytoplasmic tail domains.[21, 22] Type I and type II procollagens can be degraded by an ADAMTS (a disintegrin and metalloprotease with thrombospondin type I repeat).[23] ADAM 12 was detected immunohistochemically in breast, colon, and lung carcinomas, and overexpression of disintegrin domains of ADAM 12 and ADAM 15 promoted cell adhesion

in melanoma cells.[24] Interactions between MMPs, TIMPs, and ADAMs are believed to regulate cancer cell invasion, but their particular interactions are not fully understood.

In this report, we describe an *in vitro* assay that examines the ability of ovarian carcinoma cells to invade through mesothelial cell monolayers. This new assay more closely mimics *in vivo* conditions than the currently used cell invasion assays. In addition, gene expression analysis was performed to determine whether the expression of genes associated with cell invasion (such as MMPs, TIMPs, and ADAMS) were differentially expressed in ovarian carcinoma compared to normal ovaries. Our results suggest that complex cell-cell and cell-ECM interactions between the tumor cells and their target cells mediate ovarian carcinoma cell invasion, and that this assay may be a suitable tool for its study.

Methods

Unless otherwise stated, all standard reagents and materials were obtained from Sigma Chemical Company (St. Louis, MO), all pictures were photographed with a Nikon Coolpix 950 camera, and all experiments were performed in triplicate and repeated a minimum of three times.

Cell culture. The human ovarian carcinoma cell line NIH:OVCAR5, which mimics the progression of ovarian carcinoma when injected into *in vivo* mouse models,[25] was maintained in RPMI 1640 medium, 10% fetal bovine serum (FBS), 2 mM glutamine, 0.2 U/ml insulin, and 50 U/ml penicillin G/streptomycin (Life Technologies, Grand Island, NY). The ovarian carcinoma cell line NIH:OVCAR5 was originally established by Dr. Thomas Hamilton (Fox Chase Cancer Center)[26] and obtained from Dr. Judah Folkman, Harvard Medical School. The human peritoneal mesothelial cell line LP9 (Coriell Cell Repositories, Camden, NJ) was maintained in a medium containing a 1:1 ratio of M199 and MCDB 10 media, 15% FBS, 2 mM glutamine, 5 ng/ml epidermal growth factor, 400 ng/ml hydrocortisone, and 50 U/ml penicillin G/streptomycin. Both cell lines were maintained in 75-mm^2 tissue culture flasks in a humidified incubator with 5% CO_2 at 37°C.

Ovarian carcinoma cell invasion through live mesothelial cell monolayers. The ability of NIH:OVCAR5 ovarian carcinoma cells to invade through live mesothelial cell monolayers was assessed. Each cell line was labeled with a different fluorescent stain. LP9 mesothelial cells were grown to confluence in twelve-well tissue culture plates (Becton Dickinson, Franklin Lakes, NJ) and rinsed twice with phosphate buffered saline (PBS). The mesothelial cells were labeled with

10 μg/ml 5-chloromethylfluorescein diacetate (Molecular Probes, Inc., Eugene, OR), a green fluorescent stain, in PBS for 30 min at 37°C, and then rinsed twice with PBS. The NIH:OVCAR5 cells were released from tissue culture flasks with 0.5% trypsin, 2 mM EDTA as described previously,[27] and resuspended in PBS at a concentration of 10^6 cells/ml. The NIH:OVCAR5 cells were labeled with 10 μg/ml carboxy SNARF-1 (Molecular Probes, Inc.), a red fluorescent stain, in PBS for 30 min, and then rinsed twice with PBS. The NIH:OVCAR5 cells were added to the live mesothelial cell monolayers at a concentration of 10,000 cells/ml/well. The cocultures were maintained in a 1:1 ratio of complete media for each cell type. At 24 hr intervals, the wells were gently washed twice with PBS, and the cells were visualized with a Nikon Eclipse TE200 fluorescent microscope.

Ovarian carcinoma cell invasion through fixed mesothelial cell monolayers. The ability of NIH:OVCAR5 ovarian carcinoma cells to invade through fixed monolayers of the human LP9 mesothelial cell line was assessed. LP9 cells (10,000 cells/well) were added to twelve-well tissue culture plates and grown to confluence for 48 hr in complete medium. The mesothelial cell monolayers were rinsed twice with 1 ml PBS, fixed with 250 μl dimethyl sulfoxide for 30 min, and rinsed twice with 1 ml PBS. Single cell suspensions of NIH:OVCAR5 cells were resuspended in complete cell culture media and added to the fixed mesothelial monolayers. At 24 hr intervals for 7 days, the media was removed and the wells were gently washed twice with 1 ml PBS. 500 μl of 0.2% trypan blue solution (Sigma) was applied to each well for 15 min, and gently rinsed with 1 ml PBS. At 24 hr intervals, the wells were gently washed twice with PBS, and the cells were visualized with a light microscope.

Inhibition of ovarian carcinoma cell invasion through mesothelial cell monolayers. NIH:OVCAR5 cells were allowed to invade through mesothelial cell monolayers as described above, except that the cells were incubated in the presence of: 25 mM GM6001, a chemical inhibitor of MMP-1, -2, -3, -8, and –9 [28] (Chemicon International, Temecula, CA); 100 μg/ml GRGDSP or GRGESP peptides (Life Technologies); 1 μg/ml of normal mouse immunoglobulin (IgG); monoclonal antibody (mAb) P5D2, which blocks the adhesive activity of human β1 integrin subunits (provided by Dr. Leo Furcht, University of Minnesota); and mAb IM7, which blocks the hyaluronan-binding site of CD44 (Pharmingen, San Diego, CA). The putative blocking agents were replenished daily.

ECM Molecules. Collagen type IV, isolated from mouse Engelbreth-Holm-Swarm (EHS) tumor, was purchased from Trevigen, Gaithersburg, MD. Mouse EHS laminin, prepared as previously described,[29] was provided by Dr. Leo Furcht, University of Minnesota. Human plasma fibronectin, purified as described,[30] was provided by Dr. James McCarthy, University of Minnesota. Human umbilical cord hyaluronan, chondroitin sulfate A, and ovalbumin were purchased from Sigma. Matrigel was purchased from Becton Dickinson, Bedford, MA.

Cell proliferation assay. 96-well plates were coated with 50 μg/ml of fibronectin, laminin, collagen type IV, or ovalbumin or with 1 mg/ml hyaluronan in PBS (100 μl/well) at 4°C for 16 hr. Nonspecific binding sites were blocked with 2 mg/ml ovalbumin in PBS at 4°C for 1 hr (200 μl/well), and then rinsed twice with PBS. Single cell suspensions of NIH:OVCAR5 cells in complete medium were added at a concentration of 500 cells/200 μl/well and cultured for up to 7 days. At various time points, 2 mg/ml WST-1 (Boehringer-Mannheim Corporation, Indianapolis,

IN) was added to each well and incubated for 2 hr. The resulting formazan product was quantitated by a SpectaMax 250 scanning multi-well spectrophotometer (Molecular Devices Corporation, Sunnyvale, CA) by measuring absorbance at 450 nm. These experiments were performed in quadruplicate.

Human tissue samples. Tissue samples from 50 normal ovaries, 20 primary ovarian carcinomas, 17 secondary omental metastases, and 7 normal omenta were obtained from the Tissue Procurement Facility of the University of Minnesota Cancer Center. Samples were obtained using protocols approved by the University of Minnesota Institutional Review Board. All samples were identified, dissected, and snap frozen in liquid nitrogen within 30 min of removal from the patient. Tissue sections of each sample were prepared before freezing, and were examined by a pathologist by light microscopy after H&E staining to confirm the pathologic nature of the sample. None of the samples were necrotic.

Gene expression analysis of human tissues. The relative expression of genes associated with cell invasion in normal ovaries, primary ovarian carcinomas, secondary omental metastases, and normal omenta was studies. RNA was prepared from the human tissue samples described above and gene expression was determined at Gene Logic Inc. (Gaithersburg, MD) using Affymetrix GeneChip® U_95 arrays (Santa Clara, CA) containing approximately 12,000 known genes and 48,000 ESTs. Gene expression analysis utilized the Gene Logic GeneExpress® Software System. Genes associated with cell invasion were selected for further analysis if their mean expression changed at least 2-fold and if they were assigned mean expression intensity values

greater than or equal to 100. Clustering of the gene expression data was performed with Eisen Cluster and TreeView software (available at http://rana.lbl.gov/EisenSoftware.htm).

Results

Ovarian carcinoma cells invade through mesothelial cell monolayers.

To determine the invasive ability of ovarian carcinoma cells, we developed an *in vitro* assay that we believe more closely mimics *in vivo* conditions than the commonly used Matrigel invasion assay.[2] Namely, in our *in vitro* invasion assay, the invasive ability of ovarian carcinoma cells is determined by their ability to invade through monolayers of mesothelial cells that line the peritoneum. Our initial strategy involved the use fluorescently labeled cocultures of live cells. In these assays, the ovarian carcinoma cells and mesothelial cells were labeled with two different colored fluorescent dyes (Figure 1). At 3 days, the two cell types are indistinguishable from each other (Figure 1C) when viewed with a phase microscope. When viewed with fluorescent filters, the NIH:OVCAR5 cells (Figure 1B) could be distinguished from the mesothelial cell monolayers (Figure 1C). One cluster of NIH:OVCAR5 cells, highlighted with arrows, was observed under phase and fluorescent filters (Figure 1A, 1B), and its absence was noted from the visualized mesothelial cell monolayer (Figure 1C). The ovarian carcinoma tumor cells had invaded through the mesothelial cell monolayer and adhered to the tissue culture plate, creating a focal point of invasion. For up to 3 days, the cells were easily visualized with the fluorescent microscope. However, the fluorescent dyes diluted to undetectable levels after approximately 6-8 cell divisions and could not be used for longer time points. Furthermore, when we added putative inhibitors of cell invasion, such as RGD peptides, blocking antibodies, and chemical MMP inhibitors, the unfixed mesothelial cells detached from the tissue culture plates. Therefore, it was necessary to fix the mesothelial cell monolayers used in all subsequent assays, since fixed

mesothelial cells were not susceptible to detachment. In addition, we opted to use trypan blue dye, which stained the fixed monolayers, but did not stain the living, invasive ovarian carcinoma cells.

In the model system described here, ovarian carcinoma cells were allowed to invade through monolayers of fixed human mesothelial cells (Figure 2). At 24 hr intervals, nonadherent ovarian carcinoma cells were gently rinsed away, and the cultures were subjected to trypan blue dye staining. The fixed mesothelial cells, which were unable to exclude the stain, were dyed blue. In contrast, the live ovarian carcinoma cells remained unstained. By 1 day, ovarian carcinoma cells adhered to the surface of the mesothelial cell monolayers. By 4 days, initial invasion by the carcinoma cells through the mesothelial monolayers was observed (Figure 2, arrows). By 7 days, the foci of invasion had increased in size (Figure 2, arrows), in some cases displacing the majority of the mesothelial cell monolayers.

Ovarian carcinoma cell invasion through mesothelial cell monolayers is inhibited by an MMP inhibitor.

Ovarian carcinoma cell invasion has been shown to be mediated, in part, by the induction of MMPs.[9, 17, 18] Ovarian cancer cell invasion through mesothelial cell monolayers was inhibited by the addition of a broad-spectrum MMP inhibitor, GM6001 (Figure 2). In the presence of 25 mM GM6001, ovarian carcinoma cell invasion was completely inhibited for up to 4 days. However, by 7 days, ovarian carcinoma cell invasion was observed in the presence of GM6001 (arrows), but the areas of invasion were much smaller than those observed in the absence of the MMP inhibitor. Furthermore many noninvasive cells adhered to and spread upon the mesothelial

cell monolayers. These results suggest that ovarian carcinoma cell invasion through mesothelial cell monolayers requires MMP activity.

Ovarian carcinoma cell invasion through mesothelial cell monolayers is mediated by integrins.

We have previously shown that β1 integrins and CD44 mediate ovarian carcinoma adhesion [4, 5] and migration [31] to ECM components. To determine whether integrins affect ovarian carcinoma cell invasion through mesothelial cell monolayers, we performed the assays in the presence of exogenous RGD peptide, a ligand bound by many integrins (Figure 2).[32] At 4 days, cell invasion was partially inhibited in the presence of 100 μg/ml RGD peptides, compared to cells incubated in the presence of RGE control peptides (Figure 2). The addition of the RGD peptide inhibited most ovarian carcinoma cell invasion (not shown), but it did not completely prevent tumor cells from adhering to the mesothelial cell monolayer. By 7 days, small areas of invasion were observed, although much smaller than those present in the RGE peptide control.

To determine whether β1 integrins or CD44 mediate ovarian carcinoma cell invasion through fixed mesothelial cell monolayers, the assays were performed in the presence of normal mouse IgG or blocking antibodies against the binding sites of the β1 integrin subunit or CD44 (Figure 3). The blocking mAb against the β1 integrin subunit inhibited cell invasion by 4 and 7 days, while the blocking mAb against CD44 had no effect, compared to IgG controls. Taken together, these data suggest that β1 integrins, but not CD44, may mediate ovarian carcinoma cell invasion through mesothelial cell monolayers.

The composition of the adhesive substratum does not affect the proliferative abilities of ovarian carcinoma cells.

To examine the effects of adhesive substrata on the proliferative ability of the ovarian carcinoma cells, NIH:OVCAR5 were cultured as monolayers in 96-well plates that were coated with different ECM components found in mesothelial cells: fibronectin, laminin, collagen type IV, and hyaluronan (Figure 4).[5, 33] We observed that the NIH:OVCAR5 cells proliferated equally well in the presence of all of these ECM components as adhesive substrata.

Differential expression of genes associated with cell invasion in normal and malignant tissues.

Since cancer cell invasion is thought to be mediated by a complex interaction between MMPs, ADAMs, and TIMPs, we decided to determine whether these genes are differentially expressed in ovarian carcinoma tissues, compared to normal ovaries. GeneLogic Inc. quantitated the expression levels of 12,000 known genes and 48,000 ESTs using Affymetrix GeneChip® U_95 arrays on RNA samples obtained from 20 primary ovarian carcinoma tumors, 17 secondary omental metastases, 50 normal ovaries, and 7 normal omenta.

Fluorescent intensity values and gene expression profiles were generated for each sample. The expression values for several gene transcripts associated with cell invasion, ADAM 8, ADAM 9, MMP 7, MMP9, and MMP 11, were highly expressed in both primary ovarian carcinomas and secondary omental metastases, compared to normal ovaries and omenta (Figure 5). Comparison of the expression values assigned to these gene transcripts confirmed significant mean fold increases of these transcripts in tumor samples compared to normal tissues (Table I): the expression of MMP 7 transcripts increased over 90-fold; the expression of MMP 9 transcripts increased over 5-fold; and the expression of ADAM 8, ADAM 9, and MMP 11 transcripts

increased over 2-fold. In contrast, the expression of gene transcripts of TIMP 2, MMP 25, TIMP 1, MMP 2, and ADAMTS 1, was down-regulated in tumor tissues, when compared to normal samples (Figure 5 and Table I). Notably, ADAMTS 1, MMP 25, TIMP 2, and MMP 2 gene expression was 2-fold to 64-fold less in tumor samples compared to normal samples.

Discussion

Currently, cancer cell invasion is most commonly measured by the ability of the cells to invade through Matrigel,[2] a mixture of matrix components synthesized by mouse EHS tumors that approximates the basement membrane ECM through which cancer cells invade.[3] While the Matrigel invasion assay provides an ECM through which cancer cells can invade, there are several caveats to this procedure. Matrigel is a mixture of ECM components synthesized by mouse sarcoma cells, which is a less than ideal milieu to examine metastasis in human ovarian carcinoma cells. More importantly, this assay measures interactions between tumor cells and ECM components, but not cell-cell interactions between tumor cells and target cells. Here, we present an alternative invasion model that we believe more closely mimics *in vivo* conditions than the currently used Matrigel invasion assay.

The *in vitro* cell-based ovarian carcinoma cell invasion assay described here has several advantages over the Matrigel invasion assay. First, the *in vitro* invasion model described herein is comprised of components of human origin, unlike Matrigel, which is murine in origin. Matrigel is not completely characterized, and may contain murine-specific components that may alter the function of human cells. Interestingly, others have shown that the addition of exogenous hyaluronan to Matrigel alters glioma cell invasion,[12] suggesting that the precise composition of the invasive matrix is critical in the accurate assessment of tumor cell invasion. Second, unlike the Matrigel invasion assay, this *in vitro* invasion model is a cell-based assay that allows interactions to occur between tumor cells and fixed target cells. Although not as ideal as live mesothelial cells, the use of the fixed cells as an invasive matrix more closely approximates *in vivo* conditions than the mixture of ECM components that comprise Matrigel. Thus, our *in vitro* invasion model may provide a more accurate gauge of metastatic events. Third, our *in vitro*

model facilitates interactions between ovarian carcinoma cells and mesothelial cells, their most likely *in vivo* targets of metastasis, providing a more optimal environment in which to study ovarian carcinoma cell invasion. Furthermore, this model could easily be adapted to measure the invasive capacities of other types of tumor cells.

We initially attempted to perform invasion assays using live mesothelial monolayers. Ovarian carcinoma cells and mesothelial cells were labeled with different fluorescent dyes prior to their use in the assay. However, the fluorescent dyes dilute to undetectable levels after approximately 6-8 cell divisions, rendering this assay unsuitable within a few days. Furthermore, the addition of RGD peptides or blocking mAb against the β1 integrin subunit resulted in detachment of the mesothelial monolayers from the tissue culture plates, presumably by disrupting integrin-mediated mesothelial cell adhesion to the ECM they had established on the tissue culture plates. For these reasons, we used fixed mesothelial monolayers as a matrix of invasion.

The invasive process was easily visualized in this cell-based model. Ovarian carcinoma cells readily adhered to, spread upon, and invaded through the mesothelial cell monolayers. After the formation of invasive foci, the cancer cells proliferated and displaced the fixed mesothelial cells. Interestingly, the fixed mesothelial cells did not stimulate contact inhibition in the invading ovarian carcinoma cells. It is still possible, however, that mesothelial cells may provide an inhibitory effect upon ovarian carcinoma cell invasion or proliferation *in vivo*.

The pericellular matrices that coat mesothelial cell monolayers is comprised of numerous of ECM components, including glycoproteins and proteoglycans.[4, 7] To determine whether adhesion to a particular substrata may affect ovarian carcinoma cell proliferation, the cells were cultured atop 96-well plates coated with fibronectin, collagen type IV, laminin, or hyaluronan,

major components of mesothelial cell ECM.[8] The ovarian carcinoma cells adhered to all of the substrata and grew to confluence. The composition of the adhesive substrata failed to affect the cells' ability to proliferate, which suggests that the general phenomenon of cell adhesion mediates ovarian carcinoma cell proliferation, rather than adhesion to a particular substratum. Further studies are required to determine the role of the mesothelial cells as positive or negative effectors of secondary tumor growth in ovarian cancer.

Ovarian carcinoma cell invasion was partially inhibited by the addition of GM6001, a potent chemical inhibitor of MMPs. The presence of this inhibitor slowed cell invasion, although the phenomenon was not completely halted at 7 days. This may be due to the activity of other degradative enzymes to the accumulation of sufficient concentrations of MMPs to overcome GM6001's inhibitory effect. The use of the MMP inhibitor did not negatively affect ovarian carcinoma cell adhesion to the mesothelial cell monolayers, or subsequent spreading of the adherent tumor cells.

We have previously shown that the β1 integrins play a major role in the adhesion of ovarian carcinoma cells to mesothelial cell monolayers.[4] In addition, we have also shown that the β1 integrins play a major role in ovarian carcinoma cell migration toward ECM components.[31] Because it has been shown that CD44 also mediates ovarian carcinoma cell adhesion,[6, 7] we expected the CD44 mAb to affect cell invasion due to its ability to partially inhibit cell adhesion to mesothelial monolayers. We observed that ovarian carcinoma cell invasion through mesothelial cell monolayers was inhibited by the addition of an RGD peptide or a blocking mAb against the β1 integrin subunits, but not by the addition of a blocking mAb against CD44. This suggests that ovarian carcinoma cell invasion through mesothelial cell monolayers may be mediated by β1 integrins, but not CD44.

Because tumor cell invasion has been attributed to alterations in the net expression of MMPs, TIMPs, and ADAMs, the expression of these gene transcripts was examined in ovarian carcinoma tumors, secondary metastases, normal ovaries, and normal omenta. Several genes associated with cell invasion were differentially expressed. In primary ovarian carcinoma tumors and secondary omental metastases, the level of expression of ADAM 8, ADAM 9, MMP 7, MMP 9, and MMP 11 transcripts was much greater than that of normal ovaries and omenta (Table I). High levels of gene expression of TIMP 1, TIMP 2, MMP 2, MMP 25, and ADAMTS 1 were observed in samples obtained from normal ovaries and omenta. TIMPs complex with and inactivate MMPs. Although relatively high levels of MMP-2 were also detected in normal tissues, the simultaneous expression of the TIMPs suggest that the MMP may be present in an inactive state, or that the TIMPs are present in adequate amounts to inhibit MMP activity.

In ovarian carcinoma, increased secretion and activity of MMP 2 and TIMP 1, but not TIMP 2 has been reported.[17-20] Increased expression of MMP 7 [34, 35] and MMP 25 [36] mRNAs have also been observed in ovarian cancers. The ADAMs are a recently discovered family of cell adhesion receptors, most of which are composed of pro-, metalloprotease, disintegrin-like, cysteine-rich, EGF-like repeat, transmembrane and cytoplasmic tail domains.[21, 22] Type I and type II procollagens can be degraded by an ADAMTS,[23] which may augment cancer cell invasion. Since it is not known whether ADAMTS collagenase activity is susceptible to effectors of MMP activity, such as GM6001, members of the ADAM family may provide an alternate degradative pathway that contributes to cancer cell invasion. Upregulation of ADAM 12 and ADAM 15 domains in melanoma cells resulted in enhanced cell adhesion.[24] Cell migration in fibroblast cells was increased by the binding of an ADAM 9 fusion protein via integrin $\alpha 6\beta 1$.[37] The role of ADAMs in cancer metastasis is not well understood, but their ability to affect cellular

functions suggests that they may contribute to cancer cell invasion. MMPs, TIMPs, and ADAMs are believed to regulate cancer cell invasion, but their particular interactions are not fully understood.

In this study, we report the development of a novel *in vitro* cell-based assay to study ovarian carcinoma cell invasion. It's primary advantages over the commonly used Matrigel invasion assay lie in its similarity to *in vivo* conditions found in ovarian carcinoma. The use of mesothelial monolayers as an invasive matrix enables cell-cell interactions that are not available in Matrigel assays. Using this assay, we observed that integrins and MMPs mediate ovarian carcinoma cell invasion. Gene expression analysis revealed differential expression of MMP, TIMP, and ADAM genes in ovarian carcinoma tumors, which may help elucidate the events that regulate metastasis. The novel invasion assay described here will enable future studies of ovarian carcinoma cell invasion.

Acknowledgements

We thank the staff of Gene Logic Inc., Gaithersburg, MD, for performing the gene expression experiments with the human tissue samples and the staff of the University of Minnesota Cancer Center's Tissue Procurement Facility for assistance in collecting and processing the human tissue samples. We thank Drs. Thomas Hamilton and Judah Folkman for providing the NIH:OVCAR5 cell line, Dr. James McCarthy for providing fibronectin, and Dr. Leo Furcht for providing the mAb P5D2 against the β1 integrin subunit.

References

1. Jemal A, Thomas A, Murray T, Thun M. Cancer statistics, 2002. CA Cancer J Clin 2002, 52:23-47.
2. Hendrix MJ, Seftor EA, Seftor RE, Fidler IJ. A simple quantitative assay for studying the invasive potential of high and low human metastatic variants. Cancer Letters 1987, 38:137-147.
3. Kleinman HK, McGarvey ML, Liotta LA, Robey PG, Tryggvason K, Martin GR. Isolation and characterization of type IV procollagen, laminin, and heparan sulfate proteoglycan from the EHS sarcoma. Biochem 1982, 21:6188-6193.
4. Lessan K, Aguiar DJ, Oegema T, Siebenson L, Skubitz APN: CD44 and β1 integrins mediate ovarian carcinoma cell adhesion to peritoneal mesothelial cells. Amer J Pathol 1999, 154:1525-1537.
5. Casey RC, Burleson KM, Pambuccian S, Skubitz K, Oegema T, Skubitz APN. β1 integrins regulate formation and adhesion of ovarian carcinoma multicellular spheroids. Amer J Pathol, 159:2071-2080.
6. Cannistra SA, Kansas GF, Niloff J, et al. Binding of ovarian cancer cells to peritoneal mesothelial is partly mediated by CD44H. Cancer Res 1993; 52:3830-3838.
7. Gardner MJ, Catterall JB, Jones LM, Turner GA. Human ovarian tumour cells can bind hyaluronic acid via membrane CD44: A possible step in peritoneal metastasis. Clin Exp Metastasis 1996; 14:325-334.
8. Takenaka K, Shibuya M, Takeda Y, Hibino S, Gemma A, Ono Y, Kudoh S. Altered expression and function of beta 1 integrins in a highly metastatic human lung adenocarcinoma cell line. Int J Oncol 2000; 17:1187-1194.

9. Fishman DA, Liu Y, Ellerbroek SM, Stack MS. Lysophosphatidic acid promotes metalloproteinase (MMP) activation and MMP-dependent invasion in ovarian cancer cells. Cancer Res 2001; 61:3194-3199.

10. Herrera-Gayol A, Jothy S. CD44 modulates Hs578T human breast cancer cell adhesion, migration, and invasiveness. Exp Mol Pathol 1999; 66:99-108.

11. Peterson RM, Yu Q, Stamenkovic I, Poole BP. Perturbation of hyaluronan interactions by soluble CD44 inhibits growth of murine mammary carcinoma cells in ascites. Am J Pathol 2000; 2159-2167.

12. Radotra B, McCormick D. Glioma invasion in vitro is mediated by CD44-hyaluronan interactions. J Pathol 1997; 181:434-438.

13. Mignatti P, Rifkin DB. Biology and biochemistry of proteinases in tumor invasion. Physiol Rev 1993; 73:161-195.

14. Liotta LA, Stetler-Stevenson WG. Metalloproteinases and cancer invasion. Semin Cancer Biol 1990; 1:99-106.

15. Davies B, Brown PD, East N, Crimmin MJ, Balkwill FR. A synthetic matrix metalloproteinase inhibitor decreases tumor burden and prolongs survival of mice bearing human ovarian carcinoma xenografts. Cancer Res 1993; 53:2087-2091.

16. Gilles C, Polette M, Piette J, Munaut C, Thompson EW, Birembaut P, Foidart JM. High level of MT-MMP expression is associated with invasiveness of cervical cancer cells. Int J Canc 1996; 65:209-213.

17. Moser TL, Young TN, Rodriguez GC, Pizzo SV, Bast RC, Stack MS. Secretion of extracellular matrix-degrading proteinases is increased in epithelial ovarian carcinoma. Int J Cancer 1994; 56:552-559.

18. Sakata K, Shigemasa K, Nagai N, Ohama K. Expression of matrix metalloproteinases (MMP-2, MMP-9, MT1-MMP) and their inhibitors (TIMP-1, TIMP-2) in common epithelial tumors of the ovary.

19. Naylor MS, Stamp GW, Davies BD, Balkwill FR. Expression and activity of MMPs and their regulators in ovarian cancer. Int J Cancer 1994; 58:50-56.

20. Hoyhtya M, Fridman R, Komarek D, Porter-Kordan K, Stetler-Stevenson WG, Liotta LA, Liang CM. Immunohistochemical localization of matrix metalloproteinase 2 and its specific inhibitor TIMP-2 in neoplastic tissues with monoclonal antibodies. Int J Cancer 1994; 56:500-505.

21. Wolfsberg TG, Straight PD, Gerena RL, Huovila AP, Primakoff P, Myles DG, White JM. ADAM, a widely distributed and developmentally regulated gene family encoding membrane proteins with a disintegrin and metalloprotease domain. Dev Biol 1995; 169:378-83.

22. Huovila APJ, Almeida EA, White JM. ADAMS and cell fusion. Curr Opin Cell Biol 1996; 8:692-699.

23. Colige A, Li SW, Sieron AL, Nusgens BV, Prockop DJ, Lapiers CM. CDNA cloning and expression of bovine procollagen I N-proteinase: a new member of the superfamily of zinc-metalloproteinases with binding sites for cells and other matrix components. Proc Natl Acad Sci USA 1997; 94:2374-2379.

24. Iba KR, Albrechtsen BJ, Gilpin F, Loechel F, Wewer UM. Cysteine-rich domain of ADAM 12 (meltrin alpha) supports tumor cell adhesion. Am J Pathol 1999; 154:1489-1501.

25. Molpus KL, Koelliker D, Atkins L, Kato DT, Buczek-Thomas J, Fuller AF, Hasan T: Characterization of a xenograft model of human ovarian carcinoma which produces intraperitoneal carcinomatosis and metastases in mice. Int J Cancer 1996, 68:588-595.

26. Hamilton TC, Young RC, Ozols RF. Experimental model systems of ovarian cancer: applications to the design and evaluation of new treatment approaches. Semin Oncol 1984; 11:285-298.

27. Pattaramalai S, Skubitz KM, Skubitz APN: A novel recognition site on laminin for α3β1 integrin. Exp Cell Res 1996, 222:281-290.

28. Galardy RE, Grobelny D, Foellmer HG, Fernandez LA. Inhibition of angiogenesis by the matrix metalloprotease inhibitor N-[2R-2-(hydroxamidocarbonymethyl)-4-methylpentanoyl)]-L-tryptophan methylamide. Cancer Res 1994; 54:4715-4718.

29. McCarthy JB, Skubitz APN, Palm SL, Furcht LT. Metastasis inhibition of different tumor types by purified laminin fragments and a heparin-binding fragment of fibronectin. J Natl Cancer Inst 1988; 80:108-116.

30. Smith DE, Mosher DF, Johnson RB, Furcht LT. Immunological identification of two sulfhydryl-containing fragments of human plasma fibronectin. J Biol Chem 1982; 257:5831-5838.

31. Casey RC, Skubitz APN: CD44 and β1 integrins mediate ovarian carcinoma cell migration toward extracellular matrix proteins. Clin Exp Metastasis 2000, 18:67-75.

32. Pierschbacher MD, Ruoslahti E. Variants of the cell recognition site of fibronectin that retain attachment-promoting activity. Proc Natl Acad Sci USA 1984; 81:5985-5988.

33. Jones LM, Gardner MJ, Catterall JB, Turner GA. Hyaluronic acid secretion by mesothelial cells: A natural barrier to ovarian cancer cell adhesion. Clin Exp Metastasis 1995; 13:373-380.

34. Tanimoto H, Underwood LJ, Shigemasa K, Parmley TH, Wang Y, Yan Y, Clarke J, O'Brien TJ. The matrix metalloproteinase pump-1 (MMP-7, matrilysin): A candidate marker/target for ovarian cancer detection and treatment. Tumour Biol 1999; 20:88-98.

35. Zhai Y, Wu R, Schwartz DR, Darrah D, Reed H, Kollings FT, Nieman MT, Fearon ER, Cho KR. Role of beta-catenin/T-cell factor-regulated genes in ovarian endometrioid adenocarcinomas. Am J Pathol 2002; 160:1229-1238.

36. Davidson B, Goldberg I, Berner A, Neshland JM, Givant-Howitz V, Bryne M, Risberg B, Kristensen GB, Trope CG, Kopolovic J, Reich R. Expression of membrane-type 1, 2, and 3 matrix metalloproteinases messenger RNA in ovarian carcinoma cells in serous effusions. Am J Clin Pathol 2001; 115:517-524.

37. Nath D, Slocombe PM, Webster A, Stephens PE, Doherty AJ, Murphy G. Meltrin gamma (ADAM-9) mediates cellular adhesion through $\alpha 6\beta 1$ integrin, leading to a marked induction of fibroblast cell motility.

Figure Legends

Figure 1. Ovarian carcinoma cell invasion through live mesothelial cell monolayers. NIH:OVCAR5 ovarian carcinoma cells were allowed to invade through monolayers of live mesothelial cells. After 3 days, the assays were photographed under a phase objective to visualize the cocultures (A), or under fluorescent objectives to visualize the ovarian carcinoma cells (B), or the mesothelial cell monolayers (C). Arrows point to a cluster of NIH:OVCAR5 cells that have invaded through the mesothelial cell monolayer. Bar = 100 nm.

Figure 2. Ovarian carcinoma cell invasion through mesothelial cells monolayers is inhibited by an MMP inhibitor and RGD peptide. NIH:OVCAR5 ovarian carcinoma cells were placed atop monolayers of fixed mesothelial cells in complete media alone or in the presence of or 25 mM GM6001, 100 μg/ml RGD peptide, or 100 μg/ml RGE peptide. The ovarian carcinoma cells adhered to the mesothelial cell monolayer by 1 day. In the presence of media or the RGE peptide, ovarian carcinoma cell invasion is observed at 4 and 7 days (arrows). In the presence of GM6001 or the RGD peptide, cell invasion is completely inhibited for 4 days, and is still partly inhibited by 7 days (arrows). Bar = 200 nm.

Figure 3. Ovarian carcinoma cell invasion through mesothelial cells monolayers is inhibited by monoclonal antibodies against the β1 integrin subunit. NIH:OVAR5 ovarian carcinoma cells were placed atop monolayers of fixed mesothelial cells in the presence of 1 μg/ml mouse IgG, blocking mAb against the β1 integrin subunit, or blocking mAb against CD44. In the presence of mouse IgG or a blocking mAb against CD44, the NIH:OVCAR5 cells invaded

through the mesothelial cell monolayers (arrows). In the presence of a blocking mAb against the β1 integrin subunit, invasion through the mesothelial cell monolayer was almost completely inhibited on day 4, and still significantly inhibited on day 7. Bar = 200 nm.

Figure 4. Ovarian carcinoma cell proliferation is not affected by the composition of adhesive substrata. 96-well plates were coated with fibronectin (diamonds), collagen type IV (squares), laminin (triangles), hyaluronan (circles), or ovalbumin (crosses). NIH:OVCAR5 cells were added to ECM-coated wells at a concentration of 500 cells/well for up to 7 days. The levels of proliferation were quantitated as described in the Material and Methods. Data are expressed are mean ± SD.

Figure 5. Analysis of cell invasion genes discriminating ovarian carcinomas from normal ovaries. Columns represent individual human tissue samples; rows represent individual genes. Each cell in the matrix represents the expression level of a single transcript in a single sample, with red and green indicating transcript levels above and below the mean for that gene across all samples, respectively.

Table I. Genes associated with cell invasion are differentially expressed in ovarian carcinoma.

Protein	1° tumor:ovary	2° tumor:ovary	2° tumor:omentum
MMP 7	90.1 ↑	97.0 ↑	37.4 ↑
MMP 9	5.7 ↑	9.5 ↑	7.9 ↑
MMP 11	2.3 ↑	4.6 ↑	----
ADAM 8	2.3 ↑	2.0 ↑	----
ADAM 9	----	2.0 ↑	----
TIMP 1	----	----	3.3 ↓
ADAMTS 1	3.9 ↓	4.1 ↓	4.4 ↓
MMP 25	3.5 ↓	64.5 ↓	52.2 ↓
TIMP 2	2.2 ↓	----	----
MMP 2	2.0 ↓	----	----

The mean fold change ratio differences in gene expression were compared between 20 primary ovarian carcinoma tumors and 50 normal ovaries, and between 17 secondary omental metastases and 7 normal omenta. Unchanged tumor:normal tissue mean fold changes are denoted as ----.

Figure 1

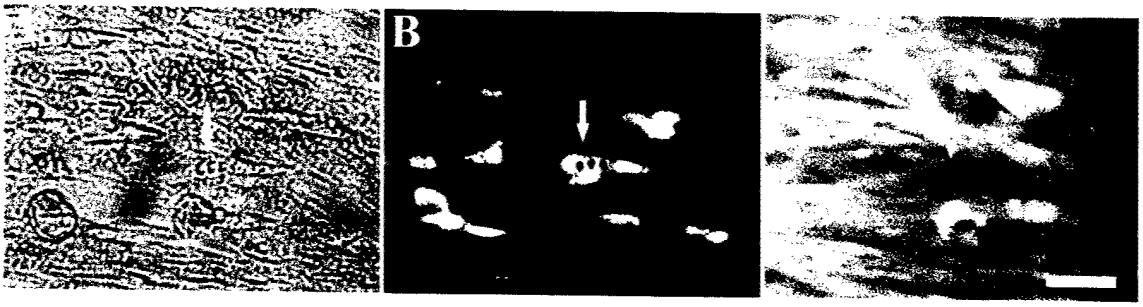

Figure 2

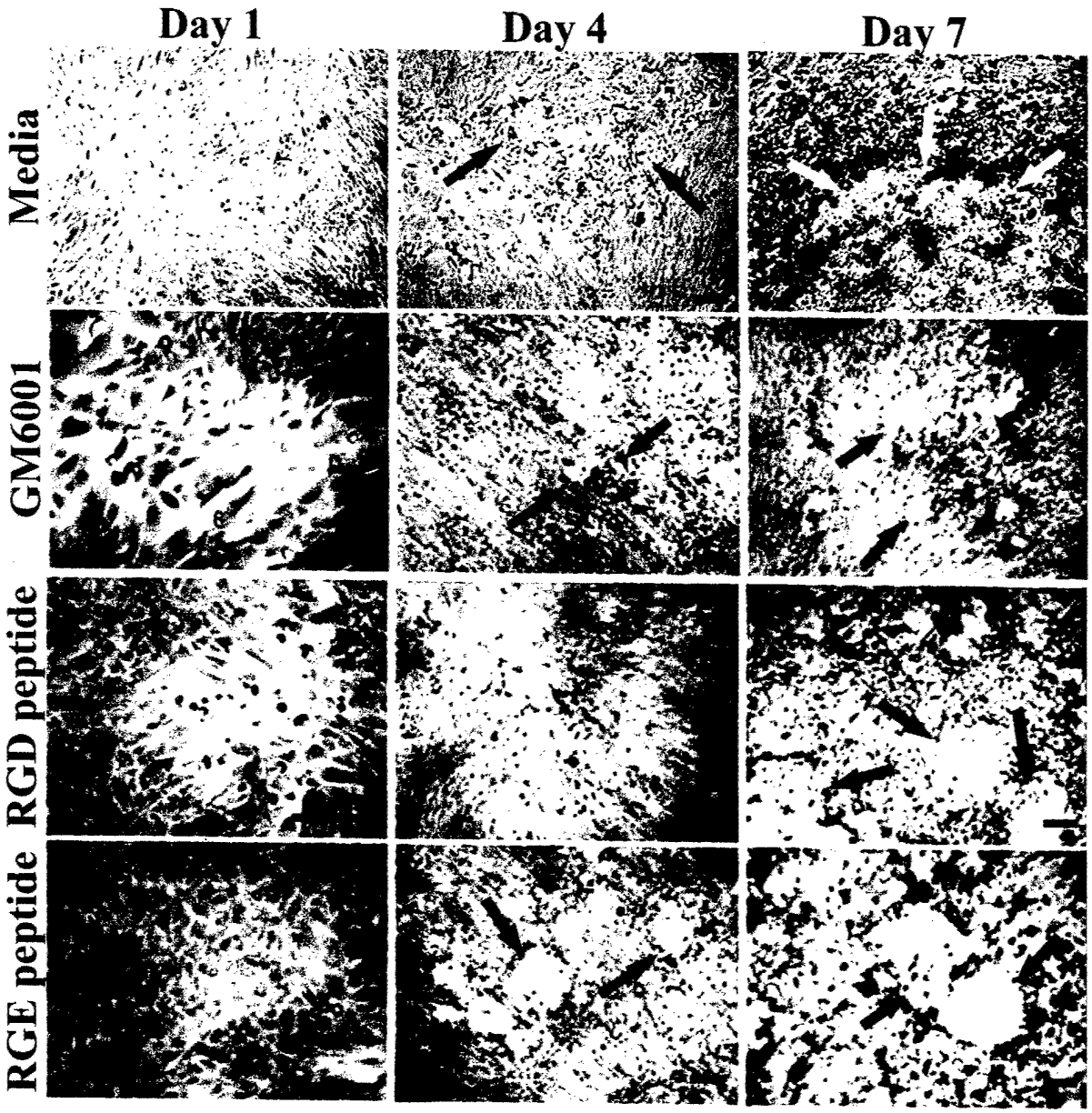

Figure 3

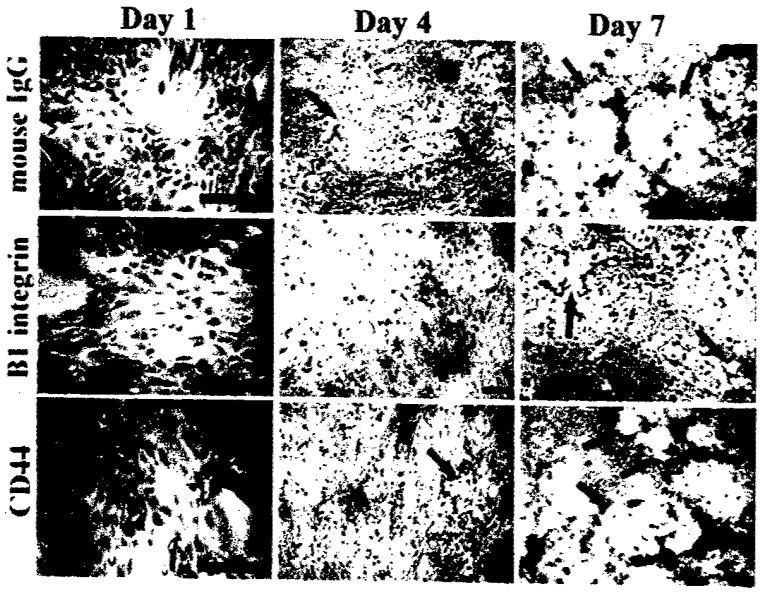

Figure 4

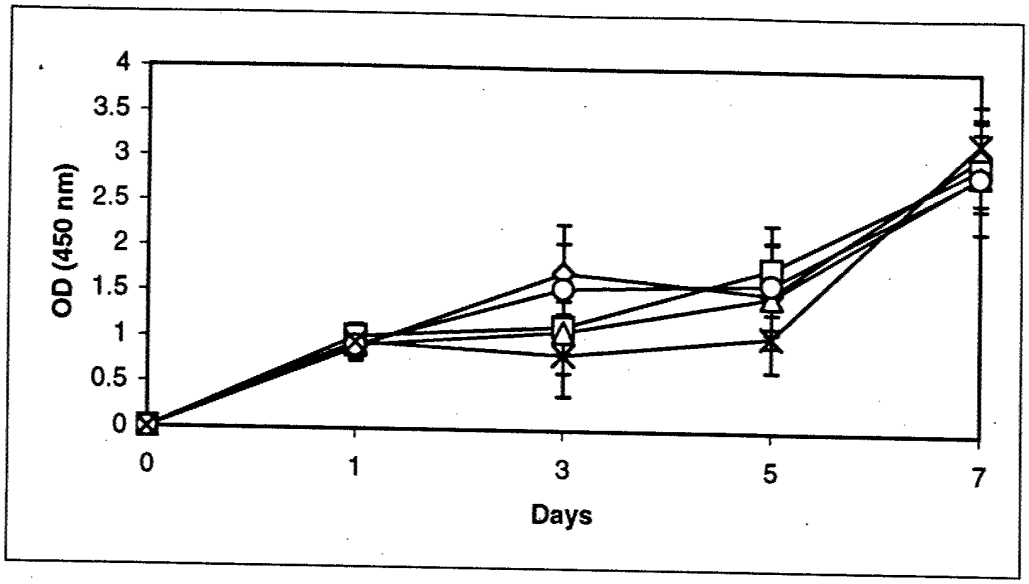

Figure 5

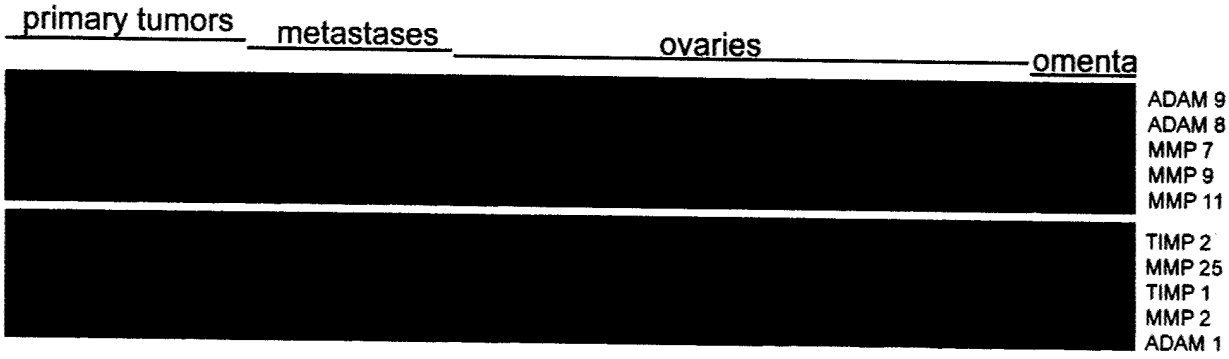
primary tumors
metastases
ovaries
omenta
ADAM 9
ADAM 8
MMP 7
MMP 9
MMP 11
TIMP 2
MMP 25
TIMP 1
MMP 2
ADAM 1

Appendix #3
Amy P.N. Skubitz

inhibit glioma cell adhesion to Matrigel nor did it affect the activity of matrix metalloproteinases (MMPs) secreted by glioma cells as demonstrated by zymography. CN also did not modulate the expression levels of tissue inhibitor of MMPs (TIMPs) and membrane-type 1 MMP (MT1-MMP) as shown by Western blotting and FACS analysis, respectively. *In vitro* wound closure assay demonstrated that CN is a potent inhibitor of migration of $\alpha v\beta 3$-positive glioma cells on Matrigel, but it did not block motility of $\alpha v\beta 3$-negative glioma cells. Further, treatment of $\alpha v\beta 3$-positive and not $\alpha v\beta 3$-negative glioma cells with CN resulted in morphological change, collapse of actin stress fibers and redistribution of focal adhesion proteins. Additional studies demonstrated that CN stimulates phosphorylation of focal adhesion kinase (FAK) at Tyr397 and Tyr576 in $\alpha v\beta 3$-positive glioma cells. In $\alpha v\beta 3$-negative glioma cells, however, CN appears only to induce autophosphorylation of FAK at Tyr397, and fails to affect Src-catalyzed FAK phosphorylation at Tyr576. Interestingly, CN was shown to hyperphosphorylate the focal adhesion protein paxillin in $\alpha v\beta 3$-positive, but not $\alpha v\beta 3$-negative glioma cells. It is concluded that inhibition of migration of $\alpha v\beta 3$-positive glioma cells by CN is likely a direct result of dysregulation of focal adhesion proteins and cytoskeletal disruption. Previous studies have shown that CN is an effective inhibitor of angiogenesis in several types of cancer. Thus, CN may be an effective anti-tumor therapy for glioma by virtue of its ability to negatively affect tumor cell invasion and angiogenesis.

#1827 Co-expression of N-cadherin and E-cadherin in prostate carcinoma cells promotes a migratory phenotype. Nelson R. Alexander, Nhan L. Tran, and Ronald L. Heimark. *University of Arizona, Tucson, AZ.*

Loss of E-cadherin function and expression is a late event in prostate cancer progression, and this de-regulation of E-cadherin is thought to contribute to prostate cancer metastasis. Gain of N-cadherin expression correlates with increasing grade of prostate cancer. It has been proposed that expression of N-cadherin in advanced prostate carcinoma confers a selective advantage to the cells, allowing them to metastasize. The purpose of this study was to elucidate whether the co-expression of both N and E-cadherin will impart a migratory phenotype to a prostate cancer cell line that normally expresses only E-cadherin. An expression vector containing a human N-cadherin-GFP fusion protein was expressed in the non-metastasizing cell line Du145. Three categories of stable clones expressing the N-cadherin-GFP fusion protein were isolated; cells expressing high levels of N-cadherin, equal levels of N and E-cadherin, and low N-cadherin high E-cadherin levels. The N-cadherin-GFP fusion protein in Du145 cells is shown to localize to cell junctions and associate with the catenins alpha, beta and p120. N-cadherin expressing clones display membrane ruffling, and immunofluorescence studies reveal modulations in the composition of focal contacts at the cell periphery. Accordingly, the actin cytoskeleton appears changed in clones expressing N-cadherin, while the relative levels of the proteins that modulate the actin cytoskeleton, the Rho Family of GTPases, remain unchanged. Clones expressing the N-cadherin-GFP fusion protein migrate faster than parental cells and empty vector control in both a serum free linear migration assay and a transwell boyden chamber assay in response to FGF1. Immunoprecipitation experiments in cells expressing both N and E cadherins show the larger isoform of p120 catenin has a higher affinity for N-cadherin than for E-cadherin. These results suggest that the motile phenotype conferred by N-cadherin expression in prostate epithelial cells is dominant to the suppression of migration phenotype mediated by E-cadherin.

#1828 Integrin α5-CD82 complex is regulated by N-glycosylation of CD82. Masaya Ono, Kazuko Handa, Donald A. Withers, and Sen-Itiroh Hakomori. *Jichi Medical School, Tochigi-ken, Japan, Pacific Northwest Research Institute, Seattle, WA, and University of Washington, Seattle, WA.*

We reported the cell motility is controlled by metastasis suppressor gene product CD82 with its glycosylation state. (Cancer Research 59,2335-2339) Tetraspan membrane protein, to which CD82 belongs, interacts with integrin family. We investigated whether the glycosylation state effects on the interaction of CD82 and integrin. CD82 was transfected to ldlD14 cell, a CHO mutant deficient in UDP-Glc 4-epimerase. In this cell, co-immunoprecipitation of CD82 and integrinα 5 occurred in the condition of incomplete glycosylation, but not complete glycosylation. Using sialidase, in the condition without sialic acid, integrin α5 co-immunoprecipitated with CD82. To clarify the responsible glycosylation site, we made CD82 mutants with N-linked consensus gene mutation at various sites. CD82 having both Asn129 and Asn198 mutation co-immunoprecipitated with integrin α5. Interaction of CD82 and integrin α5 is controlled by CD82 glycosylation. Especially the CD82 glycosylation sites of Asn129 and Asn198 are important.

#1829 Cell membrane glycosylation mediates the adhesion and migration of ovarian carcinoma cells toward extracellular matrix components and mesothelial cell monolayers. Rachael C. Casey, Theodore R. Oegema, Jr., Keith M. Skubitz, Stefan E. Pambuccian, and Amy P. Skubitz. *University of Minnesota, Minneapolis, MN.*

We have previously shown that ovarian carcinoma cell adhesion toward mesothelial cell monolayers and migration toward the extracellular matrix (ECM) proteins fibronectin, type IV collagen, and laminin is partially mediated by CD44. CD44 and other highly glycosylated proteoglycans have been shown to affect the functional abilities of ovarian carcinoma cells. The purpose of this study was to determine the role of cell membrane glycosylation in the adhesive and migratory abilities of ovarian carcinoma cells. Single-cell suspensions of radiolabeled NIH: OVCAR5 human ovarian carcinoma cells were treated with neuraminidase, chondroitinase ABC, or hyaluronidase to remove carbohydrate moieties from molecules on the surface of the cells. The adhesive abilities of the treated cells was tested with an *in vitro* adhesion assay in which 96-well plates were coated with fibronectin, type IV collagen, laminin, or confluent monolayers of LP-9 human peritoneal mesothelial cells. The radiolabeled, glycosidase-treated ovarian carcinoma cells were then monitored for their adhesive abilities. In addition, glycosidase-treated ovarian carcinoma cells were tested for their ability to migrate toward fibronectin, type IV collagen, or laminin in modified Boyden chambers. We observed that neuraminidase pretreatment had no effect on ovarian carcinoma cell adhesion, but decreased the cells' migration toward the ECM proteins. Chondoitinase ABC treatment decreased adhesion of ovarian carcinoma cells to fibronectin, laminin, and mesothelial cell monolayers, yet increased cell migration toward the ECM proteins. The removal of CD44's chief ligand, hyaluronan, by hyaluronidase treatment increased adhesion of ovarian carcinoma cells to the ECM proteins and mesothelial cell monolayers, but had no effect upon cell migration. Taken together, these results suggest that the glycosylation of ovarian carcinoma cell membrane proteoglycans affects the cells' ability to adhere and migrate toward ECM proteins and mesothelial cell monolayers, and may affect the formation and spread of secondary tumor growth.

#1830 Versican-containing fibroblast conditioned medium inhibits prostate cancer cell adhesion to fibronectin but not laminin. David J. Horsfall, Andrew J. Sakko, Carmela Ricciardelli, Keiko Mayne, Wayne D. Tilley, and Villis R. Marshall. *Dept of Surgery, Flinders University of South Australia, Bedford Park, Australia.*

Versican, a large chondroitin sulfate proteoglycan synthesized by stromal fibroblasts, including prostatic fibroblasts, is a candidate prognostic marker for prostate cancer. Increased deposition of versican into extracellular matrix of peritumoral stroma is associated with early relapse of patients treated by radical surgery for presumed organ-confined prostate cancer. Although versican is a recognised anti-cell adhesive molecule for various mesenchymal cell types including fibroblasts, smooth muscle and nerve cells and hence reportedly modulates cell motility, the effect of versican on the attachment of prostatic adenocarcinoma cells to components of extracellular matrix is unknown. In this study, conditioned medium from *in vitro* cultured prostate fibroblasts, containing unpurified native versican, was found to inhibit the attachment of LNCaP, PC3 and DU145 prostate cancer cells to fibronectin-coated, but not laminin-coated surfaces. Partial characterization of the bioactive molecule(s) present in prostate fibroblast conditioned medium revealed that chondroitin sulfate side chains were essential for inhibition of prostate cancer cell attachment to fibronectin. Furthermore, the fibronectin peptide sequence RGD partially reversed the inhibition of prostate cancer cell attachment, indicating the specificity of cellular binding. These data support versican being involved in modulating prostate cancer cell attachment to extracellular matrix. Because versican apparently modulates cancer cell adhesion to fibronectin but not laminin, it is possible that *in vivo* versican may promote local invasion of prostatic stroma by prostate cancer cells, rather than penetration of the basement membrane.

#1831 The molecular basis of inflammatory breast carcinoma. Sanford H. Barsky and Mary L. Alpaugh. *UCLA School of Medicine, Los Angeles, CA.*

Inflammatory breast cancer (IBC) is a poorly understood, little studied form of breast cancer which is very aggressive and particularly devastating in disadvantaged minority women. IBC is characterized by florid tumor emboli within lymphovascular spaces, a phenotype which distinguishes it from other forms of breast cancer. Using a novel human-scid model of IBC, we have conceptually divided this phenotype into three parts: 1) The tumor cell embolus (IBC spheroid) forms on the basis of an intact and overexpressed E-cadherin / α,β-catenin axis which mediates tumor cell-tumor cell adhesion analogous to the embryonic blastocyst and accounts for both the compactness of the embolus and its complete dissolution with anti-E-cadherin antibodies, absent Ca++, or E-cadherin dominant-negative mutant approaches. Dissolution of the tumor cell embolus by any of these approaches induces apoptosis via an anoikis pathway. The compactness of the embolus results in its resistance to chemotherapy / radiation therapy and its efficiency at metastasis formation and therefore therapeutic strategies which disadhere it are highly desirable. 2) The tumor cell embolus (IBC spheroid), in contrast, fails to bind the surrounding vascular endothelial cells because of decreased sialyl-Lewis X/A carbohydrate ligand-binding epitopes on its overexpressed MUC1 which are necessary for binding endothelial cell E-selectin. This natural tumor cell-endothelial cell aversion of the tumor cell embolus (IBC spheroid) further contributes to the compactness of the IBC spheroid and a phenomenon we term passive metastasis. 3) The tumor cell embolus finds itself within the vascular lumen in the first place because it stimulates a vascular channel to form around it rather than intravasating into pre-existing lymphatics or capillaries. The enveloping vascular channel does not form from angiogenesis but rather from vasculogenesis as evidenced by experiments where tumor cell emboli (IBC spheroids) are mixed with murine embryonal fibroblasts labeled with green fluorescent protein (GFP) and injected into scid mice. GFP-labeled fibroblasts initially devoid of endothelial cell markers are observed within the tumor stroma; tumor emboli are also observed within lymphovascular spaces where the lining

Appendix #4
Amy P.N. Skubitz

Kathryn M. Burleson

Comparison of Ovarian Carcinoma Multicellular Spheroids From Cell Lines and Patient Ascites: Do Spheroids Have Metastatic Potential?

Kathryn M. P. Burleson* 1, Rachael C. Casey 1, Stephan E. Pambuccian 1, Keith M. Skubitz 2, Theodore R. Oegema, Jr. 3, and Amy P.N. Skubitz 1
From the Departments of Laboratory Medicine and Pathology 1, Medicine 2, and Orthopedic Surgery 3, University of Minnesota, Minneapolis, Minnesota

The role that ovarian carcinoma multicellular spheroids, generally considered non-adhesive, play in the metastatic process has yet to be determined. Previously, we have shown that the NIH:OVCAR5 ovarian carcinoma cell line forms spheroids comparable to the multicellular aggregates recovered from the ascites fluid of ovarian carcinoma patients. These NIH:OVCAR5 cell spheroids adhere to laminin, fibronectin, and type IV collagen. This adhesion is partially mediated by the α2, α5, α6, and β1 integrin subunits. In this study, we demonstrate that spheroids isolated from the ascites fluid of patients with ovarian carcinoma are capable of adhering to extracellular matrix molecules, and that both NIH:OVCAR5 and ascites spheroids adhere to mesothelial monolayers in vitro. Spheroids isolated from the ascites fluid of eleven ovarian carcinoma patients were tested for their ability to adhere to extracellular matrix proteins. Most ascites spheroid samples had moderate adhesion toward fibronectin, and reduced adhesion to laminin or type IV collagen. Monoclonal antibodies against the β1 integrin subunit partially inhibited adhesion to all three proteins, suggesting that the β1 integrin subunit plays only a partial role in ascites spheroid adhesion. Furthermore, NIH:OVCAR5 and patient ascites spheroids adhered to live, but not fixed, mesothelial monolayers at a greater rate than to extracellular matrix proteins. These results suggest that ascites multicellular spheroids have limited adhesive ability partially reliant on integrin-ligand interactions. This adhesion may be enhanced by interaction with the cells lining the mesothelium, implicating spheroids as a potential source of secondary tumor growth in ovarian carcinoma.

Presented at AACR meeting "Pathobiology of Cancer Workshop"
Keystone, CO

Appendix #5
Amy P.N. Skubitz

Ovarian Carcinoma Ascites Spheroids Are Capable of Adhesion to Extracellular Matrix Proteins and Mesothelial Monolayers

Kathryn M. Burleson[§], Rachael C. Casey[§], Suzanne M. Grindle, Stephan E. Pambuccian[§], Keith M. Skubitz[†], Theodore R. Oegema, Jr.[‡], and Amy P.N. Skubitz[§]
From the Departments of Laboratory Medicine and Pathology[§], Medicine[†], and Orthopedic Surgery[‡], University of Minnesota, Minneapolis, Minnesota

Ovarian carcinoma cells form multicellular aggregates, or spheroids, in the peritoneal cavity of patients with late-stage disease. Spheroids tend to be overlooked in the metastatic process of ovarian carcinoma, and their adhesive abilities have yet to be determined. Previously, we have shown that spheroids can be generated *in vitro* using the NIH:OVCAR5 ovarian carcinoma cell line, and form multicellular aggregates similar to those recovered from the ascites fluid of ovarian carcinoma patients. NIH:OVCAR5 spheroids are capable of adhesion to laminin, fibronectin, and type IV collagen, and their adhesion is partially mediated by the α2, α5, α6, and β1 integrin subunits. In this study, ovarian carcinoma ascites spheroids from eleven patients were tested for their ability to adhere to extracellular matrix proteins, and were sorted into three groups depending on their adhesiveness. Most ascites samples showed moderate adhesion to fibronectin, and reduced adhesion to type IV collagen or laminin. Monoclonal antibodies against the β1 integrin subunit partially inhibited adhesion to all three proteins, implying that the β1 integrin subunit plays a partial role in the adhesion of ascites spheroids. Additionally, NIH:OVCAR5 and patient ascites spheroids adhered to live, but not fixed, mesothelial monolayers, at higher levels than to extracellular matrix proteins alone. We examined the gene expression of ovarian cancer ascites samples, and solid tissues from primary ovarian carcinomas, secondary ovarian carcinomas, and normal ovaries. RNA was prepared and gene expression was determined at Gene Logic Inc. (Gaithersburg, MD) using Affymetrix GeneChip® U 95 arrays. Gene expression analysis was performed with Gene Logic GeneExpress® Software System. A gene set of approximately 200 genes was generated to compare the expression of cell adhesion molecules, including integrins, proteoglycans, glycoproteins, glycosaminoglycans, extracellular matrix molecules, and basement membrane proteins. Hierarchical clustering of the samples using the cell adhesion gene set segregated the ascites samples into three distinct adhesion groups, corresponding to the results we obtained from the adhesion assays. The results suggest that ascites spheroids have a limited adhesive ability toward extracellular matrix proteins, which is partially dependent on integrin-ligand interactions. Furthermore, the variation in adhesion between ascites samples may be due to altered cell adhesion molecule expression between ovarian cancer patients. This adhesion may be further enhanced by interaction with the cells lining the mesothelium, thus implicating spheroids as a potential metastatic threat in ovarian carcinoma.

Presented at the AACR Special Conference in Cancer Research, "Proteases, Extracellular Matrix, and Cancer" October 9-13, 2002
The Westin Resort, Hilton Head Island, SC

American Journal of Pathology, Vol. 159, No. 6, December 2001

10

β1-Integrins Regulate the Formation and Adhesion of Ovarian Carcinoma Multicellular Spheroids

Rachael C. Casey,* Kathryn M. Burleson,* Keith M. Skubitz,† Stefan E. Pambuccian,* Theodore R. Oegema, Jr.,‡ Laura E. Ruff,* and Amy P. N. Skubitz*

From the Departments of Laboratory Medicine and Pathology, Medicine,† and Orthopaedic Surgery,‡ University of Minnesota, Minneapolis, Minnesota*

Ovarian carcinoma multicellular spheroids are an *in vitro* model of micrometastasis whose adhesive abilities have not been elucidated. In this study, we identified adhesion molecules that mediate the formation of ovarian carcinoma spheroids and their subsequent adhesion to extracellular matrix proteins. The NIH:OVCAR5, but not the SKOV3, ovarian carcinoma cell line formed spheroids similar to multicellular aggregates isolated from patient ascitic fluid. NIH:OVCAR5 spheroid formation was augmented by a β1-integrin-stimulating monoclonal antibody or exogenous fibronectin, but was inhibited by blocking monoclonal antibodies against the α5- or β1-integrin subunits. By immunohistochemical staining, α2-, α3-, α5-, α6-, and β1-integrin subunits, CD44, and fibronectin were detected in NIH:OVCAR5 spheroids. NIH:OVCAR5 spheroids adhered to fibronectin, laminin, and type IV collagen, and this adhesion was partially inhibited by blocking antibodies against the α5-, α6-, and α2-integrin subunits, respectively. A blocking monoclonal antibody against the β1-integrin subunit completely inhibited adhesion of the spheroids to all three proteins. These results suggest that interactions between the α5β1-integrin and fibronectin mediate the formation of ovarian carcinoma spheroids and that their adhesion to extracellular matrix proteins at sites of secondary tumor growth may be mediated by a complex interaction between multiple integrins and their ligands. *(Am J Pathol 2001, 159:2071–2080)*

Ovarian cancer is the leading cause of gynecological malignancy and the fifth leading cause of cancer death among women in the United States.[1] In ovarian carcinoma, cancer cells detach from the surface of the tumor into the peritoneal cavity. Subsequent peritoneal implants are characterized by the adhesion, migration, and invasion of the tumor cells into the peritoneum and underlying organs. Free-floating tumor cells are found in the peritoneal cavity both as both single cells and as multicellular aggregates.[2] However, because they are difficult to study and manipulate compared to single-cell suspensions, ovarian carcinoma multicellular aggregates have been primarily ignored in most studies.

Many human tumor cells and cell lines can be cultured as multicellular aggregates, which are spherical, mechanically stable, and viable.[3] Early *in vitro* studies indicated that ovarian carcinoma tumor cells and cell lines were unable to form spheroids, but remained exclusively as free-floating single cells or formed monolayers in tissue culture.[4] More recently, spheroids have been successfully generated from some ovarian cancer cells and cell lines, and used as three-dimensional *in vitro* models to study the efficacy of therapeutic strategies.[5–7] Cells in ovarian carcinoma spheroids exhibit changes in their position in the cell cycle and are protected from radiation-induced[5,6] and taxol-induced[8,9] apoptosis, compared to cells cultured as monolayers. However, the phenomena that mediate the formation of ovarian carcinoma multicellular spheroids and their subsequent abilities to adhere, migrate, invade, and proliferate at secondary growth sites have not been investigated, and their contributions to secondary tumor growth, if any, have not been assessed. It still remains unclear whether the floating multicellular aggregates found in patients' ascites fluid are capable of adhering to the extracellular matrix (ECM) of mesothelial cells or whether they are merely nonadhesive, and therefore noninvasive or benign, counterparts to the malignant ovarian carcinoma cells that adhere to the peritoneal lining.

Many cell-cell and cell-matrix interactions are regulated by integrins, a family of heterodimeric transmembrane receptors.[10] ECM proteins, which include fibronectin, type IV collagen, and laminin, affect the *in vitro* growth, morphology, survival, and differentiation of normal and malignant cells via their interactions with inte-

Supported by a Cancer Biology Training grant from the National Institutes of Health/National Cancer Institute (CA09138-25 to R. C. C.), a grant from the Department of the Army (DA/DAMD17-99-1-9564), a grant from the Minnesota Medical Foundation (SMF-2078-99), and a Grant-in-Aid of Research from the Office of the Vice President for Research and Dean of the Graduate School of the University of Minnesota (no. 18118).

The content of the information presented in this manuscript does not necessarily reflect the position of the United States Government.

Accepted for publication August 17, 2001.

Address reprint requests to Dr. Amy P. N. Skubitz, Department of Laboratory Medicine and Pathology, MMC 609, 420 Delaware St. SE, University of Minnesota, Minneapolis, MN 55455. E-mail: skubi002@tc.umn.edu.

grins.[11] In ovarian carcinoma, integrins have been shown to mediate the organization of ECM,[12] adhesion to ECM components,[13–15] and cell motility.[16–18] Integrins have also been shown to mediate interactions between ovarian carcinoma cells and the mesothelial cells that line the abdominal organs.[15] CD44, another cell surface receptor found on ovarian carcinoma cells,[15,18,19] binds the ECM glycosaminoglycan hyaluronan with high affinity[20] and also has a weak affinity for fibronectin, type IV collagen, and laminin.[21] Interactions between CD44 and hyaluronan affect cell adhesion,[15] migration,[18,19] and tumor growth[22] in ovarian carcinoma cells.

The purpose of this study was to elucidate the biological properties of ovarian carcinoma spheroids by developing an *in vitro* model from established ovarian carcinoma cell lines. We examined the roles of integrins, CD44, and ECM proteins in the formation of ovarian carcinoma spheroids. The proliferative ability and viability of ovarian carcinoma cells cultured as spheroids were also determined and compared to that of the same cell lines cultured as monolayers. We examined the expression of adhesion molecules in NIH:OVCAR5 spheroids. We assessed the ability of ovarian carcinoma spheroids to adhere to ECM molecules and identified integrin subunits that mediated these interactions. The results from this study identify adhesion molecules that participate in the formation of ovarian carcinoma spheroids and suggest that their subsequent adhesion to secondary sites of tumor growth may be integrin-dependent events. Our findings suggest that ovarian carcinoma cells present as free-floating multicellular aggregates may exhibit markedly different behavior than ovarian carcinoma single cells or monolayers. It is possible that these differences may then translate into different metastatic abilities *in vivo* and/or responses to treatments.

Materials and Methods

Unless otherwise stated, all standard reagents and materials were obtained from Sigma Chemical Company (St. Louis, MO), all pictures were photographed with a Nikon Coolpix 950 camera (Melville, NY), and all experiments were performed in triplicate and repeated a minimum of three times.

Cell Culture

The human ovarian carcinoma cell lines NIH:OVCAR5 and SKOV3 were chosen for their ability to mimic the progression of ovarian carcinoma when injected into *in vivo* mouse models.[23] These cells have also been shown to adhere to peritoneal mesothelial cells in *in vitro* models.[24,25] The ovarian carcinoma cell line SKOV3 was obtained from Dr. Robert Bast, Jr., M.D. Anderson Cancer Center, University of Texas, Houston, TX. These cells were maintained in McCoy's 5A medium supplemented with 15% fetal bovine serum, 2 mmol/L L-glutamine, and 50 U/ml penicillin G/streptomycin (Life Technologies, Grand Island, NY). The ovarian carcinoma cell line NIH:OVCAR5 was originally established by Dr. Thomas Hamilton (Fox Chase Cancer Center, Philadelphia, PA)[26] and obtained from Dr. Judah Folkman, Harvard Medical School, Boston, MA. This cell line was maintained in RPMI 1640 medium supplemented with 10% fetal bovine serum, 2 mmol/L L-glutamine, 0.2 U/ml insulin, and 50 U/ml penicillin G/streptomycin. Both cell lines were maintained in 75-mm^2 tissue culture flasks in a humidified incubator with 5% CO_2 at 37°C.

Purification of Primary Ovarian Carcinoma Cells

Primary ascites fluid samples from six patients diagnosed with serous ovarian adenocarcinoma were obtained with the approval of the University of Minnesota Institutional Review Board from the University of Minnesota Cancer Center Tissue Procurement Facility. Tumor cells were collected by centrifugation (1000 × *g*, 10 minutes). To lyse erythrocytes, the cells were resuspended in 10 mmol/L potassium bicarbonate, 155 mmol/L ammonium chloride, 0.1 mmol/L ethylenediaminetetraacetic acid, pH 7.4, for 5 minutes. The remaining cells were collected by centrifugation (1000 × *g*, 10 minutes). The tumor cells were layered on Ficoll-Paque Plus (Pharmacia Biotech, Uppsala, Sweden) and centrifuged at 2000 × *g* for 15 minutes. The tumor cells were removed from the top of the Ficoll layer and washed with RPMI 1640 medium.

Spheroid Culture

The method used to generate spheroids was based on the liquid overlay technique.[27] To prohibit cell adhesion to a substratum, the wells of 24-well tissue culture plates (Becton Dickinson, Franklin Lakes, NJ) were coated with 200 μl of 0.5% SeaKem LE agarose (BioWittaker Molecular Applications, Rockland, ME) in serum-free media, and allowed to solidify for 30 minutes at 20°C. NIH:OVCAR5 or SKOV3 cells were grown in monolayer cultures, released with 0.5% trypsin, 2 mmol/L ethylenediaminetetraacetic acid as described previously,[28] and resuspended in complete cell culture media at 5000 to 50,000 cells/ml. Cell suspensions were layered onto the top of the solid agarose-coated plates at a volume of 1 ml/well, and then incubated for 48 hours at 37°C. By this technique, cells remained afloat in the media, and did not become incorporated or implanted in the solidified agarose that coats the wells of the 24-well plates. After 48 hours, the resulting spheroids were gently removed from the surface of the solidified agarose and centrifuged at 300 × *g* for 3 minutes to remove single cells before use in subsequent experiments.

Antibodies

Purified monoclonal antibodies (mAbs) that block the adhesive activity of human integrin subunits α1 (clone FB12), α2 (clone P1E6), α3 (clone P1B5), α4 (clone P1H4), α5 (clone P1D6), α6 (clone GoH3), and αvβ3 (clone LM609) were purchased from Chemicon International (Temecula, CA). A purified mAb against the human β1-integrin subunit that stimulates cell adhesion to ECM

proteins (clone 21C8) was also purchased from Chemicon International. Purified immunoglobulin (IgG) of mouse mAb P5D2, which blocks the adhesive activity of human β1-integrin subunits, was provided by Dr. Leo Furcht (University of Minnesota). Affinity-purified IgG of mAb IM7, which blocks the hyaluronan-binding site of CD44, was purchased from Pharmingen (San Diego, CA). Polyclonal rabbit IgG against human fibronectin was purchased from Calbiochem-Novabiochem Corporation (San Diego, CA). Normal mouse IgG and normal goat serum were purchased from Sigma.

ECM Molecules

Type IV collagen, isolated from mouse Engelbreth-Holm-Swarm tumor, was purchased from Life Technologies. Mouse Engelbreth-Holm-Swarm laminin, prepared as previously described,[29] was provided by Dr. Leo Furcht, University of Minnesota. Human plasma fibronectin, purified as described,[30] was provided by Dr. James McCarthy, University of Minnesota.

Proliferation Assays

Single-cell suspensions of NIH:OVCAR5 or SKOV3 cells were added to 24-well tissue culture plates to form monolayers, or to agarose-coated 24-well plates to form spheroids, at a density of 500 cells/200 μl. The cells were cultured in complete cell culture media for up to 21 days. At various time points, 2 mg/ml WST-1 (Boehringer-Mannheim Corporation, Indianapolis, IN) was added to each well and incubated for 2 hours. WST-1 is a tetrazolium salt that is reduced by mitochondrial dehydrogenases to form a formazan dye. The formazan product was quantitated by a SpectaMax 250 scanning multiwell spectrophotometer (Molecular Devices Corporation, Sunnyvale, CA) by measuring absorbance at 450 nm. These experiments were performed in quadruplicate.

Role of Adhesion Molecules in Multicellular Aggregation

To examine the role of cell surface receptors in ovarian carcinoma spheroid formation, single-cell suspensions of NIH:OVCAR5 or SKOV3 cells in serum-free media were added to agarose-coated 24-well plates at a density of 5000 cells/200 μl in the presence of 10 μg/ml of normal mouse IgG or mAbs against integrin subunits or CD44. To examine the effect ECM proteins on spheroid formation, the cells were incubated in the presence of 25 μg/ml of fibronectin, laminin, type IV collagen, or ovalbumin. The cells were incubated at 37°C for up to 24 hours in a humidified incubator, examined under a light microscope, and photographed.

Expression of Cell Surface Receptors and ECM Molecules in Spheroids

NIH:OVCAR5 spheroids were collected by centrifugation at 300 × *g* for 3 minutes and resuspended in 80 μl of expired human plasma (American Red Cross, Minneapolis, MN). To suspend the spheroids in a semisolid clot suitable for embedding, 40 μl of 10 U/ml of human thrombin was added to the suspension. Alternately, NIH:OVCAR5 spheroids were suspended in 1% agarose. After polymerization, the clots were embedded in OCT frozen embedding material (Fisher Scientific, Pittsburgh, PA) on dry-ice. Six μm-thick sections were cut on a cryostat and collected on poly-L-lysine-coated slides. The sections were washed with phosphate-buffered saline (PBS), pH 7.6, and blocked with normal goat serum for 30 minutes. The samples were then incubated with 1 μg/ml of the primary mouse IgG for 1 hour, followed by incubation with the secondary goat anti-mouse biotinylated antibody for 30 minutes. Endogenous peroxidase was quenched by incubating the sections in 0.3% H_2O_2 in PBS for 30 minutes. The sections were incubated for 30 minutes with Vectastain ABC reagent (Vector Laboratories, Burlingame, CA) and developed with the peroxidase substrate solution to obtain optimal color. The enzymatic reaction was quenched with excess PBS, and the sections were fixed in 2% formaldehyde, followed by mounting with Cytoseal (Fisher Scientific), and examination under a light microscope. In some cases, the samples were counterstained with methyl green stain (Vector Laboratories) according to the manufacturer's instructions.

Adhesion Assays

Glass chamber slides (Nalge Nunc International, Naperville, IL) were coated with 50 μg/ml of fibronectin, laminin, type IV collagen, or ovalbumin in PBS for 16 hours at 37°C. The slides were blocked with 2 mg/ml ovalbumin in PBS for 1 hour at 37°C. Approximately 50 to 80 NIH:OVCAR5 spheroids in 200 μl of serum-free medium were added to the slides and incubated for up to 4 hours at 37°C. The total number of spheroids in each sample was manually counted, and then nonadherent cells were gently rinsed off with PBS. Adherent cells were fixed with 2% formaldehyde in PBS, stained with Diff-Quik (Dade Behring Inc., Newark, DE), sealed with Cytoseal, and manually counted under a light microscope.

Inhibition of Spheroid Adhesion

NIH:OVCAR5 spheroids were allowed to adhere to glass chamber slides as described above, except that the spheroids were incubated in the presence of 10 μg/ml of normal mouse IgG or mAbs against the α2-, α5-, α6-, or β1-integrin subunits, or CD44. After a 2-hour incubation, the total number of spheroids that were present in each chamber was manually counted before the nonadherent cells were removed as described above. The adherent spheroids were fixed, stained, manually counted, and expressed as a percentage of the total spheroids initially added to each chamber.

Statistical Analysis

Student's *t*-test was performed as a test of significance with the use of Microsoft Excel 1997 (Microsoft Co., Red-

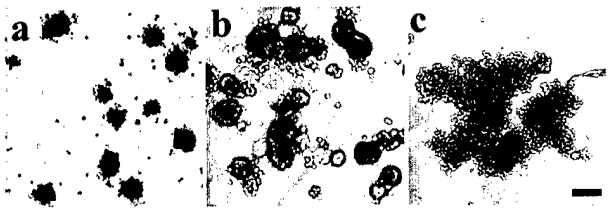

Figure 1. Ovarian carcinoma spheroid formation. Ovarian carcinoma cells obtained from patients' ascitic fluid, the NIH:OVCAR5 ovarian carcinoma cell line, or the SKOV3 ovarian carcinoma cell line were cultured in 0.5% agarose-coated 24-well plates at a density of 20,000 cells/well for 48 hours then photographed. These pictures were representatives of ovarian carcinoma cells obtained from one of the six different patients diagnosed with serous ovarian carcinoma (**a**), the NIH:OVCAR5 cell line (**b**), and the SKOV3 cell line (**c**). Scale bar, 250 μm.

mond, WA). *P* values of <0.01 were considered to indicate statistically significant differences.

Results

Formation of Ovarian Carcinoma Spheroids

Multicellular aggregates of ovarian carcinoma cells were observed in the ascitic fluid obtained from six different patients diagnosed with stage III or stage IV ovarian carcinoma. The sizes of the multicellular aggregates in the patient samples ranged from 50 to 750 μm in diameter; a representative sample is shown in Figure 1a. All of the patients' samples contained spheroids of varying sizes, and the range of sizes of the spheroids varied from patient to patient. Typically, however, the spheroids ranged in size from a score of – to ++ (see Table 1), with the majority of the spheroids scoring as ++. It was not possible to disaggregate these spheroids into a single-cell suspension, even when the spheroids were physically manipulated (via repetitive pipetting) and treated with trypsin (not shown).

Ovarian carcinoma cell lines were cultured in agarose-coated plates to determine whether spheroid phenotypes could be generated in the absence of an adhesive substratum. After 48 hours, the NIH:OVCAR5 ovarian carcinoma cell line formed spheroids (Figure 1b) that appeared similar to the multicellular aggregates found in ovarian carcinoma patients' ascites samples (Figure 1a) and were similarly resistant to physical manipulation and trypsin treatment. In addition, like the multicellular aggregates obtained from the patients' ascites samples, NIH:OVCAR cells formed spheroids of varying sizes that ranged from 60 to 400 μm in diameter, with a score of ++ in size.

In contrast, the SKOV3 ovarian carcinoma cell line formed irregular multicellular aggregates (Figure 1c) that dispersed when subjected to mild agitation. These SKOV3 cell aggregates were significantly larger than those found in patients' ascites samples; SKOV3 spheroids contained hundreds of cells and scored as +++ by our criteria (Table 1). In all cases, the cells were viable, as determined by trypan blue staining (data not shown).

Table 1. Quantitation of Spheroid Formation

Number of cells in spheroid	Score	Description of spheroid
1	–	None
2 to 5	+	Small
6 to 20	++	Medium
>20	+++	Large

In order to maintain the ovarian carcinoma cells in suspension and prohibit cell adhesion to the bottom of tissue culture plates, the wells of 24-well tissue culture plates were coated with agarose and allowed to solidify as described in the Materials and Methods section. Cell suspensions were layered onto the top of the solid agarose, and then incubated for 48 hours at 37°C. By this technique, cells remained afloat in the media, and did not become incorporated or implanted in the solidified agarose that coated the wells. After 48 hours, the resulting spheroids were gently removed from the surface of the solidified agarose and centrifuged to remove single cells before use in subsequent experiments. The sizes of the spheroids formed in the experiments were quantified based on the above scoring system.

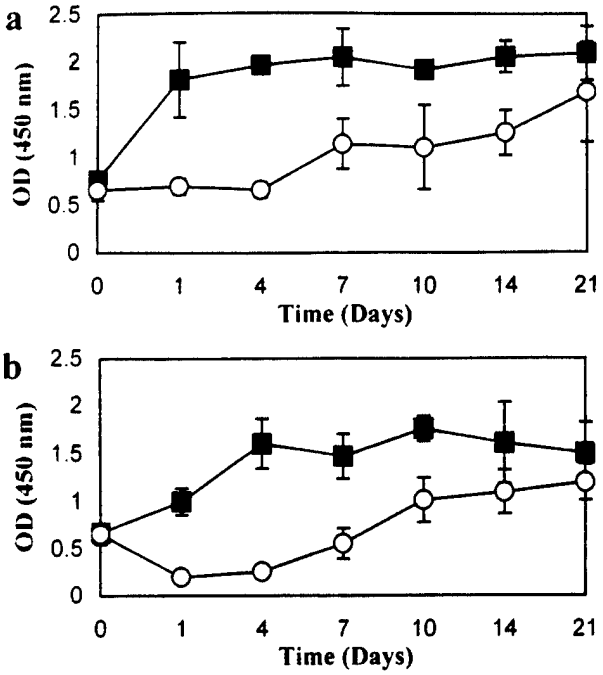

Figure 2. Proliferative index of ovarian carcinoma cells grown as monolayers or spheroids. NIH:OVCAR5 (**a**) and SKOV3 cells (**b**) were added to agarose-coated wells at a concentration of 500 cells/well and cultured as spheroids (**open circles**) or as monolayers (**filled squares**) for up to 21 days. The level of proliferation was quantitated as described in the Material and Methods. Data are expressed are mean ± SD.

Aggregation into Multicellular Spheroids Decreases the Proliferative Abilities of Ovarian Carcinoma Cell Lines

To more fully examine the effects of multicellular aggregation on the viability and proliferative ability of the cells, NIH:OVCAR5 and SKOV3 cells were cultured as monolayers or multicellular aggregates for up to 21 days (Figure 2). When cultured in tissue culture-treated plates as monolayers, the proliferation rates of the NIH:OVCAR5 cells (Figure 2a, filled squares) and SKOV3 cells (Figure 2b, filled squares) increased until 4 days, when confluence was achieved. In striking contrast, the proliferative rates of both NIH:OVCAR5 cells (Figure 2a, open circles) and SKOV3 cells (Figure 2b, open circles) cultured in

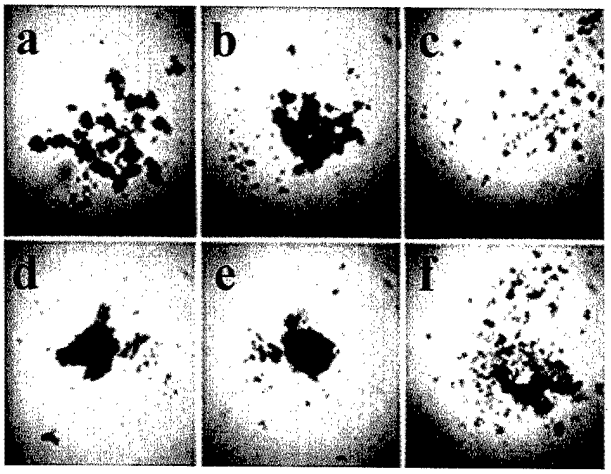

Figure 3. Formation of ovarian carcinoma spheroids is mediated by β1-integrins. Single-cell suspensions of NIH:OVCAR5 cells at a density of 5000 cells/200 μl were added to agarose-coated wells for 8 hours (**a–c**) or 24 hours (**d–f**). The cells were incubated in serum-free medium (**a** and **d**) or in the presence of 10 μg/ml of a mAb that stimulates β1-integrin subunits (**b** and **e**), or 10 μg/ml of a mAb that blocks β1-integrin subunits (**c** and **f**). Scale bar, 250 μm.

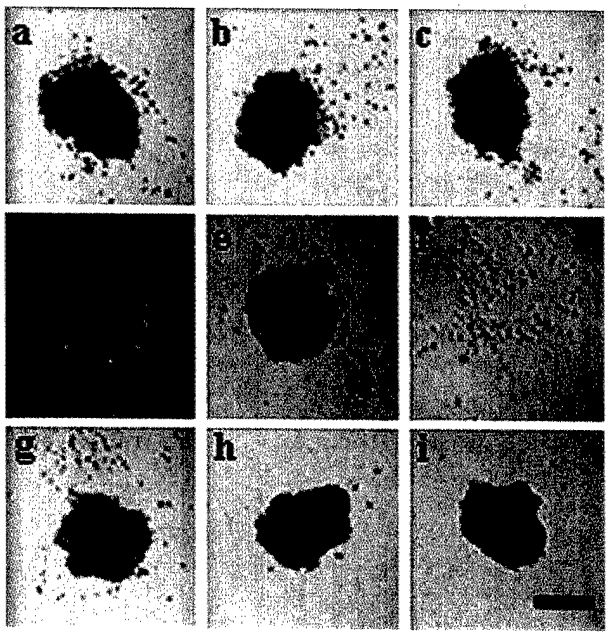

Figure 4. Formation of ovarian carcinoma spheroids is mediated by the α5-integrin subunit. NIH:OVCAR5 cells at a density of 5000 cells/200 μl were added to agarose-coated wells in serum-free medium in the presence of 10 μg/ml of mouse IgG (**a**) or 10 μg/ml of blocking mAbs against the α1-integrin subunit (**b**), α2-integrin subunit (**c**), α3-integrin subunit (**d**), α4-integrin subunit (**e**), α5-integrin subunit (**f**), α6-integrin subunit (**g**), integrin αvβ3 (**h**), or CD44 (**i**) for 16 hours. Scale bar, 500 μm.

agarose-treated 24-well plates, which prohibited the adhesion of the cells to a substratum, were initially much lower. The proliferative rates of the NIH:OVCAR5 spheroids and the SKOV3 multicellular aggregates slowly increased until they approached that of the monolayers by 21 days. The multicellular aggregates and monolayers that formed were viable, as determined by trypan blue and propidium iodide staining, which identify dead cells, and immunohistochemical staining for annexin V, which identifies apoptotic cells (data not shown). Furthermore, samples were inspected under a light microscope to ensure nearly complete incorporation of cells into spheroids and that monolayers had not formed either beneath or atop the agarose applied to the wells (not shown).

Spheroid Formation Is Mediated by α5- and β1-Integrin Subunits

We have previously shown that β1-integrin subunits mediate the adhesion of single-cell suspensions of ovarian carcinoma cells to ECM molecules and mesothelial cells.[15] We therefore hypothesized that β1-integrins also play a role in ovarian carcinoma spheroid formation. Single-cell suspensions of NIH:OVCAR5 cells were incubated in serum-free medium in the presence or absence of mAbs that blocked or stimulated the β1-integrin subunit for up to 24 hours (Figure 3). At 8 hours, spheroids began to form in serum-free medium (Figure 3a), scored as ++. Spheroid formation was accelerated by a mAb that stimulates the adhesive abilities of human β1-integrin subunits (Figure 3b), scored as +++. Spheroid formation was inhibited by a mAb that blocks the binding site of the β1-integrin subunit (Figure 3c), scored as +/−. At 24 hours, large spheroids, scored as +++, had formed in serum-free medium (Figure 3d) and in the presence of the β1-integrin-stimulating mAb (Figure 3e). The β1-integrin-blocking mAb continued to partially retard spheroid formation (Figure 3f), scored as ++/+++. These mAbs had similar effects on the aggregation of SKOV3 cells into multicellular aggregates (not shown). These data suggest that β1-integrin subunits may mediate the initial formation of ovarian carcinoma spheroids.

We have previously shown that α-integrin subunits and CD44 also mediate the adhesion of ovarian carcinoma cells to ECM molecules and mesothelial cells.[15] To determine the role of these cell surface receptors in ovarian carcinoma spheroid formation, single-cell suspensions of

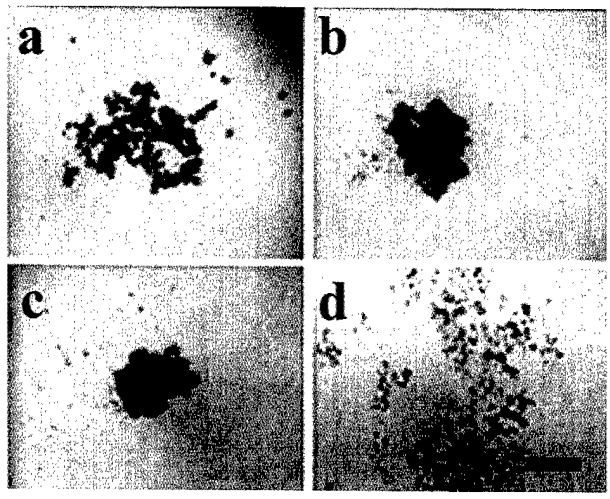

Figure 5. Addition of exogenous ECM proteins alters the formation of ovarian carcinoma spheroids. A single-cell suspension of NIH:OVCAR5 cells at a density of 5000 cells/200 μl was cultured in agarose-coated plates in serum-free medium with 25 μg/ml of ovalbumin (**a**), fibronectin (**b**), laminin (**c**), or type IV collagen (**d**) for 16 hours and then photographed. Scale bar, 250 μm.

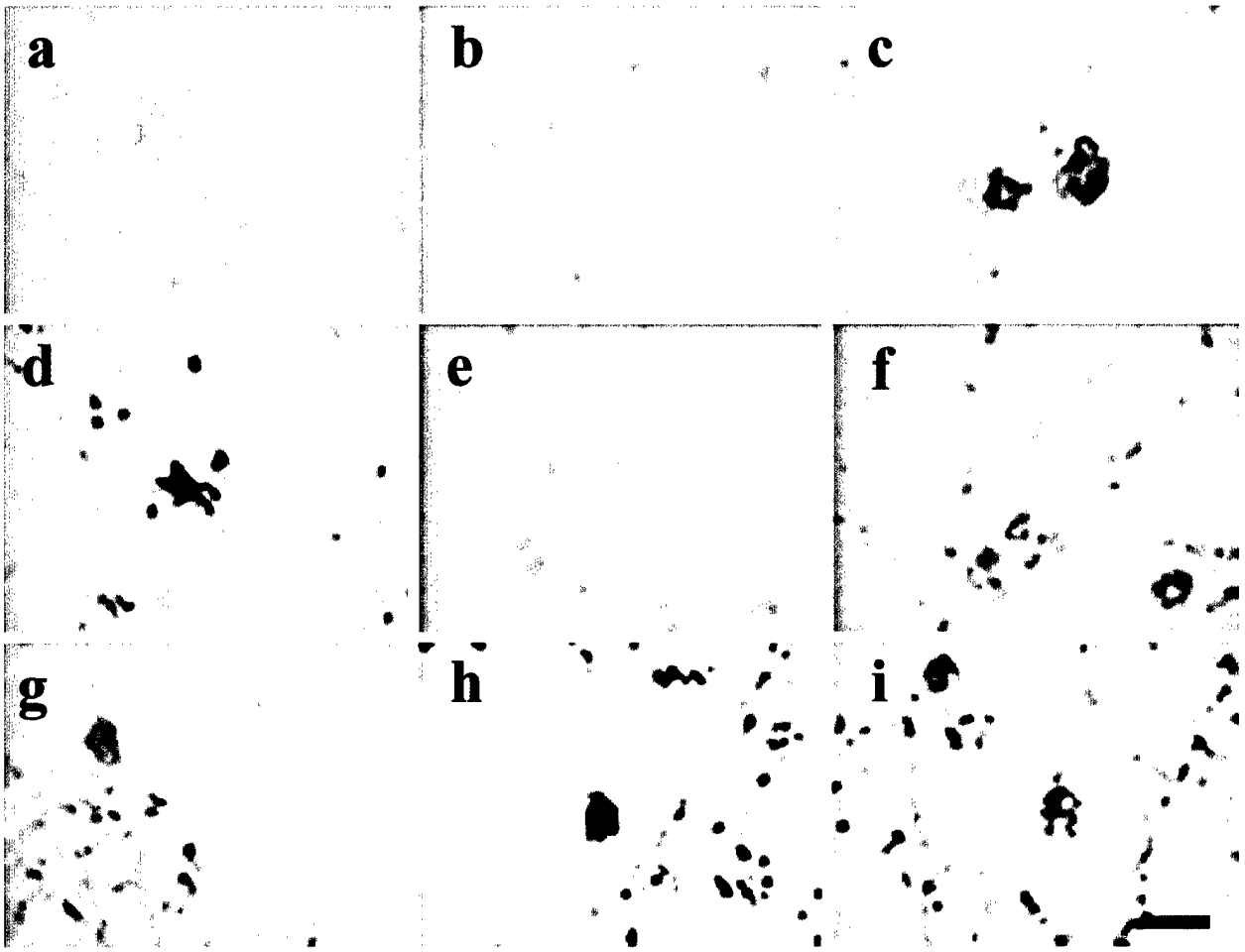

Figure 6. Spheroids express adhesion molecules. NIH:OVCAR5 spheroids were suspended in thrombin clots, embedded in OCT, sectioned at 6 μm thick, and stained with mouse IgG (**a**) or mAbs against the α1-integrin subunit (**b**), α2-integrin subunit (**c**), α3-integrin subunit (**d**), α4-integrin subunit (**e**), α5-integrin subunit (**f**), α6-integrin subunit (**g**), β1-integrin subunit (**h**), or CD44 (**i**). Scale bar, 1 mm.

NIH:OVCAR5 cells were incubated in serum-free medium in the presence of normal mouse IgG or blocking mAbs against α-integrin subunits, integrin αvβ3, or CD44 (Figure 4). Spheroid formation was inhibited by a mAb against the α5-integrin subunit (Figure 4f) and scored as +/−. In contrast, large spheroids, scored as +++, formed in the presence of normal mouse IgG (Figure 4a) or mAbs against the α1-integrin subunit (Figure 4b), α2-integrin subunit (Figure 4c), α3-integrin subunit (Figure 4d), α4-integrin subunit (Figure 4e), α6-integrin subunit (Figure 4g), integrin αvβ3 (Figure 4h), or CD44 (Figure 4i). These mAbs had similar effects on the aggregation of SKOV3 cells into multicellular aggregates (not shown). This suggests that the α5β1-integrin may mediate ovarian carcinoma spheroid formation.

To examine the effect of ECM proteins, the ligands of integrins, on spheroid formation, single-cell suspensions of NIH:OVCAR5 cells were cultured at a density of 5000 cells/well in agarose-coated wells in serum-free media in the presence of 25 μg/ml fibronectin, laminin, or type IV collagen (Figure 5). The addition of exogenous fibronectin enhanced spheroid formation (Figure 5b), scored as +++, compared to the ovalbumin control (Figure 5a), scored as +/++. Enhanced spheroid formation was also observed in the presence of laminin (Figure 5c), scored as +++, but not in the presence of type IV collagen (Figure 5d), scored as +/++. These results suggest that ECM proteins affect ovarian carcinoma spheroid formation.

Immunolocalization of Adhesion Molecules in Spheroids

The expression of integrin subunits and CD44 on NIH:OVCAR5 spheroids was analyzed by immunohistochemistry (Figure 6). The ovarian carcinoma spheroids, which were embedded in thrombin clots, stained positively for integrin subunits α2 (Figure 6c), α3 (Figure 6d), α5 (Figure 6f), α6 (Figure 6g), and β1 (Figure 6h). In addition, the ovarian carcinoma spheroids stained positively for CD44 (Figure 6i). In contrast, the integrin subunits α1 (Figure 6b) and α4 (Figure 6e) were not detected in the spheroids.

The potential interaction of the α5β1-integrin and its ligand, fibronectin, in fully formed NIH:OVCAR5 ovarian carcinoma spheroids was also assessed by immunohistochemical staining (Figure 7). Because the human plasma used to make thrombin clots contains fibronectin, the spheroids in this set of experiments were embedded

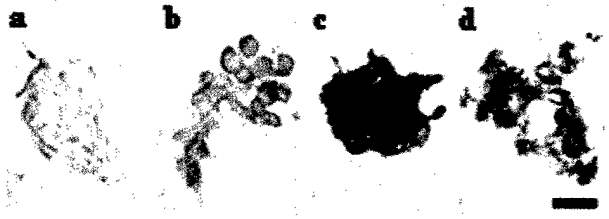

Figure 7. Localization of the α5- and β1-integrin subunits and fibronectin in spheroids. NIH:OVCAR5 spheroids were suspended in agarose clots, embedded in OCT, sectioned at 6 μm thick, and stained with normal mouse IgG (**a**), a mAb against the α5-integrin subunit (**b**), a mAb against the β1-integrin subunit (**c**), or a polyclonal antibody against fibronectin (**d**). The slides were then counterstained with methylene green. The α5- and β1-integrin subunits, as well as fibronectin, localized to the cell surface and were concentrated at points of cellular contact. Scale bar, 100 μm.

in agarose clots. Also, the samples were counterstained with methyl green stain after immunostaining. The α5- and β1-integrin subunits were detected on the surface of individual NIH:OVCAR5 cells in the spheroids (Figure 7, b and c, respectively). Fibronectin was also detected on the surface of the cells and in the ECM surrounding them (Figure 7d). This suggests that interactions between the α5β1-integrin and fibronectin may continue to mediate early adhesion events in ovarian carcinoma spheroids. No staining was observed on the surface of cells incubated in the presence of normal mouse IgG (Figure 7a).

Ovarian Carcinoma Spheroid Adhesion to ECM Proteins Is Mediated by Integrins

The ability of NIH:OVCAR5 spheroids to adhere to ECM components was assessed as a model to determine whether spheroids are inherently unable to adhere, which would explain the free-floating multicellular aggregates found in ovarian carcinoma patients' ascites fluid. Only NIH:OVCAR5 cells were used in the following series of experiments, because of their phenotypic resemblance to patient ascites cells, in that the NIH:OVCAR5 spheroids remained intact after manipulations, unlike the SKOV3 multicellular aggregates, which dispersed with even minimal manipulation. To determine the ability of ovarian carcinoma spheroids to adhere to ECM proteins, NIH:OVCAR5 spheroids were allowed to adhere to glass chamber slides coated with 50 μg/ml of fibronectin, laminin, or type IV collagen for up to 4 hours (Figure 8). Spheroid adhesion to all three ECM proteins occurred in a time-dependent manner, with maximum adhesion attained by 4 hours. Approximately 90% of the spheroids adhered to fibronectin (Figure 8, squares) and laminin (Figure 8, triangles) at 4 hours, and ~80% of the spheroids adhered to type IV collagen (Figure 8, circles) at 3 hours. The spheroids failed to adhere to chamber slides coated with ovalbumin (Figure 8, diamonds). These data suggest that ovarian carcinoma spheroids have the ability to adhere to ECM glycoproteins, despite the fact that many ovarian carcinoma multicellular aggregates are found floating in the ascitic fluid of patients and seemingly fail to adhere *in vivo*.

The role of integrin subunits in NIH:OVCAR5 spheroid adhesion toward fibronectin, laminin, and type IV collagen was investigated (Table 2). Spheroids were allowed to adhere to the ECM proteins or ovalbumin for 2 hours in the presence of blocking mAbs against integrin subunits. Spheroid adhesion to all three ECM proteins was almost completely inhibited in the presence of a blocking mAb against the β1-integrin subunit ($P < 0.001$). In addition, a mAb against the α5-integrin subunit inhibited spheroid adhesion to fibronectin by 60% ($P < 0.005$), a mAb against the α6-integrin subunit decreased spheroid adhesion to laminin by 40% ($P < 0.01$), and a mAb against the α2-integrin subunit decreased spheroid adhesion to type IV collagen by 55% ($P < 0.01$). Spheroid adhesion to all three ECM proteins was slightly increased in the presence of a β1-integrin-stimulating mAb, but was not significantly affected by blocking mAbs against the α3- or α4-integrin subunits, integrin αvβ3, or CD44 (data not shown). These results suggest that spheroid adhesion to secondary growth sites is a complex, multivalent phe-

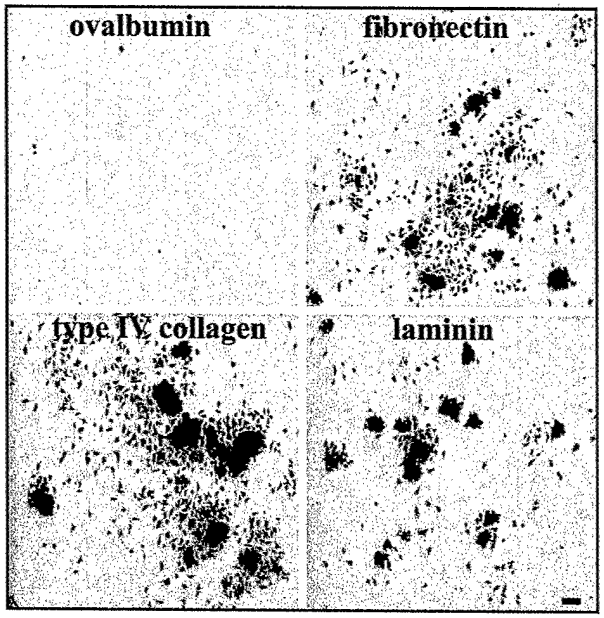

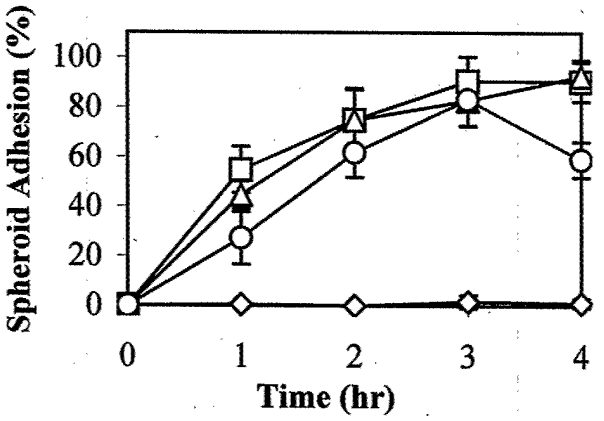

Figure 8. Adhesion of NIH:OVCAR5 spheroids to ECM proteins. NIH:OVCAR5 spheroids were incubated on glass chamber slides coated with 50 μg/ml of ovalbumin (**diamonds**), fibronectin (**squares**), laminin (**triangles**), or type IV collagen (**circles**) for up to 4 hours. Nonadherent cells were washed away, and the remaining adherent cells were fixed, stained, and photographed. Scale bar, 250 μm. Data are expressed as mean ±SD.

Table 2. Spheroid Adhesion to ECM Proteins Is Mediated by Integrins

mAb	Fibronectin	Laminin	Type IV collagen
IgG	69 ± 12	56 ± 8	55 ± 4
α2	71 ± 9	71 ± 9	24 ± 10‡
α5	25 ± 13†	50 ± 3	31 ± 8
α6	64 ± 18	35 ± 9‡	38 ± 7
β1	2 ± 9*	3 ± 5*	0 ± 0*

Glass chamber slides were coated with 50 μg/ml of fibronectin, laminin, type IV collagen, or ovalbumin. NIH:OVCAR5 spheroids were incubated on the coated slides in serum-free medium for 2 hours in the presence of 10 μg/ml of mouse IgG or 10 μg/ml of blocking mAbs against the α2-, α5-, α6-, or β1-integrin subunits. Values are expressed as a percentage of the total number of spheroids that adhered to each substrate. Fewer than 5% of cells adhered to ovalbumin under any conditions. Data are expressed as mean ± SD.

*$P < 0.001$.

†$P < 0.005$.

‡$P < 0.01$, compared to the normal mouse IgG control.

nomenon that is mediated by multiple cell-matrix interactions between integrins and ECM components.

Discussion

In ovarian carcinoma, both single cells and multicellular aggregates are found in patients' ascitic fluid.[2] Extensive research has been performed using single-cell suspensions of cell lines derived from primary ovarian carcinoma tumors and ascites cells. However, because multicellular aggregates of ovarian carcinoma cells are not suited for assays that require single-cell suspensions, they have been primarily overlooked by the scientific community. In this study, we generated ovarian carcinoma cell spheroids, which are intermediate in complexity between monolayers and solid tumors, and more closely approximate the *in vivo* conditions of ovarian carcinoma patients than single-cell suspensions or monolayers. We used this model to identify adhesion molecules that mediate the formation of ovarian carcinoma spheroids and their subsequent adhesion to ECM proteins.

Early attempts to create spheroids from ovarian cancer cells were unsuccessful.[4] Ovarian carcinoma spheroids were eventually created; however, some primary tumor cells and cell lines required weeks to form stable spheroids, whereas others did not form multicellular aggregates at all.[2,4–9] In this study, we used the liquid overlay method[27] to show that the NIH:OVCAR5 ovarian carcinoma cell line formed stable spheroids within 48 hours. These spheroids appeared similar to those present *in vivo* in patients' ascites samples. In contrast, the SKOV3 ovarian carcinoma cell line failed to form stable spheroids unless incubated for more than 14 days (not shown). Another group was able to generate SKOV3 spheroids in 10 days using an alternate method.[8] This disparity may reflect the heterogeneity of ovarian carcinoma cells, even within well-defined cell lines. It is also important to note that cell lines, which are selected for their ability to proliferate and adhere, may form spheroids at a much faster rate than ovarian carcinoma cells *in vivo*.

Condensation into spheroids or multicellular aggregates decreased the proliferative abilities of the NIH:OVCAR5 and SKOV3 ovarian carcinoma cell lines when compared to the same cells cultured as monolayers. Both cell lines underwent a marked decrease in proliferation in the absence of adhesion to a substratum. However, the proliferative rates of the spheroids eventually approached those of the confluent monolayers. The cells in the spheroids and monolayers remained viable, as determined by staining for markers of cell death and apoptosis. Previous reports show that increased percentages of ovarian carcinoma monolayer cells accumulate in G_2/M phase compared to spheroid cells when exposed to Taxol.[9] The spheroid cells may be arrested at an earlier step of the cell cycle, which may inhibit both cell proliferation and apoptosis. The slower proliferative rate of ovarian carcinoma spheroids may protect them from therapies directed against fast-growing tumor cells.

Although several groups have generated spheroids from ovarian carcinoma cells,[5–9] the biological mechanisms by which the spheroids formed have not been defined. The NIH:OVCAR5 and SKOV3 ovarian carcinoma cell lines express a variety of adhesion molecules on their surfaces, including integrins, ICAM-1, and CD44.[15,18] In this study, we report that a functional blocking mAb against the β1-integrin subunit inhibited the formation of spheroids by NIH:OVCAR5 cells at an 8-hour time point, whereas a mAb that stimulates β1-integrin-mediated cell adhesion hastened the phenomenon. These data suggest that β1-integrin subunits mediate the initial formation of ovarian carcinoma spheroids. The incomplete inhibition of the β1-integrin subunits at the 24-hour time point suggests that if the β1-integrin subunits are inactivated, the ovarian carcinoma cells may possess a compensatory mechanism to facilitate spheroid condensation. However, it is also possible that the mAbs against the β1-integrin subunits may simply be internalized by 24 hours, eventually allowing the ovarian carcinoma cells to condense into spheroids. We also report that a functional blocking mAb against the α5-integrin subunit inhibited the formation of spheroids by NIH:OVCAR5 cells. Monoclonal antibodies that blocked the functional sites of the α1-, α2-, α3-, α4-, and α6-integrin subunits, integrin αvβ3, or CD44 had no effect on spheroid formation. This suggests that ovarian carcinoma spheroid formation may be regulated by the integrin α5β1.

The chief ligand of the α5β1-integrin is fibronectin.[31] Fibronectin has been reported to promote the adhesion of ovarian carcinoma cells[32,33] and may crosslink these cells via their α5β1-integrin receptors. In our hands, the addition of exogenous fibronectin promoted ovarian carcinoma spheroid formation, which supports our theory that ovarian carcinoma spheroid formation may be mediated by the α5β1-integrin. Interestingly, the addition of exogenous laminin also enhanced spheroid formation, whereas type IV collagen inhibited spheroid formation. It is possible that these adhesion molecules may indirectly alter spheroid formation, perhaps by signal transduction mechanisms.

By immunohistochemistry, we detected α5-integrin subunits, β1-integrin subunits, and fibronectin in regions of cell-cell contact on the surface of NIH:OVCAR5 spheroids generated after 48 hours in tissue culture. These

results are consistent with our finding that the α5β1-integrin mediates NIH:OVCAR5 spheroid formation. Although we observed fibronectin on the surface of ovarian carcinoma spheroids, we did not determine whether the fibronectin was secreted by the ovarian carcinoma cells themselves or whether it was incorporated into their pericellular matrix from the complete medium in which they were initially cultured. Fibronectin has been detected in peritoneal fluids obtained from both normal and ovarian cancer patients, and elevated expression of fibronectin has been measured by others in malignant ascites fluid.[34] Therefore, we decided to perform the spheroid formation portion of this assay in the presence of sera, because this would more closely approximate *in vivo* conditions. Interestingly, NIH:OVCAR5 cells grown in fibronectin-free serum substitute media for 48 hours did form spheroids when cultured in agarose-coated wells (data not shown). Altered ECM composition has been reported in glioma cell spheroids, which were found to contain fibronectin and a small proteoglycan not detected when the cells were cultured in monolayers.[35] Such alterations may facilitate spheroid formation, suggesting that the cells themselves can manufacture the additional ECM needed or incorporate it from exogenous sources. These results suggest that cell surface α5β1-integrins may mediate ovarian carcinoma cell aggregation via interactions with fibronectin that the cells have synthesized and retained on their surfaces or sequestered from their environment.

The α5β1-fibronectin interaction may later be augmented or replaced by other cell-cell interactions, including the gap junctions, tight junctions, and desmosomes detected in mature spheroids.[36–38] Squamous epithelial cells grown as spheroids express significantly less epidermal growth factor receptors than squamous cell monolayers.[39] Altered levels of expression of ICAM-1, CD44, and LFA-1 have been reported in cancer cells grown as spheroids compared to monolayers.[40] By flow cytometric analysis, we previously detected α1-, α2-, α3-, α5-, α6-, and β1-integrin subunits on the surface of single-cell suspensions of the NIH:OVCAR5 cell line.[18] In this study, we report that the α2-, α3-, α5-, α6-, and β1-integrin subunits, but not α1-integrin subunits, were detected on NIH:OVCAR5 spheroids by immunohistochemistry. Taken together, these data suggest that condensation into multicellular aggregates resulted in decreased expression of the α1-integrin subunit, which in turn may result in a similarly decreased ability to adhere to a substratum. The condensation of ovarian carcinoma cells into spheroids or multicellular aggregates may induce other alterations in adhesion molecule expression or ECM composition, with concurrent effects on their adhesive abilities.

An earlier study of single-cell suspensions of NIH:OVCAR5 cells reported >90% adhesion of these cells to fibronectin, laminin, and type IV collagen within 30 minutes[15] However, in this study we found that NIH:OVCAR5 spheroids required 4 hours to achieve maximum adhesion. Factors that may contribute to the longer time period required for spheroid adhesion to various substrates include: decreased expression of receptors, decreased avidity of receptors, competing cell-cell and cell-matrix interactions within the spheroids, physical constraints that limit the cells' ability to spread onto the anchoring surfaces, and the effects of mechanical forces on a structure with a greater surface area/volume ratio. Any of these factors may contribute to the presence of free-floating multicellular aggregates found in ovarian carcinoma patient ascites.[2]

In this study, we report that the adhesion of ovarian carcinoma spheroids to ECM components is a β1-integrin-mediated event. The nearly complete inhibition of adhesion by a blocking mAb against the β1-integrin subunit, coupled with partial inhibition in the presence of blocking mAbs against α-integrin subunits, suggest that multiple integrin-ECM interactions are involved in the process. Our results suggest that the interactions of the α5β1-integrin with fibronectin, the α6β1-integrin with laminin, and the α2β1-integrin with type IV collagen mediate ovarian carcinoma spheroid adhesion. Recently, Kawano and colleagues,[41] reported that the α2β1-, α6β1-, α3β1-integrins mediated the adhesion of squamous epithelial multicellular aggregates to type I collagen, laminin 1, and laminin 5, respectively. Taken together, these data suggest that spheroid adhesion is an integrin-dependent event, although the precise integrin-ligand interactions involved may be tissue-specific. However, additional cell-matrix and cell-cell interactions, which have been reported in spheroids generated from other cell types,[36–40] may mediate the initial formation and continued maintenance of spheroid morphology as they progress with time.

The examination of multicellular aggregates in ovarian carcinoma may be of clinical importance. This study demonstrates that ovarian carcinoma cells cultured as spheroids exhibit decreased proliferative and adhesive properties compared to ovarian carcinoma cells cultured as monolayers. Ovarian carcinoma spheroids are less sensitive than monolayers to cancer drugs and ionizing radiation,[4,5,9,42] which may be partly because of the low proliferative rates we report in this study. Also, the kinetics of drug absorption are altered in ovarian carcinoma spheroids, compared to ovarian carcinoma monolayers.[43] Taken together, these data suggest that spheroids may represent a tenacious, long-term source of secondary tumor growth in ovarian carcinoma that is not addressed by current therapeutic strategies, which target highly proliferative cancer cells. The biological properties of ovarian carcinoma spheroids require further study to better understand their significance in secondary tumor growth and to effectively eradicate them during the treatment of the disease. The model of ovarian carcinoma spheroid formation and adhesion presented in this study will also lay the groundwork for future studies in which ovarian carcinoma spheroids isolated from patient ascites fluid can now be monitored for their cell surface receptors and adhesive properties.

Acknowledgments

We thank Dr. James McCarthy for providing fibronectin, Dr. Leo Furcht for providing laminin and the mAb P5D2

against the β1-integrin subunit, Dr. Robert C. Bast, Jr. for providing the SKOV3 cell line, Drs. Thomas Hamilton and Judah Folkman for providing the NIH:OVCAR5 cell line; and the Tissue Procurement Facility of the University of Minnesota (a Comprehensive Cancer Center designated by the National Cancer Institute, supported by a Cancer Center Support grant from NIH/NCI, grant P30CA77598) for providing the patient ascites samples.

References

1. Greenlee RT, Murray T, Bolden S, Wingo PA: Cancer statistics, 2000. CA Cancer J Clin 2000, 50:7–33
2. Allen HJ, Porter C, Gamarra M, Johnson EA: Isolation and morphologic characterization of human ovarian carcinoma cell clusters present in effusions. Exp Cell Biol 1987, 55:194–208
3. Sutherland RM: Cell and environment interactions in tumor microregions: the multicell spheroid model. Science 1988, 240:177–184
4. Jones AC, Stratford IJ, Wilson PA, Peckham MJ: In vitro cytotoxic drug sensitivity of human tumour xenografts grown as multicellular tumor spheroids. Br J Cancer 1982, 46:870–879
5. Filippovich IV, Sorokina NI, Robillard N, Chatal JF: Radiation-induced apoptosis in human ovarian carcinoma cells growing as a monolayer and as multicell spheroids. Int J Cancer 1997, 72:851–859
6. Bardies M, Thedrez P, Gestin J, Marcille BM, Guerreau D, Faivre-Chauvet A, Mahe M, Sai-Maurel C, Chatal JF: Use of multi-cell spheroids of ovarian carcinoma as an intraperitoneal radio-immunotherapy model: uptake, retention kinetics, and dosimetric evaluation. Int J Cancer 1992, 50:984–991
7. Becker JL, Prewett TL, Spaulding GF, Goodwin TJ: Three-dimensional growth and differentiation of ovarian tumor cell line in high aspect rotating-wall vessel: morphologic and embryologic considerations. J Cell Biochem 1993, 51:283–289
8. Makhija S, Taylor DD, Gibb RK, Gercel-Taylor C: Taxol-induced bcl-2 phosphorylation in ovarian cancer cell monolayer and spheroids. Int J Oncol 1999, 14:515–521
9. Frankel A, Buckman R, Kerbel RS: Abrogation of taxol-induced G_2-M arrest and apoptosis in human ovarian cancer cells grown as multicellular tumor spheroids. Cancer Res 1997, 57:2388–2393
10. Hynes RO: Integrins: versatility, modulation, and signaling in cell adhesion. Cell 1992, 69:11–25
11. Boudreau N, Bissell MJ: Extracellular matrix signalling: integration of form and function in normal and malignant cells. Curr Opin Cell Biol 1998, 10:640–646
12. Carreiras F, Cruet S, Staedel C, Sichel F, Gauduchon P: Human ovarian adenocarcinoma cells synthesize vitronectin and use it to organize their adhesion. Gynecol Oncol 1999, 72:312–322
13. Sheppard D: Epithelial integrins. BioEssays 1996, 18:655–660
14. Abe Y, Tsutsui T, Mu J, Kosugi A, Yagita H, Sobue K, Niwa O, Fujiwara H, Hamaoka T: A defect in cell-to-cell adhesion via integrin-fibronectin interactions in a highly metastatic tumor cell line. Jpn J Cancer Res 1997, 88:64–71
15. Lessan K, Aguiar DJ, Oegema T, Siebenson L, Skubitz APN: CD44 and β1 integrin mediate ovarian carcinoma cell adhesion to peritoneal mesothelial cells. Am J Pathol 1999, 154:1525–1537
16. Buczek-Thomas JA, Chen N, Hasan T: Integrin-mediated adhesion and signalling in ovarian cancer. Cell Signal 1998, 10:55–63
17. Carreiras F, Rigot V, Cruet S, Andre F, Gauduchon P, Marvaldi J: Migration properties of the human ovarian adenocarcinoma cell line IGROV1: importance of αvβ3 integrins and vitronectin. Int J Cancer 1999, 80:285–294
18. Casey RC, Skubitz APN: CD44 and β1 integrins mediate ovarian carcinoma cell migration toward extracellular matrix proteins. Clin Exp Metastasis 2000, 18:67–75
19. Cannistra SA, Abu-Jawdeh G, Niloff J, Strobel T, Swanson L, Andersen J, Ottensmeier C: CD44 variant expression is a common feature of epithelial ovarian cancer: lack of association with standard prognostic factors. J Clin Oncol 1995, 13:1912–1921
20. Aruffo A, Stamenkovic I, Melnick M, Underhill CB: CD44 is the principal cell surface receptor for hyaluronate. Cell 1990, 61:1303–1313
21. Jalkanen S, Jalkanen M: Lymphocyte CD44 binds the COOH-terminal heparin-binding domain of fibronectin. J Cell Biol 1992, 116:817–825
22. Strobel T, Swanson L, Cannistra SA: In vivo inhibition of CD44 limits intra-abdominal spread of a human ovarian cancer xenograft in nude mice: a novel role for CD44 in the process of peritoneal implantation. Cancer Res 1997, 57:1228–1232
23. Molpus KL, Koelliker D, Atkins L, Kato DT, Buczek-Thomas J, Fuller AF, Hasan T: Characterization of a xenograft model of human ovarian carcinoma which produces intraperitoneal carcinomatosis and metastases in mice. Int J Cancer 1996, 68:588–595
24. Jones LM, Gardner MJ Catterall JB, Turner GA: Hyaluronic acid secreted by mesothelial cells: a natural barrier to ovarian cancer cell adhesion. Clin Exp Metastasis 1995, 13:373–380
25. Gardner MJ, Catterall JB, Jones LM, Turner GA: Human ovarian tumour cells can bind hyaluronic acid via membrane CD44: a possible step in peritoneal metastasis. Clin Exp Metastasis 1996, 14:325–334
26. Hamilton TC, Young RC, Ozols RF: Experimental model systems of ovarian cancer: applications to the design and evaluation of new treatment approaches. Semin Oncol 1984, 11:285–298
27. Yuhas JM, Li AP, Martinez AO, Ladman AJ: A simplified method for production and growth of multicellular tumor spheroids. Cancer Res 1977, 37:3639–3643
28. Pattaramalai S, Skubitz KM, Skubitz APN: A novel recognition site on laminin for α3β1 integrin. Exp Cell Res 1996, 222:281–290
29. McCarthy JB, Skubitz APN, Palm SL, Furcht LT: Metastasis inhibition of different tumor types by purified laminin fragments and a heparin-binding fragment of fibronectin. J Natl Cancer Inst 1988, 80:108–116
30. Smith DE, Mosher DF, Johnson RB, Furcht LT: Immunological identification of two sulfhydryl-containing fragments of human plasma fibronectin. J Biol Chem 1982, 257:5831–5838
31. Ruoslahti E: Fibronectin and its receptors. Annu Rev Biochem 1988, 57:375–413
32. Strobel T, Cannistra SA: Beta-1 integrins partly mediate binding of ovarian carcinoma cells to peritoneal mesothelium in vitro. Gynecol Oncol 1999, 73:362–367
33. Cannistra SA, Ottensmeier C, Niloff J, Orta B, DiCarlo J: Expression and function of beta 1 and alpha v beta 3 integrins in ovarian carcinoma. Gynecol Oncol 1995, 58:216–225
34. Menzin AW, Loret de Mola JR, Bilker WB, Wheeler JE, Rubin SC, Feinberg RF: Identification of oncofetal fibronectin in patients with advanced epithelial ovarian cancer: detection in ascitic fluid and localization to primary sites and metastatic implants. Cancer 1998, 82:152–158
35. Glimelius B, Norling B, Nederman T, Carlsson J: Extracellular matrices in multicellular spheroids of human glioma origin: increased incorporation of proteoglycans and fibronectin as compared to monolayer cultures. APMIS 1988, 96:433–444
36. Soranzo C, Della Torre G, Ingrosso A: Formation, growth and morphology of multicellular tumor spheroids from a human colon carcinoma cell line (LoVo). Tumorigenesis 1986, 72:459–467
37. Ladman AJ, Martinez AO: Cell contacts and surface features of three murine tumors grown as multicellular spheroids. Eur J Cell Biol 1987, 45:224–229
38. Hulser DF, Brummer F: Closing and opening of gap junction pores between two- and three-dimensionally cultured tumor cells. Biophys Struct Mech 1982, 9:83–88
39. Mansbridge JN, Ausserer WA, Knapp MA, Sutherland RM: Adaptation of EGF receptor signal transduction to three-dimensional culture conditions: changes in surface receptor expression and protein tyrosine phosphorylation. J Cell Physiol 1994, 161:374–382
40. Rainaldi G, Calcabrini A, Arancia G, Santini MT: Differential expression of adhesion molecules (CD44, ICAM-1, and LFA-3) in cancer cells grown in monolayer or as multicellular spheroids. Anticancer Res 1999, 19:1769–1778
41. Kawano K, Kantak SS, Murai M, Yao CC, Kramer RH: Integrin α3β1 engagement disrupts intercellular adhesion. Exp Cell Res 2001, 262: 180–196
42. Griffon G, Marchal C, Merlin JL, Marchal S, Parache RM, Bey P: Radiosensitivity of multicellular tumour spheroids obtained from human ovarian cancers. Eur J Cancer 1995, 31:85–91
43. Embleton MJ, Charleston A, Affleck K: Efficacy and selectivity of monoclonal-antibody-targeted drugs and free methotrexate in fluorescence-labelled mixed tumor-cell monolayer cultures and multicellular spheroids. Int J Cancer 1991, 49:566–572